

Computation and Analysis of Statistical Solutions of the Incompressible Euler Equations

Doctoral Thesis**Author(s):**

Lanthaler, Samuel

Publication date:

2021

Permanent link:

<https://doi.org/10.3929/ethz-b-000521981>

Rights / license:

In Copyright - Non-Commercial Use Permitted

Diss. ETH No. 27930

Computation and Analysis of Statistical Solutions of the Incompressible Euler Equations

A thesis submitted to attain the degree of
DOCTOR OF SCIENCES of ETH ZURICH
(Dr. sc. ETH Zurich)

presented by
SAMUEL LANTHALER
M.Sc. Mathematics, ETH Zurich
born on 18.08.1989
citizen of Wängi (TG), Switzerland

accepted on the recommendation of

Prof. Dr. Siddhartha Mishra, ETH Zurich, examiner
Prof. Dr. Ulrik Fjordholm, University of Oslo, co-examiner

2021

Abstract

The inviscid, incompressible Euler equations are an idealized model for flows at high Reynolds number. Solutions of inviscid fluid models, such as the incompressible Euler equations, are highly sensitive to small perturbations of the initial data. Mathematically, this is reflected by a lack of general uniqueness and well-posedness results. For numerical approximations, this lack of stability implies that the convergence of numerical schemes to a unique limit cannot be guaranteed for general (energy-admissible) initial data. The present thesis studies the approximation of solutions of the incompressible Euler equations, focusing on spectral methods. Besides extending the convergence theory of these methods in a deterministic setting, we propose *statistical solutions* as a suitable framework to study the convergence of numerical methods for rough solutions of the Euler equations, at low regularity. These statistical solutions are time-parametrized probability measures on flow fields. The main observation of the present work is that, for the approximation of solutions at low regularity, a marked contrast is observed numerically between the failure of (strong) convergence in any classical, deterministic sense, versus the apparent stability and convergence of statistical quantities at increasing numerical resolution. In addition to presenting extensive numerical experiments to study different aspects of the convergence of statistical quantities, we develop a theoretical framework of statistical solutions. This theoretical framework allows us to interpret these empirical observations as the convergence of numerical approximants to a *limiting statistical solution*. Building on the insights gained in the analysis of statistical solutions, we next investigate the question of anomalous energy dissipation in the zero-viscosity limit of the Navier-Stokes equations, and provide a characterization of energy conservative solutions of the incompressible Euler equations in two dimensions, considerably going beyond the critical $1/3$ -Hölder regularity for energy conservation identified by Onsager. Finally, we address the practically important question of combining available observational data with the underlying fluid model in a Bayesian formulation, and the use of neural network based surrogate models to provide novel approximations of statistical solutions.

Zusammenfassung

Ein idealisiertes Modell für Strömungen hoher Reynoldszahl sind die inviziden, inkompressiblen Eulergleichungen. Lösungen von inviziden Fluidmodellen, wie den inkompressiblen Eulergleichungen, sind hochempfindlich gegenüber Störungen der Anfangsdaten. Mathematisch spiegelt sich dies wider in der Nichtverfügbarkeit von allgemeinen Ergebnissen zur Eindeutigkeit und Existenz von Lösungen. Für numerische Näherungen bedeutet dieser Mangel an Stabilität, dass die Konvergenz numerischer Schemata zu einem eindeutigen Grenzwert für allgemeine (energiezulässige) Ausgangsdaten nicht garantiert werden kann. Die vorliegende Arbeit beschäftigt sich mit der Approximation von Lösungen der inkompressiblen Eulergleichungen, mit Schwerpunkt auf spektralen Methoden. Neben der Erweiterung der Konvergenztheorie dieser Methoden in einem deterministischen Kontext schlagen wir statistische Lösungen der Eulergleichungen vor. Letzteres sind zeitparametrisierte Wahrscheinlichkeitsmasse auf dem Raum der Strömungsfelder, welche uns zu einem besseren Verständnis der Konvergenz numerischer Methoden verhelfen, insbesondere wenn die zugrunde liegende Lösung eine geringe Regularität aufweist. Die wichtigste Erkenntnis dieser Arbeit ist, dass bei der numerischen Annäherung von Lösungen mit niedriger Regularität ein deutlicher Kontrast beobachtet wird, zwischen dem Ausbleiben der (starken) Konvergenz im klassischen, deterministischen Sinne gegenüber der augenscheinlichen Stabilität und Konvergenz statistischer Größen bei steigender numerischer Auflösung. Neben der Präsentation umfangreicher numerischer Experimente zur Untersuchung verschiedener Aspekte dieser Konvergenz statistischer Größen, entwickeln wir einen theoretischen Rahmen für statistische Lösungen, der es uns ermöglicht, eine Interpretation dieser empirischen Beobachtungen als numerische Konvergenz zu einer statistischen Lösung zu geben. Aufbauend auf den gewonnenen Erkenntnissen für statistische Lösungen untersuchen wir desweiteren die Frage der anomalen Energiedissipation im Nullviskositäts-Limes der Navier-Stokes-Gleichungen; Wir geben eine Charakterisierung energieerhaltender Lösungen der inkompressiblen Eulergleichungen in zwei Dimensionen. Dieses Resultat geht deutlich über die von Onsager identifizierte kritische $1/3$ -Hölder-Regularität für die Energieerhaltung hinaus. Abschließend wenden wir uns der praktisch wichtigen Frage zu, wie vorhandener Beobachtungsdaten mit dem zugrunde liegenden Fluidmodell in einer Bayes'schen Formulierung kombiniert werden können, und wir diskutieren neuronale Netzwerk-basierte Stellvertreter-Modelle, um eine neuartige Darstellung statistischer Lösungen zu erhalten.

Contents

Abstract	i
Zusammenfassung	iii
Outline of this thesis	1
1 Introduction	3
1.1 The incompressible Euler equations	3
1.2 Physical meaning of the equations	4
1.3 Elements of the mathematical theory	6
1.4 Numerical discretization: Spectral methods	16
2 Convergence of the spectral viscosity scheme to rough solutions	21
2.1 Introduction	21
2.2 A fine-tuned SV scheme	22
2.3 Overview of the strategy	24
2.4 Spectral decay estimate	25
2.5 Short-time estimates	29
2.6 Uniform L^1 control and equi-integrability	30
2.7 Convergence in the Delort class	34
2.8 Numerical experiments	35
2.9 Discussion	45
3 Statistical solutions	47
3.1 Introduction	47
3.2 Time-Parameterized Probability Measures on $L^2(D; \mathbb{R}^d)$	49
3.3 Dissipative statistical solutions and their well-posedness	55
3.4 Numerical Approximation of Statistical Solutions	58
3.5 Numerical Experiments	65
3.6 Discussion	78
4 Physically realizable solutions and energy conservation	81
4.1 Introduction	81
4.2 Energy conservation of vanishing viscosity limits	84
4.3 Energy conservation for numerical approximations of statistical solutions	93
4.4 Numerical experiments	97
4.5 Discussion	110

5 Limitations of the approach	113
6 Bayesian inversion for fluid flows	115
6.1 Introduction	115
6.2 Bayesian inverse problem	117
6.3 Data assimilation	127
6.4 Applications	138
6.5 Discussion	144
7 Surrogate models and operator learning for fluid flows	147
7.1 Introduction	148
7.2 Approximation by Fourier Neural Operators	149
7.3 Approximation of PDEs by Ψ -FNOs	158
7.4 Approximation of statistical solutions via surrogates	164
7.5 Discussion	169
8 Conclusions and further research	171
List of symbols	175
Appendices	177
A Mathematical complements	179
A.1 Fourier analysis	179
A.2 Compactness theorems	182
B Wasserstein distance	185
Bibliography	187
Acknowledgments	197
Curriculum Vitae	199

Outline of this thesis

For the convenience of the reader, we provide a brief outline of the contents of the present thesis.

In chapter 1, we introduce the incompressible Euler equations. These equations form the main object of study of this work. After a short recapitulation of the physical meaning of the equations, we review elements of their mathematical theory. We summarize short-time existence and uniqueness of classical solutions, the concepts of weak and measure-valued solutions and point out the central role played by the vorticity in their mathematical analysis. Furthermore, we discuss rough solutions with unbounded vorticity in the two-dimensional case, and the connection of such rough solutions with physical theories of turbulence. The first chapter also introduces spectral methods, and in particular the spectral (hyper-)viscosity (SV) scheme for the numerical approximation of the incompressible Euler equations.

In chapter 2, we study the convergence of the SV scheme to rough solutions. Using compensated compactness methods, we show that a suitable choice of parameters for the SV scheme ensures that approximate solution sequences computed by this discretization converge (subsequently) to a weak solution of the incompressible Euler equations, even for rough initial data. More precisely, we provide a proof of convergence for initial data in the so-called “*Delort class*”. This result closes a long-standing gap between the available existence theory and convergence results for numerical schemes. Chapter 2 is based on the publication [LM20].

In chapter 3, we introduce statistical solutions of the incompressible Euler equations. We propose an algorithm for their numerical approximation and study the convergence of approximate statistical solutions, both analytically and by numerical experimentation. In particular, we emphasize the importance of “structure functions” for the compactness and convergence theory of statistical solutions. These structure functions are also central to physical theories of turbulence, and thus provide a natural link to these physical theories. Chapter 3 reviews the main results of [LMPP21b].

In chapter 4, we study the structure functions of the preceding chapter in further detail, and in connection with the question of anomalous energy dissipation for the incompressible Euler equations. We focus on the two-dimensional case, where we first provide a characterization of energy conservation for physically realizable solutions, *i.e.* solutions which are obtained in the zero-viscosity limit of the incompressible Navier-Stokes equations. We then discuss the energy conservation of statistical solutions computed by numerical discretization. Numerical experiments for a number of rough initial data demonstrate the relevance of the proposed estimates. This chapter summarizes the results of [LMPP21a].

In chapter 5, we point out two major limitations of the approach to statistical solutions introduced in the preceding chapters. Initial steps at addressing these limitations are undertaken in the subsequent chapters 6 and 7.

In chapter 6, we show how available measurement data can be incorporated in the framework of the present thesis, based on a Bayesian point of view: More precisely, we discuss Bayesian inversion and data

assimilation/filtering for PDEs defining ill-posed forward problems, such as the incompressible Euler equations. This chapter is based on [LMW21].

In chapter 7, we discuss the emerging field of operator learning and analyse a novel neural network architecture, Fourier neural operators (FNOs), to approximate operators defined on infinite-dimensional function spaces, *i.e.* mapping input functions to output functions. We review the universal approximation theorem for FNOs, showing that FNOs can approximate general continuous operators mapping between Sobolev spaces, to arbitrary accuracy. In addition, we use ideas from spectral methods to derive explicit complexity and error estimates for the FNO approximation of the solution operator of the incompressible Euler and Navier-Stokes equations. We also indicate how FNO surrogates can be used to provide an alternative numerical approximation of statistical solutions, and provide a rationale for their potentially improved efficiency, compared to traditional numerical methods. This chapter is mainly based on [KLM21], with elements taken from [LMK21].

Finally, in chapter 8 we present conclusions and remark on possible further research directions.

For reference, a list of commonly used symbols throughout this thesis has been included on page 175. A brief summary of basic results in harmonic analysis and measure theory are provided, respectively, in Appendices A and B.

Chapter 1

Introduction

1.1 The incompressible Euler equations

The present thesis studies the numerical approximation of the incompressible Euler equations. The incompressible Euler equations describe the motion of an ideal, incompressible fluid in the absence of viscous effects, and are given by the following system of partial differential equations (PDEs) [MB01, CM90]:

$$\begin{cases} \partial_t \mathbf{u} + (\mathbf{u} \cdot \nabla) \mathbf{u} + \nabla p = 0, \\ \operatorname{div}(\mathbf{u}) = 0, \quad \mathbf{u}(t=0) = \bar{\mathbf{u}}. \end{cases} \quad (1.1.1)$$

Here, $\mathbf{u} : D \times [0, T] \rightarrow \mathbb{R}^d$, $(x, t) \mapsto \mathbf{u}(x, t) = (u_1(x, t), \dots, u_d(x, t))$ denotes the fluid velocity as a function of the spatial location $x = (x_1, \dots, x_d) \in D$ and at time $t \in [0, T]$, with $D \subset \mathbb{R}^d$, $d \in \{2, 3\}$, the underlying domain. The function $p : D \times [0, T] \rightarrow \mathbb{R}$, $(x, t) \mapsto p(x, t)$ denotes the pressure. The vector field $\bar{\mathbf{u}} : D \rightarrow \mathbb{R}^d$ denotes the initial data, and it is assumed here and in the following that $\operatorname{div}(\bar{\mathbf{u}}) = 0$ for any initial data. The incompressible Euler equations (1.1.1) have to be complemented by suitable boundary conditions. In the present thesis we will throughout assume *periodic boundary conditions*, *i.e.* we assume that the domain $D = \mathbb{T}^d$ can be identified with the 2π -periodic torus $\mathbb{T}^d \simeq [0, 2\pi]^d$.

We also recall that $\partial_t \mathbf{u}$ is a compact notation for the partial derivative $\partial \mathbf{u} / \partial t$ with respect to t , and that $\nabla = (\partial_{x_1}, \dots, \partial_{x_d})$ denotes the (spatial) gradient operator, such that

$$\nabla p = (\partial_{x_1} p, \dots, \partial_{x_d} p) \in \mathbb{R}^d, \quad (\mathbf{u} \cdot \nabla) \mathbf{u} = \left(\sum_{j=1}^d u_j \partial_{x_j} u_1, \dots, \sum_{j=1}^d u_j \partial_{x_j} u_d \right) \in \mathbb{R}^d.$$

We define the divergence of a matrix-valued function $A : D \rightarrow \mathbb{R}^{d \times d}$, $x \mapsto A(x) = (A_{ij}(x))_{i,j}$ by $\operatorname{div}(A) = \sum_{i=1}^d \partial_{x_i} A_{ij} \in \mathbb{R}^d$. Owing to the divergence-free constraint, $\operatorname{div}(\mathbf{u}) = \sum_{i=1}^d \partial_{x_i} u_i = 0$, we then have the equality $\mathbf{u} \cdot \nabla \mathbf{u} = \operatorname{div}(\mathbf{u} \otimes \mathbf{u})$, where the tensor product $\mathbf{u} \otimes \mathbf{u}$ is the matrix with entries $(u_i u_j)_{i,j} \in \mathbb{R}^{d \times d}$. This allows us to write (1.1.1) in the (formally) equivalent form

$$\begin{cases} \partial_t \mathbf{u} + \operatorname{div}(\mathbf{u} \otimes \mathbf{u}) + \nabla p = 0, \\ \operatorname{div}(\mathbf{u}) = 0, \quad \mathbf{u}(t=0) = \bar{\mathbf{u}}. \end{cases} \quad (1.1.2)$$

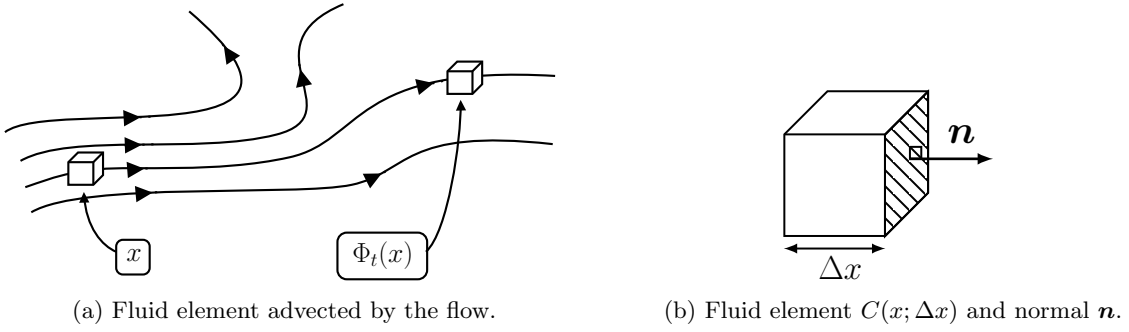


Figure 1.1: Schematic for fluid elements: (a) advection and (b) outward unit normal \mathbf{n} .

1.2 Physical meaning of the equations

1.2.1 Momentum equation and force balance

Physically, the first equation of (1.1.1) describes the acceleration of fluid elements due to the force exerted by the pressure. To see why, we consider an infinitesimal fluid element at the initial position x at $t = 0$, and follow its evolution $t \mapsto \Phi_t(x)$ over time (cp. Figure 1.1a). Here, x is treated as a parameter. The fluid element is advected by the flow, yielding

$$\frac{d\Phi_t(x)}{dt} = \mathbf{u}(\Phi_t(x), t), \quad \Phi_0(x) = x. \quad (1.2.1)$$

By Newton's second law $\mathbf{F} = m\mathbf{a}$, the acceleration of the fluid element is therefore given by

$$a = \frac{d^2\Phi_t(x)}{dt^2} \stackrel{(1.2.1)}{=} (\partial_t u + u \cdot \nabla u) \Big|_{(\Phi_t(x), t)} = \frac{F}{m}, \quad (1.2.2)$$

where \mathbf{F} is the force acting on the fluid element, and m is its mass.

The force \mathbf{F} due to the pressure acting on a small cube $C(x; \Delta x)$ of side length Δx and center x (cp. Figure 1.1b) is given by the integral of the pressure over its faces:

$$\mathbf{F} = - \int_{\partial C(x; \Delta x)} p(\xi) d\mathbf{n}(\xi),$$

where \mathbf{n} is the outward pointing normal to the surface. For small $\Delta x \ll 1$, we have

$$\mathbf{F} \approx -\sum_{j=1}^d \left[p\left(x + \frac{\Delta x}{2} \mathbf{e}_j\right) - p\left(x - \frac{\Delta x}{2} \mathbf{e}_j\right) \right] (\Delta x)^2 \mathbf{e}_j,$$

where $\mathbf{e}_j \in \mathbb{R}^d$ denotes the j -th unit vector. Assuming a constant mass density = 1, we furthermore note that

$$m = \int_{C(x; \Delta x)} 1 \, dx = (\Delta x)^3,$$

implying that the acceleration \mathbf{a} is given by (for infinitesimal fluid elements):

$$\begin{aligned} \mathbf{a} &= \lim_{\Delta x \rightarrow 0} \frac{\mathbf{F}}{m} = \lim_{\Delta x \rightarrow 0} \frac{\int_{\partial C(x; \Delta x)} p(\xi) d\mathbf{n}(\xi)}{\int_{C(x; \Delta)} 1 dx} \\ &= \lim_{\Delta x \rightarrow 0} - \sum_{j=1}^d \frac{1}{\Delta x} \left[p\left(x + \frac{\Delta x}{2} \mathbf{e}_j\right) - p\left(x - \frac{\Delta x}{2} \mathbf{e}_j\right) \right] \mathbf{e}_j = -\nabla p(x). \end{aligned}$$

Thus, if the total force acting on the fluid element is determined by the pressure alone, then (1.2.2) implies that

$$\partial_t \mathbf{u} + \mathbf{u} \cdot \nabla \mathbf{u} = -\nabla p,$$

yielding the first equation of the incompressible Euler equations (1.1.1).

We also remark that if there are additional forces acting on the fluid elements, such as the gravitational force or frictional forces between fluid elements, represented by a force density $\mathbf{f} : D \times [0, T] \rightarrow \mathbb{R}^d$, then the same argument shows that the momentum equation of the incompressible Euler equations becomes

$$\partial_t \mathbf{u} + (\mathbf{u} \cdot \nabla) \mathbf{u} + \nabla p = \mathbf{f}.$$

In particular, additional stresses due to internal friction of the fluid elements can be modeled by $\mathbf{f} = \nabla \cdot (\nu \nabla \mathbf{u}) = \nu \Delta \mathbf{u}$, where $\nu > 0$ denotes the viscosity, leading to the *incompressible Navier-Stokes equations*

$$\begin{cases} \partial_t \mathbf{u} + (\mathbf{u} \cdot \nabla) \mathbf{u} + \nabla p = \nu \Delta \mathbf{u}, \\ \operatorname{div}(\mathbf{u}) = 0, \quad \mathbf{u}(t=0) = \bar{\mathbf{u}}. \end{cases} \quad (1.2.3)$$

1.2.2 Incompressibility

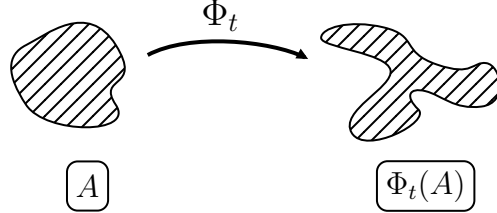


Figure 1.2: The flow map Φ_t .

We next show that the divergence-free constraint $\operatorname{div}(\mathbf{u}) = 0$ reflects the incompressibility of the underlying fluid: Indeed, if $A \subset \mathbb{R}^d$ is any bounded subdomain, then by the change of variables formula with $y = \Phi_t(x)$, the volume of the domain $\Phi_t(A)$ transported by the flow is given by

$$\operatorname{Vol}(\Phi_t(A)) = \int_{\Phi_t(A)} 1 dy = \int_A |\det(D_x \Phi_t(x))| dx. \quad (1.2.4)$$

Taking a time-derivative of the integrand, we obtain

$$\frac{\partial}{\partial t} \det(D_x \Phi_t(x)) = \det(D_x \Phi_t(x)) \operatorname{tr}([D_x \Phi_t(x)]^{-1} \cdot \partial_t D_x \Phi_t(x)),$$

where $D_x \Phi_t(x)$ denotes the Jacobian matrix of $\Phi_t(x)$, and where equation (1.2.2) implies that

$$\partial_t D_x \Phi_t(x) = D_x \partial_t \Phi_t(x) = D_x [\mathbf{u}(\Phi_t(x), t)] = D_x \mathbf{u}|_{(\Phi_t(x), t)} \cdot D_x \Phi_t(x).$$

It thus follows that

$$\begin{aligned} \frac{\partial}{\partial t} \det(D_x \Phi_t(x)) &= \det(D_x \Phi_t(x)) \operatorname{tr}([D_x \Phi_t(x)]^{-1} \cdot D_x \mathbf{u}|_{(\Phi_t(x), t)} \cdot D_x \Phi_t(x)) \\ &= \det(D_x \Phi_t(x)) \operatorname{tr}(D_x \mathbf{u}|_{(\Phi_t(x), t)}) \\ &= \det(D_x \Phi_t(x)) \operatorname{div}(\mathbf{u})|_{(\Phi_t(x), t)}. \end{aligned}$$

Hence, assuming the divergence-free constraint $\operatorname{div}(\mathbf{u}) = 0$, it follows that $\partial_t \det(D_x \Phi_t(x)) = 0$. From (1.2.4), this implies that $\frac{d}{dt} \operatorname{Vol}(\Phi_t(A)) = 0$, or equivalently

$$\operatorname{Vol}(\Phi_t(A)) = \operatorname{Vol}(\Phi_0(A)) = \operatorname{Vol}(A),$$

for any bounded subdomain $A \subset \mathbb{T}^d$, *i.e.* that the flow associated with \mathbf{u} is incompressible.

1.2.3 Kinetic energy

We finally note that the kinetic energy of a fluid element $C(x; \Delta x)$ of unit mass density, and hence of mass $m = (\Delta x)^3$, is given by $\frac{1}{2}m|\mathbf{u}|^2 = \frac{1}{2}|\mathbf{u}|^2(\Delta x)^3$. Considering infinitesimal fluid elements, this indicates that the energy density of the fluid is given by $e(x, t) = \frac{1}{2}|\mathbf{u}(x, t)|^2 dx$, and the total kinetic energy at time t is given by

$$E(t) = \frac{1}{2} \int_{\mathbb{T}^d} |\mathbf{u}(x, t)|^2 dx = \frac{1}{2} \|\mathbf{u}(t)\|_{L_x^2}^2.$$

A formal calculation based on the incompressible Euler equations (1.1.1) shows that

$$\begin{aligned} \frac{d}{dt} E(t) &= \int_{\mathbb{T}^d} \partial_t \mathbf{u} \cdot \mathbf{u} = - \int_{\mathbb{T}^d} [(\mathbf{u} \cdot \nabla) \mathbf{u} + \nabla p] \cdot \mathbf{u} dx \\ &= - \int_{\mathbb{T}^d} (\mathbf{u} \cdot \nabla) \left(\frac{1}{2} |\mathbf{u}|^2 \right) dx - \int_{\mathbb{T}^d} \nabla p \cdot \mathbf{u} dx \\ &= - \int_{\mathbb{T}^d} \operatorname{div} \left(\frac{1}{2} |\mathbf{u}|^2 \mathbf{u} \right) dx + \int_{\mathbb{T}^d} p \operatorname{div}(\mathbf{u}) dx \\ &= 0, \end{aligned}$$

where we have integrated by parts and used the divergence-free condition $\operatorname{div}(\mathbf{u}) = 0$, as well as the divergence-theorem on the last line, and we have assumed \mathbf{u} to be sufficiently regular to justify all of the manipulations. In particular, this argument shows that smooth solutions of the incompressible Euler equations are *energy-conservative*.

1.3 Elements of the mathematical theory

Even though the incompressible Euler equations were formulated by Leonhard Euler already in 1757 [Eul57] and are amongst the first PDEs to have been devised, their mathematical analysis and understanding is still very far from complete. In this section, we will review some key elements of the available mathematical theory which are pertinent to the contents and contributions of the present thesis. We refer the reader to Appendix A for a brief summary of some fundamental facts on the Fourier transform and Sobolev spaces.

1.3.1 Leray projection and Fourier transformed equations

Mathematically, the divergence-free constraint $\operatorname{div}(\mathbf{u}) = 0$ implies that the pressure can be determined (up to an unimportant constant) from the velocity field \mathbf{u} : Indeed, taking the divergence of the momentum equation, and using that the divergence of $\partial_t \mathbf{u}$ vanishes, we find

$$-\Delta p = \operatorname{div}(\operatorname{div}(\mathbf{u} \otimes \mathbf{u})), \tag{1.3.1}$$

where $\Delta p = \sum_{i=1}^d \partial_{x_i}^2 p$ denotes the Laplacian applied to p . The equation for the pressure (1.3.1) indicates that the pressure is not a true dynamic variable, but instead acts as a Lagrange multiplier in (1.1.1), to ensure the divergence-free constraint $\operatorname{div}(\mathbf{u}) = 0$. In fact, the gradient term ∇p in the incompressible Euler equations acts as a *L^2 -orthogonal projection* of the non-linear term onto divergence-free vector fields, as will be discussed next. To this end, let us first point out that in view of the close relation of the L^2 -norm with the kinetic energy of the fluid, explained in the previous section, it is natural to assume that the flow field \mathbf{u} has finite energy, *i.e.* that $\sup_{t \in [0, T]} \|\mathbf{u}\|_{L_x^2} < \infty$, for any physically admissible solution. We will implicitly assume this in the following formal calculations.

To develop a better intuition for the meaning of the pressure term, it is instructive to consider the Fourier transformed version of the incompressible Euler equations (1.1.2). To this end, we write $\mathbf{u}(x, t) = \sum_{k \in \mathbb{Z}^d} \widehat{\mathbf{u}}_k(t) e^{ik \cdot x}$, and $p(x, t) = \sum_{k \in \mathbb{Z}^d} \widehat{p}_k(t) e^{ik \cdot x}$ in terms of their Fourier series. The incompressible Euler equations then lead to the following system of equations for the Fourier coefficients $\widehat{\mathbf{u}}_k$ ($k \neq 0$):

$$\frac{d\widehat{\mathbf{u}}_k}{dt} = -ik \cdot (\widehat{\mathbf{u}} \otimes \widehat{\mathbf{u}})_k - ik\widehat{p}_k, \quad (\widehat{\mathbf{u}} \otimes \widehat{\mathbf{u}})_k = \sum_{\ell \in \mathbb{Z}^d} (\widehat{\mathbf{u}}_\ell \otimes \widehat{\mathbf{u}}_{k-\ell}). \quad (1.3.2)$$

and $\frac{d\widehat{\mathbf{u}}_0}{dt} = 0$ for $k = 0$. Equation (1.3.1) for the pressure can now be expressed as $\widehat{p}_k = -\frac{(k \otimes k)}{|k|^2} : (\widehat{\mathbf{u}} \otimes \widehat{\mathbf{u}})_k$, for $k \neq 0$, where we denote $A : B = \sum_{i,j=1}^d A_{ij} B_{ij}$ for matrices A, B . Substitution of this identity for \widehat{p}_k in (1.3.2), yields ($k \neq 0$)

$$\frac{d\widehat{\mathbf{u}}_k}{dt} = \left(I - \frac{k \otimes k}{|k|^2} \right) (-ik \cdot (\widehat{\mathbf{u}} \otimes \widehat{\mathbf{u}})_k), \quad (\widehat{\mathbf{u}} \otimes \widehat{\mathbf{u}})_k = \sum_{\ell \in \mathbb{Z}^d} (\widehat{\mathbf{u}}_\ell \otimes \widehat{\mathbf{u}}_{k-\ell}), \quad (1.3.3)$$

where $I \in \mathbb{R}^{d \times d}$ denotes the identity matrix. We furthermore observe that the divergence constraint $\operatorname{div}(\mathbf{u}) = 0$ is equivalent to the condition that $k \cdot \widehat{\mathbf{u}}_k = 0$, for all $k \in \mathbb{Z}^d$, *i.e.* that the k -th Fourier coefficient of \mathbf{u} is perpendicular to k . The matrix $I - \frac{k \otimes k}{|k|^2}$ is clearly the orthogonal projection onto the perpendicular complement of k , and hence multiplication with this matrix ensures that the right-hand side of (1.3.3) remains divergence-free.

We can define an associated operator $\mathbb{P} : L^2(\mathbb{T}^d; \mathbb{R}^d) \rightarrow L^2(\mathbb{T}^d; \mathbb{R}^d)$, $\mathbf{v} \mapsto \mathbb{P}\mathbf{v}$ via the Fourier transform as follows:

$$\mathbb{P} \left(\sum_{k \in \mathbb{Z}^d} \widehat{\mathbf{v}}_k e^{ik \cdot x} \right) := \sum_{k \in \mathbb{Z}^d \setminus \{0\}} \left(I - \frac{k \otimes k}{|k|^2} \right) \widehat{\mathbf{v}}_k e^{ik \cdot x}. \quad (1.3.4)$$

It is not hard to see that \mathbb{P} is an *L^2 -orthogonal projection onto divergence-free vector fields*. We will refer to the projection \mathbb{P} defined by (1.3.4) as the *Leray projection*. Utilizing \mathbb{P} , we can now eliminate the pressure from the incompressible Euler equations, and formally write (1.1.2) as an equation on the space of divergence-free vector fields:

$$\begin{cases} \partial_t \mathbf{u} + \mathbb{P} \operatorname{div}(\mathbf{u} \otimes \mathbf{u}) = 0, \\ \mathbf{u}(t = 0) = \overline{\mathbf{u}}. \end{cases} \quad (1.3.5)$$

This evolution equation is formally equivalent to (1.3.3), and furnishes one of the most succinct formulations of the incompressible Euler equations.

1.3.2 Well-posedness theory and the vorticity equation

Given a PDE such as the incompressible Euler equations (1.1.1), it is natural to ask whether there is a function space $X \subset L^2(\mathbb{T}^d; \mathbb{R}^d)$, on which the initial value problem is well-posed; *i.e.* there exists

a solution operator $\mathcal{S}_t : X \rightarrow X$ ($t \geq 0$), such that for any $\bar{\mathbf{u}} \in X$, the time-dependent vector field $\mathbf{u}(t) := \mathcal{S}_t(\bar{\mathbf{u}})$ is the unique solution of equation (1.1.1). Natural candidate spaces include the whole space of L^2 -bounded, divergence-free vector fields, or Sobolev spaces $H^s = H^s(\mathbb{T}^d; \mathbb{R}^d)$, $s \geq 0$, consisting of vector fields \mathbf{u} , whose Fourier coefficients $\hat{\mathbf{u}}_k$ satisfy (cp. Appendix A)

$$\sum_{k \in \mathbb{Z}^d} (1 + |k|)^{2s} |\hat{\mathbf{u}}_k|^2 < \infty.$$

Global well-posedness results have so far only been achieved in the two-dimensional case, where it can be shown that solutions to smooth initial data (e.g. $\mathbf{u} \in H^s$, for $s > 3$) remain smooth also at later times, and are unique [MB01]. In the three-dimensional case, no global in time existence and uniqueness results are available. Short-time existence and uniqueness results for solutions starting from sufficiently regular initial data are classical [MB01, Thm 3.4]:

Theorem 1.3.1 (Short-time existence and uniqueness). *Let $\bar{\mathbf{u}} \in H^s$ be initial data for the incompressible Euler equations on \mathbb{T}^d . Assume that $s > \frac{d}{2} + 2$. Then there exists a time $T > 0$, depending on $\|\bar{\mathbf{u}}\|_{H^s}$, such that there exists a unique solution $\mathbf{u} \in C([0, T]; H^s)$ of the incompressible Euler equations (1.1.1).*

The short-time existence and uniqueness Theorem 1.3.1 implies in particular, that for any initial data $\bar{\mathbf{u}}$, there exists a *maximal time* $T^* = T^*(\bar{\mathbf{u}}) > 0$, such that there exists a solution $\mathbf{u} \in C([0, T^*); H^s)$ of the incompressible Euler equations with initial data $\bar{\mathbf{u}}$. For $d \geq 3$, it is not known whether one always has $T^* = \infty$, or whether the H^s -norm of \mathbf{u} might blow-up for certain initial data $\bar{\mathbf{u}}$, at a finite time $T^* < \infty$.

A crucial tool in the study of the regularity of solutions of the incompressible Euler equations is the *vorticity equation*, describing the evolution of the vorticity $\text{curl}(\mathbf{u})$. The vorticity equation is obtained by taking the curl of (1.1.1). In the three-dimensional case, the vorticity is a vector field $\boldsymbol{\omega} = \text{curl}(\mathbf{u})$, and the vorticity equation is given by

$$\partial_t \boldsymbol{\omega} + \mathbf{u} \cdot \nabla \boldsymbol{\omega} = \boldsymbol{\omega} \cdot \nabla \mathbf{u}. \quad (1.3.6)$$

In the two-dimensional case, the vorticity is a scalar quantity $\omega = \text{curl}(\mathbf{u}) = \partial_{x_1} u_2 - \partial_{x_2} u_1$, and the vorticity equation reduces to the following transport equation

$$\partial_t \omega + \mathbf{u} \cdot \nabla \omega = 0. \quad (1.3.7)$$

Due to the divergence-free constraint $\text{div}(\mathbf{u}) = 0$, this equation can also be written in the formally equivalent form $\partial_t \omega + \text{div}(\mathbf{u} \omega) = 0$. The importance of the vorticity equation is highlighted by the following well-known blow-up criterion, due to Beale, Kato and Majda [BKM84]:

Theorem 1.3.2 (Beale-Kato-Majda criterion). *Let $s > \frac{d}{2} + 1$ be an integer, and let $\mathbf{u} \in C([0, T^*); H^s)$ be a solution of the incompressible Euler equations (1.1.8). If \mathbf{u} cannot be extended to a solution on the closed interval $[0, T^*]$, then we must have*

$$\int_0^{T^*} \|\boldsymbol{\omega}(t)\|_{L_x^\infty} dt = \infty.$$

□

A consequence of Theorem 1.3.2 and the short-time existence and uniqueness Theorem 1.3.1 is that if $\int_0^{T^*} \|\boldsymbol{\omega}\|_{L^\infty} dt < \infty$, then the solution \mathbf{u} can be extended to a strictly larger time interval $[0, T^* + \delta)$, for $\delta > 0$.

Remark 1.3.3. In the two-dimensional case, the transport equation (1.3.7) implies an *a priori* bound $\|\omega(t)\|_{L^\infty} \leq \|\bar{\omega}\|_{L^\infty}$, where $\bar{\omega} := \text{curl}(\bar{\mathbf{u}})$, at least for solutions constructed by a suitable regularization. It therefore follows from Theorem 1.3.2 that for any integer $s > d/2 + 2$ and initial data $\bar{\mathbf{u}} \in H^s$, there exists a unique global-in-time solution of the incompressible Euler equations in $\mathbf{u} \in C([0, \infty); H^s)$. Corresponding *a priori* estimates for the three-dimensional case have so far not been obtained, because of the presence of the additional (vortex stretching) term on the right-hand side of (1.3.6).

In the three-dimensional case, it is a long-standing open problem whether solutions starting from smooth initial data are globally well-defined ($T^* = \infty$), or whether there exist smooth initial data $\bar{\mathbf{u}}$ for which the corresponding (strong) solution is only defined on a finite maximal time-interval ($T^* < \infty$). A careful recent numerical study [LH19] suggests that finite-time break-down of smoothness may be possible. Even though global-in-time existence and uniqueness can be shown for solutions with sufficiently regular initial data in the two-dimensional case, many flows of interest, such as vortex sheets, do not possess the regularity required by the above well-posedness results. Hence, there is considerable interest in going beyond the well-posedness theory of Theorem 1.3.1 for both the two- and three-dimensional incompressible Euler equations.

1.3.3 Weak solutions and measure-valued solutions

As pointed out in the previous section, the question of global (in time) well-posedness of classical solutions of the incompressible Euler equations (1.1.1) in three space dimensions, even with sufficiently smooth initial data $\bar{\mathbf{u}}$, is not yet resolved. Moreover in two space dimensions, where one can prove well-posedness of classical solutions as long as the initial data is sufficiently regular, many interesting initial data of interest do not possess this regularity. Hence, it is imperative to consider *weak solutions* of (1.1.1), defined as follows:

Definition 1.3.4. A vector field $\mathbf{u} \in L^\infty([0, T); L^2(\mathbb{T}^d; \mathbb{R}^d))$ is a **weak solution** of the incompressible Euler equations with initial data $\bar{\mathbf{u}} \in L^2(\mathbb{T}^d; \mathbb{R}^d)$, if

$$\int_0^T \int_{\mathbb{T}^d} \mathbf{u} \cdot \partial_t \varphi + (\mathbf{u} \otimes \mathbf{u}) : \nabla \varphi \, dx \, dt = - \int_{\mathbb{T}^d} \bar{\mathbf{u}} \cdot \varphi(\cdot, 0) \, dx, \quad (1.3.8)$$

for all test vector fields, $\varphi(x, t) \in C_c^\infty(\mathbb{T}^d \times [0, T); \mathbb{R}^d)$ satisfying $\text{div}(\varphi) = 0$, and

$$\int_{\mathbb{T}^d} \mathbf{u} \cdot \nabla \psi \, dx = 0, \quad (1.3.9)$$

for all test functions $\psi \in C^\infty(\mathbb{T}^d)$ and for a.e. $t \in [0, T]$.

It is customary to require additional admissibility criteria in order to recover uniqueness of weak solutions. A natural criterion in this context is given by the so-called dissipative or admissible weak solutions: a weak solution \mathbf{u} is **(energy) admissible**, if

$$\|\mathbf{u}(t)\|_{L_x^2} \leq \|\bar{\mathbf{u}}\|_{L_x^2}, \quad (1.3.10)$$

for a.e. $t \in [0, T]$. In the general case, no coercive *a priori* estimates for solutions of the incompressible Euler equations are known, beyond the physically natural energy admissibility constraint (1.3.10). Although the global existence of admissible weak solutions in three space dimensions is open, one can prove global existence of admissible weak solutions in two dimensions with very general initial data.

A general strategy for constructing weak solutions of the incompressible Euler equations (1.3.8) is to start from an *a priori* *well-posed* approximation of the incompressible Euler equations, e.g. obtained via

regularization or a numerical discretization depending on a parameter $\Delta > 0$. This yields a sequence of approximate solutions \mathbf{u}^Δ indexed by $\Delta \rightarrow 0$. The aim is then to prove the existence of a (suitable) limit $\mathbf{u} = \lim_{\Delta \rightarrow 0} \mathbf{u}^\Delta$, and to show that this limit \mathbf{u} is a weak solution of the incompressible Euler equations [MB01]. A careful construction of the approximation often allows some uniform a priori control on quantities of interest for the sequence \mathbf{u}^Δ , such as a uniform bound on the L^2 -norm, $\limsup_{\Delta \rightarrow 0} \|\mathbf{u}^\Delta\|_{L^2} \leq C < \infty$. A suitable abstract notion of such approximate solution sequences has been introduced by DiPerna and Majda in [DM87b]:

Definition 1.3.5 (Approximate solution sequence). *Let $\Delta \searrow 0$ be a sequence. Let $\{\mathbf{u}^\Delta\}$ be a sequence in $L^\infty([0, T]; L^2(\mathbb{T}^d; \mathbb{R}^d))$. The sequence $\{\mathbf{u}^\Delta\}$ is an **approximate solution sequence** for the incompressible Euler equations, if the following properties are satisfied:*

1. *The sequence $\{\mathbf{u}^\Delta\}$ is uniformly bounded in $L^\infty([0, T]; L^2(\mathbb{T}^d; \mathbb{R}^d))$,*
2. *The sequence $\{\mathbf{u}^\Delta\}$ is uniformly bounded in $\text{Lip}([0, T]; H^{-L}(\mathbb{T}^d; \mathbb{R}^d))$, for some $L > 1$.*
3. *For any test vector field $\varphi \in C_c^\infty(\mathbb{T}^d \times [0, T); \mathbb{R}^d)$ with $\text{div}(\varphi) = 0$, we have:*

$$\lim_{\Delta \searrow 0} \int_0^T \int_{\mathbb{T}^d} \varphi_t \cdot \mathbf{u}^\Delta + (\nabla \varphi) : (\mathbf{u}^\Delta \otimes \mathbf{u}^\Delta) dx dt + \int_{\mathbb{T}^d} \varphi(\cdot, 0) \cdot \mathbf{u}^\Delta(\cdot, 0) dx = 0.$$

4. *$\text{div}(\mathbf{u}^\Delta) = 0$ in $\mathcal{D}'(\mathbb{T}^d \times [0, T])$, i.e. in the sense of distributions.*

While Definition 1.3.5 encompasses the available a priori estimates on approximate solution sequences obtained in the zero-viscosity limit of the Navier-Stokes equations, or from many numerical schemes, these properties are insufficient in general to guarantee the (weak) convergence to a weak solution [DM87b]. The uniform L^2 -bound for example guarantees the weak convergence (of a subsequence) $\mathbf{u}^\Delta \xrightarrow{L^2} \mathbf{u}$ in L^2 , but does not allow to pass to the limit in the quadratic term $\mathbf{u}^\Delta \otimes \mathbf{u}^\Delta \xrightarrow{\mathcal{D}'} \mathbf{u} \otimes \mathbf{u}$ of the Euler equations, even in a distributional sense. Instead, the limiting behaviour under such weak assumptions has to be encompassed by a *Young measure*, leading to the concept of a *measure-valued solution* [DiP85, DM87b]. We follow [AB97, BDLS11], and introduce the following definition of generalized Young measures.

Definition 1.3.6 (Generalized Young measure). *We denote by $\mathcal{P}(X)$ the space of Borel probability measures on a topological space X , and $\mathcal{P}(X)$ is given the topology of weak convergence of measures (cp. Appendix B). A **generalized Young measure** is a triple $(\nu_{x,t}, \lambda, \nu_{x,t}^\infty)$ consisting of the oscillation measure $\nu_{x,t}$, the concentration measure $\lambda = \lambda_t(dx) \otimes dt$, and the concentration-angle measure $\nu_{x,t}^\infty$, such that*

- $\lambda = \lambda_t(dx) \otimes dt$ is a Radon measure on $\mathbb{T}^d \times [0, T]$ that is singular with respect to Lebesgue measure $dx dt$, and $[0, T] \mapsto \mathcal{P}(\mathbb{T}^d)$, $t \mapsto \lambda_t$ is Lebesgue measurable,
- the mapping $\mathbb{T}^d \times [0, T] \rightarrow \mathcal{P}(\mathbb{R}^d)$, $(x, t) \mapsto \nu_{x,t}$ is Lebesgue measurable,
- the mapping $\mathbb{T}^d \times [0, T] \rightarrow \mathcal{P}(\mathbb{S}^{d-1})$, $(x, t) \mapsto \nu_{x,t}^\infty$ is λ -measurable.

We let \mathcal{T} denote the following space of test functions:

$$\mathcal{T} = \left\{ g \in C(\mathbb{R}^d) \mid g^\infty(\boldsymbol{\theta}) := \lim_{s \rightarrow \infty} \frac{g(s\boldsymbol{\theta})}{s^2} \text{ exists } \forall \boldsymbol{\theta} \in \mathbb{S}^{d-1} \text{ on the unit sphere} \right\}.$$

We will say that a sequence of functions $\mathbf{u}_k \in L^2$ converges **in the sense of Young measures** to $(\nu, \lambda, \nu^\infty)$, denoted $\mathbf{u}_k \xrightarrow{\mathcal{Y}} (\nu, \lambda, \nu^\infty)$, provided that

$$g(\mathbf{u}_k) dx dt \xrightarrow{*} \langle \nu_{x,t}, g \rangle dx dt + \langle \nu_{x,t}^\infty, g^\infty \rangle \lambda_t(dx) dt,$$

converges in the sense of measures, for every $g \in \mathcal{T}$, where

$$\langle \nu_{x,t}, g \rangle := \int_{\mathbb{R}^d} g(\xi) \nu_{x,t}(d\xi), \quad \langle \nu_{x,t}^\infty, g^\infty \rangle := \int_{\mathbb{S}^{d-1}} g^\infty(\theta) \nu_{x,t}^\infty(d\theta).$$

We also define a **Young measure** as a generalized Young measure without concentration, i.e. for which $\lambda \equiv 0$.

Remark 1.3.7. We note that the quadratic term in the incompressible Euler equations (1.1.2), $g(\xi) = \xi \otimes \xi$, belongs to the space of test functions \mathcal{T} of Definition 1.3.6, with $g^\infty(\theta) = \theta \otimes \theta$.

Based on these Young measures, we extend the weak solutions of the incompressible Euler equations given in Definition 1.3.4, to the notion of a measure-valued solution, following [DM87b]:

Definition 1.3.8 (Measure-valued solution). A generalized Young measure $(\nu, \lambda, \nu^\infty)$ is a **measure-valued solution** of the incompressible Euler equations (1.1.1) with initial data $\bar{\mathbf{u}}$, provided that it satisfies

$$\begin{aligned} & \int_0^T \int_{\mathbb{T}^d} \langle \nu_{x,t}, \xi \rangle \cdot \partial_t \varphi + \langle \nu_{x,t}, \xi \otimes \xi \rangle : \nabla \varphi \, dx \, dt \\ & + \int_0^T \int_{\mathbb{T}^d} \langle \nu_{x,t}^\infty, \theta \otimes \theta \rangle : \nabla \varphi \lambda_t(dx) \, dt = - \int_{\mathbb{T}^d} \bar{\mathbf{u}} \cdot \varphi(\cdot, 0) \, dx, \end{aligned} \tag{1.3.11}$$

for all test vector fields, $\varphi(x, t) \in C_c^\infty(\mathbb{T}^d \times [0, T); \mathbb{R}^d)$ such that $\operatorname{div}(\varphi) = 0$, and

$$\int_{\mathbb{T}^d} \langle \nu_{x,t}, \xi \rangle \cdot \nabla \psi \, dx = 0, \tag{1.3.12}$$

for all test functions $\psi \in C^\infty(\mathbb{T}^d)$ and for a.e. $t \in [0, T]$. A measure-valued solution $(\nu, \lambda, \nu^\infty)$ is said to be **(energy) admissible**, if

$$\frac{1}{2} \int_{\mathbb{T}^d} \langle \nu_{x,t}, |\xi|^2 \rangle \, dx + \frac{1}{2} \lambda_t(\mathbb{T}^d) \leq \frac{1}{2} \int_{\mathbb{T}^d} |\bar{\mathbf{u}}|^2 \, dx \quad \text{for a.e. } t \in [0, T].$$

Remark 1.3.9. We note that if $(\nu, \lambda, \nu^\infty)$ is a measure-valued solution, such that $\lambda \equiv 0$, and $\nu_{x,t} = \delta_{\mathbf{u}(x,t)}$ is a Dirac measure, then $\mathbf{u}(x, t)$ is a weak solution of the incompressible Euler equations. Hence, measure-valued solutions extend the notion of weak solutions.

We can now state the following convergence theorem to measure-valued solutions, due to DiPerna and Majda (cp. [DM87b, Prop. 5.1]):

Theorem 1.3.10. If $\{\mathbf{u}^\Delta\}$, $\Delta \rightarrow 0$ is an approximate solution sequence of the incompressible Euler equations, then there exists a subsequence $\Delta_k \rightarrow 0$, and a generalized Young measure $(\nu, \lambda, \nu^\infty)$, such that \mathbf{u}^{Δ_k} converges to $(\nu, \lambda, \nu^\infty)$ in the sense of Young measures. Any Young measure limit $(\nu, \lambda, \nu^\infty)$ that can be obtained from the sequence \mathbf{u}^Δ is a measure-valued solution of the incompressible Euler equations.

One consequence of Theorem 1.3.10 is that for any L^2 initial data $\bar{\mathbf{u}}$, there exists a (global-in-time) measure-valued solution $(\nu, \lambda, \nu^\infty)$ of the Euler equations with initial data $\bar{\mathbf{u}}$.

Clearly, admissible measure-valued solutions are a very weak solution concept, with a lot of scope for non-uniqueness. One may thus wonder whether this notion is in fact too weak to be of any practical significance. We end our summary of weak and measure-valued solutions with the following two remarkable results: The first results has been obtained in [BDLS11, Thm. 2], and shows that – in the presence of a classical solution \mathbf{u} – any admissible measure-valued solution collapses to a Dirac delta concentrated on \mathbf{u} .

Theorem 1.3.11 (Weak-strong uniqueness). *Assume that $\mathbf{u} \in C([0, T]; L^2(\mathbb{T}^d; \mathbb{R}^d))$ is a solution of the incompressible Euler equations with $\int_0^T \|\nabla \mathbf{u}\|_{L^\infty} dt < \infty$, and let $(\nu, \lambda, \nu^\infty)$ be any admissible measure-valued solution with the same initial data. Then $\lambda \equiv 0$, and $\nu_{x,t} = \delta_{\mathbf{u}(x,t)}$ for a.e. $(x, t) \in \mathbb{T}^d \times [0, T]$.*

Finally, we summarize the following result from [SW12], which shows that, in a precise sense, admissible weak solutions actually have the same scope for non-uniqueness as admissible measure-valued solutions (MVS).

Theorem 1.3.12 (MVS are generated by weak solutions). *A Young measure $(\nu, \lambda, \nu^\infty)$ is an admissible measure-valued solution of the Euler equations with initial data $\bar{\mathbf{u}}$ if, and only if, there exists a sequence \mathbf{u}_n of admissible weak solutions to the Euler equations, such that $\mathbf{u}_n(t = 0) \rightarrow \bar{\mathbf{u}}$ strongly in L^2 and \mathbf{u}_n converges to $(\nu, \lambda, \nu^\infty)$ in the sense of Young measures.*

1.3.4 Rough solutions in two dimensions

As pointed out in the last section, the two-dimensional Euler equations benefit from additional a priori control on the solutions due to the fact that the (scalar) vorticity $\omega = \partial_{x_1} u_2 - \partial_{x_2} u_1$ (formally) satisfies a transport equation $\partial_t \omega + \mathbf{u} \cdot \nabla \omega = 0$. This statement can be made precise for the two-dimensional incompressible Navier-Stokes equations (1.2.3), allowing the construction of solutions of the Euler equations with similar bounds by passing to the zero-viscosity limit $\mathbf{u}^\nu \rightarrow \mathbf{u}$, $\nu \rightarrow 0$. For the incompressible Navier-Stokes equations, we have the following well-posedness result (cp. [Lio96, Thm. 3.1]):

Theorem 1.3.13 (Navier-Stokes well-posedness, $d = 2$). *For any divergence-free $\bar{\mathbf{u}} \in L^2(\mathbb{T}^2; \mathbb{R}^2)$, there exists a unique weak solution $\mathbf{u}^\nu \in L^2([0, T]; H^1) \cap C([0, T]; L^2)$ of the incompressible Navier-Stokes equations (1.2.3) with viscosity $\nu > 0$ on \mathbb{T}^2 . Furthermore, the solution $\mathbf{u}^\nu(t)$ is smooth for any $t > 0$, and satisfies the energy identity*

$$\frac{1}{2} \|\mathbf{u}^\nu(t)\|_{L_x^2}^2 + \nu \int_0^t \|\nabla \mathbf{u}^\nu(s)\|_{L_x^2}^2 ds = \frac{1}{2} \|\bar{\mathbf{u}}\|_{L_x^2}^2. \quad (1.3.13)$$

Remark 1.3.14. We recall that, as shown by a straight-forward calculation,

$$\|\nabla \mathbf{u}^\nu\|_{L_x^2} = \|\omega^\nu\|_{L_x^2}, \quad (1.3.14)$$

holds for any $\mathbf{u}^\nu \in H_x^1$, such that $\operatorname{div}(\mathbf{u}^\nu) = 0$, $\operatorname{curl}(\mathbf{u}^\nu) = \omega^\nu$. One may therefore write (1.3.13) in the equivalent form

$$\frac{1}{2} \|\mathbf{u}^\nu(t)\|_{L_x^2}^2 + \nu \int_0^t \|\omega^\nu(s)\|_{L_x^2}^2 ds = \frac{1}{2} \|\bar{\mathbf{u}}\|_{L_x^2}^2. \quad (1.3.15)$$

In particular, the smoothness guaranteed by Theorem 1.3.13 allows us to rigorously take the curl of the Navier-Stokes equations at times $t > 0$. In fact, we have the following (folklore) results:

Theorem 1.3.15 (Navier-Stokes vorticity, $d = 2$). *Let \mathbf{u}^ν be a solution of the Navier-Stokes equations (1.2.3) with initial data $\bar{\mathbf{u}} \in L^2(\mathbb{T}^2; \mathbb{R}^2)$. The vorticity $\omega^\nu = \operatorname{curl}(\mathbf{u}^\nu)$ is a smooth solution of*

$$\partial_t \omega^\nu + \mathbf{u}^\nu \cdot \nabla \omega^\nu = \nu \Delta \omega^\nu, \quad (1.3.16)$$

for any $t > 0$. The enstrophy $\mathcal{E} = \frac{1}{2} \|\omega^\nu\|_{L_x^2}^2$ satisfies

$$\frac{d}{dt} \frac{1}{2} \|\omega^\nu\|_{L_x^2}^2 = -\nu \|\nabla \omega^\nu\|_{L_x^2}^2. \quad (1.3.17)$$

Furthermore, the vorticity satisfies the following a priori estimates in terms of the initial vorticity $\bar{\omega} = \operatorname{curl}(\bar{\mathbf{u}})$:

$$\|\omega^\nu(t)\|_{L_x^p} \leq \|\bar{\omega}\|_{L_x^p}, \quad \forall p \in [1, \infty], t \geq 0, \quad (1.3.18)$$

$$\|\omega^\nu(t)\|_{L_x^2} \leq \frac{\|\bar{\mathbf{u}}\|_{L_x^2}}{\sqrt{\nu t}}, \quad \forall t > 0. \quad (1.3.19)$$

Sketch of proof. We note that due to the smoothness of solutions at $t > 0$ (cp. Theorem 1.3.13), equation (1.3.16) is immediate from taking the curl of the Navier-Stokes equations (1.2.3), which is rigorously justified in this case. The enstrophy equation (1.3.17) follows from (1.3.16) upon multiplication by ω^ν and spatial integration. The a priori L^p estimate on ω^ν can be derived similarly by multiplying with $\omega^\nu |\omega^\nu|^{p-2}$ and integrating over \mathbb{T}^2 . Finally, the vorticity bound (1.3.19) can be derived from the enstrophy equation, by observing that after an integration by parts we have

$$\int_{\mathbb{T}^2} |\omega^\nu|^2 dx = - \int_{\mathbb{T}^2} \mathbf{u}^\nu \cdot \nabla^\perp \omega^\nu dx \leq \left(\int_{\mathbb{T}^2} |\mathbf{u}^\nu|^2 dx \right)^{1/2} \left(\int_{\mathbb{T}^2} |\nabla \omega^\nu|^2 dx \right)^{1/2},$$

where $\nabla^\perp = (-\partial_{x_2}, \partial_{x_1})$ is a ‘‘rotated’’ gradient; using also the energy identity (1.3.13), this implies that $\|\omega^\nu\|_{L_x^2} \leq \|\bar{\mathbf{u}}\|_{L_x^2}^{1/2} \|\nabla \omega^\nu\|_{L_x^2}^{1/2}$, or equivalently, $-\nu \|\nabla \omega^\nu\|_{L_x^2}^2 \leq -\nu \|\omega^\nu\|_{L_x^2}^4 / \|\bar{\mathbf{u}}\|_{L_x^2}^2$ (assuming wlog $\bar{\mathbf{u}} \neq 0$). Substitution in the enstrophy equation (1.3.17) then shows that $y_\nu(t) = \|\omega^\nu(t)\|_{L_x^2}^2$ satisfies the differential inequality $\frac{dy_\nu}{dt} \leq -\nu y_\nu^2 / \|\bar{\mathbf{u}}\|_{L_x^2}^2$. Integrating this differential inequality, it is straight-forward to show that $y_\nu(t) \leq \|\bar{\mathbf{u}}\|_{L_x^2}^2 / (\nu t)$, for all $t > 0$, yielding (1.3.19). \square

The preceding theorem can be used to show the existence of solutions of the incompressible Euler equations for initial data with *unbounded* vorticity $\bar{\omega} \in L^p$, using the a priori L^p -estimate (1.3.18) on the approximate solution sequence \mathbf{u}^ν obtained by considering the zero-viscosity limit of the Navier-Stokes equations. Such an existence result for vorticity $\bar{\omega} \in L^p$, $1 < p < \infty$ has first been obtained by DiPerna and Majda [DM87a], utilizing the fact that a sequence \mathbf{u}^ν with uniformly bounded vorticity $\omega^\nu \in L^p$ is *strongly compact* in L^2 , by Sobolev embedding. The existence of a weak solution of the Euler equations for initial data $\bar{\mathbf{u}} \in L^2$ with $\bar{\omega} \in L^p$ can thus be established by passing to the (subsequential) limit $\mathbf{u}^\nu \rightarrow \mathbf{u}$, as $\nu \rightarrow 0$. Further extensions of the result of DiPerna and Majda can be obtained by similar compactness methods for initial vorticity $\bar{\omega}$ belonging to Orlicz spaces such as $\bar{\omega} \in L \log(L)^\alpha$, $\alpha \geq 1/2$, which are compactly embedded in H^{-1} [Mor92, Cha93, Cha94, LFNLT00]. These methods break down for $\bar{\omega} \in L^1$, as there is no compact embedding $L^1 \not\hookrightarrow H^{-1}$ in this case. We also note that in the special case where the initial vorticity is bounded, $\bar{\omega} \in L^\infty$, existence had already been shown by Yudovich [Yud63], who not only proved the existence but also the *uniqueness* of solutions in this case. The uniqueness result of [Yud63] has later been extended to vorticities belonging to slightly more general spaces in [Vis98, Vis99, Yud95]. The uniqueness of the solutions constructed by DiPerna and Majda in [DM87a], with initial vorticity in L^p spaces for $p < \infty$, however, remains an open problem.

In his celebrated work [Del91], Delort has shown the existence of weak solutions to the Euler equations with even more general initial vorticity $\bar{\omega} = \bar{\omega}' + \bar{\omega}''$, where $\bar{\omega}'$ is a finite, non-negative *Radon measure* belonging to H^{-1} , and $\bar{\omega}'' \in L^1 \cap H^{-1}$. We will subsequently refer to this set of initial data as the *Delort class*. These initial data include the interesting case of *vortex sheets*, i.e. vorticity concentrated on curves in the two-dimensional spatial domain [MB01]. In [Del91] a rigorous proof of this existence result has been given for $\bar{\omega}'' \in L^p$, $p > 1$, with a remark on the possible extension to $p = 1$. A detailed proof of the extension to $\bar{\omega}'' \in L^1$ has subsequently been provided by Vecchi and Wu [VW93]. We recall from the last section, that approximate solution sequences, as e.g. obtained by considering the zero-viscosity limit, converge (subsequentially) $\mathbf{u}^\nu \xrightarrow{\mathcal{Y}} (\nu, \lambda, \nu^\infty)$ to a measure-valued solution in the sense of Young measures

(cp. Theorem 1.3.10). If the initial vorticity is a bounded measure, then it can be shown that there are no oscillation effects in this limit, *i.e.* the oscillation measure $\nu = \delta_{\mathbf{u}}$ is a Dirac measure. Delort's main observation is a compensated compactness result, which shows that for initial data in the Delort class, the structure of the concentration measure satisfies additional constraints, which ensure that

$$\int_0^T \int_{\mathbb{T}^2} \langle \nu_{x,t}^\infty, \boldsymbol{\theta} \otimes \boldsymbol{\theta} \rangle : \nabla \varphi \lambda_t(dx) dt = 0,$$

for any solenoidal test function φ . Delort's result should thus be viewed as a statement about the fine properties of the concentration-angle measure ν^∞ ; in particular, no claim is made that $\lambda \equiv 0$, *i.e.* concentration effects are not ruled out, and hence there may be lack of strong L^2 -convergence $\mathbf{u}^\nu \not\rightarrow \mathbf{u}$ in the limit $\nu \rightarrow 0$. However, possible concentration effects in this limit are not seen upon integration against a test function in the definition of measure-valued solutions (1.3.11), and hence the barycenter $\mathbf{u} = \langle \delta_{\mathbf{u}}, \boldsymbol{\xi} \rangle = \langle \nu, \boldsymbol{\xi} \rangle$ of the (Dirac) oscillation measure defines a weak solution.

Apart from a generalization relying on special symmetry properties [LFLX01], the result of Delort [Del91] remains the most general existence result for the incompressible Euler equations in two dimensions. The question of existence of solutions beyond this *Delort class*, for instance, when $\bar{\omega}$ is an arbitrary bounded measure in H^{-1} with varying sign, remains open. The uniqueness of rough solutions in the Delort class also remains unknown.

1.3.5 Turbulence and anomalous energy dissipation

The incompressible Euler equations (1.1.1) can formally be obtained as the zero-viscosity limit $\nu \rightarrow 0$ of the incompressible Navier-Stokes equations (1.2.3). These equations have received considerable attention in particular due to their connection with turbulence. Turbulence is conventionally described as an energy cascade process, where energy cascades from large scales of the flow to ever smaller scales [Fri95]. For a given viscosity $\nu > 0$, the incompressible Navier-Stokes equations formally satisfy an energy balance equation of the form

$$\frac{d}{dt} \frac{1}{2} \int_D |\mathbf{u}^\nu|^2 dx = -\nu \int_D |\nabla \mathbf{u}^\nu|^2 dx.$$

Here, the left-hand side describes the time evolution of the kinetic energy $E(t) = \frac{1}{2} \|\mathbf{u}(t)\|_{L_x^2}^2$, while the right-hand side term describes the energy dissipation (at small scales) by viscosity. Formally, taking the limit $\nu \rightarrow 0$ in these equations suggests that solutions of the incompressible Euler equations should be energy conservative. This is certainly true for sufficiently smooth solutions \mathbf{u} of (1.1.1); e.g. if $\mathbf{u}^\nu \rightarrow \mathbf{u}$ and $\|\nabla \mathbf{u}^\nu\|_{L_x^2}$ remains uniformly bounded as $\nu \rightarrow 0$, then the dissipation term will tend to zero. However, in general, $\|\nabla \mathbf{u}^\nu\|_{L_x^2}$ may diverge as $\nu \rightarrow 0$, so it is not clear a priori, whether $\nu \int_0^t \|\nabla \mathbf{u}^\nu\|_{L_x^2}^2 dt \rightarrow 0$ in the limit $\nu \rightarrow 0$. In three dimensions, it is one of the fundamental postulates of Kolmogorov's 1941 physical theory of fully developed, homogeneous turbulence that $\langle \nu \|\nabla \mathbf{u}^\nu\|_{L_x^2}^2 \rangle \rightarrow \epsilon_0 > 0$, as $\nu \rightarrow 0$ [Kol91, KLH⁺91]. Here, $\langle \dots \rangle$ refers to a suitable averaging over an ensemble of solutions. Based on a series of physical arguments [Fri95], the following “2/3-law” is then derived for fully developed, homogeneous turbulence:

$$\langle |\mathbf{u}(x+h) - \mathbf{u}(x)|^2 \rangle \lesssim |h|^{2/3}, \quad \text{for length scales } |h| \gg \eta,$$

where $\eta \sim \nu^{3/4}$ is the Kolmogorov dissipation scale, beyond which viscosity dominates. This indicates that turbulent, dissipative solutions of the Euler equations, which are obtained in the zero-viscosity limit, should (on average) obey a Hölder-type regularity condition with exponent $\alpha = 1/3$.

The question of whether or not such anomalous energy dissipation is present in turbulent flows described by the Euler equations has also been posed by Onsager [Ons49], see also [ES06] for a modern account of this topic. In [Ons49], it was first argued that Hölder continuous solutions of the incompressible Euler equations $\mathbf{u} \in C^\alpha$ should conserve energy provided that $\alpha > 1/3$, whereas solutions at lower regularity $\alpha < 1/3$ might exhibit *anomalous dissipation* of energy, even in the zero viscosity limit $\nu \rightarrow 0$. Onsager did not provide a rigorous proof of this claim, and his observation has subsequently been formulated as a mathematical conjecture by Eyink [Eyi94], who referred to it as *Onsager's conjecture*. Eyink also gave the first mathematically rigorous proof of energy conservation assuming a somewhat stronger regularity condition on \mathbf{u} (which in turn implies $\mathbf{u} \in C^\alpha$, for some $\alpha > 1/3$). For this positive direction of Onsager's conjecture (energy conservation for fractional regularity $\alpha > 1/3$), a very short and elegant proof has been found by Constantin, Titi, E [CET94], who prove energy conservation if $\mathbf{u} \in L^3([0, T]; B_3^{1/3+\epsilon, \infty})$, $\epsilon > 0$, where $B_p^{\alpha, q}$ denotes the Besov spaces.

The negative direction of Onsager's conjecture is the statement that for any $\epsilon > 0$, there exists an energy dissipative solution $u \in C^{1/3-\epsilon}$. A proof of this assertion has only recently been achieved by Isett [Ise18] and Buckmaster, DeLellis, Székelyhidi and Vicol [BdLSV19], based on a series of technical improvements of the celebrated break-through work of DeLellis and Székelyhidi [DLS09]. In [DLS09], the authors formulated a concept of subsolutions for the incompressible Euler equations; they show that convex integration techniques can be used in this framework to construct solutions, in analogy with the geometric convex integration developed by Nash [Nas54] in the context of isometric embeddings of manifolds. The technique introduced by these authors in fact does not only exhibit single instances of Hölder continuous energy dissipative flows, but shows that there is a dense set in L_x^2 of initial data for the incompressible Euler equations for which there exist infinitely many weak solutions of the incompressible Euler equations, infinitely of which conserve energy and infinitely of which dissipate energy at any given (smooth) energy dissipation rate.

1.3.6 Anomalous energy dissipation in two dimensions

While the positive direction of Onsager's conjecture is independent of the spatial dimension d , the negative direction is so far restricted to $d \geq 3$. Since two-dimensional flows are more constrained than higher-dimensional ones, it is not clear whether the Onsager critical exponent $\alpha = 1/3$ can also be achieved for $d = 2$. In general, the convex integration technique shows the existence (and density) of wild initial data for which there exist infinitely many dissipative solutions of the incompressible Euler equations. It does not, however, give any explicit examples of such wild initial data. In this direction, Székelyhidi [Szé11] has been able to show that the flat vortex sheet (with distinguished sign) is an explicit example of initial data for which the convex integration method can be applied to construct infinitely many weak solutions. We recall that vortex sheet initial data are initial data $\bar{u} \in L_x^2$ for which the distributional vorticity $\bar{\omega} = \text{curl}(\bar{u}) \in \mathcal{M}$ is a bounded measure; in the case of the flat vortex sheet, $\bar{\omega}$ is concentrated uniformly on a straight line.

For vortex sheet initial data in two dimensions, it can be shown by a priori estimates that if a solution is obtained in the zero-viscosity limit $\nu \rightarrow 0$, then its vorticity $\omega(t) \in \mathcal{M}$ is a bounded measure, and in fact $\|\omega(t)\|_{\mathcal{M}} \leq \|\bar{\omega}\|_{\mathcal{M}}$ for $t \geq 0$, where $\|\cdot\|_{\mathcal{M}}$ denotes the total variation norm. In contrast, for weak solutions constructed via convex integration methods, there is no a priori bound on the vorticity, and it is not a bounded measure in general. Thus, it remains unclear what the physical relevance of these wild solutions is. It might also hint at the important role played by additional constraints on weak solutions of the incompressible Euler equations, which are imposed by considering *physically realizable* solutions, obtained in the zero-viscosity limit.

In two dimensions, it can be shown that Onsager-critical Hölder regularity of u is achieved for $\bar{\omega} \in$

$L^{3/2+\epsilon}$, $\epsilon > 0$ [CFLS16]. This poses the question whether energy dissipative weak solutions of the incompressible Euler equations can be constructed with vorticity bounded in L^p , $p < 3/2$, and if so, whether such energy dissipative solutions can be obtained in the physically relevant zero-viscosity limit $\nu \rightarrow 0$. Recently, the group of authors [CFLS16] have been able to give a negative answer to this last question: They prove that if a weak solution of the incompressible Euler equations \mathbf{u} with initial data having vorticity $\bar{\omega} \in L^p$, $p > 1$, is obtained as the limit $\mathbf{u}^\nu \rightarrow \mathbf{u}$ of solutions \mathbf{u}^ν of the ν -Navier-Stokes equations, then \mathbf{u} is energy conservative. These solutions do not belong to any Hölder space C^α , $\alpha > 1/3$, for $p < 3/2$. Thus – at least in two dimensions – Onsager criticality is not the last word on the question of anomalous dissipation. We will come back to this question of anomalous energy dissipation in chapter 4, where we provide a characterization of physically realizable energy conservative solutions of the Euler equations in the deterministic case, and study the question of energy conservation also at the level of statistical solutions. Our results imply that an *arbitrary* uniform Hölder bound ($\alpha > 0$) on the sequence \mathbf{u}^ν suffices to ensure energy conservation in the limit, thus going far beyond the Onsager criticality in this case.

1.4 Numerical discretization: Spectral methods

A wide variety of numerical methods have been developed to robustly approximate the incompressible Euler and the closely related incompressible Navier-Stokes equations. These include spectral methods [DGO84], finite element methods [SS17], finite difference-projection methods [Cho68, JBBG89] and vortex methods [Kra86b, Kra86a, MB01].

Although finite difference and finite element methods are very useful when discretizing the Euler equations in domains with complex geometry, spectral methods, based on projecting (1.1.1) into a finite number of Fourier modes are the method of choice for approximating (1.1.1) with periodic boundary conditions. These methods are very efficient to implement (aided by the fast Fourier transform (FFT)), fast to run and have *spectral*, *i.e.* superpolynomial convergence rates for smooth solutions of (1.1.1) [DGO84]. Consequently, spectral methods are widely used in the simulation of homogeneous and isotropic turbulence [Gho96, KK00]. In the present section we will review spectral methods, discuss the concept of spectrally vanishing viscosity, first introduced by Tadmor in [Tad89], and discuss elements of their implementation in the SPHINX code, on which the numerical experiments presented in this thesis are based. For further details on this code, we refer to the thesis [Leo18].

1.4.1 Fourier spectral methods: the SV scheme

To employ Fourier spectral methods for the numerical discretization of the incompressible Euler equations, we consider, for $N \in \mathbb{N}$, the finite-dimensional subspace $L_N^2 \subset L^2$, spanned by real-valued vector fields $\mathbf{u}^\Delta \in L^2(\mathbb{T}^d; \mathbb{R}^d)$, of the form

$$\mathbf{u}^\Delta(x) = \sum_{|k|_\infty \leq N} \hat{\mathbf{u}}_k e^{ik \cdot x}, \quad (\hat{\mathbf{u}}_k \in \mathbb{C}^d), \quad (1.4.1)$$

where we denote $|k|_\infty := \max_{i=1,\dots,d} |k_i|$. Throughout this thesis, we will consistently denote by

$$\Delta \equiv 1/N \quad (1.4.2)$$

the “grid size” parameter, defined as the reciprocal of N . Clearly, Δ is a measure of the numerical resolution of the scheme, with $\Delta \rightarrow 0$ the limit of infinite resolution. The requirement that \mathbf{u}^Δ in (1.4.1) be real-valued imposes the constraint $\hat{\mathbf{u}}_{-k} = \text{conj}(\hat{\mathbf{u}}_k)$ on the coefficients $\hat{\mathbf{u}}_k$, where $\text{conj}(\cdot)$ denotes the complex conjugate.

We will denote by $P_N : L^2 \rightarrow L_N^2$ the orthogonal projection onto this subspace. In analogy with the Leray projection $\mathbb{P} : L^2(\mathbb{T}^d; \mathbb{R}^d) \rightarrow L^2(\mathbb{T}^d; \mathbb{R}^d)$ onto divergence-free vector fields introduced in (1.3.4), we introduce the *truncated Leray projection* $\mathbb{P}_N : L^2(\mathbb{T}^d; \mathbb{R}^d) \rightarrow L_N^2(\mathbb{T}^d; \mathbb{R}^d)$ by $\mathbf{v} \mapsto \mathbb{P}_N \mathbf{v} := P_N \mathbb{P} \mathbf{v}$, which is equivalently defined by

$$\mathbb{P}_N \left(\sum_{k \in \mathbb{Z}^d} \widehat{\mathbf{v}}_k e^{ik \cdot x} \right) := \sum_{0 < |k|_\infty \leq N} \left(I - \frac{k \otimes k}{|k|^2} \right) \widehat{\mathbf{v}}_k e^{ik \cdot x}, \quad (1.4.3)$$

for all \mathbf{v} .

Spectral hyper-viscosity scheme (SV scheme)

We consider the following spectral viscosity approximation of the incompressible Euler equations, which follows an idea first proposed by Tadmor for the numerical approximation of scalar conservation laws [Tad89, Tad04]:

$$\begin{cases} \partial_t \mathbf{u}^\Delta + \mathbb{P}_N (\mathbf{u}^\Delta \cdot \nabla \mathbf{u}^\Delta) = -\epsilon_N |\nabla|^{2s} (Q_N * \mathbf{u}^\Delta), \\ \operatorname{div}(\mathbf{u}^\Delta) = 0, \quad \mathbf{u}^\Delta|_{t=0} = \mathbb{P}_N \bar{\mathbf{u}}. \end{cases} \quad (1.4.4)$$

Here \mathbb{P}_N is the spatial truncated Leray projection operator (1.4.3) and Q_N is a Fourier multiplier of the form

$$Q_N(x) = \sum_{m_N < |k| \leq N} \widehat{Q}_k e^{ik \cdot x}, \quad (1.4.5)$$

and we assume $0 \leq \widehat{Q}_k \leq 1$, and $\widehat{Q}_k \equiv 0$ for $|k| \leq m_N$, so that dissipation is only applied on the upper part of the spectrum, *i.e.* for $|k| > m_N$, thus preserving the formal spectral accuracy of the method, while at the same time enabling us to enforce a sufficient amount of energy dissipation on the small scale Fourier modes which is needed to stabilize the method. The additional hyperviscosity parameter $s \geq 1$ in (1.4.4) can be chosen larger to enforce more numerical dissipation on the high Fourier modes, thus allowing a larger part of the Fourier spectrum to remain free of numerical diffusion, while still ensuring stability of the resulting numerical scheme. The sequence $\epsilon_N > 0$ allow us to control the amount of dissipation applied. A minimal requirement is that $\epsilon_N \rightarrow 0$, as $N \rightarrow \infty$, to ensure consistency with the limiting Euler equations (1.1.2).

Following the derivation of the Fourier transformed Euler equations (1.3.3) on page 7, we also note that equation (1.4.4) is equivalent to the following set of ODEs for the Fourier coefficients $\widehat{\mathbf{u}}_k(t)$, $0 < |k|_\infty \leq N$:

$$\frac{d\widehat{\mathbf{u}}_k}{dt} = \left(I - \frac{k \otimes k}{|k|^2} \right) \cdot \left(\sum_{|\ell|_\infty, |k-\ell|_\infty \leq N} (-ik \cdot \widehat{\mathbf{u}}_\ell) \widehat{\mathbf{u}}_{k-\ell} \right) - \epsilon_N |k|^{2s} \widehat{Q}_k \widehat{\mathbf{u}}_k. \quad (1.4.6)$$

Hence (1.4.4) uniquely determines the numerical evolution of the Fourier coefficients, and thus defines a semi-discretization of the incompressible Euler equations (1.1.1), through the system of ODEs (1.4.6). We obtain a fully discretized scheme by combining (1.4.6) with a time-stepping scheme of our choice.

1.4.2 Numerical implementation and 2/3-dealiasing

As already mentioned at the beginning of this section, the numerical experiments presented in this thesis have been obtained with the SPHINX code, written by F. Leonardi [Leo18]. The SPHINX code solves

the ODE system (1.4.6), employing the strongly stability preserving Runge-Kutta (SSP-RK) scheme [GST01] of order 3 with adaptive time-stepping, and allows for parallel computations based on MPI and OpenMP, and the use of GPUs based on CUDA kernels.

A direct implementation of the ODE system in the form (1.4.6) would require $O(N^{2d})$ multiplication operations, and hence imply a quadratic computational cost in the number of degrees of freedom ($O(N^d)$) of the numerical scheme. Such a quadratic scaling would be prohibitive for the large-scale simulations required for the numerical experiments of the following chapters. Therefore, the SPHINX code relies on the so-called 2/3-dealiasing rule to reduce the computational cost to $O(N^d \log(N))$. The 2/3-dealiasing rule allows for the efficient computation of the non-linear term

$$[\widehat{\mathbf{u}^\Delta \cdot \nabla \mathbf{u}^\Delta}]_k = \sum_{\ell} (-ik \cdot \widehat{\mathbf{u}}_\ell) \widehat{\mathbf{u}}_{k-\ell}, \quad (1.4.7)$$

based on the availability of the fast Fourier-transform (FFT) algorithm [CT65], which computes the d -dimensional Fourier transform (and its inverse) in $O(N^d \log(N))$ operations. More precisely, given the function values $\mathbf{u}^\Delta(x_j)$ on a equispaced grid $\{x_j\}_{j \in \mathcal{J}_N} \subset \mathbb{T}^d$ with grid spacing $\Delta x = 2\pi/(2N+1)$ in each direction (cf. Appendix A), the FFT computes the *discrete Fourier transform*

$$\widehat{\mathbf{u}}_k = \frac{1}{(2N+1)^d} \sum_{j \in \mathcal{J}_N} \mathbf{u}^\Delta(x_j) e^{-ik \cdot x_j},$$

for all $k \in \mathbb{Z}^d$, $|k|_\infty \leq N$, and its inverse

$$\mathbf{u}^\Delta(x_j) = \sum_{|k|_\infty \leq N} \widehat{\mathbf{u}}_k e^{ik \cdot x_j}.$$

To reduce the computation complexity of the evaluation of (1.4.7), the idea is to replace the direct evaluation in Fourier space of the quadratic term (1.4.7), by the following composition

$$\widehat{\mathbf{u}}_k \mapsto \begin{bmatrix} \widehat{\mathbf{u}}_k \\ ik \otimes \widehat{\mathbf{u}}_k \end{bmatrix} \xrightarrow{\text{IFFT}} \begin{bmatrix} \mathbf{u}^\Delta(x_j) \\ \nabla \mathbf{u}^\Delta(x_j) \end{bmatrix} \mapsto \mathbf{u}^\Delta(x_j) \cdot \nabla \mathbf{u}^\Delta(x_j) \xrightarrow{\text{FFT}} [\widehat{\mathbf{u}^\Delta \cdot \nabla \mathbf{u}^\Delta}]_k,$$

where the computational complexity of these mappings is $O(N^d)$, $O(N^d \log(N))$, $O(N^d)$ and $O(N^d \log(N))$, respectively; hence the total computation only takes $O(N^d \log(N))$ operations, substantially outperforming the naive $O(N^{2d})$ -algorithm for large N . The main difficulty is that the Fourier expansion of the non-linear term $\mathbf{u}^\Delta \cdot \nabla \mathbf{u}^\Delta$ is

$$\mathbf{u}^\Delta \cdot \nabla \mathbf{u}^\Delta = \sum_{|k|_\infty, |\ell|_\infty \leq N} (i\ell \cdot \widehat{\mathbf{u}}_k) \widehat{\mathbf{u}}_\ell e^{i(k+\ell) \cdot x},$$

and hence includes wavenumbers for which $|k + \ell|_\infty > N$. Thus, when the Fourier coefficients of $[\widehat{\mathbf{u}^\Delta \cdot \nabla \mathbf{u}^\Delta}]_k$, $|k|_\infty \leq N$, are computed based on a discrete Fourier transform on the grid points x_j , this inevitably leads to “aliasing errors”, as explained in detail in [Leo18, Chapter 6.2]. The 2/3-dealiasing rule states that such aliasing errors can be avoided by computing the discrete Fourier transform on a larger grid with a finer grid spacing $\widetilde{\Delta x} \sim \frac{2}{3} \Delta x$. In practice, this can be accomplished in a numerical implementation by zero-padding the Fourier spectrum of \mathbf{u}^Δ , *i.e.* writing

$$\mathbf{u}^\Delta(x) = \sum_{|k|_\infty \leq N'} \widehat{\mathbf{u}}_k e^{ik \cdot x},$$

where $N' > \frac{3}{2}N$, and setting $\widehat{\mathbf{u}}_k := 0$, for $|k|_\infty > N$. For further details, and the mathematical justification of the 2/3 dealiasing technique, we refer to [Leo18, Chapter 6.2]. This technique is used in the SPHINX code to efficiently compute the non-linear term in the SV scheme.

1.4.3 Stability properties of the SV scheme

Multiplying the evolution equation (1.4.4) by \mathbf{u}^Δ and integrating by parts, we note the following energy balance:

$$\|\mathbf{u}^\Delta(t)\|_{L_x^2}^2 + 2(2\pi)^d \epsilon_N \int_0^t \sum_{|k|_\infty \leq N} \widehat{Q}_k |k|^{2s} |\widehat{\mathbf{u}}_k^\Delta(\tau)|^2 d\tau = \|\mathbf{u}^\Delta(t=0)\|_{L_x^2}^2 \leq \|\overline{\mathbf{u}}\|_{L_x^2}^2. \quad (1.4.8)$$

In particular, this implies that approximate solutions \mathbf{u}^Δ computed with the SV scheme satisfy the a priori energy admissibility condition $\|\mathbf{u}^\Delta(t)\|_{L_x^2} \leq \|\overline{\mathbf{u}}\|_{L_x^2}$ for all $t \in [0, T]$.

In fact, the approximations obtained by the spectral viscosity method are approximate solutions in the sense of Definition 1.3.5. To show the Lip-boundedness, we simply note that for any $\varphi \in C^\infty(\mathbb{T}^d; \mathbb{R}^d)$, and $0 \leq t_1 < t_2 \leq T$, we have from (1.4.4)

$$\begin{aligned} \langle \varphi, \mathbf{u}^\Delta(\cdot, t_2) - \mathbf{u}^\Delta(\cdot, t_1) \rangle &\leq C(t_2 - t_1) \|\nabla \varphi\|_{L_x^\infty} \|\mathbf{u}^\Delta\|_{L^\infty([0, T]; L_x^2)}^2 \\ &\quad + \epsilon_N(t_2 - t_1) \||\nabla|^{2s} \varphi\|_{L_x^\infty} \|\mathbf{u}^\Delta\|_{L^\infty([0, T]; L_x^2)} \\ &\leq CE_0(t_2 - t_1) \|\nabla \varphi\|_{L_x^\infty} + \epsilon_N \sqrt{E_0}(t_2 - t_1) \||\nabla|^{2s} \varphi\|_{L_x^2}, \end{aligned}$$

where $E_0 = \int_{\mathbb{T}^d} |\overline{\mathbf{u}}|^2 dx$ is (twice) the kinetic energy of the initial data $\overline{\mathbf{u}}$ (cp. (1.4.8)). Now we choose L large enough so that, by Sobolev embedding:

$$H^L(\mathbb{T}^d; \mathbb{R}^d) \hookrightarrow W^{1,\infty}(\mathbb{T}^d; \mathbb{R}^d) \cap H^{2s}(\mathbb{T}^d; \mathbb{R}^d).$$

Then

$$\langle \varphi, \mathbf{u}^\Delta(\cdot, t_2) - \mathbf{u}^\Delta(\cdot, t_1) \rangle \leq C|t_2 - t_1| \|\varphi\|_{H^L},$$

with a constant C depending on $\sup_N \epsilon_N$ (assumed finite) and E_0 , but independent of N . Taking the supremum of all $\varphi \in H^L(\mathbb{T}^d; \mathbb{R}^d) \cap C^\infty(\mathbb{T}^d; \mathbb{R}^d)$ with $\|\varphi\|_{H^L} \leq 1$ on the left, we find

$$\|\mathbf{u}^\Delta(\cdot, t_2) - \mathbf{u}^\Delta(\cdot, t_1)\|_{H^{-L}} \leq C|t_2 - t_1|,$$

proving that $\mathbf{u}^\Delta \in \text{Lip}((0, T); H^{-L})$, with a uniformly bounded Lipschitz constant. The other two properties are easily shown; The consistency property has been shown in [LM15, Lemma 3.2], the divergence-free property is satisfied exactly. Thus, we have shown:

Theorem 1.4.1. *The sequence \mathbf{u}^Δ obtained from the SV scheme for the incompressible Euler equations form an approximate solution sequence in the sense of Definition 1.3.5.*

By Theorem 1.3.10, this immediately implies convergence to a measure-valued solution as $\Delta \rightarrow 0$:

Theorem 1.4.2. *Let $\{\mathbf{u}^\Delta\} \subset L^2$, $\Delta = 1/N \rightarrow 0$ be the sequence obtained by solution of the SV scheme (1.4.4) at resolution Δ for given initial data $\overline{\mathbf{u}}$. Then there exists a subsequence $\Delta_k \rightarrow 0$ and a generalized Young measure $(\nu, \lambda, \nu^\infty)$, such that $\mathbf{u}^{\Delta_k} \xrightarrow{\nu} (\nu, \lambda, \nu^\infty)$ converges in the sense of Young measures.*

As a consequence of weak-strong uniqueness, Theorem 1.3.11, we can also conclude:

Corollary 1.4.3. *If the initial data $\overline{\mathbf{u}}$ admits a solution \mathbf{u} , such that $\int_0^T \|\nabla \mathbf{u}(t)\|_{L_x^\infty} dt < \infty$, then the sequence \mathbf{u}^Δ computed by the SV scheme (1.4.4) converges $\mathbf{u}^\Delta \rightarrow \mathbf{u}$ strongly in $L^2(\mathbb{T}^d \times [0, T])$.*

Chapter 2

Convergence of the spectral viscosity scheme to rough solutions

2.1 Introduction

As explained in the last chapter, there is considerable interest in the analysis and the numerical approximation of rough solutions of the incompressible Euler equations, in both two and three spatial dimensions. In the present chapter, we will discuss the numerical approximation of rough solutions of the *two-dimensional* incompressible Euler equations by spectral methods. As opposed to the three-dimensional case, the mathematical theory of solutions in two dimensions, even at low regularity, is considerably more mature and several existence results for rough solutions (and, to a lesser extent, uniqueness results) have been established, leveraging the additional a priori control on the vorticity in this setting. In particular, we will focus on the convergence of numerical schemes for initial data in the “Delort class”, *i.e.* having vorticity $\bar{\omega}$ of the form $\bar{\omega} = \bar{\omega}' + \bar{\omega}''$, where $\bar{\omega}' \in \mathcal{M}_+ \cap H^{-1}$ is a finite, non-negative Radon measure bounded in H^{-1} , and $\bar{\omega}'' \in L^1 \cap H^{-1}$. These initial data include the interesting case of signed vortex sheets, *i.e.* initial data for which the (non-negative) vorticity is concentrated on curves in the two-dimensional spatial domain.

For numerical approximations of the incompressible Euler equations, rigorous convergence results have been mostly available when the underlying solution is sufficiently smooth, see [BT15] for spectral methods, [LMS16] for finite-difference projection methods, [SS17] for discontinuous Galerkin methods and [MB01] for vortex methods. For rough initial data, only a few rigorous results are available. And usually, these results either only prove convergence in a very weak sense (*e.g.* to a measure-valued solution), or they rely on a direct discretization of the vorticity equation to provide the necessary a priori control and hence the resulting numerical methods are specific to the two-dimensional case; A notable result in this regard is the convergence of a *central finite difference scheme* ([LT97]) for the vorticity formulation (cp. (1.3.7)) of the two-dimensional Euler equations [LT97]. This scheme was shown to possess a discrete maximum principle for the vorticity. Hence, one can prove that it converges to a weak solution of (1.3.7), as long as the initial vorticity $\bar{\omega} \in L^p$ for $1 < p \leq \infty$ [LFNL00]. However, it is unclear if the convergence analysis for this scheme can be extended to the case where the initial data $\bar{\omega} \in L^1 \cap H^{-1}$, let alone in the Delort class. Similarly for spectral methods and for finite difference-projection methods, the only available results for (1.1.1), are of convergence to the significantly weaker solution framework of dissipative measure-valued solutions in [LM15] and in [Leo18], respectively.

When $\bar{\omega} \in \mathcal{M} \cap H^{-1}$ is a bounded measure, the best available convergence results to date have been

achieved by Liu and Xin for the vortex blob method in [LX95] and by Schochet for both the vortex point and blob methods in [Sch96] (see also the related work by Liu and Xin [LX01]). In [LX95, Sch96, LX01], it is shown that for initial data with vorticity $\bar{\omega} \in H^{-1}$ a finite, non-negative Radon measure in \mathcal{M}_+ , the vortex methods will converge weakly to a weak solution of the incompressible Euler equations with $\omega \in \mathcal{M}_+ \cap H^{-1}$. The assumption on the definite sign (either positive or negative in the whole domain) of the initial vorticity appears to be an essential ingredient in these convergence results [LX95, Sch96, LX01]: If $\bar{\omega}$ has a definite sign, then the conserved Hamiltonian of these vortex methods can be leveraged to provide a priori control the concentration of the discretized vorticity. When the initial vorticity $\bar{\omega}$ is not necessarily of definite sign, then the Hamiltonian no longer provides control on vorticity concentration and the available convergence results are somewhat weaker in this case. Without any sign restriction, convergence of the vortex point/blob methods has been shown by Schochet [Sch96] for initial data with vorticity $\bar{\omega} \in L(\log L)$. The fundamental difficulty that prevents the convergence results for vortex methods to be extended to initial data of the form $\bar{\omega} = \bar{\omega}' + \bar{\omega}''$, $\bar{\omega}' \in \mathcal{M}_+ \cap H^{-1}$, $\bar{\omega}'' \in L^1 \cap H^{-1}$ considered by Delort [Del91, VW93], apparently lies in the fact that at the continuous level, concentration of $\bar{\omega}'' \in L^1$ is prevented by the *incompressibility* of the advecting flow. However, in the case of vortex methods, incompressibility of the advecting flow is not known to be sufficient to prevent concentration of the discretized vortices. In the definite sign case ($\bar{\omega}'' = 0$), it turns out that the discrete energy conservation can be used to circumvent this issue [Maj93, LX95, Sch96, LX01]. Without any sign restriction, but assuming that $\bar{\omega} \in L(\log L)$, the conservation of phase-space volume (Liouville's theorem) can be used to show that no concentration occurs for suitable vortex approximations to the initial data $\bar{\omega}$ [Sch96]. Therefore a considerable gap remains between the existence result of Delort and the available convergence results for numerical methods, including even very specialized schemes such as vortex methods.

In the present chapter, we will present rigorous convergence results based on (compensated) compactness techniques, for approximations by the spectral viscosity scheme of the two-dimensional Euler equations with rough initial data in the afore-mentioned *Delort class*. The discussion in this chapter is based on the original publication [LM20], where detailed proofs of all results, as well as refined estimates on L^p vorticity control for $1 < p < \infty$ can be found. Here, we will streamline the discussion and focus instead only on the Delort case, requiring as one key ingredient a priori L^1 -control on the approximations, *i.e.* $\sup_{\Delta} \|\omega^{\Delta}\|_{L^1} < \infty$.

2.2 A fine-tuned SV scheme

In the following, we will consider the following *fine-tuned* spectral vanishing viscosity (SV) scheme for the incompressible Euler equations, which is a slight adaptation of the general SV scheme outline in chapter 1.4 ensuring additional a priori bounds even for very rough initial data: Given $N \in \mathbb{N}$, we fix a “grid-scale” $\Delta = 1/N$, and consider the following approximation of the incompressible Euler equations

$$\begin{cases} \partial_t \mathbf{u}^{\Delta} + \mathbb{P}_N(\mathbf{u}^{\Delta} \cdot \nabla \mathbf{u}^{\Delta}) = \epsilon_N \Delta (Q_N * \mathbf{u}^{\Delta}), \\ \operatorname{div}(\mathbf{u}^{\Delta}) = 0, \quad \mathbf{u}^{\Delta}|_{t=0} = K_{a_N} * \bar{\mathbf{u}}, \end{cases} \quad (2.2.1)$$

with periodic boundary conditions. Here \mathbb{P}_N is the truncated Leray projection operator (1.4.3), mapping onto divergence-free vector fields. Q_N is a Fourier multiplier of the form

$$Q_N(x) = \sum_{m_N < |k| \leq N} \hat{Q}_k e^{ik \cdot x}, \quad (2.2.2)$$

and we assume

$$0 \leq \widehat{Q}_k \leq 1, \quad \widehat{Q}_k = \begin{cases} 0, & |k| \leq m_N, \\ 1, & |k| > 2m_N. \end{cases} \quad (2.2.3)$$

The choice of parameters m_N and ϵ_N will be specified later.

Remark 2.2.1. In equation (2.2.3), we have assumed that the coefficients \widehat{Q}_k change only in the interval $|k| \in [m_N, 2m_N]$. This assumption could have been replaced by taking $[m_N, cm_N]$, for any constant $c > 1$, without changing the results of this chapter. We have chosen $c = 2$ here for simplicity, and in order not to introduce further parameters into the numerical scheme. In practice, a different choice may be more suitable.

As a slight extension to the SV scheme discussed in chapter 1.4, we have introduced an additional Fourier kernel K_{a_N} . This kernel gives an another degree of freedom in our numerical method, and will be necessary to obtain suitably approximated initial data, providing further control on the numerical solution. The Fourier kernel K_{a_N} is a trigonometric polynomial of the form

$$K_{a_N}(x) = \sum_{|k| \leq a_N} \widehat{K}_k e^{ik \cdot x}, \quad |\widehat{K}_k| \leq 1.$$

The exact form of the kernel K_{a_N} and the choice of parameters a_N will be specified later. However, we shall assume that K_{a_N} satisfies a bound of the form

$$\|K_{a_N}\|_{L^1} \leq C \log(N)^2, \quad \text{for all } N \in \mathbb{N}. \quad (2.2.4)$$

The above discretization of the initial conditions will be necessary in our convergence proofs for unbounded initial vorticity, and in particular if the initial data is a vortex sheet as considered by Delort [Del91].

Remark 2.2.2. The SV scheme for the incompressible Euler equations depends on the three parameter sequences ϵ_N, m_N, a_N . To fix ideas, we note that we will later on choose $\epsilon_N \rightarrow 0$, $a_N \sim m_N \sim N^\theta \rightarrow \infty$ for some $\theta \leq \frac{1}{2}$.

Since the \mathbf{u}^Δ are smooth, and since the Fourier projection commutes with differentiation, it turns out that we can equivalently write the system (2.2.1) in its vorticity form

$$\begin{cases} \partial_t \omega^\Delta + P_N(\mathbf{u}^\Delta \cdot \nabla \omega^\Delta) = \epsilon_N \Delta(Q_N * \omega^\Delta), \\ \operatorname{curl}(\mathbf{u}^\Delta) = \omega^\Delta, \\ \omega^\Delta|_{t=0} = \operatorname{curl}(K_{a_N} * \bar{\mathbf{u}}). \end{cases} \quad (2.2.5)$$

Here, $P_N : L^2 \rightarrow L_N^2$ is the L^2 -orthogonal Fourier projection (cp. Appendix A for further details). We recall the following simple result, which will be of fundamental importance for the current work:

Proposition 2.2.3 (Lemma 3.10, [LM15]). *The systems (2.2.1) for \mathbf{u}^Δ and (2.2.5) for ω^Δ are equivalent.*

Remark 2.2.4. Proposition 2.2.3 allows us to focus on the vorticity formulation (2.2.5). The strategy is then as follows: The vorticity formulation will be used to obtain uniform a priori control on the L^p -norm of the approximate vorticities ω^Δ , for some $1 \leq p \leq \infty$. The bounds on ω^Δ in turn provide additional control on the velocity \mathbf{u}^Δ , which can be used to prove the convergence of the non-linear terms in the primitive variable formulation (2.2.1). The convergence of the non-linear terms will rely

either on establishing pre-compactness of the sequence \mathbf{u}^Δ in $L^2(\mathbb{T}^2; \mathbb{R}^2)$, following the original ideas of Diperna and Majda [DM87a], or by employing compensated compactness results established by Delort [Del91, VW93, Sch95]. It is thus the interplay between the primitive and the vorticity formulation, which will allow us to obtain convergence proofs even for rough initial data.

As a first step towards proving the convergence of the SV method, we make the error terms more apparent. We rewrite the system (2.2.5) in the following form

$$\partial_t \omega^\Delta + \mathbf{u}^\Delta \cdot \nabla \omega^\Delta - \epsilon_N \Delta \omega^\Delta = \underbrace{(I - P_N)(\mathbf{u}^\Delta \cdot \nabla \omega^\Delta)}_{=: \text{err}_1} + \underbrace{\epsilon_N \Delta R_{m_N} * \omega^\Delta}_{=: \text{err}_2}. \quad (2.2.6)$$

The left-hand side corresponds to the vorticity formulation of the Navier-Stokes equations in 2d with viscosity ϵ_N . The right hand side consists of a projection error (err_1), and a "viscosity" error (err_2), which is written in terms of a convolution with $R_{m_N} \equiv 1 - Q_N$. We note that $R_{m_N}(x)$ has Fourier coefficients

$$0 \leq \hat{R}_k \leq 1, \quad \hat{R}_k = \begin{cases} 1, & |k| \leq m_N, \\ 0, & |k| > 2m_N. \end{cases} \quad (2.2.7)$$

Similar to (2.2.4), we will assume a bound of the form

$$\|R_{m_N}\|_{L^1} \leq C \log(N)^2, \quad \text{for all } N \in \mathbb{N}, \quad (2.2.8)$$

for the kernel R_{m_N} . For the construction of a kernel satisfying the last estimate, see Maday and Tadmor [MT89, Appendix], which generalizes to the two dimensional case via a tensor product.

2.3 Overview of the strategy

Given initial data $\bar{\mathbf{u}}$ in the Delort class, with vorticity $\bar{\omega} \in (\mathcal{M}_+ + L^1) \cap H^{-1}$, our goal is to show that – up to the extraction of a subsequence – the sequence $\mathbf{u}^\Delta(t) \in L^2$ computed by the SV method converges $\mathbf{u}^\Delta \rightharpoonup \mathbf{u}$ weakly in L^2 to a *weak solution* $\mathbf{u} \in L^\infty([0, T]; L^2(\mathbb{T}^2; \mathbb{R}^2))$ of the incompressible Euler equations. In fact, we will show that any (weak) limit of this sequence is a weak solution. Our proof of convergence will rely on the following fact, first (implicitly) established by Delort [Del91], and later explicitly pointed out by Vechhi and Wu [VW93], see also the discussion in [Sch95].

Theorem 2.3.1 (Delort [Del91], Vecchi and Wu [VW93], Shocet [Sch95]). *Let $\omega^\Delta(x, t)$ be a sequence of vorticities, satisfying the following conditions:*

- (i) $\|\omega^\Delta(\cdot, t)\|_{H^{-1}} \leq M$, uniformly for $\Delta > 0$, and for $t \in [0, T]$,
- (ii) $\|\omega^\Delta(\cdot, t)\|_{L^1} \leq M$, uniformly for $\Delta > 0$, and for $t \in [0, T]$,
- (iii) for all $\epsilon > 0$, there exists $\delta > 0$, such that

$$|A| < \delta \implies \int_A [\omega^\Delta]_-(\cdot, t) dx < \epsilon, \quad \forall t \in [0, T], \forall \Delta > 0,$$

where $[\omega^\Delta]_- := \max(0, -\omega^\Delta) \geq 0$ denotes the absolute value of the negative part of ω^Δ .

Then there exists a subsequence $\Delta_k \rightarrow 0$, and a measure $\omega \in (\mathcal{M}_+ + L^1) \cap H^{-1}$, such that $\omega^{\Delta_k} \rightharpoonup \omega$ in the sense of measures. Furthermore, for the corresponding sequence of velocities \mathbf{u}^{Δ_k} , one has $\mathbf{u}^{\Delta_k} \rightharpoonup \mathbf{u}$ weakly in L^2 , and for any divergence-free test function $\varphi \in C^\infty([0, T] \times \mathbb{T}^2; \mathbb{R}^2)$, we have

$$\lim_{k \rightarrow \infty} \int_0^T \int_{\mathbb{T}^2} (\mathbf{u}^{\Delta_k} \otimes \mathbf{u}^{\Delta_k}) : \nabla \varphi dx dt = \int_0^T \int_{\mathbb{T}^2} (\mathbf{u} \otimes \mathbf{u}) : \nabla \varphi dx dt.$$

In particular, Theorem 2.3.1 implies that one can pass to the limit in the non-linear term of the incompressible Euler equations, in the weak formulation.

To apply this theorem, our goal will thus be to prove (i) a uniform a priori bound on $\mathbf{u}^\Delta \in L^2$, (ii) a uniform L^1 -bound on the vorticity ω^Δ , and (iii) uniform control on the negative parts of the vorticity (equi-integrability). The required L^2 -bound is straightforward, since Fourier spectral methods are adapted to L^2 -spaces (cp. Proposition 2.4.1). To control the L^1 -norm of the vorticity and show equi-integrability of the negative parts, we will rely on (2.2.6). To this end, we multiply (2.2.6) by $\phi'(\omega^\Delta)$ for convex, Lipschitz continuous ϕ , and integrate against x , to obtain

$$\frac{d}{dt} \int_{\mathbb{T}^2} \phi(\omega^\Delta) dx \leq \text{Lip}(\phi) \left(\|(I - P_N)(\mathbf{u}^\Delta \cdot \nabla \omega^\Delta)\|_{L^1} + \|\epsilon_N \Delta R_{m_N} * \omega^\Delta\|_{L^1} \right).$$

We will show that the error terms in the bracket converge to 0, as $N \rightarrow \infty$, implying uniform control

$$\int_{\mathbb{T}^2} \phi(\omega^\Delta(x, t)) dx \leq \int_{\mathbb{T}^2} \phi(\omega^\Delta(x, 0)) dx + o(1) \leq M + o(1),$$

provided that $\phi(\omega^\Delta(x, 0)) \leq M$ is uniformly bounded (cp. Proposition 2.6.8). For $\phi(\omega) := |\omega|$, this yields L^1 -control. Equi-integrability of the negative parts will be deduced from the choice $\phi(\omega) = [\omega + c]_- = \max(0, -(\omega + c))$ for suitable $c > 0$ (cf. Lemmas 2.6.9, 2.6.10).

The main difficulty in the proof will be the a priori control of the non-linear projection error $\|(I - P_N)(\mathbf{u}^\Delta \cdot \nabla \omega^\Delta)\|_{L^1}$. To control this error, we split $\mathbf{u}^\Delta = \mathbb{P}_{N/2}\mathbf{u}^\Delta + (I - \mathbb{P}_{N/2})\mathbf{u}^\Delta$ and $\omega^\Delta = P_{N/2}\omega^\Delta + (I - P_{N/2})\omega^\Delta$ into the contributions of Fourier modes with wavenumber $|k| \leq N/2$ and $|k| > N/2$, respectively. Since the Fourier spectrum of the product $\mathbb{P}_{N/2}\mathbf{u}^\Delta \cdot \nabla P_{N/2}\omega^\Delta$ is confined to Fourier modes $\leq N$, it follows that

$$(I - P_N)(\mathbf{u}^\Delta \cdot \nabla \omega^\Delta) = (I - P_N) \left(\mathbf{u}^\Delta \cdot \nabla (I - P_{N/2})\omega^\Delta \right) + (I - P_N) \left((I - \mathbb{P}_{N/2})\mathbf{u}^\Delta \cdot \nabla P_{N/2}\omega^\Delta \right), \quad (2.3.1)$$

involves products, where at least one of the factors only includes high wavenumbers. To control these terms, we shall show that with a sufficient amount of spectral viscosity, the Fourier modes in the range $N/2 < |k| \leq N$ decay (exponentially) in N (see section 2.4). In particular, this provides very strong decay estimates on both $(I - P_{N/2})\omega^\Delta$ and $(I - \mathbb{P}_{N/2})\mathbf{u}^\Delta$, as $N \rightarrow \infty$, which will allow us to control the non-linear projection error (cp. Lemma 2.4.6). A technical caveat is that the spectral viscosity requires a short initial time $t_N^* > 0$ in order to provide this damping of the high Fourier components, and hence the spectral decay estimates can only be established for $t \in [t_N^*, \infty)$. Thus, the above spectral decay estimate has to be complemented by short-time control over the initial time-interval $[0, t_N^*]$, which ensures bounds on the vorticity before the viscosity can act to control the small scale behaviour. Short-time control is the subject of section 2.5. Since the required estimates are often somewhat involved, we will focus on providing an overview of the main results, and provide detailed references to the original publication [LM20], where the complete technical proofs can be found.

2.4 Spectral decay estimate

As outlined in the last section, before establishing more detailed L^1 -estimates for the vorticity, we note that L^2 estimates for the approximate solutions, \mathbf{u}^Δ and ω^Δ are readily obtained.

Proposition 2.4.1. *If $\bar{\mathbf{u}} \in L^2$, then the approximation sequence \mathbf{u}^Δ satisfies*

$$\|\mathbf{u}^\Delta(\cdot, t)\|_{L^2} \leq \|\mathbf{u}^\Delta(\cdot, 0)\|_{L^2} \leq \|\bar{\mathbf{u}}\|_{L^2}.$$

In particular, this implies that we have a uniform bound

$$\|\omega^\Delta(\cdot, t)\|_{H^{-1}} \leq \|\bar{\mathbf{u}}\|_{L^2}.$$

Proof. Multiply (2.2.1) by \mathbf{u}^Δ , integrate over the spatial variable, we find

$$\frac{d}{dt} \int_{\mathbb{T}^2} |\mathbf{u}^\Delta|^2 dx = - \int_{\mathbb{T}^2} \nabla \mathbf{u}^\Delta : \nabla (Q_N * \mathbf{u}^\Delta) dx \stackrel{\text{(Parseval)}}{=} -(2\pi)^2 \sum_k \hat{Q}_k |k|^2 |\widehat{(\mathbf{u}^\Delta)}_k|^2 \leq 0.$$

Integration over time yields the first inequality. The second inequality follows from

$$\|\mathbf{u}^\Delta(\cdot, 0)\|_{L^2}^2 = \|K_{a_N} * \bar{\mathbf{u}}\|_{L^2}^2 = (2\pi)^2 \sum_k \hat{K}_k^2 |\widehat{(\bar{\mathbf{u}})}_k|^2 \leq (2\pi)^2 \sum_k |\widehat{(\bar{\mathbf{u}})}_k|^2 = \|\bar{\mathbf{u}}\|_{L^2}^2.$$

The non-linear terms in (2.2.1) cancel out after multiplication with \mathbf{u}^Δ in the above estimate. The upper bound for $\|\omega\|_{H^{-1}}$ is trivial. \square

The main tool employed to prove the convergence results in this chapter will be the decay estimate for the vorticity stated below in Proposition 2.4.2. A similar idea has in fact been used in the context of the one-dimensional Burgers equation to prove the uniform L^∞ -boundedness of the numerical approximations by the SV method [MT89]. The method employed in [MT89], which is based on a bootstrap argument adapted from [HKR90], does not appear to allow a straightforward extension to the present case. Instead, we shall adapt a different method from [DT95].

To state the next proposition, we first need to define the operators $e^{\alpha|\nabla|}$ for $\alpha \in \mathbb{R}$, and $|\nabla|$. They are defined as distributions $\mathcal{D}'(\mathbb{T}^2)$ via their Fourier coefficients, as follows:

$$\widehat{(e^{\alpha|\nabla|})}_k = e^{\alpha|k|}, \quad \widehat{(|\nabla|)}_k = |k|. \quad (2.4.1)$$

We can now state the spectral decay estimate, based on the method employed in [DT95].

Proposition 2.4.2. *Let ω^Δ be a solution of the voriticty equation (2.2.5), with arbitrary parameters $\epsilon_N, m_N, a_N > 0$. Let*

$$\begin{cases} \beta_N = \alpha^2 + 8\epsilon_N^2 m_N^2, \\ \gamma_N = C \log(N), \end{cases} \quad (2.4.2)$$

where C is a constant such that ($k \in \mathbb{Z}^2$)

$$\sum_{|k| \leq N} \frac{1}{|k|^2} \leq C \log(N).$$

Then for any $\alpha > 0$, we have the estimate

$$\|e^{\alpha t|\nabla|} \omega^\Delta(\cdot, t)\|_{L^2}^2 \leq \frac{\|\omega^\Delta(\cdot, 0)\|_{L^2}^2 e^{\beta_N t/\epsilon_N}}{1 - \frac{\gamma_N \|\omega^\Delta(\cdot, 0)\|_{L^2}^2}{\beta_N} [e^{\beta_N t/\epsilon_N} - 1]}, \quad (2.4.3)$$

for all $t < t^*$, with

$$t^* = \frac{\epsilon_N}{\beta_N} \log \left(1 + \frac{\beta_N}{\gamma_N \|\omega^\Delta(\cdot, 0)\|_{L^2}^2} \right).$$

Sketch of proof. For all details of the proof, we refer to [LM20, Prop. 4.4]. Here, we sketch the main ideas: To prove the spectral decay estimate, we consider the evolution equation for $e^{\alpha t|\nabla|}\omega^\Delta$. We find from

$$\partial_t \omega^\Delta = \epsilon_N \Delta \omega^\Delta + \epsilon_N \Delta (R_{m_N} * \omega^\Delta) - P_N(\mathbf{u}^\Delta \cdot \nabla \omega^\Delta),$$

that $\|e^{\alpha t|\nabla|}\omega^\Delta\|_{L^2}^2$ satisfies the following differential inequality

$$\frac{d}{dt} \|e^{\alpha t|\nabla|}\omega^\Delta\|_{L^2}^2 \leq \frac{\beta_N}{\epsilon_N} \|e^{\alpha t|\nabla|}\omega^\Delta\|_{L^2}^2 + \frac{\gamma_N}{\epsilon_N} \|e^{\alpha t|\nabla|}\omega^\Delta\|_{L^2}^4,$$

where $\beta_N := \alpha^2 + 8\epsilon_N^2 m_N^2$ and $\gamma_N = C \log(N)$. Integration of this inequality can then be shown to yield

$$\|e^{\alpha t|\nabla|}\omega^\Delta\|_{L^2}^2 \leq \frac{\|\omega^\Delta(\cdot, 0)\|_{L^2}^2 e^{\beta_N t/\epsilon_N}}{1 - \frac{\gamma_N \|\omega^\Delta(\cdot, 0)\|_{L^2}^2}{\beta_N} [e^{\beta_N t/\epsilon_N} - 1]}.$$

□

Note that the L^2 norm on the left provides a very crude upper bound for the Fourier coefficients of ω^Δ via

$$e^{2\alpha t|k|} |\widehat{\omega}_k|^2 \leq \|e^{\alpha t|\nabla|}\omega^\Delta\|_{L^2}^2. \quad (2.4.4)$$

Next, we can employ Proposition 2.4.2 together with a simple a priori estimate on $\|\omega^\Delta(\cdot, 0)\|_{L^2} = \|K_{a_N} * \bar{\omega}\|_{L^2}$, to arrive at the following theorem (cf. [LM20, Thm. 4.8]):

Theorem 2.4.3. *Let $\bar{\mathbf{u}} \in L^2$ be given initial data for the incompressible Euler equations. Then there exist absolute constants $A, B > 0$ such that the approximations, $\omega^\Delta = \text{curl}(\mathbf{u}^\Delta)$, obtained from the spectral viscosity method satisfy the following estimate on their Fourier coefficients:*

$$|\widehat{\omega}_k(t)|^2 \leq A a_N^2 \|\bar{\mathbf{u}}\|_{L^2}^2 \left(1 + \frac{\beta_N}{B \log(N) a_N^2 \|\bar{\mathbf{u}}\|_{L^2}^2}\right) e^{-2\alpha t^* |k|},$$

for $t \in [t^*, T]$, and

$$t^* = \frac{\epsilon_N}{\beta_N} \log \left(1 + \frac{\beta_N}{B \log(N) a_N^2 \|\bar{\mathbf{u}}\|_{L^2}^2}\right).$$

□

We next observe that we can choose the sequences $\epsilon_N \rightarrow 0$, $m_N, a_N \rightarrow \infty$ in a suitable manner, such that the Fourier coefficients in the range $N/2 \leq |k| \leq N$ decay superpolynomially in N . This is the content of the next theorem:

Theorem 2.4.4. *With the notation of Theorem 2.4.3. Choose the free parameters ϵ_N, a_N, m_N as follows*

$$m_N \lesssim N^\theta, \text{ where } 0 \leq \theta < \frac{1}{3}, \quad a_N \sim N^\theta, \quad \epsilon_N \sim \frac{a_N \log(N)^s}{N}, \quad (s > 6). \quad (2.4.5)$$

Then, for any $\sigma > 0$, there exists a constant $C_\sigma > 0$, such that

$$|\widehat{\omega}_k(t)| \leq C_\sigma N^{-\sigma}, \quad \text{for } N/2 \leq |k| \leq N, \quad t \in [t^*, \infty), \quad (2.4.6)$$

where $t^* \rightarrow 0$, at a convergence rate

$$t^* \ll \frac{1}{a_N N \log(N)^2}. \quad (2.4.7)$$

It will be convenient to state the following definition:

Definition 2.4.5. *We will say that a choice of parameters ϵ_N, m_N, a_N and Fourier kernels Q_N, K_{a_N} for the SV method ensures spectral decay, provided that the conclusions (estimates (2.4.6), (2.4.7)) of Theorem 2.4.4 hold true.*

As a consequence of Theorem 2.4.4 and the identity (2.3.1), expressing the fact that only high-frequencies contribute to the projection error, one can now readily show that the projection error vanishes in the limit $N \rightarrow \infty$, at least for $t \geq t_N^*$. This is the content of the next lemma:

Lemma 2.4.6. *If the parametrization for the SV method ensures spectral decay, then the projection error can be bounded from above, i.e. there exists a constant $C > 0$ depending on the initial data $\bar{\mathbf{u}}$, but independent of N , such that for all $t \in [t_N^*, \infty)$ and for any $1 \leq p < \infty$:*

$$\|(I - P_N)(\mathbf{u}^\Delta(t) \cdot \nabla \omega^\Delta(t))\|_{L^p} \leq CN^{-1}\|\omega^\Delta(t)\|_{L^p}.$$

Alternatively, one can find a constant $C' > 0$, again depending on the initial data, but independent of N , such that

$$\|(I - P_N)(\mathbf{u}^\Delta(t) \cdot \nabla \omega^\Delta(t))\|_{L^p} \leq C'N^{-1}.$$

□

For a detailed proof, we refer to [LM20, Lemma 4.12]. We also remark that the asymptotic decay N^{-1} was chosen arbitrarily, and could have been replaced by any polynomial rate $N^{-\sigma}$, $\sigma > 0$.

The next lemma summarizes that the second discretization error can also be bounded from above.

Lemma 2.4.7. *Under the present assumptions on the SV method (cp. (2.2.8)), We have*

$$\|\Delta(R_{m_N} * \omega^\Delta)\|_{L^1} \leq 2m_N^2 \|R_{m_N}\|_{L^1} \|\omega^\Delta\|_{L^1} \leq 2m_N^2 \log(N)^2 \|\omega^\Delta\|_{L^1}.$$

□

Based on Lemmas 2.4.6 and 2.4.7, we can now control the error terms on the right hand side. We conclude this section by proving the following theorem, stating that the L^1 -norm is uniformly controlled for $t \geq t_N^*$.

Theorem 2.4.8 (L^1 control after short time). *If the numerical parameters ensure spectral decay, then there exists a sequence $c_N \rightarrow 0$ such that*

$$\|\omega^\Delta(\cdot, t)\|_{L^1} \leq (1 + c_N t) \|\omega^\Delta(\cdot, t_N^*)\|_{L^1}, \quad \text{for all } t \geq t_N^*.$$

Proof. We start from equation (2.2.6):

$$\partial_t \omega^\Delta + \mathbf{u}^\Delta \cdot \nabla \omega^\Delta - \epsilon_N \Delta \omega^\Delta = (I - P_N)(\mathbf{u}^\Delta \cdot \nabla \omega^\Delta) + \epsilon_N \Delta R_{m_N} * \omega^\Delta.$$

Multiplying by $\text{sign}(\omega^\Delta)$ (or smooth approximations thereof; we will forego the details here), and integrating over x , we find

$$\frac{d}{dt} \|\omega^\Delta(\cdot, t)\|_{L^1} \leq \|\text{err}_1\|_{L^1} + \|\text{err}_2\|_{L^1}.$$

Using Lemmas 2.4.6 and 2.4.7, we obtain (for $t \geq t_N^*$)

$$\frac{d}{dt} \|\omega^\Delta(\cdot, t)\|_{L^1} \leq C [N^{-1} \|\bar{\mathbf{u}}\|_{L^2} + \epsilon_N m_N^2 \log(N)^2] \|\omega^\Delta(\cdot, t)\|_{L^1}.$$

After an integration over $[t_N^*, t]$, it follows that

$$\|\omega^\Delta(\cdot, t)\|_{L^1} \leq \|\omega^\Delta(\cdot, t_N^*)\|_{L^1} \exp(c_N t),$$

where $c_N = C [N^{-1} \|\bar{\mathbf{u}}\|_{L^2} + \epsilon_N m_N^2 \log(N)^2] \rightarrow 0$. □

2.5 Short-time estimates

In the last section, we have shown that the numerical parameters can be chosen to ensure the spectral decay of the Fourier modes $N/2 \leq |k| \leq N$ for $t \in [t_N^*, +\infty)$, where (cp. (2.4.7))

$$t_N^* \ll \frac{1}{a_N N \log(N)^2}. \quad (2.5.1)$$

As a consequence, we have proven L^1 -control of the vorticity for $t \geq t_N^*$ in terms of $\|\omega^\Delta(\cdot, t_N^*)\|_{L^1}$. In this section, we will bridge the gap $[0, t_N^*]$ and prove short time L^1 control of the vorticity for the initial interval $0 \leq t \leq t_N^*$ in terms of $\|\omega^\Delta(\cdot, 0)\|_{L^1}$. We will prove the following theorem,

Theorem 2.5.1. *If $\omega^\Delta(\cdot, 0) \in L^1$, then there exists a sequence $c_N \rightarrow 0$ (depending only on the initial data $\bar{\omega}$), such that*

$$\|\omega^\Delta(\cdot, t)\|_{L^1} \leq (1 + c_N) \|\omega^\Delta(\cdot, 0)\|_{L^1} + c_N, \quad \text{for all } t \in [0, t_N^*].$$

Proof. We begin by observing that

$$\partial_t \omega^\Delta = -P_N(\mathbf{u}^\Delta \cdot \nabla \omega^\Delta) + \epsilon_N \Delta \omega^\Delta + \epsilon_N \Delta(R_{m_N} * \omega^\Delta). \quad (2.5.2)$$

Using also the operator norm bound $\|P_N\|_{L^1 \rightarrow L^1} \leq C \log(N)^2$ (cp. Proposition A.1.1 in Appendix A), the identity (2.5.2) implies that,

$$\begin{aligned} \frac{d}{dt} \|\omega^\Delta\|_{L^1} &\leq \|P_N(\mathbf{u}^\Delta \cdot \nabla \omega^\Delta)\|_{L^1} + \epsilon_N \|\Delta(R_{m_N} * \omega^\Delta)\|_{L^1} \\ &\leq C \log(N)^2 \|\mathbf{u}^\Delta \cdot \nabla \omega^\Delta\|_{L^1} + C \epsilon_N m_N^2 \log(N)^2 \|\omega^\Delta\|_{L^1}, \end{aligned} \quad (2.5.3)$$

for some constant $C > 0$. Setting $\delta_N := C \epsilon_N m_N^2 \log(N)^2$, we note that $\delta_N \rightarrow 0$ and $\delta_N \geq 0$, we find

$$\frac{d}{dt} (\|\omega^\Delta\|_{L^1} e^{-\delta_N t}) \leq C \log(N)^2 \|\mathbf{u}^\Delta \cdot \nabla \omega^\Delta\|_{L^1}. \quad (2.5.4)$$

On the right hand side, we have used the simple estimate $e^{-\delta_N t} \leq 1$. We will now show that if $\omega^\Delta(\cdot, 0) \in L^1$, then there exists a constant $C > 0$ such that

$$\|\omega^\Delta(\cdot, t)\|_{L^1} \leq \|\omega^\Delta(\cdot, 0)\|_{L^1} e^{\delta_N t_N^*} + C \|\bar{\mathbf{u}}\|_{L^2}^2 [a_N N \log(N)^2] t_N^*,$$

for all $t \in [0, t_N^*]$. Here $\delta_N \rightarrow 0$. The claimed estimate then follows from the observation that $\delta_N t_N^* \rightarrow 0$ (is independent of the initial data), and from (2.5.1).

To this end, we start by noting that

$$\begin{aligned} \|\mathbf{u}^\Delta(t) \cdot \nabla \omega^\Delta(t)\|_{L^1} &\leq C \|\mathbf{u}^\Delta(t)\|_{L^2} \|\nabla \omega^\Delta(t)\|_{L^2} \\ &\leq C N \|\mathbf{u}^\Delta(t)\|_{L^2} \|\omega^\Delta(t)\|_{L^2}. \end{aligned}$$

From the a priori L^2 -bounds for $\mathbf{u}^\Delta, \omega^\Delta$, we can furthermore estimate the right-hand side by $\|\mathbf{u}^\Delta(\cdot, t)\|_{L^2} \leq \|\bar{\mathbf{u}}\|_{L^2}$, and

$$\|\omega^\Delta(\cdot, t)\|_{L^2} \leq \|\omega^\Delta(\cdot, 0)\|_{L^2} = \|K_{a_N} * \bar{\omega}\|_{L^2} \leq C a_N \|K_{a_N} * \bar{\mathbf{u}}\|_{L^2} \leq C a_N \|\bar{\mathbf{u}}\|_{L^2}.$$

From (2.5.4), we now find

$$\frac{d}{dt} (\|\omega^\Delta(\cdot, t)\|_{L^1} e^{-\delta_N t}) \leq C N a_N \log(N)^2 \|\bar{\mathbf{u}}\|_{L^2}^2.$$

Integrating in time from 0 to t , we find, for some constant C ,

$$\|\omega^\Delta(\cdot, t)\|_{L^1} \leq \|\omega^\Delta(\cdot, 0)\|_{L^1} e^{\delta_N t} + C N a_N e^{\delta_N t} \log(N)^2 \|\bar{u}\|_{L^2}^2 t.$$

The right hand side is uniformly bounded for $t \in [0, t_N^*]$, by

$$\|\omega^\Delta(\cdot, t)\|_{L^1} \leq \|\omega^\Delta(\cdot, 0)\|_{L^1} e^{\delta_N t_N^*} + C N a_N e^{\delta_N t_N^*} \log(N)^2 \|\bar{u}\|_{L^2}^2 t.$$

Furthermore, since $\delta_N t_N^* \rightarrow 0$, we can absorb the (uniformly bounded) factor $e^{\delta_N t_N^*}$ by increasing constant C , yielding the claimed estimate. \square

2.6 Uniform L^1 control and equi-integrability

Combining Theorems 2.4.8 and 2.5.1 of the last two sections, we can now conclude that the L^1 -norm of the vorticity can be uniformly controlled on compact intervals $[0, T]$.

Theorem 2.6.1 (vorticity L^1 control). *Let $\bar{u} \in L^2(\mathbb{T}^2; \mathbb{R}^2)$ be given initial data for the incompressible Euler equations. Let $T > 0$ be given. If the parameters for the spectral viscosity approximation ensure spectral decay, then there exists a sequence $c_N \rightarrow 0$, such that*

$$\|\omega^\Delta(\cdot, t)\|_{L^1} \leq (1 + c_N) \|\omega^\Delta(\cdot, 0)\|_{L^1} + c_N.$$

Remark 2.6.2. *We point out that Theorem 2.6.1 provides a bound on the L^1 -norm of $\omega^\Delta(\cdot, t)$, in terms of the L^1 -norm of $\omega^\Delta(\cdot, 0)$, rather than \bar{u} . This is made necessary because the Fourier projections*

$$P_{a_N} : L^1 \rightarrow L^1, \bar{u} \mapsto P_{a_N} \bar{u}, \quad (N \in \mathbb{N}),$$

do not define a family of uniformly bounded operators on L^1 (and even less so for $\bar{u} \in \mathcal{M}_+$ a measure); indeed we only have $\|P_{a_N}\|_{L^1 \rightarrow L^1} \lesssim \log(a_N)^2$ by Proposition A.1.1 in Appendix A. Thus, for Delort initial data, a more careful approximation of the initial data needs to be made to ensure uniform boundedness in L^1 of the approximation sequence ω^Δ , i.e. we can not choose the initial data projection kernel $K_{a_N} = D_{a_N}$ as the Dirichlet kernel, in this case.

We recall that, in order to apply Theorem 2.3.1 to the approximate solution sequence generated by the SV scheme, we need to establish (i) uniform H^{-1} control, (ii) uniform L^1 control and (iii) equi-integrability. The required uniform H^{-1} -bound on the vorticity has been obtained in Proposition 2.4.1. The uniform L^1 -bound on the vorticity has been established in Theorem 2.6.1, provided that $\omega^\Delta(\cdot, 0)$ remains uniformly bounded in L^1 . As indicated in the last remark, this restriction is a non-trivial issue. A discussion of one possible way to obtain suitable approximations of the initial data will now be given.

Remark 2.6.3. *The uniform L^1 -boundedness of the sequence $\omega^\Delta(\cdot, 0)$ requires an initial approximation for which the vorticity does not only converge in H^{-1} , but also in the sense of (signed) measures with a uniform L^1 -bound. One way to ensure L^1 boundedness is as follows: Fix a mollifier $\psi \in C^\infty$ with support in a unit ball $B_1(0)$. Denote $\psi_\rho(x) := \rho^{-2} \psi(x/\rho)$. We will obtain the initial data for the numerical approximation by convolution with a smoothing kernel $\bar{u} \mapsto \psi_\rho * \bar{u}$, and subsequently project to the lowest Fourier modes $\leq N$, viz.*

$$\bar{u} \mapsto D_N * (\psi_\rho * \bar{u}) = (D_N * \psi_\rho) * \bar{u},$$

where $D_N(x) = \sum_{|k|_\infty \leq N} \exp(ik \cdot x)$ is the Dirichlet kernel. Since ψ_ρ is smooth, we are assured that $D_N * \psi_\rho \rightarrow \psi_\rho$ uniformly as $N \rightarrow \infty$ (for fixed $\rho > 0$). In particular, it follows that $\|D_N * \psi_\rho\|_{L^1} \rightarrow \|\psi_\rho\|_{L^1}$. The idea is now to choose a sequence ρ_N , such that $N \gg \rho_N^{-1}$ (i.e. such that the convolution kernel is asymptotically resolved by the numerical approximation). If the convolution is adequately resolved, then we would expect that $K_N := D_N * \psi_{\rho_N}$ is a suitable kernel to ensure convergence of the initial data.

The following proposition confirms the intuition pointed out in the last remark. As the proof does not provide any further insight beyond Remark 2.6.3, we refer the interested reader to [LM20, Prop. 6.4] for details of the argument.

Proposition 2.6.4. *Let $\Psi \in C_c^\infty(\mathbb{R}^2)$ be a non-negative function, $\int_{\mathbb{R}^2} \Psi(x) dx = 1$, and assume that Ψ is compactly supported in $(-\pi, \pi)^2$. Define $\Psi_\rho := \rho^{-2}\Psi(x/\rho)$, a compactly supported mollifier. Let ψ_ρ be the periodization of Ψ_ρ , such that we can consider ψ_ρ as an element in $C^\infty(\mathbb{T}^2)$. For $M \in \mathbb{N}$, let $K_M := D_M * \psi_{\rho_M}$ for some sequence $\rho_M \rightarrow 0$. If $\rho_M \sim M^{-1+\delta}$ with $\delta > 0$, then K_M is a good kernel, in the sense that $K_M * \phi \rightarrow \phi$ for all $\phi \in C^\infty(\mathbb{T}^2)$, and there exists a constant C , such that $\|K_M\|_{L^1} \leq C$. In addition, we have*

$$\|\psi_{\rho_M} - K_M\|_{L^1} \rightarrow 0, \quad \text{as } M \rightarrow \infty.$$

□

The observations of Proposition 2.6.4 will allow us to control numerical approximations for initial data in the Delort class, and in particular, will ensure that $\|\omega^\Delta(\cdot, 0)\|_{L^1}$ remains uniformly bounded. We make the following

Definition 2.6.5. *We will say that the SV method has suitably approximated initial data, if $\omega^\Delta(\cdot, 0) = K_{a_N} * \bar{\omega}$ (for $a_N \in \mathbb{N}$ specified in the scheme) is obtained by convolution with a kernel K_M as described in Proposition 2.6.4.*

Our final ingredient in the convergence proof requires equi-integrability of the negative parts. The following proposition gives us some control on the negative part $[\omega^\Delta]_- := \max(0, -\omega^\Delta)$ of ω^Δ , if the initial approximation is chosen as in Proposition 2.6.4:

Proposition 2.6.6. *Consider initial data $\bar{\omega} = \bar{\omega}' + \bar{\omega}'' \in H^{-1}$, where $\bar{\omega}' \in \mathcal{M}_+$ is a finite non-negative measure and $\bar{\omega}'' \in L^1$. If $\omega^\Delta(\cdot, 0)$ is obtained as suitably approximated initial data for the SV method, then for any $\epsilon > 0$, there exists $c > 0$ and $N_0 \in \mathbb{N}$, such that*

$$\int_{\mathbb{T}^2} [\omega^\Delta(\cdot, 0) + c]_- dx < \epsilon, \quad \Delta \equiv 1/N, \quad \forall N \geq N_0.$$

Remark 2.6.7. *Note that $[\omega^\Delta(\cdot, 0) + c]_- \neq 0$, only on the set $\{x \mid \omega^\Delta(x, 0) < -c\}$. The above proposition therefore gives us some control on the size of the negative part of the approximation ω^Δ . The proposition will be used below to show that the negative vorticity cannot concentrate on small sets.*

Proof. Note that $w \mapsto [w]_- := \max(0, -w)$ is convex, homogeneous and bounded from above by $|w|$. From these properties, it follows that

$$[\omega^\Delta(\cdot, 0) + c]_- \leq |\omega^\Delta(\cdot, 0) - \psi_{\rho_N} * \bar{\omega}| + [\psi_{\rho_N} * \bar{\omega} + c]_-.$$

Next, note that $\psi_{\rho_N} \geq 0$ and $c > 0$, implies that

$$[\psi_{\rho_N} * \bar{\omega} + c]_- \stackrel{(\bar{\omega}' \geq 0)}{\leq} [\psi_{\rho_N} * \bar{\omega}'' + c]_- \stackrel{(\text{Jensen})}{\leq} \psi_{\rho_N} * [\bar{\omega}'' + c]_-.$$

Therefore, we obtain upon spatial integration, using also that $\int_{\mathbb{T}^2} \psi_{\rho_N} dx = 1$:

$$\int_{\mathbb{T}^2} [\omega^\Delta(\cdot, 0) + c]_- dx \leq \|\omega^\Delta(\cdot, 0) - \psi_{\rho_N} * \bar{\omega}\|_{L^1} + \int_{\mathbb{T}^2} [\bar{\omega}'' + c]_- dx.$$

Since $\bar{\omega}'' \in L^1$, we can now choose $c > 0$ large enough to ensure that the second term is smaller than $\epsilon/2$. From the estimate

$$\|\omega^\Delta(\cdot, 0) - \psi_{\rho_N} * \bar{\omega}\|_{L^1} = \|(K_N - \psi_{\rho_N}) * \bar{\omega}\|_{L^1} \leq \|K_N - \psi_{\rho_N}\|_{L^1} \|\bar{\omega}\|_{\mathcal{M}},$$

and the fact that $\|K_N - \psi_{\rho_N}\|_{L^1} \rightarrow 0$, by Proposition 2.6.4, we can find $N_0 \in \mathbb{N}$, such that $\|\omega^\Delta(\cdot, 0) - \psi_{\rho_N} * \bar{\omega}\|_{L^1} < \epsilon/2$. For this choice of $c > 0$ and $N_0 \in \mathbb{N}$, we then have

$$\int_{\mathbb{T}^2} [\omega^\Delta(\cdot, 0) + c]_- dx < \epsilon, \quad \Delta \equiv 1/N, \text{ for all } N \geq N_0.$$

□

The next goal is to show that the result of Proposition 2.6.6 remains true also at later times $t > 0$. To this end, we first show the following improvement on the mere L^1 -boundedness implied by Theorem 2.6.1.

Proposition 2.6.8. *Let $\phi \in C^1$ be a convex function, such that $|\phi'(\omega)| \leq D$, for some constant D . If there exists a constant M , such that*

$$\int_{\mathbb{T}^2} |\omega^\Delta(\cdot, 0)| dx \leq M, \quad \Delta \equiv 1/N, \text{ for all } N \in \mathbb{N},$$

then the numerical solutions $\omega^\Delta(x, t)$ (computed with parameters ensuring spectral decay) satisfy, in addition

$$\int_{\mathbb{T}^2} \phi(\omega^\Delta(\cdot, t)) dx \leq \int_{\mathbb{T}^2} \phi(\omega^\Delta(\cdot, 0)) dx + c_N, \quad \text{for } t \in [0, T], \quad (2.6.1)$$

with a sequence c_N converging to zero, $c_N \rightarrow 0$. Furthermore, the sequence c_N depends on ϕ only via the constant D , i.e. the bound on $|\phi'|$.

Sketch of proof. The proof again relies on a combination of a short-time estimate on the interval $[0, t_N^*]$, combined with the spectral decay estimate for $t \geq t_N^*$. The short-time estimate is very similar to the short-time estimate for the L^1 -norm, and the reader is referred to [LM20, Prop. 6.7] for details. The result is that for $0 \leq t \leq t_N^*$, we have an estimate of the form

$$\int_{\mathbb{T}^2} \phi(\omega^\Delta(\cdot, t)) dx \leq \int_{\mathbb{T}^2} \phi(\omega^\Delta(\cdot, 0)) dx + \underbrace{CDNa_N \log(N)^2 t_N^*}_{\rightarrow 0 \text{ (as } N \rightarrow \infty\text{)}},$$

where we note that the last term on the right-hand side converges to 0, by assumption on the parameters ensuring spectral decay (cp. (2.4.7)).

To finish the proof, we observe that for $t \geq t_N^*$, we find from the evolution equation for ω^Δ (equation (2.2.6)):

$$\begin{aligned} \frac{d}{dt} \int_{\mathbb{T}^2} \phi(\omega^\Delta) dx &\leq \langle \phi'(\omega^\Delta), (I - P_N)(\mathbf{u}^\Delta \cdot \nabla \omega^\Delta) \rangle + \langle \phi'(\omega^\Delta), \epsilon_N \Delta(R_{m_N} * \omega^\Delta) \rangle \\ &\leq D \|(I - P_N)(\mathbf{u}^\Delta \cdot \nabla \omega^\Delta)\|_{L^1} + D \|\epsilon_N \Delta(R_{m_N} * \omega^\Delta)\|_{L^1}. \end{aligned}$$

The two terms on the right hand side, can be estimated using Lemma 2.4.6 and 2.4.7, yielding $\|(I - P_N)(\mathbf{u}^\Delta \cdot \nabla \omega^\Delta)\|_{L^1} \leq CN^{-1}$, and $\|\epsilon_N \Delta(R_{m_N} * \omega^\Delta)\|_{L^1} \leq C\epsilon_N m_N^2 \log(N)^2$, for a constant $C > 0$ depending only on the initial data. It now follows that

$$\frac{d}{dt} \int_{\mathbb{T}^2} \phi(\omega^\Delta) dx \leq \underbrace{CD(N^{-1} + \epsilon_N m_N^2 \log(N)^2)}_{\rightarrow 0 \text{ (as } N \rightarrow \infty\text{)}},$$

for some constant C , independent of N and ϕ . Integrating in time, it follows that for $t \in [t_N^*, T]$:

$$\int_{\mathbb{T}^2} \phi(\omega^\Delta(\cdot, t)) dx \leq \int_{\mathbb{T}^2} \phi(\omega^\Delta(\cdot, t_N^*)) dx + c_N^{(1)} \leq \int_{\mathbb{T}^2} \phi(\omega^\Delta(\cdot, 0)) dx + c_N^{(1)} + c_N^{(2)},$$

with

$$c_N^{(1)} := CD(N^{-1} + \epsilon_N m_N^2 \log(N)^2)T \rightarrow 0, \quad (\text{as } N \rightarrow \infty).$$

and

$$c_N^{(2)} := CDN a_N \log(N) t_N^* \rightarrow 0, \quad (\text{as } N \rightarrow \infty),$$

This proves the claim with $c_N := c_N^{(1)} + c_N^{(2)}$. \square

Applying the above Proposition 2.6.8 with a suitable sequence of smooth approximations $\phi_\epsilon(\omega) \rightarrow [\omega + c]_-$, and relying on Proposition 2.6.6, it is now straightforward to show the following result:

Lemma 2.6.9. *If ω^Δ is obtained from the SV method, with suitably approximated initial data and parameters ensuring spectral decay, then for any $\epsilon > 0$, there exists a $c > 0$ and $N_0 \in \mathbb{N}$, such that*

$$\int_{\mathbb{T}^2} [\omega^\Delta(\cdot, t) + c]_- dx < \epsilon, \quad \text{for all } t \in [0, T], \text{ and for all } \Delta = 1/N, N \geq N_0.$$

As a consequence of Lemma 2.6.9, we now prove that the sequence $[\omega^\Delta]_-$ satisfies the equi-integrability property (iii) of Theorem 2.3.1.

Lemma 2.6.10. *Under the assumptions of Lemma 2.6.9, the sequence $[\omega^\Delta]_-$ is uniformly equi-integrable on $[0, T]$, in the following sense: For all $\epsilon > 0$, there exists a $\delta > 0$, such that*

$$|A| < \delta \implies \int_A [\omega^\Delta]_-(\cdot, t) dx < \epsilon, \quad \text{for all } \Delta = 1/N > 0, \text{ and } t \in [0, T]. \quad (2.6.2)$$

Proof. Let $\epsilon > 0$. We have to find $\delta > 0$, such that (2.6.2) is satisfied. By Lemma 2.6.9, there exists $c > 0$ and $N_0 \in \mathbb{N}$, $\Delta_0 = 1/N_0$, such that

$$\int_{\mathbb{T}^2} [\omega^\Delta(\cdot, t) + c]_- dx < \epsilon/2,$$

for all $\Delta \leq \Delta_0$ and $t \in [0, T]$. We now observe that for any subset $A \subset \mathbb{T}^2$, we have

$$\int_A [\omega^\Delta]_-(\cdot, t) dx \leq \int_A (c + [\omega^\Delta(\cdot, t) + c]_-) dx = c|A| + \int_A [\omega^\Delta(\cdot, t) + c]_- dx.$$

Since the second term is smaller than $\epsilon/2$ by our choice of c , it now suffices to choose $\delta < \epsilon/(2c)$, to find

$$|A| < \delta \implies \int_A [\omega^\Delta]_-(\cdot, t) dx < \epsilon, \quad \text{for all } \Delta \leq \Delta_0, \text{ and all } t \in [0, T].$$

On the other hand, let $M := \sup_{\Delta > \Delta_0} \|\omega^\Delta\|_{L^\infty([0, T] \times \mathbb{T}^2)} = \sup_{N < N_0} \|\omega^\Delta\|_{L^\infty([0, T] \times \mathbb{T}^2)}$, where we recall that by definition, $\Delta = 1/N$ depends on the grid size $N \in \mathbb{N}$, and $\Delta_0 = 1/N_0$ for some $N_0 \in \mathbb{N}$. Note that for $N = 1, \dots, N_0 - 1$, each ω^Δ is a smooth function on $[0, T] \times \mathbb{T}^2$. In particular, this implies that $M < \infty$ is finite. Choosing now $\delta < \epsilon/M$, it follows that we also have

$$|A| < \delta \implies \int_A [\omega^\Delta]_-(\cdot, t) dx < \epsilon, \quad \text{for } \Delta \equiv 1/N, N = 1, \dots, N_0 - 1, \text{ and for } t \in [0, T].$$

This proves the claim. \square

2.7 Convergence in the Delort class

In this section, we will finally prove that any (weak) limit point of the approximate solution sequence generated by the SV method is in fact a weak solution of the incompressible Euler equations, for initial data in the Delort class.

Theorem 2.7.1. *Let $\omega^\Delta = \operatorname{curl}(\mathbf{u}^\Delta)$, \mathbf{u}^Δ be obtained by solving the approximate Euler equations, with parameters ensuring spectral decay, and with suitably approximated initial data obtained from $\bar{\omega} = \bar{\omega}' + \bar{\omega}''$, where $\bar{\omega}' \in \mathcal{M}_+ \cap H^{-1}$ and $\bar{\omega}'' \in L^1 \cap H^{-1}$. Then the sequence \mathbf{u}^Δ converges weakly (up to the extraction of a subsequence) to a weak solution $\mathbf{u} \in L^2$ of the Euler equations. Furthermore, the limiting vorticity $\omega = \operatorname{curl}(\mathbf{u})$ is an element of $\omega \in (\mathcal{M}_+ + L^1) \cap H^{-1}$, i.e. ω can be written as a sum $\omega = \omega_+ - \omega_-$, where $\omega_+(\cdot, t) \in \mathcal{M}_+$ is a finite, non-negative measure on \mathbb{T}^2 , and $\omega_-(\cdot, t) \in L^1(\mathbb{T}^2)$.*

Proof. By Proposition 2.4.1, we have $\|\mathbf{u}^\Delta(\cdot, t)\|_{L^2} \leq \|\bar{\mathbf{u}}\|_{L^2}$ for all N and $t \in [0, T]$. Therefore there exists a subsequence \mathbf{u}^Δ , and $\mathbf{u} \in L^\infty([0, T]; L^2(\mathbb{T}^2; \mathbb{R}^2))$, such that $\mathbf{u}^\Delta \rightharpoonup \mathbf{u}$ weakly in $L^2([0, T] \times \mathbb{T}^2)$. By Theorem 2.6.1, the associated sequence of vorticities ω^Δ satisfies uniform bounds $\|\omega^\Delta(\cdot, t)\|_{L^1} \leq M$, for all $t \in [0, T]$. By Lemma 2.6.10, we also have uniform equi-integrability. From this, it then follows that the relevant non-linear terms in the incompressible Euler equations converge in the sense of distributions, according to Delort's result (Theorem 2.3.1). Thus, from the weak consistency of the spectral approximation (cp. Theorem 1.4.1), we conclude that $\mathbf{u}^\Delta \rightharpoonup \mathbf{u}$ in L^2 , and that \mathbf{u} is a weak solution of the incompressible Euler equations.

Furthermore, since the non-negative parts $[\omega^\Delta]_+$ are uniformly bounded in $L^1([0, T] \times \mathbb{T}^2)$, we can extract a subsequence of $[\omega^\Delta]_+ dx dt$, converging weakly in the sense of measures to a limiting measure $\omega_+ \geq 0$. Since the sequence $[\omega^\Delta]_+$ is uniformly bounded in $L^\infty([0, T]; L^1(\mathbb{T}^2))$, there exists a constant M , such that for any $t_1 < t_2$, $t_1, t_2 \in [0, T]$:

$$\int_{(t_1, t_2) \times \mathbb{T}^2} d\omega_+ \leq \liminf_{N \rightarrow \infty} \int_{t_1}^{t_2} \int_{\mathbb{T}^2} [\omega^\Delta]_+ dx dt \leq M(t_2 - t_1).$$

In particular, it follows that ω_+ is “absolutely continuous with respect to dt ”, in the sense that we can disintegrate $\omega_+ = \omega_+(\cdot, t) dt$, with $\omega_+(\cdot, t)$ a finite, non-negative measure on \mathbb{T}^2 for $t \in [0, T]$, and for any $f \in C(\mathbb{T}^2)$, the mapping

$$t \mapsto \int_{\mathbb{T}^2} f(x) \omega_+(dx, t)$$

is Lebesgue-measurable.

On the other hand, by the equi-integrability of the negative parts $[\omega^\Delta]_-$, the Dunford-Pettis theorem A.2.2 now implies that the sequence $[\omega^\Delta]_-$ is weakly compact in $L^1([0, T] \times \mathbb{T}^2)$. Furthermore, we again have for any $t_1 < t_2$, with $t_1, t_2 \in [0, T]$:

$$\int_{t_1}^{t_2} \int_{\mathbb{T}^2} [\omega^\Delta]_- dx dt \leq M(t_2 - t_1).$$

Passing to the limit $\Delta \rightarrow 0$ (employing weak compactness, $[\omega^\Delta]_- \rightharpoonup \omega_-$ in L^1 , and possibly after the extraction of a further subsequence), it follows that also

$$\int_{t_1}^{t_2} \int_{\mathbb{T}^2} \omega_- dx dt \leq M(t_2 - t_1).$$

Hence, we conclude that $\int_{\mathbb{T}^2} \omega_-(x, t) dx \leq M$ for almost all $t \in [0, T]$. Since $\omega_- \geq 0$, this implies in particular that $\omega_- \in L^\infty([0, T]; L^1(\mathbb{T}^2))$.

Using finally the uniform a priori bound

$$\|\omega^\Delta(\cdot, t)\|_{H^{-1}} \leq \|\mathbf{u}^\Delta(\cdot, t)\|_{L^2} \leq \|\bar{\mathbf{u}}\|_{L^2},$$

we conclude that the numerical approximation converges to a Delort-type solution with limiting vorticity $\omega(\cdot, t) = \omega_+(\cdot, t) - \omega_-(\cdot, t) \in (\mathcal{M}_+ + L^1) \cap H^{-1}$. \square

2.8 Numerical experiments

In this section, we will present a suite of numerical experiments to illustrate the convergence results proved in the last section. We start with a brief description of some essential details of the implementation of the spectral viscosity method.

2.8.1 Numerical implementation

We adapt the implementation of the spectral viscosity method (2.2.1), based on the the *SPHINX* code, presented in chapter 1.4. We recall that in the *SPHINX* code, the spectral scheme is implemented in the primitive formulation (2.2.1), and remark that in the numerical implementation, the domain has been chosen to be a torus of unit periodicity, $T^2 = [0, 1]^2$, rather than $\mathbb{T}^2 = [0, 2\pi]^2$. Clearly, the results of the previous sections remain true, up to rescaling.

For our simulations, the diffusion parameter ϵ_N in (2.2.1) is chosen to be of the form $\epsilon_N = \epsilon/N_G = \epsilon/(2N)$, where ϵ is a fixed constant and where $N_G = 2N$ denotes the number of grid points $\{x_{i,j}\}_{i,j=1,\dots,N_G}$, in each direction. This scaling for ϵ_N with N_G has been found to be sufficient to cause the required decay of the highest Fourier modes, to ensure vorticity control.

It has been suggested in [Tad89] (in the context of the Burgers equation), that the numerical stability of the SV method is greatly enhanced in practice, if the Fourier coefficients \hat{Q}_k are smooth functions of k . Therefore, for all following simulations carried out with the spectral viscosity method, we have set \hat{Q}_k as a smooth cutoff function of the form

$$\hat{Q}_k = 1 - \exp(-(|k|/k_0)^\alpha),$$

where $k_0 = N/3$ (or $k_0 = N/8$), and $\alpha = 18$. The coefficients \hat{Q}_k so obtained are depicted in Figure 2.1a, as a function of $|k|/N$. We remark that for $|k| = 0.1N$, we have $\hat{Q}_k < 10^{-9}$, whereas for $|k| = 0.4N$, we find $\hat{Q}_k > 1 - 10^{-11}$. For all practical purposes, this implies that $m_N \approx 0.1N$, and that \hat{Q}_k effectively changes from 0 to 1 over the interval $|k| \in [m_N, 4m_N]$ (rather than over the interval $[m_N, 2m_N]$). As has already been noted in Remark 2.2.1, the choice of a factor 2 is not essential for the theoretical results established in the previous sections.

2.8.2 Sinusoidal vortex sheet

In our first numerical experiment, we consider approximations to a vortex sheet, *i.e.* vorticity concentrated along curves in the two-dimensional periodic domain. In particular, we take initial data of the following form,

$$\bar{\omega}(x) := \delta(x - \Gamma) - \int_{T^2} d\Gamma.$$

Note that we have added a second term to ensure that $\int \bar{\omega} dx = 0$. We define the curve Γ as the graph $\Gamma := \{(x_1, x_2) \mid x_1 \in [0, 1], x_2 = d \sin(2\pi x_1)\}$, and we choose $d = 0.2$. We define a mollifier as the following

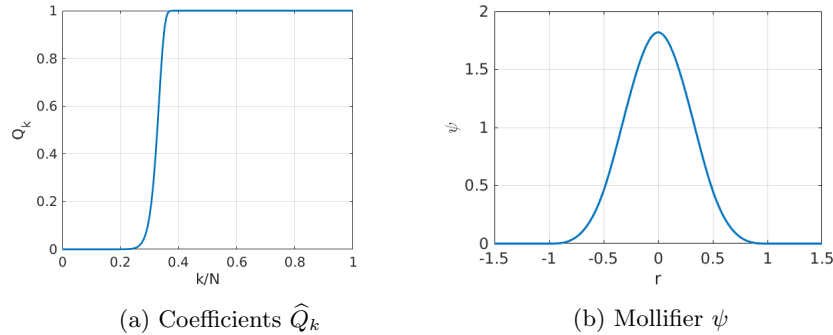


Figure 2.1: Coefficients defining the SV projection (left) and mollifier used in the approximation of the vortex sheet initial data (right).

third order B-spline

$$\psi(r) := \frac{80}{7\pi} \left[(r+1)_+^3 - 4(r+1/2)_+^3 + 6r_+^3 - 4(r-1/2)_+^3 + (r-1)_+^3 \right].$$

The mollifier is depicted in Figure 2.1b. We define $\psi_s(x) := s^{-2}\psi(|x|/s)$. The numerical approximation to the above initial data is obtained by setting

$$\omega^\Delta(x_{i,j}, 0) := (\bar{\omega} * \psi_{\rho_N})(x_{i,j}),$$

where ρ_N determines the thickness (smoothness) of the approximate vortex sheet, and $x_{i,j}$, $i, j \in \{1, \dots, N_G\}$ denote the grid points. The convolution at a point $x \in \mathbb{T}^2$ is computed by numerical quadrature:

$$\begin{aligned} (\bar{\omega} * \psi_{\rho_N})(x) &= \int \psi_{\rho_N}(x - y) d\Gamma(y) \\ &= \int_0^1 \psi_{\rho_N}(x - (\xi, g(\xi))) \sqrt{1 + |g'(\xi)|^2} d\xi \\ &\approx \frac{\rho_N}{M} \sum_{i=-M}^M \psi_{\rho_N}(x - (\xi_i, g(\xi_i))) \sqrt{1 + |g'(\xi_i)|^2}, \end{aligned}$$

with $\xi_i = x^1 + i\rho_N/M$ are equidistant quadrature points in x^1 , and $g(\xi) = d \sin(2\pi\xi)$, $g'(\xi) = 2\pi d \cos(\xi)$. The additional factor $\sqrt{1 + |g'(\xi)|^2}$ is the length element along the graph $\xi \mapsto (\xi, g(\xi))$. For our simulations, we have used $M = 400$.

Smoothed (fat) vortex sheet

First we consider a smoothed vortex sheet, where ρ_N is a fixed constant, independent of N . Consequently, the resulting vorticity is smooth. The initial data (on a sequence of successively finer resolutions) is shown in Figure 2.2. As seen from the figure, we have already resolved the vorticity at 512 grid points (in each direction). Hence, this test case can serve as a benchmark for the performance of the spectral viscosity method when the initial data (and solution) is smooth.

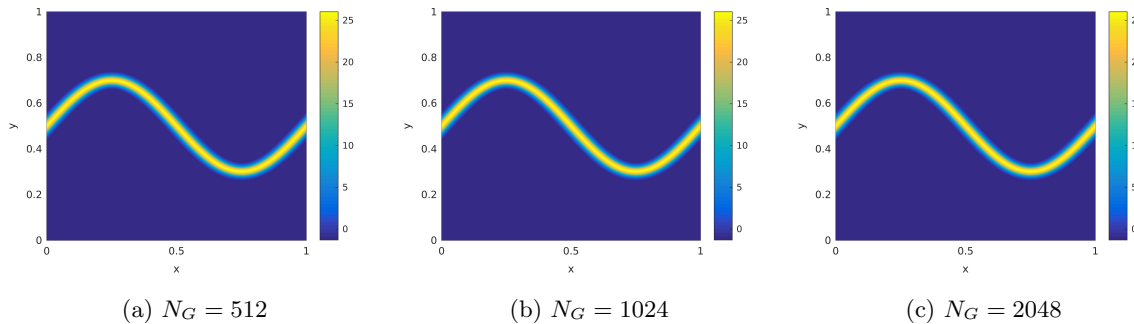


Figure 2.2: Numerical approximation of the initial data (vorticity) for the smoothed (fat) vortex sheet with $\rho_N = 0.05$, at three different spectral resolutions.

We approximate the solution of the two-dimensional Euler equations with this initial data with two variations of the spectral viscosity method. To this end, we first consider the *pure spectral method* by setting $\epsilon = 0$ in (2.2.1). This is justified as the initial data is smooth and the classical convergence theory (see [BT15]) holds for the spectral method, without any added viscosity. In Figure 2.3, we present the evolution of this smoothed vortex sheet over time, at the highest resolution of $N_G = 2048$ grid points in each direction. As seen from this figure, the initial (fat) vortex sheet has started folding by the time $t = 0.4$ and has folded into two distinct vortices at time $t = 0.8$.

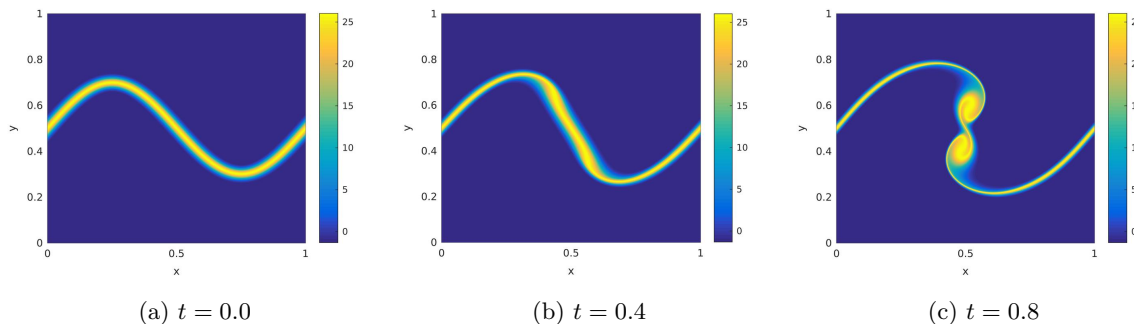


Figure 2.3: Evolution in time for the smoothed vortex sheet with the pure spectral method, *i.e.* $(\epsilon, \rho) = (0, 0.05)$, at the highest resolution of $N_G = 2048$.

The convergence of the pure spectral method in this case is presented in Figure 2.4 where we present the approximated vorticities, at time $t = 1$, on three different levels of resolution. From this figure, we observe that the pure spectral method appears to converge and the vorticity is very well resolved, already at a resolution of $N_G = 512$ grid points in each direction. This convergence can be quantified by computing the following L^2 -error (of the velocity field):

$$E_{N_G}(t) := \|\mathbf{u}_{N_G}(\cdot, t) - \mathbf{u}_{N_{G,\max}}(\cdot, t)\|_{L^2}, \quad (2.8.1)$$

Here, $N_{G,\max} = 2048$ and \mathbf{u}_{N_G} is the velocity field computed at resolution N_G (grid size). In other words, we compute error with respect to a reference solution computed on a very fine grid. This error (as a function of resolution) is plotted in Figure 2.5 (A). We observe from this figure that there is convergence with respect to increasing spectral resolution and the errors are already very low at resolutions

of approximately 512^2 grid points. We further analyze the performance of the numerical method by computing the Fourier energy spectrum of ω^Δ at the highest resolution, which we define by

$$E(\kappa) := \sum_{|k|_\infty = \kappa} |\widehat{\omega}_k|^2. \quad (2.8.2)$$

The spectrum (for three different times) is shown in Figure 2.5 (B) and shows that the bulk of the energy (with respect to the vorticity) is concentrated in the low Fourier modes (large scales). Moreover, this spectrum decays very fast and there is almost no contribution from the high Fourier modes. This is along expected lines as the underlying solution is smooth.

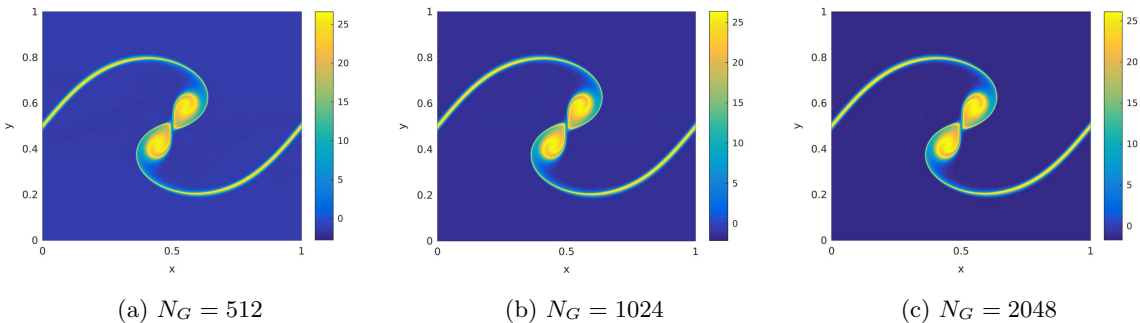


Figure 2.4: Numerical approximations at three different spectral resolutions of the smoothed vortex sheet with the pure spectral method, *i.e.* $(\epsilon, \rho) = (0, 0.05)$, at time $t = 1$

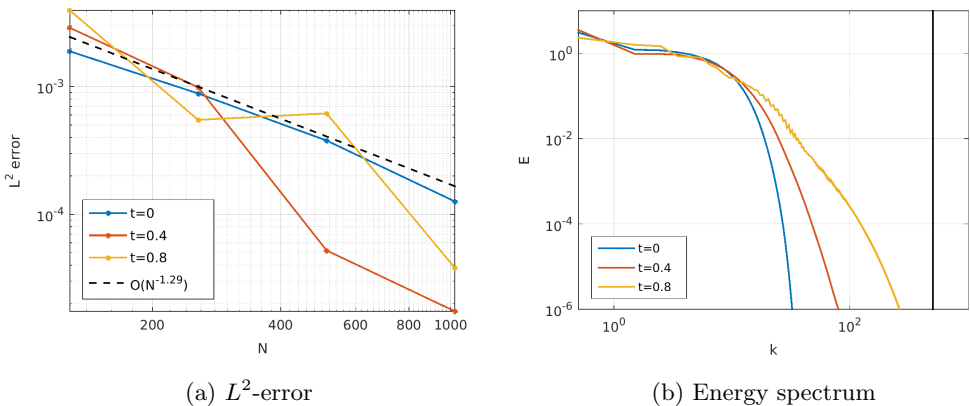


Figure 2.5: Results for the smoothed vortex sheet with the pure spectral method, *i.e.* $(\epsilon, \rho) = (0, 0.05)$ at time $t = 1$. (A): Error of the approximate velocity field (2.8.1) in L^2 (B): Energy spectrum (2.8.2) for the highest resolution of $N_G = 2048$ at different times.

Next, we approximate solutions of the two-dimensional Euler equations with the smoothed vortex sheet initial data, but with a spectral viscosity method, *i.e.* with parameters described at the beginning of this section, in particular with $\epsilon = 0.05$ and the cut-off parameter $k_0 = N/3$. The computed vorticities (for successively refined spectral resolutions) at time $t = 1$ are shown in Figure 2.6. As seen from this figure, the computed vorticities look almost indistinguishable from the vorticities computed with the

pure spectral method (compare with Figure 2.4). This is further corroborated by the computed energy spectrum (2.8.2), shown in Figure 2.7 (B), which is also indistinguishable from the pure spectral case (Figure 2.5(B)). Moreover, we plot the L^2 error of the velocity (2.8.1) in Figure 2.7 (A) and observe that the method converges with increasing resolution. Furthermore, the convergence is cleaner than the one seen for the pure spectral method case (compare Figure 2.7 (A) with Figure 2.5 (A)). This suggests that adding a little bit of viscosity in the higher modes (as we do with the spectral viscosity method) might improve observed convergence, even for underlying smooth solutions.

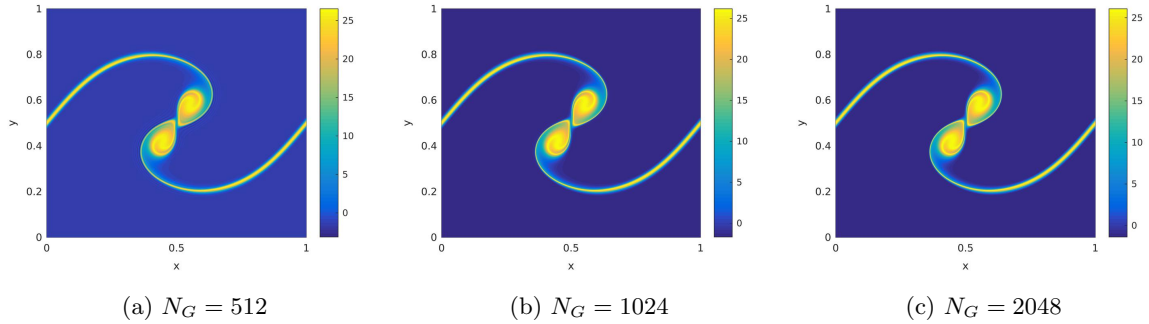


Figure 2.6: Numerical approximations at three different spectral resolutions of the smoothed vortex sheet with the spectral viscosity method, *i.e.* $(\epsilon, \rho) = (0.05, 0.05)$, at time $t = 1$

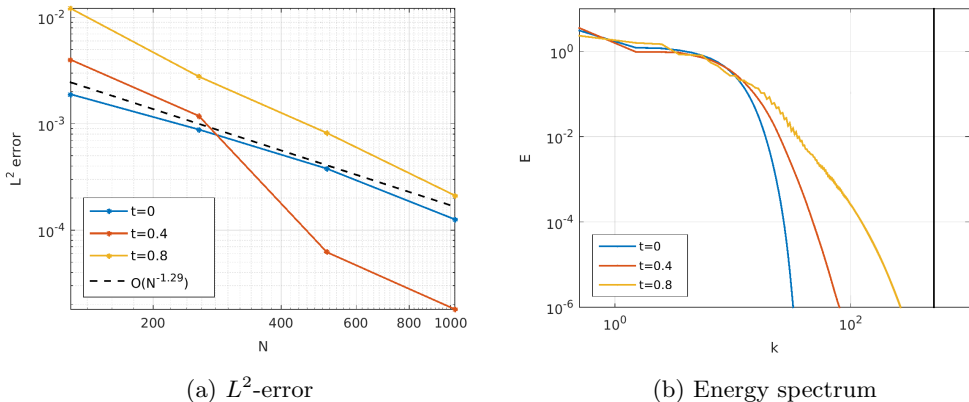


Figure 2.7: Results for the smoothed vortex sheet with the spectral viscosity method, *i.e.* $(\epsilon, \rho) = (0.05, 0.05)$ at time $t = 1$. (A): Error of the approximate velocity field (2.8.1) in L^2 (B): Energy spectrum (2.8.2) for the highest resolution of $N_G = 2048$ at different times.

Singular (thin) vortex sheet

Next, we consider an initial data which belongs to the *Delort class* by setting $\rho_N = \rho/N_G = \rho/(2N)$, where ρ is a fixed constant. In particular, this implies that the vortex sheet becomes *thinner* with increasing resolution, in contrast to the case of the smoothed (fat) vortex sheet (Figure 2.2). This can also be observed from Figure 2.8, where we depict the initial data, for successively increasing resolutions and $\rho = 10$. Moreover, this initial data is *well approximated*, as stipulated by the theory presented in the last section.

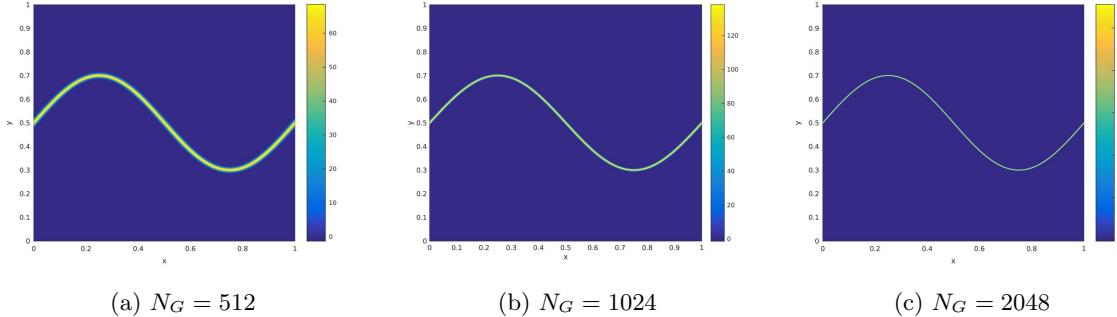


Figure 2.8: Numerical approximation of the initial data (vorticity) for the singular vortex sheet with $\rho_N = 10/N$, at three different spectral resolutions. Compare with the smoothed vortex sheet of Figure 2.2.

It is clear that a pure spectral method will not suffice in this case. In fact, our numerical experiments showed that the pure spectral method was unstable. Hence, we have to use the spectral viscosity method to approximate the solutions in this case. At the first instance, we consider a spectral viscosity method with the parameters, $\theta = 0$ in (2.4.5) and $\epsilon = 0.05$. We remark that this particular case of the spectral viscosity method, corresponds to a *vanishing viscosity* method as a Navier-Stokes type viscous damping is applied to every (even low) Fourier modes, *i.e.* $m_N = 0$ in (2.2.1). Consequently, this method will only be (formally) first-order accurate. On the other hand, it can be expected to more stable than just applying viscous damping to the high Fourier modes. The evolution of the approximate vortex sheet in time, at the highest resolution of $N_G = 2048$ is shown in Figure 2.9.

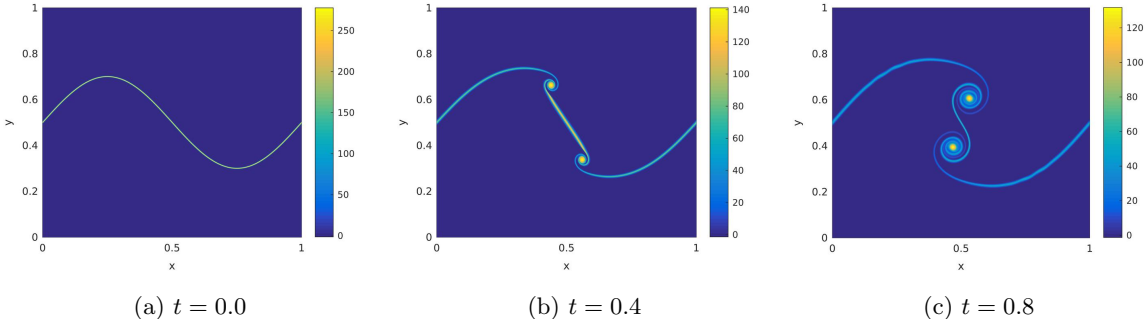


Figure 2.9: Evolution in time for the singular (thin) vortex sheet with the vanishing viscosity method, *i.e.* $(\epsilon, \rho) = (0.05, 10)$, at the highest resolution of $N_G = 2048$.

We observe from this figure that as in the case of the smoothed vortex sheet, the initial vortex sheet rolls up and spirals around two vorticities, but with structures that are considerably thinner than in the case of the smoothed vortex sheet (compare with Figure 2.3).

The convergence of the numerical method is investigated qualitatively in Figure 2.10, where we plot the computed vorticities at time $t = 1$, at three successively finer resolutions and observe convergence as the resolution is increased. However, we do notice that by time $t = 1$, there are small wave like instabilities that are developing along both spiral arms of the rolled up sheet. Nevertheless, these structures do not seem to impede convergence in L^2 norm, which is depicted in Figure 2.11 (A). We also plot the computed spectrum (2.8.2) in Figure 2.11 (B). We see from this figure that the spectrum, even for the initial data,

decays much more slowly with wave number, when compared to the smoothed vortex sheet (Figure 2.5 (B)). Nevertheless, there seems to be enough dissipation in the system to damp the spectrum at high wave numbers and enable a stable computation of the vortex sheet.

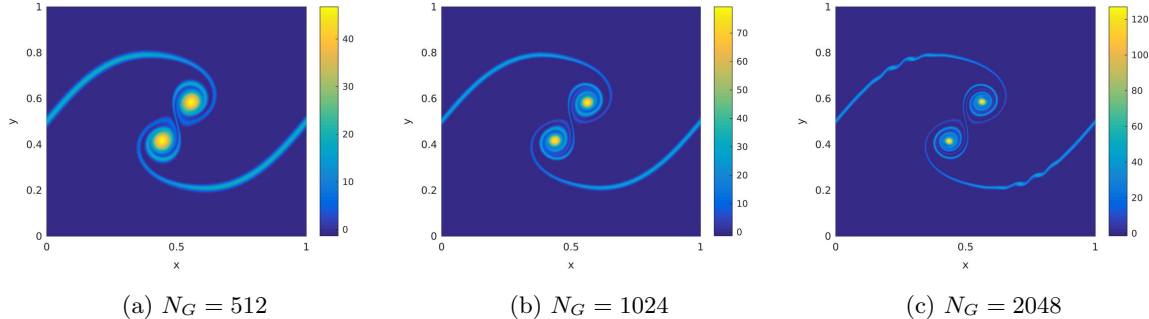


Figure 2.10: Numerical approximations at three different spectral resolutions of the singular vortex sheet with the vanishing viscosity method with $(\epsilon, \rho) = (0.05, 10)$, at time $t = 1$

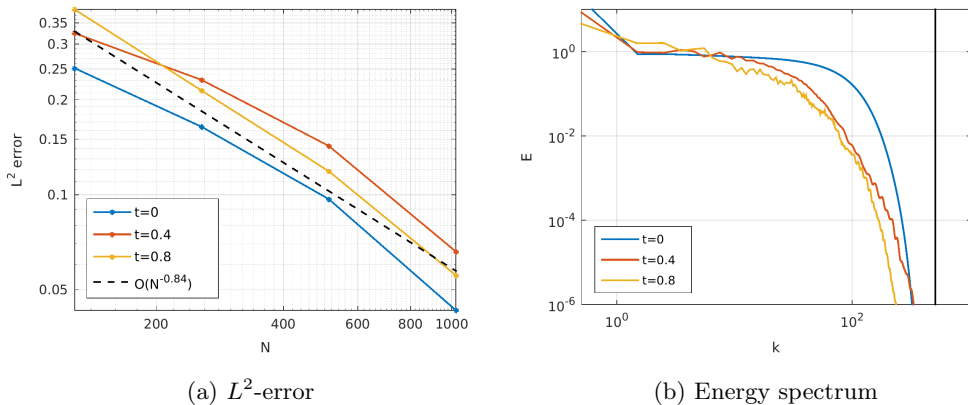


Figure 2.11: Results for the singular (thin) vortex sheet with the vanishing viscosity method, i.e. $(\epsilon, \rho) = (0.05, 10)$ at time $t = 1$. (A): Error of the approximate velocity field (2.8.1) in L^2 (B): Energy spectrum (2.8.2) for the highest resolution of $N_G = 2048$ at different times.

Next, we approximate the singular vortex sheet with a spectral viscosity method, as described in section 2.8.1. As for the smoothed vortex sheet, we consider a cut-off parameter $k_0 = \frac{N}{3}$ and viscosity parameter $\epsilon = 0.05$. The time evolution of the computed vorticity with this scheme is shown in Figure 2.12. In contrast to the situation for the vanishing viscosity method (Figure 2.9), there is a marked appearance of instabilities in the form of small wave like structures along the spiral arms by time $t = 0.4$. By a later time of $t = 0.8$, these structures evolve into a large number of small vortices and the whole sheet breaks up into small scale structures. The spontaneous emergence of these small scale numerical instabilities clearly impedes convergence of this version of the spectral viscosity method. This lack of convergence is seen from Figure 2.13 where plot the approximate vorticities, computed with this spectral viscosity method at time $t = 1$, at three successively finer mesh resolutions. From this figure, we observe that although the computed vortex sheet is stable at a moderate resolution of 512^2 Fourier modes, it

starts becoming unstable at the next level of refinement, *i.e.* $N_G = 1024$, with the appearance of small vortices along the outer spiral arms. These vortices appear to break up into even smaller structures at the finest level of refinement, *i.e.* $N_G = 2048$ and the whole sheet disintegrates into a soup of small incoherent vortices. The lack of convergence (at least at later times) is also observed from Figure 2.14 (A) where we plot the L^2 error (2.8.1), with respect to the velocity field at the finest resolution. Clearly, there is no observed convergence at the time $t = 0.8$. The appearance of structures at small scales can also be inferred from the spectrum (2.8.2), plotted in Figure 2.14 (B). In comparison to the spectrum computed with the vanishing viscosity method (Figure 2.11 (B)), we observe that the spectrum with this spectral viscosity method shows that a non-negligible amount of energy is contained in the small scales (high wave numbers).

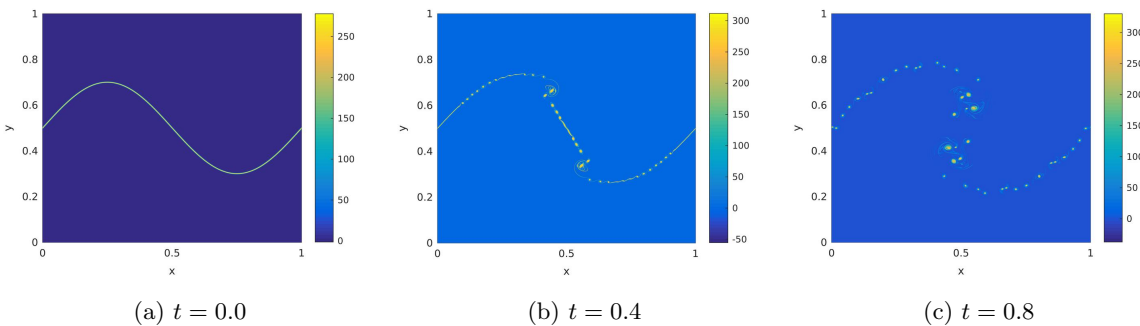


Figure 2.12: Evolution in time for the singular (thin) vortex sheet with the spectral viscosity method, *i.e.* $(\epsilon, \rho, k_0) = (0.05, 10, N/3)$, at the highest resolution of $N_G = 2048$.

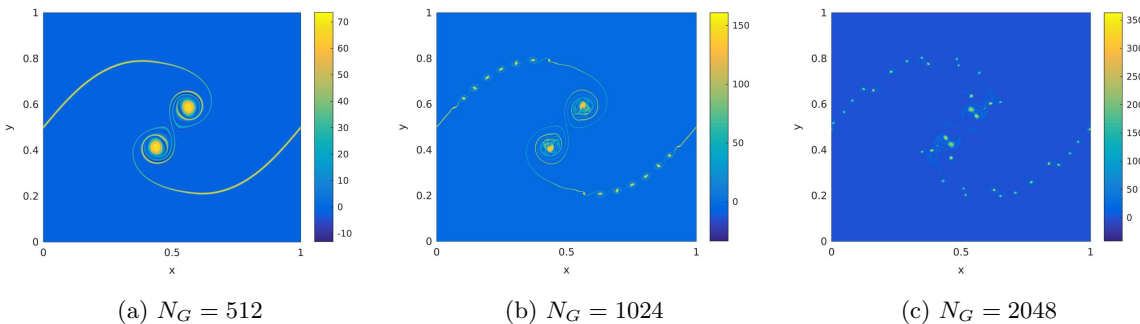


Figure 2.13: Numerical approximations at three different spectral resolutions of the singular vortex sheet with the spectral viscosity method with $(\epsilon, \rho, k_0) = (0.05, 10, N/3)$, at time $t = 1$

These numerical results lead to an interesting dilemma. We have proved in Theorem 2.7.1 that, up to a subsequence, the spectral viscosity method converges as the spectral resolution is increased. On the other hand, we see in this experiment that this method may not converge, at least on moderately long time scales. Is there a way to reconcile these two facts. We argue that there is no contradiction between the theorem and the numerical observations. As it happens, the solutions of the Euler equations with rough initial data are highly unstable [MB01]. In particular, very small differences in the initial data can be amplified by possibly double exponential instabilities that lead to very large separation between the underlying solutions, after even a short period of time. Computations of the Euler equations are

necessarily approximate and it can happen that even small round off errors are amplified in time and yield small scale vortical structures that eventually can lead to the disintegration of the sheet. These instabilities are damped at low to moderate resolutions but will appear at very high resolutions. Moreover, they tend to accumulate in time and only seems to appear at later times.

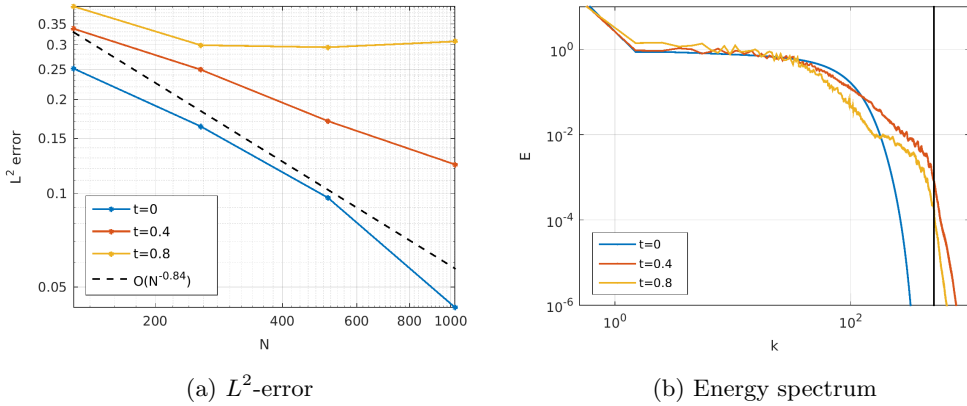


Figure 2.14: Results for the singular (thin) vortex sheet with the with the spectral viscosity method with $(\epsilon, \rho, k_0) = (0.05, 10, N/3)$ at time $t = 1$. (A): Error of the approximate velocity field (2.8.1) in L^2 (B): Energy spectrum (2.8.2) for the highest resolution of $N_G = 2048$ at different times.

It is interesting to contrast the lack of convergence of the spectral viscosity method (Figure 2.14 (A)) with the apparent convergence of the vanishing viscosity method (Figure 2.11 (A)). Clearly the vanishing viscosity method, at least for the parameters considered above, is significantly more dissipative than the spectral viscosity method at the same resolution. This is seen from the computed spectrum (comparing Figure 2.11 (B) and Figure 2.14 (B)) as we observe that the vanishing viscosity method damps the small scale instabilities and prevents the transfer of energy into the smallest scales. However, the amount of viscosity is $\epsilon_N = \frac{\epsilon}{N}$. Thus, increasing the resolution further with the vanishing viscosity method can reduce the viscous damping and possibly to the instabilities building up and leading to the disintegration of the sheet. Given that it is unfeasible to increase the resolution beyond $N_G = 2048$, we mimic this possible behavior by reducing the constant to $\epsilon = 0.01$ in the vanishing viscosity method. The resulting approximate vorticities at time $t = 1$, for three different resolutions is shown in Figure 2.15. We observe from this figure that the results are very similar to the spectral viscosity method (compare with Figure 2.13) and the sheet disintegrates into a soup of small vortices at the highest resolution. Consequently, there is no convergence of the velocity in L^2 as seen from Figure 2.16 (A) and the spectrum shows that more energy is transferred to the smallest scales now than it was when $\epsilon = 0.05$ (compare with Figure 2.11 (B)).

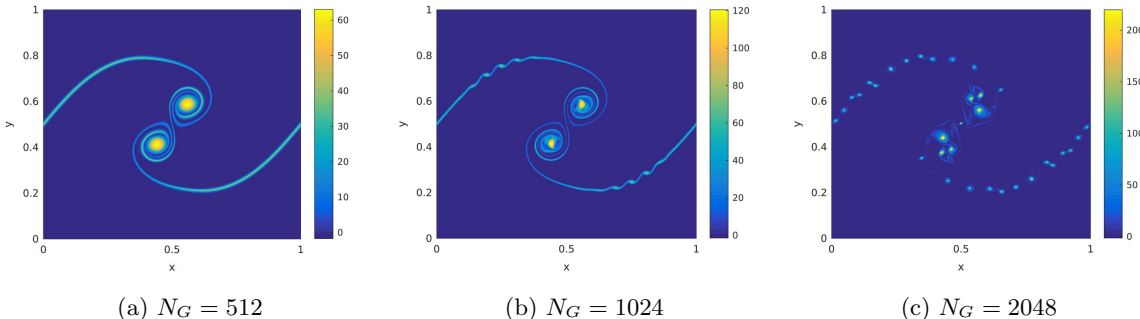


Figure 2.15: Numerical approximations at three different spectral resolutions of the singular vortex sheet with the vanishing viscosity method with $(\epsilon, \rho) = (0.01, 10)$, at time $t = 1$

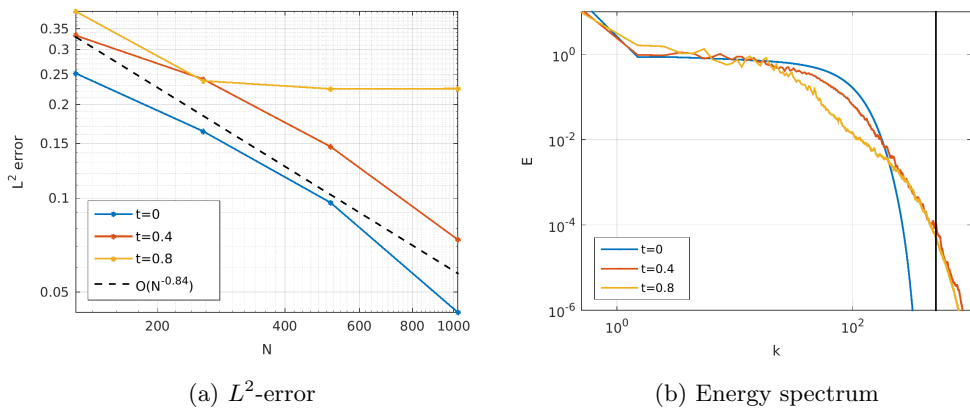


Figure 2.16: Results for the singular (thin) vortex sheet with the vanishing viscosity method *i.e.* $(\epsilon, \rho) = (0.01, 10)$ at time $t = 1$. (A): Error of the approximate velocity field (2.8.1) in L^2 (B): Energy spectrum (2.8.2) for the highest resolution of $N_G = 2048$ at different times.

The lack of convergence of computations of singular vortex sheets, on account of the formation and amplification of small scale instabilities, is well known and can be traced back to the pioneering work of Krasny [Kra86b, Kra86a] and reference therein. In those papers, the author computed singular vortex sheets by solving the Birkhoff-Rott equations of vortex dynamics and was able to ensure stable computation by controlling the round-off errors with an adaptive increase of the arithmetic precision of the computation. We believe that this fix is only relevant for a few levels of increasing resolution and ultimately at very high resolutions, the vortex sheet will disintegrate into smaller vortices. This is already evidenced by our computations at different resolutions, at different times and with different values of the viscosity parameter ϵ . Paraphrasing [MB01], the phenomenon of the exponential growth of small instabilities ‘is a feature of the underlying equation itself as opposed to an instability of the numerical method.’

2.9 Discussion

In this chapter, we have considered the two-dimensional incompressible Euler equations. In contrast to the three-dimensional case, global well-posedness results are available in two space dimensions. In particular, existence and uniqueness of weak solutions can be proved under the assumption that the initial vorticity is in L^∞ . Moreover, global (in time) existence of weak solutions is proved for significantly less regular initial data, for instance when the initial vorticity belongs to the so-called *Delort class*. Such rough initial data are encountered in practice when one considers the evolution of vortex sheets in an ideal fluid.

Although many different numerical methods have been developed to approximate the incompressible Euler equations, convergence results for these schemes have mostly been available in the regime where the initial data and the underlying solutions were smooth. Notable exceptions were considered in [LT97] and [LFNL00], where the authors prove convergence of central finite difference schemes for the vorticity formulation of the equations under the assumption that the initial vorticity is in L^p , for $1 < p \leq \infty$, and more generally if the vorticity belongs to a rearrangement invariant space that is compactly supported in H^{-1} . For vortex methods [LX95, Sch96, LX01], convergence is known when the initial vorticity is a bounded measure of definite sign, or if the vorticity is in $L(\log L)$ without any sign restriction. However, no rigorous convergence results are available for the case of Delort class initial data. Thus, there has so far remained a considerable gap between the mathematical existence results and rigorous convergence results for numerical approximations.

In this chapter, based on the original publication [LM20], we have proposed a *spectral viscosity* method to approximate the two-dimensional Euler equations. Based on the spectral viscosity framework of Tadmor [Tad89] and references therein, our method is a spectral method that discretizes the Euler equations in Fourier space. Viscosity (damping) is only added in the high wave-number Fourier modes. Consequently, the method is formally spectrally (superpolynomially) accurate for smooth solutions. Until now, convergence of this method was only proved for smooth solutions of the incompressible Euler equations [BT15].

We prove that the spectral viscosity method converges to a weak solution as long as the initial data belongs to the Delort class. This also closes the gap between available existence results for the underlying PDE and convergence results for numerical approximation.

The proof relies on the following key ingredients:

- The equivalence of the spectral viscosity method for the velocity-pressure formulation (2.2.1) and the vorticity formulation (2.2.5). This equivalence holds for any resolution *i.e.* truncation of the underlying Fourier expansion.
- A spectral decay estimate for the high wave-number modes.
- A patching up of long-time estimates on the vorticity (obtained by the spectral decay estimate) and short-time estimates.
- A novel approximation of rough initial data that amounts to resolving the initial singularities.
- Application of the compensated compactness theorems of Delort by controlling the negative part of the approximated vorticity. In particular, we ensure that the negative part of the vorticity, as approximated by the spectral viscosity method, cannot concentrate on sets of small measure.

It is unclear if these ingredients, particularly the equivalence between the velocity-pressure and vorticity formulations, can be transferred to other numerical methods. Thus, for the time being, the spectral viscosity method is the only method that can rigorously be proved to converge to weak solutions for the

incompressible Euler equations with rough initial data. As the results summarized in this chapter are based on a spectral Fourier expansion, they are inherently limited to the periodic case. It is not clear, whether the method can be extended to other boundary conditions, and in particular to schemes providing numerical approximations of flows in the whole plane. Furthermore, due to the lack of theoretical existence results on domains with boundary, a convergence proof on such domains appears to be out of reach at present.

We also present representative numerical experiments to test the proposed spectral viscosity method. We observe from the experiments that the spectral viscosity method performs as well as the pure (standard) spectral method for smooth initial data. We also computed vortex sheets with the spectral and vanishing viscosity methods and observed convergence to complicated roll-ups of the sheet, particularly for small times. However for very high spectral resolutions and for long times, the computed solutions contained small scale instabilities that amplified (either with time or in resolution or both) and led to the disintegration of the vortex sheet into a soup of small vortices. We argue that this phenomena is generic to such rough data and cannot be alleviated at the level of numerical computations, particularly at very high resolutions. On the other hand, many papers in recent years such as [FMT16, LM15, Leo18] and references therein, have presented computations of vortex sheets and demonstrated that although each deterministic simulation can be unstable, yet statistical quantities (ensemble averages) are computed robustly. This implies that statistical notions of solutions such as dissipative measure-valued solutions [DM87a, LM15, FMT16] and the more recent statistical solutions [FLM17, FW18, LMPP21b] might be more appropriate as a solution framework for the incompressible Euler equations, certainly from the perspective of numerical approximation. The concept of *statistical solutions* of the incompressible Euler equations will be discussed in detail in the next chapter.

Chapter 3

Statistical solutions

3.1 Introduction

In the last chapter, we have seen that convergence results for carefully designed numerical schemes such as the spectral viscosity scheme can be obtained for the two-dimensional incompressible Euler equations, even for rough initial data such as signed vortex sheets (*i.e.* with distinguished sign). These convergence results are a precise analogue of the available analytic existence theory, providing sufficient control on the numerical approximate solution sequence to ensure that any limit of this sequence is a weak solution of the incompressible Euler equations, and satisfying all known natural a priori bounds. However, even in the two-dimensional case, the available existence theory does not include many flows of interest, such as *unsigned* vortex sheets, *i.e.* vortex sheets with varying sign of the vorticity, or even rougher initial data such as L^2 -energy admissible $\bar{\mathbf{u}}$ which are only Hölder continuous. Available existence results for rough solutions also do not extend to the three-dimensional case, since the vorticity equation includes a vortex-stretching term which cannot be controlled (cf. chapter 1.3.2), and therefore a priori bounds on the vorticity are no longer available. Furthermore, as seen in the numerical experiments of the last chapter, even when rigorous convergence (or rather, compensated compactness) results *are* available, this does not necessarily mean that *strong* convergence (in L^2) of the numerically computed solutions is observed upon mesh refinement. In fact, numerical experiments considering irregular initial data have found a *lack of convergence* of numerical schemes in any conventional, deterministic sense. Similar results have also been found for compressible, inviscid models such as the compressible Euler equations and other hyperbolic conservation laws [FKMT17, FLMW20]. This lack of convergence can be generally attributed to the appearance of additional small-scale instabilities, which are revealed only upon an increase of the numerical resolution, and which prevent convergence in the limit. Closely related to this non-convergence of numerical schemes is the lack of general stability and uniqueness estimates for weak solutions, strongly indicating that the underlying issues are not only related to numerical discretization errors, but may represent a more fundamental feature of inviscid, turbulent models such as the incompressible Euler equations. In the present chapter, we will therefore go beyond the classical paradigm of deterministic weak solutions, formalizing and investigating a *statistical* solution concept for the incompressible Euler equations, following similar work in [FLM17] in the context of hyperbolic conservation laws and a related formulation [FW18] in the context of the incompressible Euler equations. The present chapter will follow the original publication [LMPP21b].

3.1.1 Measure-valued and statistical solutions

Given the lack of well-posedness results for weak solutions and the lack of convergent numerical approximations, there is considerable scope for the design of alternative solution frameworks for (1.1.1). One such framework is that of measure-valued solutions [DM87b], where the sought for solutions are no longer functions but space-time parameterized probability measures on state space. The global existence of measure-valued solutions, even in three space dimensions, was shown in [DM87b] and has been reviewed in chapter 1.3.3 of the present thesis (cf. Theorem 1.3.10). A convergent numerical method (of the spectral viscosity type) and an efficient algorithm to compute measure-valued solutions was proposed in [LM15]. However, measure-valued solutions are generically non-unique. This holds true even for the much simpler case of the one-dimensional Burgers equation [Sch90]. In [FLM17], the authors implicated the lack of information about multi-point (spatial) correlations in the non-uniqueness of measure-valued solutions. Moreover, they also proposed a framework of *statistical solutions* as an attempt to recover uniqueness.

In the formulation of [FLM17], statistical solutions are time-parameterized probability measures on L^p , for $1 \leq p < \infty$, that are consistent with the underlying PDE in a weak sense. They were shown to be equivalent to a family of *correlation measures*, where the k -th member of this family is a Young measure representing correlations (or joint probabilities) of the solution at k distinct spatial points. Thus, one can interpret statistical solutions as measure-valued solutions, augmented with information about all possible multi-point correlations. The consideration of multi-point statistics is one of the main differences of the present work with earlier contributions such as [LM15], which focused on the computation of a measure-valued solution, *i.e.* single-point statistics. A priori, statistical solutions contain much more information than measure-valued solutions. Moreover, statistical solutions encode statistical (ensemble averaged) properties of the solutions of the underlying PDE. Thus, statistical solutions provide a suitable framework for uncertainty quantification (UQ) [FLM17, AM18]. This is particularly relevant for the incompressible Euler equations as it is well-known that the flow of fluids, at very high-Reynolds numbers, can be turbulent and only averaged (or statistical) properties can be inferred from measurements [Fri95].

Statistical solutions for scalar conservation laws were considered in [FLM17], wherein well-posedness was shown under an entropy condition. In particular, information about infinitely many correlations was necessary to ensure uniqueness. In [FLM18, FLMW20], a Monte Carlo algorithm, based on the ensemble averaging algorithm of [FKMT17], was proposed and analyzed for scalar conservation laws and multi-dimensional hyperbolic systems of conservation laws, respectively. In contrast to [FLMW20] where multi-dimensional hyperbolic systems of conservation laws were considered, we focus on the case of incompressible Euler equations in this chapter.

Independent notions of statistical solutions of the incompressible Navier-Stokes equations have been proposed in [FRT10] and in [VF77]. While the statistical solutions of Foias, Rosa and Temam [FRT10] are formulated in terms of the evolution equations of integrals of functionals $\int_H \Phi(\mathbf{u}) d\mu_t(\mathbf{u})$ on a suitable Hilbert space H , the statistical solutions in the present work are formulated in terms of an infinite family of PDEs for the multi-point correlation measures $\nu_{t,x_1,\dots,x_k}^k(\xi_1, \dots, \xi_k)$. These correlation measures encode the probability of the flow field $\mathbf{u}(t, x)$ attaining certain values at points x_1, \dots, x_k and time t , *i.e.* one might informally write

$$\nu_{t,x_1,\dots,x_k}^k(\xi_1, \dots, \xi_k) = \text{Prob} [\mathbf{u}(x_1, t) = \xi_1, \dots, \mathbf{u}(x_k, t) = \xi_k].$$

Despite the apparent differences between the current work and [FRT10], the two approaches can be related to each other, using the correspondence between multi-point correlation measures and infinite-dimensional measures established in [FLM17].

3.1.2 Overview of this chapter

The main goal of this chapter is to review a statistical solution concept for the incompressible Euler equations (1.1.1) introduced in [LMPP21b], where a notion of dissipative statistical solutions was proposed. Statistical solutions are formulated as a time-parameterized probability measure on $L^2(D; \mathbb{R}^d)$ on the underlying domain D , whose k -point correlations are consistent with the incompressible Euler equations in a suitable sense. Well-posedness of such dissipative statistical solutions can be proven in special cases, including short-time well-posedness results and global well-posedness results for sufficiently regular initial data in two spatial dimensions. This chapter will also review a numerical algorithm, based on Monte-Carlo ensemble averaging and the spectral viscosity discretization, to approximate statistical solutions, showing that the approximations converge in an appropriate topology to a statistical solution, under reasonable and verifiable hypotheses on the numerical method. A selection of numerical experiments will be used to illustrate interesting properties of the computed statistical solutions and to verify the theory. For further numerical experiments, the interested reader is referred to the original publication [LMPP21b].

The rest of this chapter is organized as follows: in section 3.2, we present time-parameterized probability measures on $L^2(D; \mathbb{R}^d)$ and characterize convergence in a suitable topology on this space of measures. In section 3.3, we define statistical solutions of (1.1.1) and present partial well-posedness results. The numerical approximation of statistical solutions and its convergence is presented in section 3.4 and numerical experiments are summarized in section 3.5.

3.2 Time-Parameterized Probability Measures on $L^2(D; \mathbb{R}^d)$

As mentioned in the introduction, statistical solutions are time-parameterized probability measures on L^2 , where L^2 energy bound is enforced by the incompressible Euler equations. In this section, we will describe time-parameterized probability measures, characterize them and describe a suitable topology on them. Although different in several details, similar considerations have previously appeared in different contexts in [FLM17, FLMW20]. To streamline our discussion we will merely state the core results in this section, and provide the main ideas of the proofs where appropriate. Complete and detailed proofs of these results can be found in the publication [LMPP21b], on which this chapter is based.

Given a (Borel) probability measure $\mu \in \mathcal{P}(L_x^2)$ on L_x^2 , we define the *2nd order structure function* as the following quantity:

$$S_2(\mu; r) := \left(\int_{L_x^2} \int_D \int_{B_r(0)} |\mathbf{u}(x+h) - \mathbf{u}(x)|^2 dh dx d\mu(\mathbf{u}) \right)^{1/2}. \quad (3.2.1)$$

The structure function $S_2(\mu; r)$ provides a measure of the average two-point correlation of the underlying functions, a quantity that is natural to consider in the context of turbulent flows [Fri95]. The following results shows that structure functions are also closely related compactness of probability measures in $\mathcal{P}(L_x^2)$:

Theorem 3.2.1. *Let $\mathcal{F} \subset \mathcal{P}(L_x^2)$ be a family of probability measures on L_x^2 . Assume that there exists $M > 0$, such that $\mu(B_M(0)) = 1$ for all $\mu \in \mathcal{F}$, where $B_M(0) = \{\mathbf{u} \in L_x^2 \mid \|\mathbf{u}\|_{L_x^2} < M\}$. Then the following statements are equivalent:*

- (i) $\mathcal{F} \subset L_x^2$ has compact closure (with respect to the weak topology),
- (ii) There exists a modulus of continuity ϕ , such that we have a uniform bound on the structure function:

$$S_2(\mu; r) \leq \phi(r), \quad \forall \mu \in \mathcal{F}.$$

The proof of this theorem can be found in [LMPP21b, Appendix A]. Rather than discussing the details of the proof, we point out that uniform bounds on the structure function are precisely a probabilistic version of the equicontinuity property of Kolmogorov's compactness theorem on L^p spaces, and hence this result may not be unexpected, see also the next remark.

Remark 3.2.2. *Theorem 3.2.1 is closely related to Kolmogorov's characterization of compact subset of L_x^2 : Indeed, there is a natural isometric embedding*

$$(L_x^2, \|\cdot\|_{L_x^2}) \hookrightarrow (\mathcal{P}_1(L_x^2), W_1), \quad u \mapsto \delta_u.$$

Thus, a bounded set $K \subset L_x^2$ has compact closure if, and only if, its image under this embedding $\{\delta_u \mid u \in K\} \subset \mathcal{P}(L_x^2)$ has compact closure. Using Theorem 3.2.1, we conclude that a bounded set $K \subset L_x^2$ has compact closure if, and only if, satisfies Kolmogorov's equicontinuity property, which corresponds to property (2) in Theorem 3.2.1.

3.2.1 Time parameterized probability measures

As mentioned before, statistical solutions are time-parameterized probability measures, in the sense of the following definition:

Definition 3.2.3. We denote by $L_t^1(\mathcal{P}) = L^1([0, T]; \mathcal{P})$ the space of weak-* measurable mappings $[0, T] \rightarrow \mathcal{P}(L_x^2)$, namely mappings $t \mapsto \mu_t$ such $t \mapsto \int_{L_x^2} F(\mathbf{u}) d\mu_t(\mathbf{u})$ is measurable for a.e $t \in [0, T]$, for all $F \in C_b(L_x^2)$ and with the property that

$$\int_0^T \int_{L_x^2} \|\mathbf{u}\|_{L_x^2} d\mu_t(\mathbf{u}) dt < \infty.$$

Denoting by δ_0 the Dirac measure concentrated on $0 \in L_x^2$, the above condition can equivalently be written as

$$\int_0^T W_1(\delta_0, \mu_t) dt < \infty.$$

This leads us to define a natural metric on $L^1([0, T]; \mathcal{P})$ by

$$d_T(\mu_t, \nu_t) := \int_0^T W_1(\mu_t, \nu_t) dt. \tag{3.2.2}$$

We then have the following proposition, whose proof is presented in [LMPP21b, Appendix B], closely mimicking the proof of completeness of L^p -spaces found in many textbooks on measure-theory.

Proposition 3.2.4. *The metric space $(L_t^1(\mathcal{P}), d_T)$ is a complete metric space.*

Our next objective is to find natural sufficient conditions for compactness on $L_t^1(\mathcal{P})$. To this end, it would be natural to extend the compactness Theorem 3.2.1 to time-parameterized probability measures and find a suitable version of the weak topology. This necessitates formalizing some notion of time-continuity or time-regularity of underlying functions.

Fix a (time-independent) divergence-free test function $\varphi \in C_c^\infty(D; \mathbb{R}^d)$. Formally, solutions of the incompressible Euler equations (1.1.1) satisfy for $s, t \in [0, T]$,

$$\int_D [\mathbf{u}(x, t) - \mathbf{u}(x, s)] \cdot \varphi(x) dx = \int_s^t \int_D \mathbf{u}(x, \tau) \otimes \mathbf{u}(x, \tau) : \nabla \varphi(x) dx d\tau,$$

so that

$$\left| \int_D [\mathbf{u}(x, t) - \mathbf{u}(x, s)] \cdot \varphi(x) dx \right| \leq C \|\mathbf{u}\|_{L_t^\infty L_x^2} \|\nabla \varphi\|_{L_x^\infty} |t - s|.$$

Furthermore, we have a natural energy bound $\|\mathbf{u}\|_{L_t^\infty L_x^2} \leq \|\bar{\mathbf{u}}\|_{L_x^2}$, in terms of the initial data $\bar{\mathbf{u}}$. If $L > 0$ is large enough such that by Sobolev embedding $H_x^L = H^L(D; \mathbb{R}^d) \hookrightarrow C^1(D; \mathbb{R}^d)$, then it follows that

$$\left| \int_D [\mathbf{u}(x, t) - \mathbf{u}(x, s)] \cdot \varphi(x) dx \right| \leq C \|\varphi\|_{H_x^L} |t - s|,$$

where the constant $C > 0$ depends only on the initial data. Taking the supremum over all $\varphi \in H_x^L$ with $\|\varphi\|_{H_x^L} \leq 1$, it follows, at least formally, that

$$\|\mathbf{u}(t) - \mathbf{u}(s)\|_{H_x^{-L}} \leq C|t - s|, \quad \forall s, t \in [0, T]. \quad (3.2.3)$$

Given these considerations, it is natural to assume that statistical solutions of the Euler equations satisfy some version of this time continuity. A formalization is provided in the following definition,

Definition 3.2.5. *A weak-* measurable, time-parameterized probability measure $t \mapsto \mu_t \in \mathcal{P}(L_x^2)$ is called **time-regular**, if there exists a constant $L > 0$, and a mapping $s, t \mapsto \pi_{s,t} \in \mathcal{P}(L_x^2 \times L_x^2)$, such that for almost all $s, t \in [0, T]$:*

- *The measure $\pi_{s,t}$ is a transport plan from μ_s to μ_t ,*
- *There exists a constant $C > 0$, such that $\pi_{s,t}$ satisfies the following regularity condition*

$$\int_{L_x^2 \times L_x^2} \|\mathbf{u} - \mathbf{v}\|_{H_x^{-L}} d\pi_{s,t}(\mathbf{u}, \mathbf{v}) \leq C|t - s|.$$

*A family $\{\mu_t^\Delta\}_{\Delta>0}$ of time-parameterized probability measures is **uniformly time-regular**, provided that each μ_t^Δ is time-regular, and the constants $L, C > 0$ above can be chosen independently of $\Delta > 0$.*

Remark 3.2.6. Note that if μ_t is of the form

$$\mu_t = \frac{1}{J} \sum_{j=1}^J \delta_{\mathbf{u}_j(t)},$$

with $t \mapsto \mathbf{u}(t)$ weak solutions of the incompressible Euler equations satisfying (3.2.3), then we can define suitable transfer plans

$$\pi_{s,t} = \frac{1}{J} \sum_{j=1}^J \delta_{\mathbf{u}_j(s)} \otimes \delta_{\mathbf{u}_j(t)}.$$

The time-regularity property follows from the estimate (3.2.3) for the \mathbf{u}_j (cp. also the definition of an approximate solution sequence, Definition 1.3.5 in chapter 1).

We now show that a family μ_t^Δ , $\Delta > 0$, of uniformly time-regular probability measures is relatively compact, provided that they satisfy a time-averaged version of the second property of Theorem 3.2.1. To this end, we define the time-averaged structure function of $(t \mapsto \mu_t) \in L_t^1(\mathcal{P})$ (weak-* measurable) as the following quantity (where the value ∞ is allowed):

$$S_2^T(\mu_t; r) := \left(\int_0^T \int_{L_x^2} \int_D \int_{B_r(0)} |\mathbf{u}(x+h) - \mathbf{u}(x)|^2 dh dx d\mu_t(\mathbf{u}) dt \right)^{1/2}. \quad (3.2.4)$$

The main result of the present section is the following compactness result:

Theorem 3.2.7. Let $\mu_t^\Delta \in L_t^1(\mathcal{P})$ be a family of uniformly time-regular probability measures, for $\Delta > 0$, for which there exists $M > 0$, such that $\mu_t^\Delta(B_M(0)) = 1$ for all $\Delta > 0$, a.e. $t \in [0, T]$. Here $B_M(0) := \{\|\mathbf{u}\|_{L_x^2} < M\}$. If there exists a modulus of continuity $\phi(r)$ such that

$$S_2^T(\mu_t^\Delta; r) \leq \phi(r), \quad \forall \Delta > 0,$$

then μ_t^Δ is relatively compact in $L_t^1(\mathcal{P})$.

The idea behind Theorem 3.2.7 is to use the spatial regularity of the sequence to show that the weak time-regularity assumption of Definition 3.2.5 implies a similar time-regularity with respect to a stronger spatial norm, where H^{-L} is replaced by L^2 . The details of the required technical argument are provided in [LMPP21b, Appendix C], and utilize ideas of the folklore Aubin-Lions lemma and the characterization of compact subsets in Bochner spaces of [Sim86]. Rather than repeating the lengthy technical argument in this thesis, we will illustrate the main ideas at the deterministic level in the next remark:

Remark 3.2.8 (Leveraging time-regularity). Suppose we are given a bounded family of functions $\mathbf{u} \in \mathcal{F} \subset L_{x,t}^2(D \times [0, T])$, which satisfies a uniform Lipschitz bound $\sup_{\mathbf{u} \in \mathcal{F}} \|\mathbf{u}(\cdot, t) - \mathbf{u}(\cdot, s)\|_{H_x^{-L}} \leq C|s-t|$ for some (large) $L > 0$. Assume, in addition, that there exist $M, \delta > 0$, such that $\int_0^T \|\mathbf{u}(\cdot, t)\|_{H_x^\delta}^2 dt \leq M$. Note that the latter condition is a simple way to ensure uniform control $\sup_{\mathbf{u} \in \mathcal{F}} S_2(\mathbf{u}; r) \leq Mr^\delta$, on the structure functions (here, this stronger condition is assumed to simplify the argument). Then, using the interpolation inequality between H_x^{-L} and H_x^δ , it follows that

$$\|\mathbf{u}(\cdot, t) - \mathbf{u}(\cdot, s)\|_{L_x^2} \leq \|\mathbf{u}(\cdot, t) - \mathbf{u}(\cdot, s)\|_{H_x^{-L}}^\theta \|\mathbf{u}(\cdot, t) - \mathbf{u}(\cdot, s)\|_{H_x^\delta}^{1-\theta},$$

where $\theta = \delta/(L + \delta) \in (0, 1)$ is chosen such that $-\theta L + (1 - \theta)\delta = 0$. This implies that for any (small) $h > 0$, we have

$$\begin{aligned} \int_0^{T-h} \|\mathbf{u}(\cdot, t+h) - \mathbf{u}(\cdot, t)\|_{L_x^2}^2 dt &\stackrel{(Interpol.)}{\leq} (C|h|)^\theta \int_0^{T-h} \|\mathbf{u}(\cdot, t+h) - \mathbf{u}(\cdot, t)\|_{H_x^\delta}^{1-\theta} dt \\ &\stackrel{(Hölder)}{\leq} C^\theta T^{(1+\theta)/2} |h|^\theta \left(\int_0^{T-h} \|\mathbf{u}(\cdot, t+h) - \mathbf{u}(\cdot, t)\|_{H_x^\delta}^2 dt \right)^{(1-\theta)/2} \\ &\stackrel{(H^\delta\text{-bound})}{\leq} C^\theta T^{(1+\theta)/2} (2M)^{(1-\theta)/2} |h|^\theta. \end{aligned}$$

In particular, this shows that $\sup_{\mathbf{u} \in \mathcal{F}} \int_0^{T-h} \|\mathbf{u}(\cdot, t+h) - \mathbf{u}(\cdot, t)\|_{L_x^2}^2 dt \lesssim |h|^\theta$, and hence \mathcal{F} satisfies a temporal equi-integrability condition in $L_{t,x}^2$, in addition to the spatial equi-integrability ensured by the H_x^δ -bound. From this, it immediately follows that $\mathcal{F} \subset L_{t,x}^2$ is relatively compact [Sim86]. The proof of Theorem 3.2.7 relies on the same basic ideas, but requires several additional technical ingredients, and an extension to the statistical context. We refer the interested reader to [LMPP21b, Appendix C] for the details of the required argument.

Let us also remark that a limit $\mu_t^\Delta \rightarrow \mu_t$ of a uniformly time-regular sequence μ_t^Δ is itself time-regular (see [LMPP21b, Appendix D] for the straight-forward proof):

Proposition 3.2.9. Let $\mu_t^\Delta \in L_t^1(\mathcal{P})$ be a family of uniformly time-regular probability measures, for $\Delta > 0$. And such that there exists $M > 0$ with $\mu_t^\Delta(B_M(0)) = 1$ for all $\Delta > 0$, a.e. $t \in [0, T]$, where $B_M(0) := \{\|\mathbf{u}\|_{L_x^2} < M\}$. If $\mu_t^\Delta \rightarrow \mu_t$ in $L_t^1(\mathcal{P})$, then μ_t is time-regular in the sense of Definition 3.2.5, with the same time-regularity constants $C, L > 0$ as for the family μ_t^Δ .

3.2.2 Time-dependent correlation measures and their compactness

It has been shown in [FLM17] that there is a one-to-one correspondence between probability measures on L_x^2 and so-called correlation measures. Correlation measures are defined as infinite hierarchies of Young measures, taking into account spatial correlations, or more precisely,

Definition 3.2.10. A **correlation measure** is a collection $\boldsymbol{\nu} = (\nu^1, \nu^2, \dots)$ of maps $\nu^k : D^k \rightarrow \mathcal{P}(U^k)$, where $U = \mathbb{R}^d$ denotes the state-space, satisfying the following properties:

1. *Weak-* measurability:* Each map $\nu^k : D^k \rightarrow \mathcal{P}(U^k)$ is weak-* measurable, in the sense that the map $x \mapsto \langle \nu_x^k, f \rangle$ from $x \in D^k$ into \mathbb{R} is Borel measurable for all $f \in C_0(U^k)$ and $k \in \mathbb{N}$. In other words, ν^k is a Young measure from D^k to U^k .
2. *L^2 -boundedness:* $\boldsymbol{\nu}$ is L^2 -bounded, in the sense that

$$\int_D \langle \nu_x^1, |\xi|^2 \rangle dx < +\infty. \quad (3.2.5)$$

3. *Symmetry:* If σ is a permutation of $\{1, \dots, k\}$ and $f \in C_0(\mathbb{R}^k)$ then $\langle \nu_{\sigma(x)}^k, f(\sigma(\xi)) \rangle = \langle \nu_x^k, f(\xi) \rangle$ for a.e. $x \in D^k$. Here, we denote $\sigma(x) = \sigma(x_1, x_2, \dots, x_k) = (x_{\sigma_1}, x_{\sigma_2}, \dots, x_{\sigma_k})$. $\sigma(\xi)$ is denoted analogously.

4. *Consistency:* If $f \in C_0(U^k)$ is of the form $f(\xi_1, \dots, \xi_k) = g(\xi_1, \dots, \xi_{k-1})$ for some $g \in C_0(U^{k-1})$, then $\langle \nu_{x_1, \dots, x_k}^k, f \rangle = \langle \nu_{x_1, \dots, x_{k-1}}^{k-1}, g \rangle$ for almost every $(x_1, \dots, x_k) \in D^k$.

5. *Diagonal continuity (DC):* If $B_r(x) := \{y \in D : |x - y| < r\}$ then

$$\lim_{r \rightarrow 0} \int_D \int_{B_r(x)} \langle \nu_{x,y}^2, |\xi_1 - \xi_2|^2 \rangle dy dx = 0. \quad (3.2.6)$$

Each element ν^k is called a **correlation marginal**. We let $\mathfrak{L}^2 = \mathfrak{L}^2(D, U)$ denote the set of all correlation measures from D to U .

It has been shown in [FLM17], that if $\mu \in \mathcal{P}(L_x^2)$, then we can associate to it a unique correlation measure $\boldsymbol{\nu}$, with the interpretation that for $A_1, \dots, A_k \subset U$:

$$\mu[\mathbf{u}(x_i) \in A_i, i = 1, \dots, k] = \nu_{x_1, \dots, x_k}^k(A_1 \times \dots \times A_k).$$

More precisely, we have the following theorem [FLM17]:

Theorem 3.2.11. For every correlation measure $\boldsymbol{\nu} \in \mathfrak{L}^2(D, U)$ there exists a unique probability measure $\mu \in \mathcal{P}(L^2(D; U))$ satisfying

$$\int_{L_x^2} \|\mathbf{u}\|_{L_x^2}^2 d\mu(\mathbf{u}) < \infty, \quad (3.2.7)$$

such that

$$\int_{D^k} \int_{U^k} g(x, \xi) d\nu_x^k(\xi) dx = \int_{L_x^2} \int_{D^k} g(x, \mathbf{u}(x)) dx d\mu(\mathbf{u}), \quad (3.2.8)$$

for all $g \in C_0(D^k \times U^k)$ and $k \in \mathbb{N}$ (where $\mathbf{u}(x)$ denotes the vector $(u(x_1), \dots, u(x_k))$). Conversely, for every probability measure $\mu \in \mathcal{P}(L^2(D; U))$ with finite moment (3.2.7), there exists a unique correlation measure $\boldsymbol{\nu} \in \mathfrak{L}^2(D, U)$ satisfying (3.2.8). The relation (3.2.8) is also valid for any measurable $g : D \times U \rightarrow \mathbb{R}$ such that $|g(x, \xi)| \leq C|\xi|^2$ for a.e. $x \in D$.

Moreover, the moments

$$m^k : D^k \mapsto U^{\otimes k}, \quad m^k(x) = \langle \nu_x^k, \xi_1 \otimes \xi_2 \otimes \dots \otimes \xi_k \rangle, \quad (3.2.9)$$

uniquely determine the correlation measure ν and hence the underlying probability measure μ .

Remark 3.2.12. We note that Theorem 3.2.11 effectively expresses a form of Fubini's theorem, and abusing notation, (3.2.8) might have been stated as

$$\int_{D^k} \left(\int_{L_x^2} g(x, \mathbf{u}(x_1), \dots, \mathbf{u}(x_k)) d\mu(\mathbf{u}) \right) dx = \int_{L_x^2} \left(\int_{D^k} g(x, \mathbf{u}(x_1), \dots, \mathbf{u}(x_k)) dx \right) d\mu(\mathbf{u}).$$

The central difficulty in deriving Theorem 3.2.11 is that point-wise evaluations are not well-defined on L_x^2 , and hence $\int_{L_x^2} g(x, \mathbf{u}(x_1), \dots, \mathbf{u}(x_k)) d\mu(\mathbf{u})$ needs to be interpreted in the appropriate way, leading to correlation marginals based on Young measures [FLM17].

The following result is obtained as a consequence of Theorem 3.2.7 (for a proof, see [LMPP21b, Appendix E]):

Theorem 3.2.13. Let $\{\mu_t^\Delta\}_{\Delta>0}$ be a family of uniformly time-regular probability measures in $L_t^1(\mathcal{P})$, and assume that there exists $M > 0$, such that $\mu_t^\Delta(B_M) = 1$ for all $\Delta > 0$ and $t \in [0, T]$. Let $\boldsymbol{\nu}_t^\Delta = (\nu_t^{\Delta,1}, \nu_t^{\Delta,2}, \dots)$ denote the corresponding time-parameterized correlation measures. If there exists a uniform modulus of continuity $\phi(r)$, such that

$$\int_0^T \int_D \int_{B_r(x)} \langle \nu_{t,x,y}^{\Delta,2}, |\xi_1 - \xi_2|^2 \rangle dy dx dt \leq \phi(r), \quad \forall \Delta > 0,$$

then $\{\mu_t^\Delta\}_{\Delta>0}$ is relatively compact in $L_t^1(\mathcal{P})$, i.e. there exists a subsequence $\Delta_j \rightarrow 0$ ($j \in \mathbb{N}$), and a time-parameterized probability measure $\mu_t \in L_t^1(\mathcal{P})$, such that

$$\int_0^T W_1(\mu_t^{\Delta_j}, \mu_t) dt \rightarrow 0, \quad \text{as } j \rightarrow \infty.$$

Furthermore, denoting by $\boldsymbol{\nu}_t = (\nu_t^1, \nu_t^2, \dots)$ the correlation measure corresponding to the limit μ , we have

- L^2 -bound: $\int_D \langle \nu_{t,x}^1, |\xi|^2 \rangle dx \leq M^2$, for a.e. $t \in [0, T]$,
- the two-point correlations satisfy

$$\int_0^T \int_D \int_{B_r(x)} \langle \nu_{t,x,y}^2, |\xi_1 - \xi_2|^2 \rangle dy dx dt \leq \phi(r),$$

- We define admissible observables, in terms of test functions $g \in C([0, T] \times D^k \times U^k)$, which satisfy the following bounds,

$$\begin{aligned} |g(t, x, \xi)| &\leq C \prod_{i=1}^k (1 + |\xi_i|^2), \\ |g(t, x, \xi) - g(t, x, \xi')| &\leq C \sum_{i=1}^k \Pi_i(\xi, \xi') \sqrt{1 + |\xi_i|^2 + |\xi'_i|^2} |\xi_i - \xi'_i|, \end{aligned} \quad (3.2.10)$$

where $C > 0$ is a fixed constant, independent of $t \in [0, T)$, $x \in D^k$ and $\xi, \xi' \in U^k$. Here $\Pi_i(\xi, \xi')$ is defined as

$$\Pi_i(\xi, \xi') := \prod_{\substack{j=1 \\ j \neq i}}^k (1 + |\xi_j|^2 + |\xi'_j|^2), \quad \xi, \xi' \in U^k. \quad (3.2.11)$$

Then, these admissible observables converge strongly in $L_{t,x}^1$, in the sense that

$$\lim_{j \rightarrow \infty} \int_0^T \int_{D^k} |\langle \nu_{t,x}^{\Delta_j,k}, g(x, \xi) \rangle - \langle \nu_{t,x}^k, g(x, \xi) \rangle| dx dt = 0,$$

A particular point of interest in the statement of previous theorem is the characterization of a suitable set of “admissible observables”, whose convergence is assured by the convergence $\mu_t^\Delta \rightarrow \mu_t$ in $L_t^1(\mathcal{P})$.

Remark 3.2.14. We note that the uniform modulus of continuity estimate in Theorem 3.2.13 can equivalently be expressed as

$$S_2^T(\mu_t^\Delta; r)^2 = \int_0^T \int_{L_x^2} \int_D \int_{B_r(0)} |\mathbf{u}(x+h) - \mathbf{u}(x)|^2 dh dx d\mu_t^\Delta(\mathbf{u}) dt \leq \phi(r),$$

for all $\Delta > 0$.

3.3 Dissipative statistical solutions and their well-posedness

Given the discussion on time-parameterized probability measures in the last section, we can now define statistical solutions of (1.1.1) as,

Definition 3.3.1. A time-parameterized probability measure $\mu_t \in L_t^1(\mathcal{P})$ is a **statistical solution** of the incompressible Euler equations with initial data $\bar{\mu}$, if $t \mapsto \mu_t$ is time-regular, and the associated correlation measure ν_t satisfies:

- Given $\varphi_1, \dots, \varphi_k \in C^\infty([0, T) \times D; \mathbb{R}^d)$ with $\operatorname{div}(\varphi_i) = 0$ for all $i = 1, \dots, k$, set

$$\varphi(t, x) = \varphi_1(t, x_1) \otimes \cdots \otimes \varphi_k(t, x_k), \quad \text{where } x = (x_1, \dots, x_k).$$

Let us denote $F(\xi) := \xi \otimes \xi$ and define a contraction by

$$(\xi_1 \otimes \cdots \otimes F(\xi_i) \otimes \cdots \otimes \xi_k) : \nabla_{x_i} \varphi = \left[\prod_{j \neq i} (\xi_j \cdot \varphi_j) \right] (\xi_i \cdot \nabla_{x_i} \varphi_i) \cdot \xi_i.$$

Then $\nu^k = \nu_{t,x_1, \dots, x_k}^k$ satisfies

$$\begin{aligned} & \int_0^T \int_{D^k} \left\{ \langle \nu^k, \xi_1 \otimes \cdots \otimes \xi_k \rangle : \partial_t \varphi \right. \\ & \quad \left. + \sum_i \langle \nu^k, \xi_1 \otimes \cdots \otimes F(\xi_i) \otimes \cdots \otimes \xi_k \rangle : \nabla_{x_i} \varphi \right\} dx dt \\ & \quad + \int_{D^k} \langle \bar{\nu}^k, \xi_1 \otimes \cdots \otimes \xi_k \rangle : \varphi(0, x) dx = 0. \end{aligned}$$

Here $\bar{\nu}$ is the correlation measure corresponding to the initial data $\bar{\mu}$.

2. For all $\psi \in C_c^\infty(D)$, we have

$$\int_{D^2} \langle \nu_{t,x_1,x_2}^2, \xi_1 \otimes \xi_2 \rangle : (\nabla \psi(x_1) \otimes \nabla \psi(x_2)) dx_1 dx_2 = 0,$$

for a.e. $t \in [0, T]$.

The above PDEs specify the time-evolution of the moments (3.2.9) for all k and by Theorem 3.2.11, determine the evolution of the probability measure μ_t .

Remark 3.3.2. As ν^1 above is a standard Young measure, it is straightforward to observe that the corresponding identity for the evolution of ν^1 corresponds to the definition of measure-valued solution of (1.1.1), in the sense of Definition 1.3.8 in chapter 1, under the further assumption that there is no concentration. Hence, one can think of statistical solutions as measure-valued solutions coupled with information about all possible multi-point correlations.

We first show that the second property of Definition 3.3.1 is equivalent to the requirement that μ_t be supported on divergence-free vector fields for almost all t .

Lemma 3.3.3. Let $\mu \in \mathcal{P}(L_x^2)$, with associated correlation measure ν . Then μ is concentrated on divergence-free vector fields if, and only if,

$$\int_{D^2} \langle \nu_{x_1,x_2}^2, \xi_1 \otimes \xi_2 \rangle : (\nabla \psi(x_1) \otimes \nabla \psi(x_2)) dx_1 dx_2 = 0,$$

for all $\psi \in C_c^\infty(D)$.

Sketch of proof. Let $\psi \in C_c^\infty(D)$. Then we have the following identity

$$\int_{L_x^2} \left[\int_D \mathbf{u} \cdot \nabla \psi dx \right]^2 d\mu(\mathbf{u}) = \int_D \langle \nu_{x_1,x_2}^2, \xi_1 \otimes \xi_2 \rangle : (\nabla \psi(x_1) \otimes \nabla \psi(x_2)) dx_1 dx_2. \quad (3.3.1)$$

Therefore the stated condition in this lemma is equivalent to the claim that for all $\psi \in C_c^\infty(D)$, we have $\int_D \mathbf{u} \cdot \nabla \psi dx = 0$, μ -a.s.. A simple continuity argument based on a countable family of suitable test functions ψ then implies that this is in fact equivalent to the statement that, for μ -a.e. \mathbf{u} , we have $\int_D \mathbf{u} \cdot \nabla \psi dx = 0$ for all $\psi \in C_c^\infty(D)$. \square

Note that if $\rho, \mu \in \mathcal{P}(L_x^2)$ are probability measures, and if ρ is of the form

$$\rho = \sum_{j=1}^J \alpha_j \delta_{\mathbf{u}_j},$$

where $\alpha_j > 0$, $\sum_{j=1}^J \alpha_j = 1$, and $\mathbf{u}_j \in L_x^2$, then a transport plan from μ to ρ is necessarily of the form [FLM17]:

$$\pi = \sum_{j=1}^J \alpha_j \mu_j \otimes \delta_{\mathbf{u}_j},$$

where $\mu_j \in \mathcal{P}(L_x^2)$, and $\sum_{j=1}^J \alpha_j \mu_j = \mu$. Therefore, given $\alpha = (\alpha_1, \dots, \alpha_J)$ as above, and $\mu \in \mathcal{P}(L_x^2)$, we denote

$$\Lambda(\alpha, \mu) := \left\{ (\mu_1, \dots, \mu_J) \mid \mu_j \in \mathcal{P}(L_x^2), \sum_{j=1}^J \alpha_j \mu_j = \mu \right\}.$$

Note that the set $\Lambda(\alpha, \mu)$ is non-empty, since it contains (μ, \dots, μ) .

In analogy with work [FLM17, FLMW20] on entropy statistical solutions for hyperbolic systems of conservation laws, we define

Definition 3.3.4 (Dissipative statistical solution). A statistical solution $\mu_t \in L_t^1(\mathcal{P})$ is called dissipative, if for every choice of coefficients $\alpha_j > 0$ with $\sum_{j=1}^J \alpha_j = 1$ and for every $(\bar{\mu}_1, \dots, \bar{\mu}_J) \in \Lambda(\alpha, \bar{\mu})$, there exists a function $t \mapsto (\mu_{1,t}, \dots, \mu_{J,t}) \in \Lambda(\alpha, \mu_t)$, such that $t \mapsto \mu_{j,t}$ is weak-* measurable, $\mu_{j,t}|_{t=0} = \bar{\mu}_j$, such that each $\mu_{j,t}$ satisfies

$$\int_0^T \int_{L_x^2} \int_D [\mathbf{u} \cdot \partial_t \varphi + (\mathbf{u} \otimes \mathbf{u}) : \nabla \varphi] dx d\mu_{j,t}(\mathbf{u}) dt = - \int_{L_x^2} \int_D \mathbf{u} \cdot \varphi(0, x) dx d\bar{\mu}_j(\mathbf{u}),$$

for all $\varphi \in C_c^\infty([0, T) \times D)$, $\operatorname{div}(\varphi) = 0$, and all $j = 1, \dots, J$. And, in addition, we have for almost every $t \in [0, T]$:

$$\int_{L_x^2} \|\mathbf{u}\|_{L_x^2}^2 d\mu_{j,t}(\mathbf{u}) \leq \int_{L_x^2} \|\mathbf{u}\|_{L_x^2}^2 d\bar{\mu}_j(\mathbf{u}), \quad j = 1, \dots, J.$$

3.3.1 Existence and uniqueness of dissipative solutions

As already pointed out in the introduction, the initial-value problem for the incompressible Euler equations is ill-posed for general initial data $\bar{\mathbf{u}} \in L_x^2$, i.e. there exists an exceptional set of initial data $\mathcal{E} \subset L_x^2$ for which there either might exist no suitable solutions at all, or for which there exist infinitely many suitable solutions. In practice, one may nevertheless hope that the “probability of encountering” such exceptional initial data is 0, so that the subsequent evolution would then be well-defined at least for initial data encountered in practice. In this section, we provide a formal description of a suitable set of statistical initial data $\bar{\mu}$ for which this intuition holds true, and show existence and partial uniqueness of dissipative statistical solutions μ_t for initial data $\bar{\mu}$ in this class. In particular, the results in this section imply a weak-strong uniqueness result for statistical solutions. In contrast, an analogous weak-strong uniqueness result for measure-valued solutions only holds for *atomic* initial data, i.e. when the initial data is a function, but fails for non-atomic Young measure-valued initial data (see e.g. Example 1 in [FKMT17] for an explicit example in the context of conservation laws).

More precisely, we show based on topological arguments, that if the set of C^1 -regular initial data admitting classical solutions of (1.1.1), over a given time-interval $[0, T)$ is dense in L_x^2 , then there exists a (topologically) generic set $\mathcal{G} \subset L_x^2$, containing these regular initial data, with the following property: For any initial data $\bar{\mu} \in \mathcal{P}(L_x^2)$ which is concentrated on this generic set $\mathcal{G} \subset L_x^2$, i.e. satisfying $\bar{\mu}(\mathcal{G}) = 1$, we have *existence and uniqueness in the class of dissipative statistical solutions*. By a “generic” set \mathcal{G} , we denote a set whose complement $\mathcal{E} = L_x^2 \setminus \mathcal{G}$ is a countable union of nowhere dense sets (implying that \mathcal{E} is a meagre set in the topological sense). We say that $\bar{\mu}$ is concentrated on \mathcal{G} , if $\bar{\mu}(\mathcal{G}) = 1$.

The construction of such a generic \mathcal{G} under the above mentioned assumption has first been carried out in [Lio96]. Let us first review the construction of \mathcal{G} . We let $\mathcal{C} \subset C^1(D; U)$ denote the set of initial data $\bar{\mathbf{v}}$ admitting a classical solution $\mathbf{v}(t)$ on $[0, T)$, with $C(\bar{\mathbf{v}}) := \sup_{t \in [0, T)} \|\nabla \mathbf{v}(t)\|_{L^\infty}$ finite, i.e. $C(\bar{\mathbf{v}}) < \infty$. For $n \in \mathbb{N}$, define the open set \mathcal{G}_n , by

$$\mathcal{G}_n := \left\{ \bar{\mathbf{u}} \in L_x^2 \mid \exists \bar{\mathbf{v}} \in \mathcal{C} \text{ s.t. } \|\bar{\mathbf{u}} - \bar{\mathbf{v}}\|_{L_x^2} < \frac{1}{n} e^{-C(\bar{\mathbf{v}})T} \right\} \quad (3.3.2)$$

Finally, we let $\mathcal{G} = \bigcap_{n \in \mathbb{N}} \mathcal{G}_n$.

Remark 3.3.5. If there exists a dense set of initial data $\bar{\mathbf{v}} \in \mathcal{C}$, then \mathcal{G} is generic in the topological sense (more precisely a G_δ set), being the countable intersection of the dense open sets \mathcal{G}_n . By the Baire category theorem, the set \mathcal{G} is non-empty and dense in this case. In particular, this would hold true if there is no finite-time blow-up for sufficiently smooth classical solutions of the incompressible Euler equations (e.g. for $C^{1,\alpha}$ initial data $\bar{\mathbf{v}}$ possessing a Hölder continuous derivative), which is an established fact in two space dimensions, but an open question in three space dimensions.

We can now state the main theorem of the present section:

Theorem 3.3.6. *Define the generic set \mathcal{G} as above (cp. equation (3.3.2)). If $\bar{\mu} \in \mathcal{P}(L_x^2)$ is initial data such that $\bar{\mu}(\mathcal{G}) = 1$ and there exists $M > 0$ such that $\bar{\mu}(B_M(0)) = 1$, then there exists a unique dissipative statistical solution μ_t of the incompressible Euler equations with initial data $\bar{\mu}$.*

The proof of Theorem 3.3.6 has been provided in detail in [LMPP21b, Appendix F]. We can now easily derive the following corollaries from Theorem 3.3.6.

Corollary 3.3.7 (Short-time existence and uniqueness). *If $m > d/2 + 1$, and if there exists a $C > 0$, such that $\bar{\mu} \in \mathcal{P}(L_x^2)$ is concentrated on*

$$\{\bar{\mathbf{u}} \in H_x^m \mid \|\bar{\mathbf{u}}\|_{H_x^m} \leq C\},$$

then there exists $T^ > 0$ (depending only on C) and a statistical solution $\mu_t : [0, T^*] \rightarrow \mathcal{P}(L_x^2)$ with initial data $\bar{\mu}$. Furthermore, μ_t is unique in the class of dissipative statistical solutions for $t \in [0, T^*]$.*

Proof. Classical short-time existence results for the Euler equations [MB01] show that there exists $T^* > 0$, such that for initial data $\bar{\mathbf{u}}$ with $\|\bar{\mathbf{u}}\|_{H_x^m} \leq C$, there exists a unique solution $\mathbf{u}(t)$ such that

$$\sup_{t \in [0, T^*]} \|\mathbf{u}(t)\|_{H_x^m} \leq C' \|\bar{\mathbf{u}}\|_{H_x^m}.$$

Since $H_x^m \hookrightarrow C^1$, this implies that $\bar{\mu}$ is concentrated on $\bar{\mathbf{u}} \in \mathcal{C}$. In particular, we conclude that $\bar{\mu}(\mathcal{G}) = 1$, and the result now follows from Theorem 3.3.6. \square

Corollary 3.3.8 (Weak-Strong uniqueness in 2d). *Let $d = 2$, and let $\alpha \in (0, 1)$. If $\bar{\mu}$ is concentrated on $C^{1,\alpha}(D; U)$ and if there exists $M > 0$, such that $\bar{\mu}(B_M(0)) = 1$, then there exists a dissipative statistical solution μ_t with initial data $\bar{\mu}$. Furthermore, μ_t is unique in the class of dissipative statistical solutions with initial data $\bar{\mu}$.*

Proof. Again, we observe that for any $\bar{\mathbf{u}} \in C^{1,\alpha}$, there exists a unique solution $\mathbf{u}(t) \in C^{1,\alpha}$. Hence, we have $\bar{\mathbf{u}} \in \mathcal{C}$ for all such $\bar{\mathbf{u}}$. In particular, it follows that $\bar{\mu}$ is concentrated on \mathcal{G} . The claim follows from Theorem 3.3.6. \square

3.4 Numerical Approximation of Statistical Solutions

3.4.1 Monte-Carlo algorithm based on the SV method

In this section, we will propose an algorithm for computing statistical solutions of the incompressible Euler equations (1.1.1). As mentioned before, this algorithm is very similar to the one proposed in [FLMW20] for computing statistical solutions of hyperbolic systems of conservation laws, which in turn was inspired by the ensemble averaging algorithms of [FKMT17], also used in [LM15], for computing measure-valued solutions. This algorithm requires a spatio-temporal discretization and a Monte Carlo sampling of the underlying probability space. We propose to combine Monte-Carlo sampling with the spectral viscosity discretization described in detail in chapter 1.4,

$$\begin{cases} \partial_t \mathbf{u}^\Delta + \mathbb{P}_N(\mathbf{u}^\Delta \cdot \nabla \mathbf{u}^\Delta) = -\epsilon_N |\nabla|^{2s} (Q_N * \mathbf{u}^\Delta), \\ \operatorname{div}(\mathbf{u}^\Delta) = 0, \quad \mathbf{u}^\Delta|_{t=0} = \mathbb{P}_N \bar{\mathbf{u}}. \end{cases} \quad (3.4.1)$$

Following [FLMW20], the computation of statistical solutions of (1.1.1) can be accomplished via the the following Monte Carlo sampling algorithm:

Algorithm 3.4.1 (Monte Carlo). *Given $\bar{\mu} \in \mathcal{P}(L_x^2)$, and a grid scale $\Delta = 1/N$, we determine an approximate statistical solution μ_t^Δ , as follows: For $m = m(N)$,*

- (1) *Generate i.i.d. samples $\bar{\mathbf{u}}_1, \dots, \bar{\mathbf{u}}_m \sim \bar{\mu}$,*
- (2) *Evolve the samples, using the numerical scheme $\mathbf{u}_i^\Delta(t) := \mathcal{S}_t^\Delta(\bar{\mathbf{u}}_i)$, where \mathcal{S}_t^Δ denotes the solution operator, defined by the scheme (1.4.4).*
- (3) *The approximate statistical solution μ_t^Δ is given by the so-called empirical measure,*

$$\mu_t^\Delta := \frac{1}{m} \sum_{i=1}^m \delta_{\mathbf{u}_i^\Delta(t)}. \quad (3.4.2)$$

□

We remark that in practice, the samples $\bar{\mathbf{u}}_i$ for $1 \leq i \leq m$ are random realizations with respect to a certain underlying probability space.

Remark 3.4.2. *The Monte Carlo algorithm 3.4.1, when restricted only to the computation of the first correlation marginal ν^1 , reduces to the ensemble averaging algorithm proposed in [LM15] for computing measure-valued solutions of the incompressible Euler equations.*

3.4.2 Convergence to statistical solutions

In this section, we will investigate the convergence of the empirical measure μ_t^Δ (3.4.2), generated by the Monte Carlo algorithm 3.4.1, to a statistical solution of (1.1.1). To this end, we seek to apply the convergence theorem 3.2.7 to these approximations. We start by verifying the temporal regularity of the empirical measures in the following lemma,

Lemma 3.4.3. *There exists $L \in \mathbb{N}$ and constants $C, C' > 0$, such that if \mathbf{u}^Δ is obtained from the spectral hyper-viscosity method (1.4.4), with $\Delta = 1/N$ and initial data $\bar{\mathbf{u}} \in L_x^2$, then*

$$\partial_t \mathbf{u}^\Delta + \operatorname{div}(\mathbf{u}^\Delta \otimes \mathbf{u}^\Delta) + \nabla p^\Delta = \mathbf{E}^\Delta,$$

where $\|\mathbf{E}^\Delta\|_{H_x^{-L}} \leq C\Delta(1 + \|\mathbf{u}^\Delta\|_{L_x^2}^2)$. Furthermore, there exists a constant C' , such that

$$\|\mathbf{u}^\Delta(t) - \mathbf{u}^\Delta(s)\|_{H_x^{-L}} \leq C'(1 + \|\bar{\mathbf{u}}\|_{L_x^2}^2)|t - s|.$$

The detailed proof can be found in [LMPP21b, Lemma 4.1], and will not be repeated here. It is essentially a repetition of the argument on page 19, showing that the SV scheme produces an approximate solution sequence in the sense of DiPerna and Majda (cp. Definition 1.3.5).

From Lemma 3.4.3, it is now easy to see that if μ_t^Δ is generated by the Monte-Carlo algorithm 3.4.1, i.e.

$$\mu_t^\Delta = \frac{1}{m} \sum_{i=1}^m \delta_{\mathbf{u}_i^\Delta(t)},$$

with $\mathbf{u}_i^\Delta(t)$ computed by the spectral hyper-viscosity scheme (1.4.4), then the transport plan defined by

$$\pi_{s,t}^\Delta := \frac{1}{m} \sum_{i=1}^m \delta_{\mathbf{u}_i^\Delta(s)} \otimes \delta_{\mathbf{u}_i^\Delta(t)},$$

satisfies the properties required by the definition of time-regularity, Definition 3.2.5. This provides the required temporal regularity required by Theorem 3.2.13.

Next, we turn our attention to the spatial regularity bounds of Theorem 3.2.7. In particular, we need to obtain uniform estimates on the structure function (3.2.4). We start with the following simple observation (cp. [LMPP21b, Lemma 4.2]):

Lemma 3.4.4. *For any $r \geq 0$, we have*

$$\int_{B_r(0)} |e^{ik \cdot h} - 1|^2 dh \leq C \min(|k|^2 r^2, 1) \leq C |k|^2 r^2,$$

where $C = 4$. □

The next result is an estimate on the structure function (3.2.4) at the grid scale Δ .

Lemma 3.4.5. *If μ_t^Δ is an approximate statistical solution obtained from the spectral hyper-viscosity method with $\Delta = 1/N$, and initial data $\bar{\mu}$ for which there exists $M > 0$ such that $\bar{\mu}(B_M(0)) = 1$ where $B_M(0) = \{\|\mathbf{u}\|_{L_x^2} < M\}$, then*

$$S_2^T(\mu_t^\Delta; \Delta) \leq CM\Delta^{1/(2s)},$$

for some absolute constant $C > 0$. The same estimate is also true for $r \leq \Delta$, i.e. we have

$$S_2^T(\mu_t^\Delta; r) \leq CMr^{1/(2s)}, \quad \text{for all } r \leq \Delta.$$

□

The proof of Lemma 3.4.5 relies on the a priori bound

$$\epsilon_N \int_0^T \sum_{|k|_\infty \leq N} Q_k |k|^{2s} |\hat{\mathbf{u}}_k(t)|^2 dt \leq \|\bar{\mathbf{u}}\|_{L^2}^2,$$

of solutions of the SV scheme, which is sufficient to ensure control on the approximate solution at small scales $r \lesssim \Delta$. The details of the proof are provided in [LMPP21b, Lemma 4.3].

As in [FLMW20] section 4.2, we have uniform estimates on the structure function at (or below) the grid scale. Large scale features are in any case independent of the resolution Δ . However, we lack any information on the *intermediate scales*, in between the two. To close this information gap, we follow [FLMW20] and make an assumption on scaling of the structure function (3.2.4) at intermediate scales. The resulting theorem is:

Theorem 3.4.6. *Consider the incompressible Euler equations with initial data $\bar{\mu} \in \mathcal{P}(L_x^2)$, such that $\text{supp}(\bar{\mu}) \subset B_M$, with B_M the ball of radius M in L_x^2 , for some $M > 0$. Define the approximate statistical solution μ_t^Δ by the Monte-Carlo algorithm 3.4.1. If the approximate statistical solutions μ_t^Δ satisfy:*

- *Approximate scaling: For every $\ell > 1$, there exists a constant $0 < \lambda_\ell \leq 1/(2s)$, fixed $C > 0$ possibly depending on the initial data, but independent of ℓ and the grid size N , such that*

$$S_2^T(\mu_t^\Delta; \ell\Delta) \leq C\ell^{\lambda_\ell} S_2^T(\mu_t^\Delta; \Delta), \quad (T > 0).$$

Then the approximate statistical solutions μ_t^Δ converge (up to a subsequence still denoted by Δ), as $\Delta \rightarrow 0$, to some $\mu_t \in L_t^1(\mathcal{P})$.

Proof. By Lemma 3.4.5, there exists a constant $C > 0$, such that

$$S_2^T(\mu_t^\Delta; r) \leq \bar{C}r^{1/(2s)}, \tag{3.4.3}$$

for all $r \leq \Delta$. If $r > \Delta$, then by the assumed approximate scaling property, we write $r = \ell\Delta$, with $\ell > 1$, and obtain

$$S_2^T(\mu_t^\Delta; r) = S_2^T(\mu_t^\Delta; \ell\Delta) \leq C\ell^{\lambda_\ell} S_2^T(\mu_t^\Delta; \Delta) \leq C\overline{C}\ell^{1/(2s)}\Delta^{1/(2s)} = C\overline{C}r^{1/(2s)},$$

for some constant $C\overline{C} > 0$. The convergence now follows from Theorem 3.2.13. \square

Remark 3.4.7. *The scaling assumption (3.4.3) can be interpreted as a weaker version of the scaling assumptions of Kolmogorov (see hypothesis H2, equation 6.3, page 75 of [Fri95]) that was instrumental in the K41 theory for homogeneous, isotropic turbulence. In contrast to the exact scaling relation postulated by Kolmogorov, Theorem 3.4.6 only requires an upper bound on the structure functions; we do not assume (or indeed even conjecture) that the structure functions exhibit any precise scaling. The scaling assumption is fundamentally an assumption about the compactness properties (encoded in two-point correlations) of the approximate statistical solutions, stating that if we can control the smallest scales by diffusion, the large scales are expected to be reasonably well-behaved. This intuition is motivated by numerical experiments presented in section 5. We also note that the inequalities in (3.4.3) can accommodate intermittency in the form of deviations for the standard Kolmogorov determination of the exponent 1/3 for the structure function (3.2.4).*

Remark 3.4.8 (Convergence without scaling assumption). *Let $\overline{\mu}$ be concentrated on a set of initial data $\mathcal{G} \subset L_x^2$, such that for any $\overline{\mathbf{u}} \in \mathcal{G}$ there exists a strong (i.e. Lipschitz continuous) solution $\mathbf{u}(x, t)$ for $t \in [0, T]$. Denote by $\mathcal{S}_t : \mathcal{G} \rightarrow L_x^2$ the solution operator mapping $\overline{\mathbf{u}} \mapsto \mathbf{u}(x, t) = \mathcal{S}_t(\overline{\mathbf{u}})$, and let $\mathcal{S}_t^\Delta : \mathcal{G} \rightarrow L_x^2$, $\overline{\mathbf{u}} \mapsto \mathcal{S}_t^\Delta(\overline{\mathbf{u}})$ denote the discretized solution operator. The corresponding (exact/approximate) statistical solution are in this case given by the push-forward $\mu_t = \mathcal{S}_{t,\#}\overline{\mu}$, $\mu_t^\Delta = \mathcal{S}_{t,\#}^\Delta\overline{\mu}$. From the definition (3.2.2) of the metric d_T on $L_t^1(\mathcal{P})$, and the Kantorovich duality formula (cp. (B.0.3) in Appendix B), we readily obtain the inequality*

$$d_T(\mu_t, \mu_t^\Delta) \leq \int_0^T \int_{\mathcal{G}} \|\mathcal{S}_t(\overline{\mathbf{u}}) - \mathcal{S}_t^\Delta(\overline{\mathbf{u}})\|_{L_x^2} d\overline{\mu}(\overline{\mathbf{u}}) dt. \quad (3.4.4)$$

Since $\mathcal{S}_t(\overline{\mathbf{u}})$ is a strong solution for all $\overline{\mathbf{u}} \in \mathcal{G}$, the pointwise convergence $\mathcal{S}_t^\Delta(\overline{\mathbf{u}}) \rightarrow \mathcal{S}_t(\overline{\mathbf{u}})$ follows from Corollary 1.4.3 in chapter 1. Hence, the integrand on the right-hand side of (3.4.4) is uniformly bounded and converges to zero pointwise, as $\Delta \rightarrow 0$. By the dominated convergence theorem, it follows that $\mu_t^\Delta \rightarrow \mu_t$ in $L_t^1(\mathcal{P})$. In particular, the approximate statistical solution μ_t^Δ computed by algorithm 3.4.1 converges to the unique dissipative statistical solution μ_t in this case, without any additional assumptions on the structure functions.¹ In three dimensions, this implies the convergence of approximate statistical solutions to the unique dissipative statistical solution under the assumptions of Corollary 3.3.7 (short-time existence and uniqueness). In the two-dimensional case, this shows the convergence to the unique dissipative statistical solution under the assumptions of Corollary 3.3.8 (global existence and uniqueness for $C^{1,\alpha}$ initial data).

3.4.3 Decay of energy spectrum

In this section, we will provide an alternative criterion to ensure convergence of probability measures with respect to the metric (3.2.2).

This criterion is motivated from well-known experimental and theoretical concepts in the study of turbulent flows and is based on the energy spectrum $E(\mathbf{u}; K)$ ($K \in \mathbb{N}_0$) associated to a vector field \mathbf{u} ,

¹In fact, it can be shown that the convergence $\mu_t^\Delta \rightarrow \mu_t$ in turn implies a uniform decay of the structure functions as $\Delta \rightarrow 0$ (cp. [LMW21, Prop. A.2])

defined as

$$E(\mathbf{u}; K) = \frac{1}{2} \sum_{K-1 < |k| \leq K} |\hat{\mathbf{u}}(k)|^2.$$

Note that the kinetic energy is obtained as a sum

$$\frac{1}{2} \int_D |\mathbf{u}|^2 dx = (2\pi)^d \sum_{K=1}^{\infty} E(\mathbf{u}; K).$$

Given a probability measure $\mu \in \mathcal{P}(L_x^2)$, let us similarly define:

$$E(\mu; K) = \int_{L_x^2} E(\mathbf{u}, K) d\mu(\mathbf{u}),$$

so that $E(\delta_{\mathbf{u}}; K) = E(\mathbf{u}; K)$, for $\mathbf{u} \in L_x^2$. Finally, we denote by $E_T(\mu_t; K)$ the time-integrated energy spectrum

$$E_T(\mu_t; K) = \int_0^T E(\mu_t; K) dt.$$

It is an experimentally observed fact [Fri95] that the typical energy spectrum of turbulent flows with a sufficiently strong dissipation mechanism at small scales typically takes a shape similar to the one shown in Figure 3.1: Visible are three parts of the energy spectrum. The left-most part (small K) corresponds to large-scale features for the flow, the middle part (intermediate K) is referred to as the inertial range, while the right-most part (large K) may be referred to as the dissipation range. The appearance of these three parts is heuristically explained as follows. Starting from initial data (with a sufficiently fast decay of the energy spectrum) initially fixes the large-scale features of the flow. Due to the non-linear nature of the evolution equation, these large-scale features decay to smaller scales, corresponding to energy cascading from small values of K to larger values of K . While a satisfactory mathematical treatment of the precise nature of this energy cascade remains an outstanding challenge, there is evidence by physical reasoning and as well as from numerical and real-world experiments that typically the energy spectrum resulting from this cascade process satisfies at least an upper bound of the form $E(K) \lesssim K^{-\gamma}$, for some fixed γ that is associated with the non-linearity. In the presence of a dissipative mechanism acting on small scale features of the flow, this “free” energy cascade to larger values of K due to the non-linearity is finally interrupted by the dissipation. Thus, energy is dissipated at dissipative scales.

From this heuristic point of view, we would expect the large-scale features to depend mostly on the initial data, while the decay of the energy spectrum at the largest values of K can be controlled in a numerical approximation scheme by a suitable choice of the numerical dissipation. On the other hand, there is no a priori information on the decay of the spectrum in the intermediate, *inertial* range. Hence, we make the following, rather natural, assumption:

Assumption 3.4.9. *There exist $\beta > 0$ and constant $C > 0$ such that the computed energy spectra with algorithm 3.4.1 scale as,*

$$E_T(\mu_t^\Delta, K) \leq CK^{-2\beta}, \quad \forall \Delta > 0. \tag{3.4.5}$$

◊

Under this assumption on the energy spectrum, we have the following convergence theorem:

Theorem 3.4.10. *If μ_t^Δ is obtained by the spectral viscosity method through algorithm 3.4.1, and if the energy spectra $E_T(\mu_t^\Delta; K)$ satisfy the inertial range Assumption 3.4.9 with $\beta > 1/2$, then there exists a subsequence (not relabeled) $\Delta \rightarrow 0$ and a time-parameterized probability measure μ_t , such that $\mu_t^\Delta \rightarrow \mu_t$ in $L_t^1(\mathcal{P})$.*

Proof. From Parseval's identity (A.1.3) and Lemma 3.4.4, we have

$$\begin{aligned} S_2^T(\mu_t; r)^2 &= \int_0^T \int_{L_x^2} \int_{B_r(0)} \int_{\mathbb{T}^d} |\mathbf{u}(x+h) - \mathbf{u}(x)|^2 dx dh d\mu_t(\mathbf{u}) dt \\ &\lesssim \int_0^T \int_{L_x^2} \sum_k \min(|k|^2 r^2, 1) |\widehat{\mathbf{u}}(k)|^2 d\mu_t(\mathbf{u}) dt \\ &\sim r^2 \sum_{K \leq 1/r} K^2 E_T(\mu_t; K) + \sum_{K > 1/r} E_T(\mu_t; K). \end{aligned}$$

Hence, based on the Assumption 3.4.9, we now obtain the estimate,

$$\begin{aligned} S_2^T(\mu_t^\Delta; r)^2 &\lesssim r^2 \sum_{K \leq 1/r} K^2 K^{-2\beta} + \sum_{K > 1/r} K^{-2\beta} \\ &\sim r^2 (1 + r^{2\beta-3}) + r^{2\beta-1} \\ &\sim r^{\min(2, 2\beta-1)}, \quad \text{as } r \rightarrow 0. \end{aligned}$$

Therefore, the scaling assumption on the average energy spectrum leads to the uniform diagonal continuity:

$$E_T(\mu_t^\Delta, K) \lesssim K^{-2\beta} \Rightarrow S_2^T(\mu_t^\Delta; r) \lesssim r^{\beta-1/2}, \quad \text{if } 1 < 2\beta < 3. \quad (3.4.6)$$

From Theorem 3.2.13, we obtain compactness of the sequence μ_t^Δ . \square

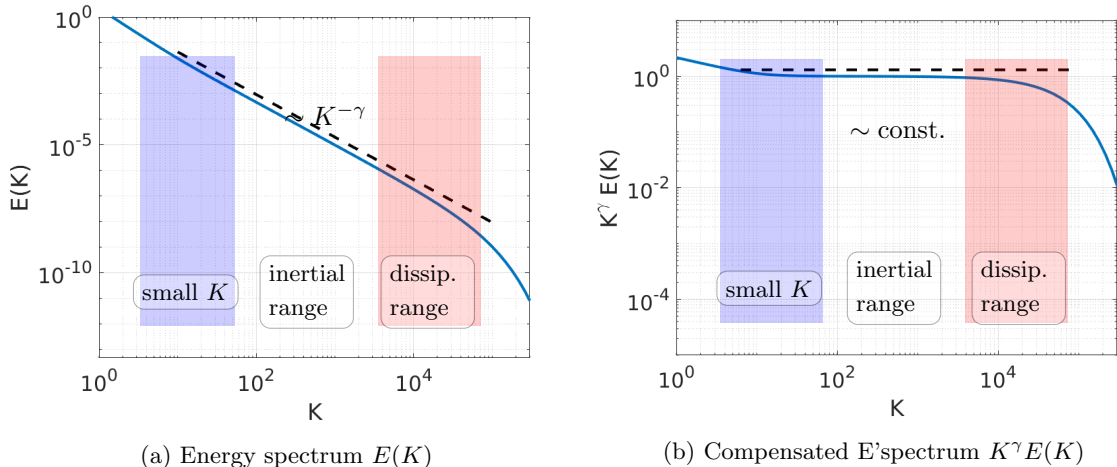


Figure 3.1: Typical energy spectrum for turbulent flows

Remark 3.4.11. As indicated in Figure 3.1 (B), a convenient way to check the scaling Assumption 3.4.9 in practice is to consider the **compensated energy spectrum**, which is defined as $K^\gamma E(K)$, where γ is the (proposed) scaling exponent in the inertial range. Proposition 3.4.10 says that if there exists $\gamma > 1$, such that the compensated energy spectrum $K^\gamma E_T(\mu_t^\Delta; K)$ is uniformly bounded by a constant, and independently of Δ , then $\{\mu_t^\Delta | \Delta > 0\}$ is compact in $L^1(\mathcal{P})$.

Remark 3.4.12. If $d = 3$ and $p = 2$, then Kolmogorov's theory states that for fully developed turbulence $S_2 \sim r^{1/3}$. Based on our estimate, this requires $\beta = \frac{5}{6}$. So that the (expected) energy spectrum is $E(K) \sim$

$K^{-2\beta} \sim K^{-5/3}$. Such an assumed scaling is consistent with many real, as well as numerical, experiments reported in the literature, and is sufficient for compactness in the space of probability measures $L_t^1(\mathcal{P})$ (cp. Proposition 3.4.10).

3.4.4 Lax-Wendroff type theorem

We have used a compactness argument to show that under some reasonable hypotheses on the approximations, numerical solutions computed by the spectral hyper-viscosity converge to a limiting time-parameterized probability measure. In this section, we show that such a limit necessarily is a statistical solution of the incompressible Euler equations in the sense of Definition 3.3.1.

Theorem 3.4.13 (Lax-Wendroff type theorem). *Let μ_t^Δ be computed by the spectral hyper-viscosity scheme with initial data $\bar{\mu}$, and assume $\mu_t^\Delta \rightarrow \mu_t$ in $L_t^1(\mathcal{P})$, as $\Delta \rightarrow 0$. Then μ_t is a statistical solution of the incompressible Euler equations with initial data $\bar{\mu}$.*

Proof. Fix $k \in \mathbb{N}$. Let $\varphi_1, \dots, \varphi_k \in C_c^\infty(D \times [0, \infty))$ be given solenoidal test functions. Set $\varphi := \varphi_1 \otimes \dots \otimes \varphi_k$ and denote $\nu^k = \nu_{x_1, \dots, x_k, t}^k$. Let \mathbf{u}^Δ be obtained from the spectral method, with initial data $\bar{\mathbf{u}}$. Let us denote $(\mathbf{u}, \varphi) := \int_D \mathbf{u} \cdot \varphi dx$. Then, as a consequence of Lemma 3.4.3, we can write

$$\frac{d}{dt}(\mathbf{u}^\Delta, \varphi_i) = (\mathbf{u}^\Delta, \partial_t \varphi_i) + (\mathbf{u}^\Delta \otimes \mathbf{u}^\Delta, \nabla \varphi_i) + (\mathbf{E}^\Delta, \varphi_i),$$

where there exists $L > 0$ independent of Δ and the initial data $\bar{\mathbf{u}}$, such that the error term \mathbf{E}^Δ satisfies $\|\mathbf{E}^\Delta\|_{H^{-L}} \leq C\Delta(1 + \|\bar{\mathbf{u}}\|_{L_x^2}^2)$. Taking the product over $i = 1, \dots, k$, we find

$$\frac{d}{dt} \prod_{i=1}^k (\mathbf{u}^\Delta, \varphi_i) = \sum_{i=1}^k \left[\prod_{j \neq i} (\mathbf{u}^\Delta, \varphi_j) \right] \{ (\mathbf{u}^\Delta, \partial_t \varphi_i) + (\mathbf{F}(\mathbf{u}^\Delta), \nabla \varphi_i) + (\mathbf{E}^\Delta, \varphi_i) \},$$

where $\mathbf{F}(\mathbf{u}) := \mathbf{u} \otimes \mathbf{u}$. Recognizing the special structure of the empirical measure μ_t^Δ (3.4.2) as a convex combination, denoting by $\nu^{k,\Delta} = \nu_{x_1, \dots, x_k, t}^{k,\Delta}$ the k -point correlation measure corresponding to μ_t^Δ , we obtain from the above identity that,

$$\begin{aligned} & \int_0^T \int_{D^k} \langle \nu^{k,\Delta}, \xi_1 \otimes \dots \otimes \xi_k \rangle : \partial_t \varphi \\ & \quad + \sum_i \langle \nu^{k,\Delta}, \xi_1 \otimes \dots \otimes \mathbf{F}(\xi_i) \otimes \dots \otimes \xi_k \rangle : \nabla_{x_i} \varphi dx dt \\ & \quad + \int_{D^k} \langle \bar{\nu}^{k,\Delta}, \xi_1 \otimes \dots \otimes \xi_k \rangle : \varphi(x, 0) dx \\ & = \int_0^T \int_{L_x^2} \sum_{i=1}^k \left[\prod_{j \neq i} (\mathbf{u}^\Delta, \varphi_j) \right] (\mathbf{E}^\Delta, \varphi_i) d\mu_t^\Delta dt. \end{aligned} \tag{3.4.7}$$

The right-hand side can be bounded by

$$\int_0^T \int_{L_x^2} \|\mathbf{u}^\Delta\|_{L_x^2}^{k-1} \sum_{i=1}^k \prod_{j \neq i} \|\varphi_j\|_{L_x^2} \|\mathbf{E}^\Delta\|_{H_x^{-L}} \|\varphi_i\|_{H_x^L} d\mu_t^\Delta dt,$$

which, by Lemma 3.4.3 is further bounded by

$$\leq C(\varphi, k) \Delta \int_0^T \int_{L_x^2} (1 + \|\mathbf{u}^\Delta\|_{L_x^2}^2)^k d\mu_t^\Delta(\mathbf{u}) dt.$$

Note that if $\bar{\mu}$ is supported on $\overline{B_M(0)} \subset L_x^2$, then it follows that μ_t^Δ is supported on $\overline{B_M(0)}$, as well. This is a consequence of the a priori L^2 -bound (1.4.8). Hence the error term in equation (3.4.7) is in this case bounded by $C\Delta$, where $C = C(\varphi, k, M, T)$ is a constant independent of Δ .

Let us also note that the terms on the left-hand side of (3.4.7) converge strongly in $L_{t,x}^1$ as $\Delta \rightarrow 0$. Indeed, it is not difficult to see that all terms on the left-hand side, e.g.

$$g(t, x, \xi) := (\xi_1 \otimes \cdots \otimes \mathbf{F}(\xi_i) \otimes \cdots \otimes \xi_k) : \nabla_{x_i} \varphi(x, t),$$

are admissible observables in the sense of (3.2.10). For such observables, the $L_{t,x}^1$ -convergence of

$$\langle \nu_{t,x}^{k,\Delta}, g(t, x, \xi) \rangle \rightarrow \langle \nu_{t,x}^k, g(t, x, \xi) \rangle, \quad \text{as } \Delta \rightarrow 0,$$

has been established in Theorem 3.2.13. The same holds true for the other two terms on the left-hand side.

Passing to the limit $\mu_t^\Delta \rightarrow \mu_t$, it thus follows that

$$\begin{aligned} & \int_0^T \int_{D^k} \langle \nu_{t,x}^k, \xi_1 \otimes \cdots \otimes \xi_k \rangle : \partial_t \varphi \\ & + \sum_i \langle \nu_{t,x}^k, \xi_1 \otimes \cdots \otimes \mathbf{F}(\xi_i) \otimes \cdots \otimes \xi_k \rangle : \nabla_{x_i} \varphi \, dx \, dt \\ & + \int_{D^k} \langle \bar{\nu}_x^k, \xi_1 \otimes \cdots \otimes \xi_k \rangle : \varphi(x, 0) \, dx = 0. \end{aligned}$$

The fact that μ_t is concentrated on incompressible vector fields follows immediately from the corresponding property of the approximations μ_t^Δ (cp. Lemma 3.3.3). Furthermore, from Proposition 3.2.9, it also follows that the limit μ_t is time-regular. This finishes the proof that μ_t is a statistical solution of the incompressible Euler equations with initial data $\bar{\mu}$. \square

Remark 3.4.14. *It is straightforward to show that if μ_t^Δ are generated from the spectral hyper-viscosity scheme (1.4.4), and if they satisfy the assumptions of Theorem 3.4.13, the limit μ_t is in fact a dissipative statistical solution in the sense of Definition 3.3.4.*

3.5 Numerical Experiments

In this section, we will present a suite of numerical experiments to demonstrate the effectiveness of the Monte Carlo algorithm 3.4.1 in computing statistical solutions of the incompressible Euler equations. For our numerical experiments, we use the implementation of the spectral hyper-viscosity scheme (1.4.4) provided by the SPHINX code, which has been reviewed in chapter 1.4. For the numerical experiments reported below, we use a spectral viscosity operator of order $s = 1$ (cp. equation (1.4.4)), with $\epsilon_N = \epsilon/N$, $\epsilon = 1/20$ unless otherwise stated. The Fourier multiplier Q_N is chosen with Fourier coefficients

$$\hat{Q}_k = \begin{cases} 1 - N/|k|^2 & |k| \geq \sqrt{N}, \\ 0, & \text{otherwise.} \end{cases}$$

corresponding to $m_N = \sqrt{N}$. Although the theory of section 3.4 is valid for both two and three space dimensions and the SPHINX code is available for both cases, we restrict our focus to two space dimensions in this section, on account of affordable computational costs.

3.5.1 Flat vortex sheet

Vortex sheets occur in many models in physics and are an important test bed for numerical experiments for the Euler equations, [LM15] and references therein. We first consider a randomly perturbed version of the *flat vortex sheet* that corresponds to the following initial data also considered in [LM15],

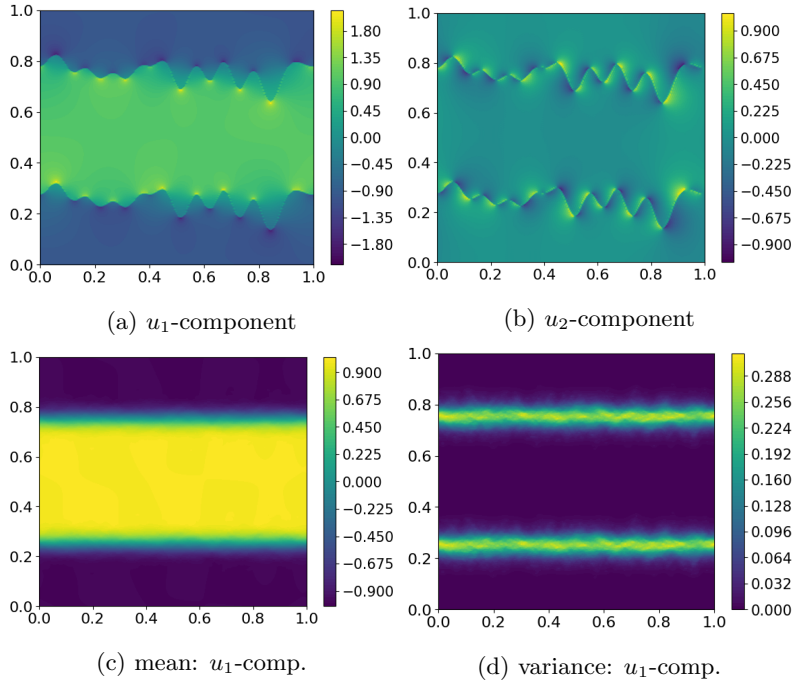


Figure 3.2: Initial data for the perturbed discontinuous flat vortex sheet ($\rho = 0$), samples for $u_{1,2}$, and mean and variance of u_1

Initial data

Given a smoothing parameter $\rho > 0$, and a parameter $\delta \geq 0$ (measuring the size of the random perturbation of the interface), this vortex sheet initial data is of the form

$$\bar{\mathbf{u}}^{\rho,\delta}(x) = \mathbb{P}(\mathbf{U}^\rho(x_1, x_2 + \sigma_\delta(x_1))), \quad (3.5.1)$$

where \mathbb{P} denotes the Leray projection, $\mathbf{U}^\rho(x) = (U_1^\rho(x), U_2^\rho(x))$ is the following smoothed flat vortex sheet initial data:

$$U_1^\rho(x) := \begin{cases} \tanh\left(\frac{x_2 - 1/4}{\rho}\right), & (x_2 \leq 1/2), \\ \tanh\left(\frac{3/4 - x_2}{\rho}\right), & (x_2 > 1/2), \end{cases} \quad U_2^\rho(x) = 0.$$

and $\sigma_\delta(x)$ is a random function, which for a given (random) choice of parameters $\alpha_1, \dots, \alpha_q \in (0, \delta)$, $\beta_1, \dots, \beta_q \in [0, 2\pi]$, is defined by

$$\sigma_\delta(x_1) = \sum_{k=1}^q \alpha_k \sin(2\pi x_1 - \beta_k). \quad (3.5.2)$$

We will also consider the discontinuous case of initial data that are obtained in the limit $\rho \rightarrow 0$ resulting in

$$U_1^0(x) := \begin{cases} +1, & (1/4 < x_2 \leq 3/4), \\ -1, & (\text{otherwise}), \end{cases} \quad U_2^0(x) = 0.$$

For our simulations, we fix $q = 10$ modes for the perturbations. The coefficients α_k are drawn independently, uniformly in $(0, 1)$, and then multiplied by δ . The coefficients β_k are i.i.d., with a uniform distribution on $[0, 2\pi]$. The initial data for the statistical solution $\bar{\mu}_\rho^\delta \in \mathcal{P}(L_x^2)$ is defined as the law of these random perturbations. It depends on the two parameters $\rho \geq 0$, $\delta \geq 0$. While ρ controls the smoothness of the initial data, δ measures the amplitude of the perturbation. We fix $\delta = 0.025$ in the following and consider different values of ρ . Note that the choice $\rho = 0$ corresponds to an initial measure supported on discontinuous flows with a very sharp transition (see figure 3.2 (A,B) for realizations (samples) of this initial data). In figure 3.2 (C,D), we present the initial mean and variance that correspond to the random variations of the initial interface location.

Clearly when $\rho > 0$, the corresponding initial data for every sample is smooth. Consequently, smooth solutions of (1.1.1) are well-posed and the spectral viscosity method converges to this solution as $N \rightarrow \infty$ [BT15]. However for $\rho = 0$, which corresponds to the case of a discontinuous vortex sheet, there are no well-posedness results even for weak solutions, as the vorticity corresponding to the initial data (for each sample) is a sign changing measure and does not belong to the *Delort class*. In [LM15], the authors had presented multiple numerical experiments to illustrate the approximate solutions, computed with a spectral viscosity method, may not converge (or converge too slowly to be of practical interest) for individual samples (see figures 5 and 6 of [LM15]). Hence, it would be interesting to study if approximate statistical solutions, generated by algorithm 3.4.1 converge in this case.

Structure functions and Compensated Energy spectra

The convergence theorem 3.4.6, based on the compactness theorem 3.2.7, provides us with verifiable criteria to check convergence of algorithm 3.4.1. In particular, we need to check certain decay conditions on the structure function (3.2.4) for small correlation lengths. To this end, we consider the following instantaneous version of the structure function (3.2.4),

$$S_{r,t}^{2,\Delta}(\mu_t) := \left(\int_{L_x^2} \int_{\mathbb{T}^2} \int_{B_r(0)} |\mathbf{u}(x+h) - \mathbf{u}(x)|^2 dh dx d\mu_t^\Delta(\mathbf{u}) \right)^{1/2}, \quad (3.5.3)$$

Note that the above is a formal definition and it can be made rigorous in terms of the time-dependent correlation measures. It is much simpler to compute the instantaneous quantity (3.5.3) than the time-averaged version (3.2.4).

Our objective is to check whether the structure function (3.2.4), or rather its instantaneous version (3.5.3), decays (uniformly in resolution Δ) as $r \rightarrow 0$. Such a decay would automatically imply convergence of the approximations to a statistical solutions by theorems 3.2.7 and 3.4.13.

Clearly if $\rho > 0$ in (3.5.1), the spectral viscosity method converges to the unique classical solution as $\Delta \rightarrow 0$. Moreover, a straightforward calculation shows that the structure function (3.5.3) should scale as,

$$S_{r,t}^{2,\Delta}(\mu_t) \approx r, \quad \forall \Delta, t. \quad (3.5.4)$$

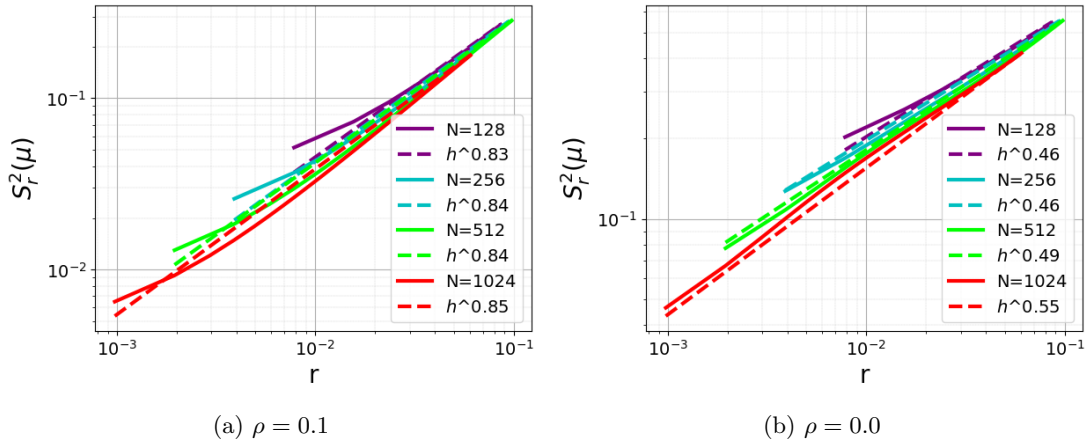


Figure 3.3: Instantaneous structure function (3.5.3) vs correlation length r for different resolutions ($N \sim \Delta^{-1}$) for different values of smoothness parameter ρ , at $t = 0.4$

This is indeed verified from figure 3.3 (A) where we plot the structure function (3.5.3) at $t = 0.4$ and $\rho = 0.1$ for different values of the mesh parameter. We see from this figure that $S_{r,0.4}^{2,\Delta}(\mu_t) \approx r^{0.9}$, at fine resolutions, which is very close to the expected value of 1 for the scaling exponent of the structure function.

On the other hand, for $\rho = 0$, corresponding to the discontinuous flat vortex sheet, the lack of smoothness inhibits us from inferring a particular form of decay of (3.2.4) (or (3.5.3)) a priori.

Remark 3.5.1. We note that for the discontinuous flat vortex sheet, we have $\bar{\mathbf{u}} = (\bar{u}_1(x_2), 0)$, and hence

$$\begin{aligned} S_2(\bar{\mathbf{u}}; r)^2 &= \int_{\mathbb{T}^2} \iint_{B_r(0)} |\bar{\mathbf{u}}(x+h) - \bar{\mathbf{u}}(x)|^2 dh dx \\ &\leq \frac{1}{\pi r^2} \int_{\mathbb{T}^2} \int_{|h_1|, |h_2| \leq r} |\bar{u}_1(x_2 + h_2) - \bar{u}_1(x_2)|^2 dh_2 dh_1 dx \\ &= \frac{4}{r} \int_{-\pi}^{\pi} \int_{|h_2| \leq r} |\bar{u}_1(x_2 + h_2) - \bar{u}_1(x_2)|^2 dh_2 dx_2. \end{aligned}$$

Furthermore, since $|h_2| \leq r$, we have that

$$|\bar{u}_1(x_2 + h_2) - \bar{u}_1(x_2)| = \begin{cases} 0, & (x_2 + h_2 > 0, x_2 > 0), \\ 2, & (x_2 + h_2 > 0, x_2 < 0), \\ 2, & (x_2 + h_2 < 0, x_2 > 0), \\ 0, & (x_2 + h_2 < 0, x_2 < 0). \end{cases} \leq 2 \cdot 1_{|x_2| \leq r},$$

and hence

$$S_2(\overline{u}; r) \leq \left(\frac{16}{r} \int_{|x_2| \leq r} \int_{|h_2| \leq r} dh_2 dx_2 \right)^{1/2} = 8r^{1/2}.$$

At least initially, the calculations of the previous remark imply that $S_{r,0}^{2,\Delta}(\bar{\mu}) \sim r^{\frac{1}{2}}$, for the discontinuous flat vortex sheet. Surprisingly, we find from figure 3.3 (B) that at fine resolutions, $S_{r,t}^{2,\Delta}(\mu_t) \approx r^{0.52}$ also at $t = 0.4$, which agrees with the decay of the structure function of the initial data. Although

we do not present the results there, we observe that the structure function (3.5.3) scales as r^{θ_t} , with $\theta_t \geq 0.5$ for all t . This implies an uniform decay of the structure function (3.2.4) and convergence of the approximations to a statistical solution of the Euler equations (1.1.1), even for this case of discontinuous vortex sheet data. Note that the computed structure functions (3.5.3) in figure 3.3 clearly satisfy the approximate scaling hypothesis (3.4.3) and thus imply convergence through Theorem 3.4.6.

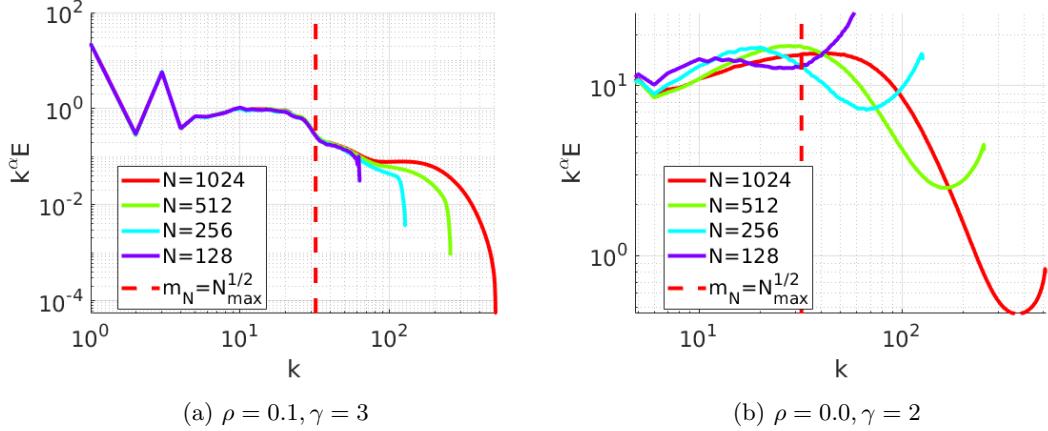


Figure 3.4: The instantaneous compensated energy spectrum $\mathcal{C}_{\gamma,t}^{\Delta}(\mu_t; K)$ (3.5.5) for the flat vortex sheet, at time $t = 0.4$. Note different values of γ for the smooth and discontinuous vortex sheets

An alternative criterion for convergence of statistical solutions is provided by the energy spectrum decay in the inertial range (3.4.5). To check whether this criterion is satisfied, we follow Theorem 3.4.10 and compute the following instantaneous *compensated energy spectrum*,

$$\mathcal{C}_{\gamma,t}^{\Delta}(\mu_t; K) := K^{\gamma} E(\mu_t, K). \quad (3.5.5)$$

Following the arguments in the proof of Theorem 3.4.10, we can relate the decay of the instantaneous energy spectrum to the corresponding decay of the structure function (3.5.3) by a direct analogue of (3.4.6).

For $\rho = 0.1$ in (3.5.1), we plot the compensated energy spectrum $\mathcal{C}_{3,0.4}^{\Delta}(\mu_t; K)$ for all K and at time $t = 0.4$, with compensating factor $\gamma = 3$ in figure 3.4 (A). Note that this choice of γ is consistent with a decay exponent of 1 for the structure function in (3.4.6), *i.e.* $S_2^T(\mu_t^{\Delta}; r) \lesssim r$. We observe from this figure that as expected for this case, the compensated energy spectrum is clearly bounded and in fact, decays faster than the expected rate for the entire range of wave numbers.

On the other hand, we plot the compensated energy spectrum $\mathcal{C}_{2,0.4}^{\Delta}(\mu_t; K)$ (3.5.5) for the discontinuous flat vortex sheet case, *i.e.* $\rho = 0$ in (3.5.1), in figure 3.4 (B). In this case, we expect from the structure function computations (see figure 3.3(B)) that the instantaneous structure function decays with an exponent of ≈ 0.5 . From (3.4.6), we see that this corresponds to the choice of $\gamma = 2$ as the exponent of compensation in (3.5.5). Moreover, in figure 3.4 (B), we also plot the line corresponding to wave number $m_N \approx \sqrt{N}$, which for the spectral viscosity method (1.4.4) represents the wave number after which the spectral viscosity is activated and hence, demarcates the separation between inertial and dissipation ranges. We observe from figure 3.4 (B) that the compensated energy spectrum is clearly uniformly bounded (in terms of the resolution Δ) for the whole inertial range and for all resolutions Δ barring the coarsest resolution, and decays fast in the dissipation range, although there is a slight kink upwards at the very end of the dissipation range, almost at the grid scale. This might be attributed to

numerical errors, which are dominant at this range. Translating these results to the energy spectrum, we see that the spectrum decays as K^{-2} in the inertial range uniformly with respect to resolution. Hence, according to theorems 3.4.10 and 3.4.13, the sequence of approximations will converge to a statistical solution of (1.1.1).

Convergence in Wasserstein Metrics

Given the computational results on the structure function and the compensated energy spectra, results in section 3.4 clearly imply convergence of the approximations μ_t^Δ , generated by the Monte Carlo algorithm 3.4.1 to a statistical solution of the incompressible Euler equations. Moreover from the discussion in section 3.2, we should observe with respect to the following *Cauchy rates*:

$$d_T(\mu_t^\Delta, \mu_t^{\Delta/2}) = \int_0^T W_1(\mu_t^\Delta, \mu_t^{\Delta/2}) dt. \quad (3.5.6)$$

Unfortunately, the calculation of the Wasserstein distance between probability measures defined on high-dimensional (or indeed ∞ -dimensional) spaces is a highly non-trivial issue, which we cannot tackle with present computational resources.

On the other hand, one can compute finite-dimensional *marginals* of (3.5.6) by utilizing the complete characterization of $L_t^1(\mathcal{P})$ in terms of *correlation measures* as given in Theorem 3.2.11. Following [FLMW20, Thm. 5.7], one can prove that,

$$\int_{D^k} W_1(\nu_{t,x}^{\Delta,k}, \nu_{t,x}^{\Delta/2,k}) dx \leq C_k W_1(\mu_t^\Delta, \mu_t^{\Delta/2}), \quad \text{a.e. } t \quad (3.5.7)$$

Here, $k \geq 1$ and $\nu_{t,x}^{\Delta,k}$ is the k -th correlation marginal corresponding to the approximate statistical solution μ_t^Δ . Note that we consider instantaneous versions of the Wasserstein metric (3.5.6) for reasons of computational convenience.

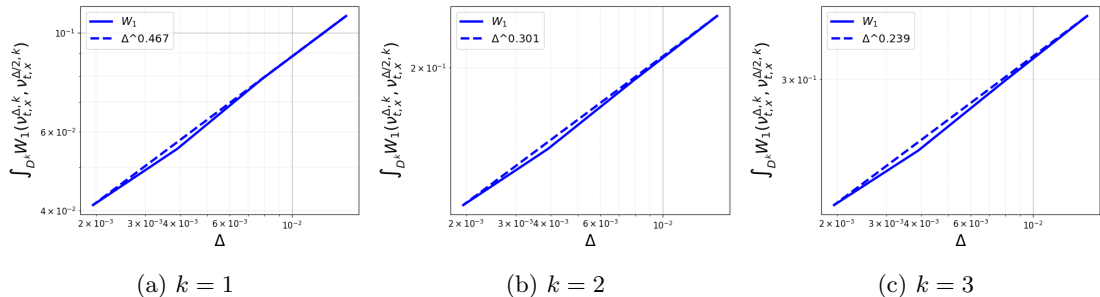


Figure 3.5: The Wasserstein distances between correlation marginals $\int_{D^k} W_1(\nu_{t,x}^{\Delta,k}, \nu_{t,x}^{\Delta/2,k}) dx$ for $k = 1, 2, 3$, at time $t = 0.4$ with respect to resolution

We remark that computing the Wasserstein distances $W_1(\nu_{t,x}^{\Delta,k}, \nu_{t,x}^{\Delta/2,k})$ for small k is much more tractable. We have computed these Wasserstein distances using the algorithm of [BvdPPH11] (as implemented in [FC17]) and the corresponding results for $k = 1, 2, 3$, at time $t = 0.4$ for the discontinuous flat vortex sheet, *i.e.* $\rho = 0$ in (3.5.1) are presented in figure 3.5. As seen from this figure, we observe a clear convergence of these Wasserstein distances (in the Cauchy sense as in (3.5.7)) for the one-point, two-point and three-point correlation measures, albeit at a slow rate for the second and third correlation marginals. This, together with the results on the structure function and compensated energy spectra,

provides considerable evidence that the approximate statistical solutions, generated by algorithm 3.4.1, converge to a statistical solution of (1.1.1). Moreover, given Theorem 3.2.13, results shown in figure 3.5 establish convergence with respect to any admissible observable in the sense of (3.2.10), corresponding of one-point, two-point and three-point statistical quantities of interest. These include mean, variance, structure functions, energy spectra as well as three-point correlation functions.

3.5.2 Sinusoidal vortex sheet

In this section, we will consider a random perturbation of the so-called sinusoidal vortex sheet, *i.e.* the initial vorticity is concentrated on a sine curve. This test case was extensively studied in a recent paper [LM20] in the context of the numerical approximation of weak solutions (in Delort class) of the two-dimensional incompressible Euler equations. Whereas [LM20] considered the deterministic problem with fixed initial data, we will here follow a statistical approach, considering an initial measure $\bar{\mu}$ supported on small random perturbations of the sinusoidal vortex sheet. As discussed in [LM20], due to inherent Kelvin-Helmholtz instabilities the computed numerical approximations for sinusoidal vortex sheet initial data experience vortex sheet roll-up at ever smaller length-scales at increasing resolution $\Delta \rightarrow 0$ (and at low diffusivity). These small-scale Kelvin-Helmholtz instabilities slow down, and at even smaller values of Δ ultimately prevent the strong convergence of the numerical approximants to a limiting solution. In this section, we will compare the convergence properties of the deterministic problem with the corresponding perturbed statistical approach. In contrast to the deterministic problem, the quantities of interest in the statistical setting, such as the mean, variance (as well as higher-order correlations), appear to retain some smoothness even after the complex vortex sheet roll-up. This makes them amenable to numerical approximation, even though the deterministic evolution cannot be stably resolved.

Initial Data

We fix a sinusoidally perturbed vortex sheet, where the initial vorticity is a Borel measure of the form

$$\omega_0 = \delta(x - \Gamma) - \int_{\mathbb{T}^2} d\Gamma,$$

such that $\int_{\mathbb{T}^2} \omega_0 dx = 0$, and up to a constant, ω_0 is uniformly distributed along a curve Γ , which is defined as the graph:

$$\Gamma = \{(x, y) \mid y = d \sin(2\pi x), x \in [0, 1]\}.$$

We chose $d = 0.2$ for our simulations.

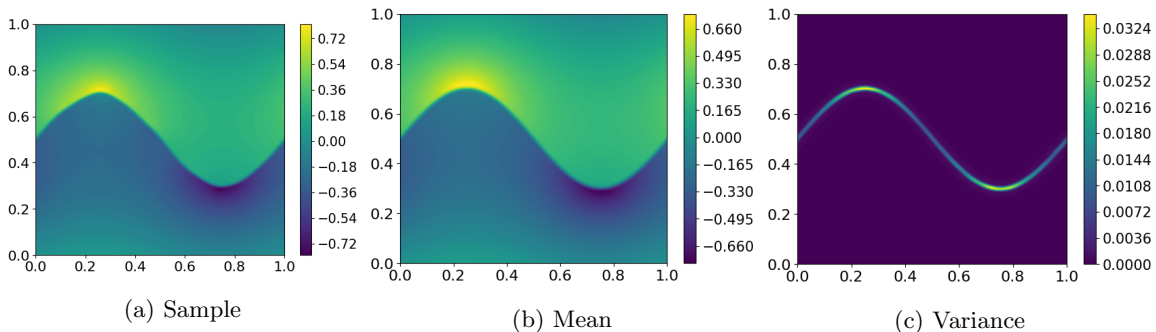


Figure 3.6: Initial conditions for the horizontal velocity u_1 for the sinusoidal vortex sheet.

The numerical initial data is obtained from the mollification of this initial data with a parameter $\rho > 0$. As a mollifier, we consider the third-order B-spline

$$\psi(r) := \frac{80}{7\pi} [(r+1)_+^3 - 4(r+1/2)_+^3 + 6r_+^3 - 4(r-1/2)_+^3 + (r-1)_+^3].$$

Next, we define $\psi_\rho(x) = \rho^{-2}\psi(|x|/\rho)$. The numerical approximation of the perturbed vortex sheet is now defined by setting

$$\omega_0^\rho(x) := \int_{\Gamma} \psi_\rho(x-y) \omega_0(y) dy$$

where ρ determines the thickness (smoothness) of the approximate vortex sheet. The convolution at $x = (x_1, x_2) \in \mathbb{T}^2$ is evaluated via numerical quadrature:

$$(\omega_0 * \psi_\rho)(x) \approx \frac{\rho}{Q} \sum_i \psi_\rho(x - (\xi_i, g(\xi_i))) \sqrt{1 + |g'(\xi_i)|^2},$$

with $\xi_i = x_1 + i\rho/Q$ equidistant quadrature points in x_1 , and $g(\xi)$ the function whose graph is Γ , *i.e.* $g(\xi) = d \sin(2\pi\xi)$. We choose $Q = 400$ quadrature points. We denote by $\mathbf{U}^\rho(x_1, x_2)$ the velocity field such that $\operatorname{div}(\mathbf{U}^\rho) = 0$ and $\operatorname{curl}(\mathbf{U}^\rho) = \omega_0^\rho$.

Similar to the case of the flat vortex sheet, we carry out random perturbations of the sinusoidal vortex sheet as follows:

$$\bar{\mathbf{u}}^{\rho, \delta}(x) := \mathbb{P}(\mathbf{U}^\rho(x_1, x_2 + \sigma_\delta(x_1))).$$

Here, $\mathbb{P} : L_x^2 \rightarrow L_x^2$ denotes the Leray projection onto divergence-free vector fields, and we again fix a random function $\sigma_\delta(x)$,

$$\sigma_\delta(x_1) = \sum_{k=1}^q \alpha_k \sin(2\pi x_1 - \beta_k),$$

depending on a parameter $\delta \geq 0$ and a choice of (random) coefficients $\alpha_1, \dots, \alpha_q \in (0, \delta)$, $\beta_1, \dots, \beta_q \in [0, 2\pi]$. For our simulations, we fix $q = 10$ modes for the perturbations. In practice, the coefficients α_k are first drawn independently, uniformly in $(0, 1)$, and then multiplied by δ . The coefficients β_k are i.i.d., with a uniform distribution on $[0, 2\pi]$. The initial data for the statistical solution $\bar{\mu}_\rho^\delta \in \mathcal{P}(L_x^2)$ is defined as the law of these random perturbations. It depends on the two parameters $\rho \geq 0$, $\delta \geq 0$. While ρ controls the smoothness of the initial data, δ measures the amplitude of the perturbation. We fix $\delta = 0.003125$ in the following and vary ρ as a function of the grid size N . To approximate vortex sheet initial data, we must scale $\rho = \rho(N)$ with N , such that $\rho \rightarrow 0$ as $N \rightarrow \infty$. We use $\rho = 5/N$ for our simulations. The additional diffusion parameter ϵ of the spectral viscosity scheme is set to $\epsilon = 0.01$. With this choice of parameters, we will drop the sub- and superscripts and denote the initial data at a given resolution simply by $\bar{\mu} \in \mathcal{P}(L_x^2)$.

Computation of individual samples

For any single realization of the random perturbation $\sigma_\delta(x)$, the resulting vorticity of the initial data (sample) is a positive measure, concentrated on a sine curve (see figure 3.6 (A) for horizontal component of velocity u_1). Hence, any single sample of the initial data in the Delort class. Therefore, by the results of [LM20], the approximate solutions generated by the spectral viscosity method (1.4.4) will converge, on increasing resolution, to a weak solution of (1.1.1). However, as noted in [LM20], this convergence can be very slow as the flow breaks down into smaller and smaller vortices. In fact, this phenomenon is also seen from figure 3.7 (Top row), where we plot the horizontal component of velocity u_1 at time $t = 1.2$ and different resolutions. At this time, the initial vortex sheet has rolled over and broken down into a

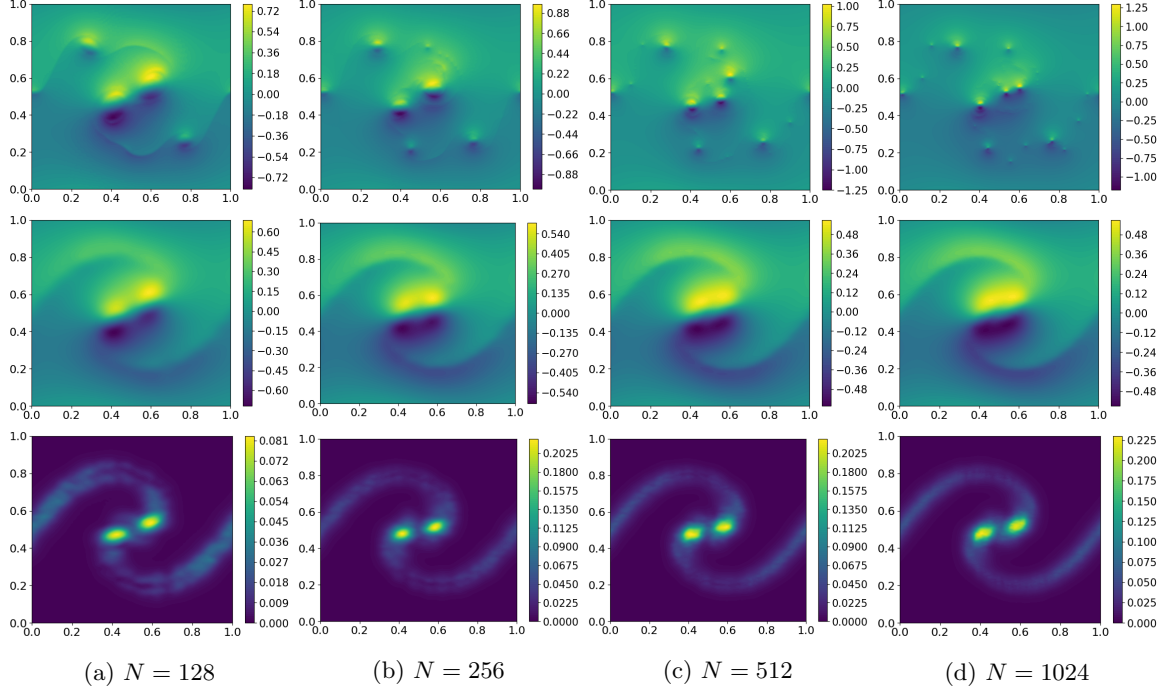
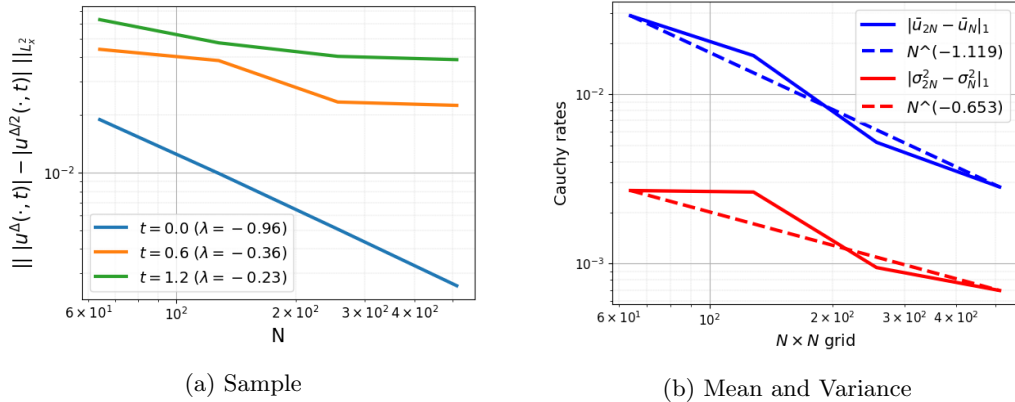


Figure 3.7: Results at time $T = 1.2$ for the horizontal velocity u_1 of the sinusoidal vortex sheet, at different resolutions. Top Row: Sample; Middle Row: Mean; Bottom Row: Variance.



succession of small vortices, whose location and amplitude are different for different resolutions. This very slow convergence is also displayed in figure 3.8 (A), where we plot the Cauchy rates $\|\mathbf{u}^\Delta(t) - \mathbf{u}^{\Delta/2}(t)\|_{L_x^2}$, with \mathbf{u}^Δ denoting the approximate solution computed with the spectral viscosity method (1.4.4), for three different times $t = 0, 0.6, 1.2$. As seen from this figure, the rate of convergence decreases very rapidly and at time $t = 1.2$, it appears as if there is no convergence on mesh refinement.

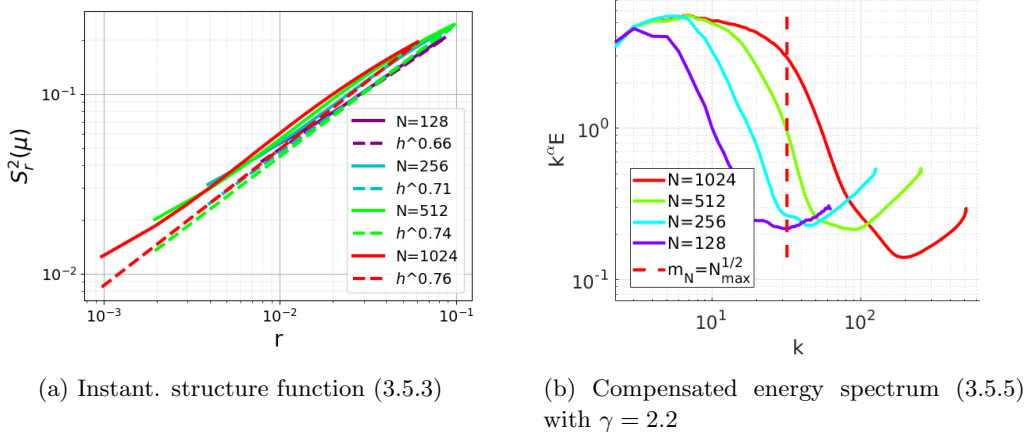


Figure 3.9: The structure function and compensated energy spectrum for the sinusoidal vortex sheet at time $T = 1.2$

Structure functions and Compensated energy spectra

Given this apparent non-convergence of individual samples, it is pertinent to investigate if computing the statistics will be more convergent. To this end, we consider the initial data to be the initial probability measure $\bar{\mu}$. The mean and variance (of the horizontal component u_1) are plotted in figure 3.6 (B,C). From this figure, we observe that the initial probability measure is concentrated on very small perturbations of the underlying sinusoidal vertex sheet, as reflected in the initial variance.

In order to investigate the convergence of approximations to the statistical solution, generated by the algorithm 3.4.1, we follow the template of the previous numerical experiment and compute the (instantaneous) structure function (3.5.3) and the compensated energy spectrum (3.5.5) in figure 3.9. From this figure, we observe that the structure function at time $t = 1.2$ scales with an exponent of ≈ 0.7 at the finest resolutions. From (3.4.6), this implies roughly a $\gamma = 2.4$ in the scaling of the energy spectrum (3.5.5). A better fit to the scaling of the energy spectrum is found with $\gamma = 2.2$. We plot the compensated energy spectrum with the latter value of γ in figure 3.9 (B). From this figure, we see that for the inertial range, the energy spectrum clearly decays (faster than) a rate of 2.2. Thus, the assumptions of theorems 3.2.7, 3.4.10 are satisfied and the approximations will converge to a statistical solution of (1.1.1).

Convergence of observables and Wasserstein Distances

Given the results on the computed structure functions and energy spectra, the approximations will converge. But is this convergence at a better rate than that of single samples? To investigate this issue, we consider two different sets of computations. First, we compute the mean and the variance of the velocity field at different resolutions and plot them (for the horizontal velocity at time $t = 1.2$) in figure

3.7 (Middle and Bottom rows). Clearly, the one-point statistics appear much more convergent than the single sample results. The mean flow consists of a coherent set of large vortices, which is in stark contrast to the large number of vortices formed in the single sample simulations. Moreover, we also plot Cauchy rates for the mean and the variance, corresponding to the norm $\sqrt{u_1^2 + u_2^2}$ at time $t = 1.2$, and different resolutions in figure 3.8 (B).

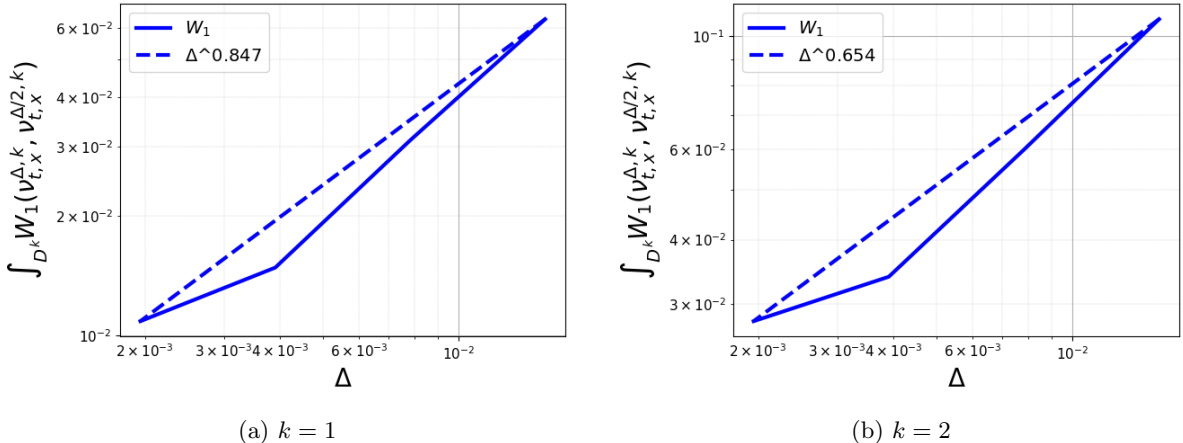


Figure 3.10: The metrics $\int_{D^k} W_1(\nu_{t,x}^{\Delta,k}, \nu_{t,x}^{\Delta/2,k})dx$ for the one- and two-point correlation marginals for the sinusoidal vortex sheet at time $t = 1.2$

Again, we observe that these one-point statistics converge at a significantly faster rate than the single sample. These results indicate that one can expect significantly better convergence of approximations for statistics than for individual realizations of fluid flows, even if the initial probability measure is a small perturbation of the underlying deterministic data and further reinforces the results of Refs. [FKMT17, LM15, FLMW20] in this direction.

Finally, we plot the Wasserstein distances (3.5.7) for $k = 1, 2$, corresponding to the one- and two-point correlation marginals, at time $t = 1.2$, in figure 3.10. The results clearly show convergence in these metrics at a significantly faster rate than for individual samples and indicate possible convergence in the metric (3.2.2) on probability measures on L^2 .

3.5.3 Fractional Brownian motion

The study of the evolution of initial ensembles corresponding to (fractional) Brownian motion stems from Refs. [SAF92, Sin92], where the authors model interesting aspects of Burgers turbulence by evolving Brownian motion initial data for the (scalar) Burgers' equation, see [FLM18] for a more recent numerical study. Similarly in [FLMW20], the authors consider the compressible Euler equations with (fractional) Brownian motion initial data. Following these articles, we will consider the two-dimensional Euler equations (1.1.1) with initial data corresponding to fractional Brownian motion, *i.e.* the following initial data:

$$u_0^{x,H}(\omega; x) := B_1^H(\omega; x), \quad u_0^{y,H}(\omega; x) := B_2^H(\omega; x). \quad \text{for } \omega \in \Omega, \quad x \in D \quad (3.5.8)$$

where B_1^H and B_2^H are two independent two-dimensional fractional Brownian motions with the Hurst index $H \in (0, 1)$. Standard Brownian motion corresponds to a Hurst index of $H = 1/2$. The initial probability measure $\bar{\mu}$ is the law of the above random field.

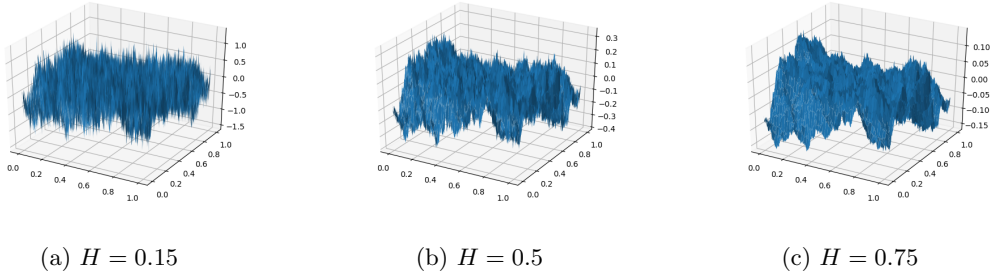


Figure 3.11: A single sample of initial horizontal velocity u_1 for the fractional Brownian motion initial data (3.5.8) for three different Hurst indices

To generate fractional Brownian motion, we use the random midpoint displacement method originally introduced by Lévy [Lév92] for Brownian motion, and later adapted for fractional Brownian motion, see [FLMW20] section 6.6.1.

Considering fractional Brownian motion initial data (3.5.8) is a significant deviation from the vortex sheet initial data in the following respects,

- For the vortex sheet initial data, the initial measure $\bar{\mu} \in \mathcal{P}(L_x^2)$ was concentrated on a 20-dimensional subset of L_x^2 (corresponding to the choice of 20 free parameters α_k, β_k). On the other hand, in the limit of infinite resolution ($\Delta \rightarrow 0$), the fractional Brownian motion initial data corresponds to a measure concentrated on an infinite dimensional subset of L_x^2 .
- For any $0 < H < 1$, and for any sample $\omega \in \Omega$, the initial vorticity for (3.5.8) is not a Radon measure. Consequently, the initial data does not belong to the Delort class and there are no existence results for the corresponding samples. Hence, fractional Brownian motion does not fall within the ambit of any of the available well-posedness theories for two-dimensional Euler equations.
- The Hurst index H in (3.5.8) controls the regularity (and also roughness) of the initial data (pathwise). Roughly speaking, each sample is Hölder continuous with exponent H . Hence, we can consider a very wide range of scenarios in terms of roughness of the initial data by varying the Hurst-index H , see figure 3.11 for realizations of the horizontal velocity field for three different Hurst indices. In particular, one can observe from this figure that lowering the value of H leads to oscillations of both higher amplitude and frequency in the initial velocity field.

Structure functions and Compensated energy spectra

In order to verify convergence of the approximations, generated by algorithm 3.4.1, for the fractional Brownian motion initial data (3.5.8), we will check if the computed structure functions (3.5.3) decay uniformly with respect to resolution, on decreasing correlation lengths. In figure 3.12 (Top Row), we plot the structure function at time $T = 1$ for three different Hurst indices of $H = 0.75, 0.5, 0.15$ and observe that the structure functions indeed decay to zero at a certain exponent (independent of resolution). These exponents are approximately 0.8 for initial $H = 0.75$, 0.6 for the standard Brownian motion initial data ($H = 0.5$) and 0.55 for the initially rough $H = 0.15$. These results indicate that the conditions of the compactness theorem 3.2.7 are fulfilled and the approximations converge to a statistical solution of (1.1.1).

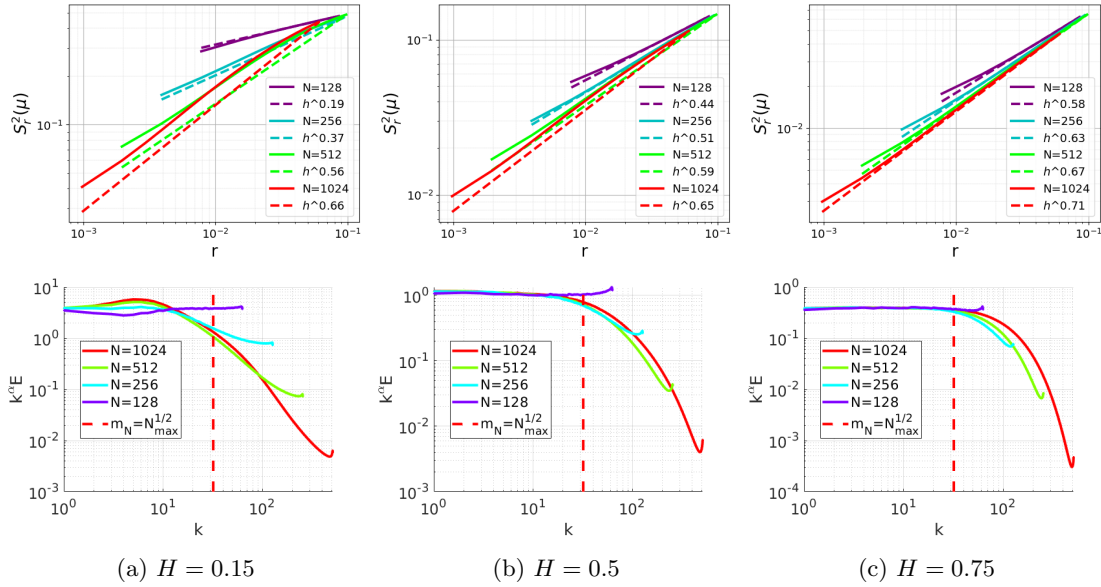


Figure 3.12: Instantaneous structure function (3.5.3) (Top Row) and Compensated energy spectrum (3.5.5) (Bottom Row) for Fractional Brownian motion initial data with three different Hurst indices at time $T = 1$. The compensated energy spectrum (3.5.5) is computed with $\gamma = 1.3$ ($H = 0.15$), $\gamma = 2.0$ ($H = 0.5$) and $\gamma = 2.5$ ($H = 0.75$)

This convergence is further reinforced by the computed compensated energy spectra (3.5.5), at time $T = 1$, for the three different Hurst indices shown in figure 3.12 (Bottom Row). Based on the value of the Hurst index, we choose the compensating index $\gamma = 2.5, 2, 1.3$ for the $H = 0.75, H = 0.5, H = 0.15$, respectively. These values of γ are chosen to provide the correct scaling of the energy spectra at the initial time $t = 0$. As seen from figure 3.12, the compensated energy spectra remain bounded up to the final time $t = T$, independent of the spectral resolution. Hence, the energy spectrum decays at least at the rate of $K^{-\gamma}$ for increasing wave number K , in the inertial range. Consequently, we can readily apply Proposition 3.4.10 and conclude that the approximations, generated by the algorithm 3.4.1, converge to a statistical solution, for all three values of the Hurst index H in (3.5.8).

Convergence in Wasserstein distance

Next, we seek to verify convergence of observables (statistical quantities of interest). To this ends, we follow the previous section and compute the Wasserstein distances $\int_{D^k} W_1(\nu_{t,x}^{\Delta,k}, \nu_{t,x}^{\Delta/2,k})dx$, corresponding to the k -point correlation marginals for the three different Hurst indices of $H = 0.75, 0.5, 0.15$. In figure 3.13, these metrics are computed at time $T = 1$, for $k = 1, 2$, corresponding to one-point and two-point statistical quantities of interest. As observed from the figure, the approximations clearly converge in this metric for both one- and two-point statistics, at rates which are independent of the underlying initial Hurst index. The two-point correlation marginals appear to converge at a slower rate than the one-point Young measures. These results validate convergence of all one- and two-point statistical quantities of interest. Taken together with the results for the structure function, compensated energy spectra and Theorem 3.2.7, they strongly suggest convergence in metric d_T (3.2.2) on $L_T^1(\mathcal{P})$.

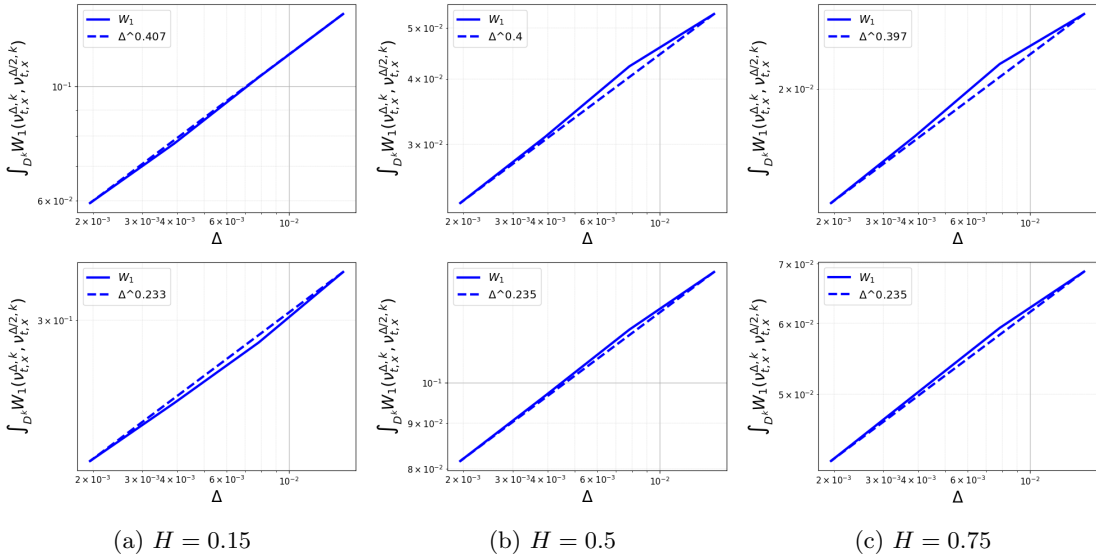


Figure 3.13: Wasserstein distances $\int_{D^k} W_1(\nu_{t,x}^{\Delta,k}, \nu_{t,x}^{\Delta/2,k}) dx$ for $k = 1$ (Top Row) and $k = 2$ (Bottom Row) for Fractional Brownian motion initial data with three different Hurst indices at time $t = 1$.

3.6 Discussion

We have considered the numerical approximation of solutions of the incompressible Euler equations (1.1.1) in this chapter. The existence of classical (or weak) solutions is an outstanding open question in three space dimensions. Although weak solutions are known to exist in two space dimensions, even for very rough initial data, they may not be unique. Similarly, numerical experiments reveal that standard numerical methods may not converge, or converge very slowly, to weak solutions on increasing resolution.

Given these inadequacies of traditional notions of solutions, it is imperative to find solution concepts for (1.1.1) that are well-posed and amenable to efficient numerical approximation. In this context, we consider the solution framework of statistical solutions. Statistical solutions are time-parameterized probability measures on $L^2(D; \mathbb{R}^d)$. Given the characterization of probability measures on L^p spaces in [FLM17], these measures are equivalent to so-called *correlation measures*, *i.e.* Young measures on tensor-products of the underlying domain and phase space that represent multi-point spatial correlations. Furthermore, we require statistical solutions to satisfy an infinite number of PDEs (see Definition 3.3.1) for the moments of the underlying correlation measure. Hence, a statistical solution can be interpreted as a measure-valued solution (cp. Definition 1.3.8), augmented with information about the evolution of all possible multi-point spatial correlations.

Our aim in this chapter was to study the well-posedness and efficient numerical approximation of statistical solutions. To this end, first, we had to characterize convergence on a weak topology on the space $L_t^1([0, T]; \mathcal{P}(L^2(D; \mathbb{R}^d)))$, under an assumption of *time-regularity* on the underlying measures. Convergence in this topology amounted to convergence of a very large class of observables (or statistical quantities of interest). We then proposed a notion of dissipative statistical solutions and also proved partial well-posedness results for them in a generic sense, namely when the initial measure is concentrated on functions sufficiently near initial data for which smooth solutions exist. This led to short-time well-posedness if the initial probability measure is concentrated on smooth functions. In two space dimensions, we proved global well-posedness for statistical solutions when the initial data is concentrated on smooth

functions. Moreover, we also proved a suitable variant of weak-strong uniqueness.

The main contribution of the work summarized in this chapter is the proposal of an algorithm 3.4.1 to approximate statistical solutions of the Euler equations. This Monte Carlo type algorithm is a variant of the algorithms proposed recently [FKMT17, LM15, FLMW20] and is based on an underlying spectral hyper-viscosity spatial discretization. Under verifiable hypotheses, we prove that the approximations converge in our proposed topology to a statistical solution. These hypotheses either rely on a suitable scaling (or uniform decay) for the structure function, or equivalently, on finding an inertial range (of wave numbers) on which the energy spectrum decays (uniformly in resolution). These hypotheses are very common in the extensive literature on turbulence (see [Fri95] and references therein). A key novelty in the work summarized in the present chapter is the rigorous proof of the fact that easily verifiable conditions on the structure functions or energy spectrum imply a rather strong form of convergence for (multi-point) statistical quantities of interest. For instance, we observe a surprising fact that a bound on the compensated energy spectrum (3.5.5) implies that k -point statistics of interest, even for large k , converge. The convergence results also provide a conditional global existence result for statistical solutions in both two and three space dimensions.

We present results of several numerical experiments for the two-dimensional Euler equations. From the numerical experiments, we observe that:

- Our convergence theory is validated by all the numerical experiments. The assumptions on the structure functions and energy spectra appear to be very clearly fulfilled in practice. Moreover, the computed solutions converge to a statistical solution in suitable Wasserstein metrics on multi-point correlation marginals. In particular, all admissible observables of interest such as mean, variance, higher moments, structure functions, spectra, multi-point correlation functions, converge on increasing resolution and sample augmentation.
- In clear contrast to the deterministic case where computed solutions may converge very slowly even if one can prove convergence of the underlying numerical method (see [LM20] and figure 3.8), statistical quantities of interest seem to be better behaved and converge faster.
- For our numerical examples, we observe convergence of approximations even when the initial data was quite rough such as when the initial vorticity may not have definite sign (as in the flat vortex sheet) or may not even be a Radon measure (as in the fractional Brownian motion with any Hurst index $H \in (0, 1)$). For such initial data, the samples are not in the Delort class and the convergence (and existence) theory for two-dimensional Euler equations is no longer valid. On the other hand, we find neat convergence to a statistical solution.

Based on the above discussion, we conclude that statistical solutions are a promising solution framework for the incompressible Euler equations. In particular, there is some scope for proving well-posedness results within this class, possibly with further admissibility criteria. Moreover, numerical approximation of statistical solutions is feasible with ensemble averaging algorithms. Statistical solutions can be a suitable framework for uncertainty quantification and Bayesian inversion for the Euler equations and to encode and explain numerous computational and experimental results for turbulent fluid flows.

There are several limitations of the work summarized in the current chapter, which provide directions for future work. At the theoretical level, we seek to either relax the criteria on scaling of structure functions or prove it. This will pave the way for global existence results. Similarly, the weak-strong uniqueness results of this paper could be improved.

In terms of numerical approximation, the main issue with the Monte Carlo type algorithm 3.4.1 is the slow convergence (in terms of number of samples). This necessitates a very high computational

cost, particularly in three space dimensions. Future work could consider efficient variants such as multi-level Monte Carlo [FLM18, MSS12, LMS16], Quasi-Monte Carlo and deep learning algorithms [LMR20], for computing statistical solutions of the incompressible Euler equations in three space dimensions. A rationale for the potentially improved efficiency of approximations of statistical solutions deep learning algorithms, leveraging neural network based surrogate models, will be discussed in chapter 7 of the present thesis.

Chapter 4

Physically realizable solutions and energy conservation

In the last chapter, we have established a theoretical framework for statistical solutions of the incompressible Euler equations. A central quantity in the study of the convergence of numerical schemes to a limiting statistical solution was given by the (2nd-order) structure function $S_2^T(\mu_t^\Delta; r)$, measuring the average two-point correlations in the flow. Numerical experiments indicate that these (statistical) structure functions are very well-behaved in practical computations, exhibiting a uniform decay at increasing numerical resolution for a wide range of initial data. In the present chapter we aim to further study the role of these structure functions in relation to one of the core questions of turbulence, namely the question of anomalous energy dissipation in the zero-viscosity limit. We will consider this question in both a deterministic and a statistical setting, and we will restrict our discussion to the two-dimensional case. The present chapter summarizes the results of [LMPP21a].

4.1 Introduction

Turbulence is a defining feature of fluid flows at high Reynolds numbers [Fri95]. It is characterized by the dynamic generation of structures (eddies) at small scales and by the cascade of energy from large scale features of the flow to ever smaller scales.

Arguably, the famous K41 theory of Kolmogorov provides the most coherent explanation for fully-developed turbulence. As presented in [Fri95], it is based on the incompressible Navier-Stokes equations with initial data $\bar{\mathbf{u}}$, given by (cp. (1.2.3) in chapter 1),

$$\begin{cases} \partial_t \mathbf{u}^\nu + \mathbf{u}^\nu \cdot \nabla \mathbf{u}^\nu + \nabla p^\nu = \nu \Delta \mathbf{u}^\nu, \\ \operatorname{div}(\mathbf{u}^\nu) = 0, \quad \mathbf{u}^\nu|_{t=0} = \bar{\mathbf{u}}, \end{cases} \quad (4.1.1)$$

Here, the velocity field is denoted by $\mathbf{u}^\nu \in \mathbb{R}^d$ (for $d = 2, 3$), and the pressure is denoted by $p^\nu \in \mathbb{R}$. For any given *viscosity* $\nu > 0$, it is straightforward to see that the incompressible Navier-Stokes equations formally satisfy an energy balance equation of the form

$$\frac{d}{dt} \frac{1}{2} \int_D |\mathbf{u}^\nu|^2 dx = -\nu \int_D |\nabla \mathbf{u}^\nu|^2 dx.$$

Here, the left-hand side describes the time evolution of the kinetic energy $E(t) = \frac{1}{2} \|\mathbf{u}^\nu(t)\|_{L_x^2}^2$, while the right-hand side term describes the energy dissipation at small scales by viscosity. It is clear from this

equation that we should expect $E(t)$ to be non-increasing in time, $E(t) \leq E(0)$ for all $t \geq 0$; in fact, we should at least expect that suitable solutions of (4.1.1) satisfy

$$E(0) - E(t) \sim \nu \int_0^t \|\nabla \mathbf{u}^\nu\|_{L_x^2}^2 dx \quad (4.1.2)$$

Given that turbulence appears at high Reynolds number (low viscosity), the behavior of the energy dissipation (the right hand side of the energy balance (4.1.2)) is of great interest. In fact, one of the fundamental postulates of Kolmogorov's K41 physical theory of fully developed homogeneous isotropic turbulence is that $\langle \nu \|\nabla \mathbf{u}^\nu\|_{L_x^2}^2 \rangle \rightarrow \epsilon_0 > 0$, as $\nu \rightarrow 0$ [Kol91, KLH⁺91]. Here, $\langle \dots \rangle$ refers to a suitable ensemble average (or long time average under an ergodicity hypothesis). In other words, a cornerstone of Kolmogorov's theory is the assumption of *anomalous*, i.e. *finite, non-zero* energy dissipation in the infinite Reynolds number limit.

Formally, taking the infinite Reynolds number limit ($\nu \rightarrow 0$) in the Navier-Stokes equations and assuming that $\mathbf{u}^\nu \rightarrow \mathbf{u}$, implies that \mathbf{u} satisfies the *incompressible Euler equations*:

$$\begin{cases} \partial_t \mathbf{u} + \mathbf{u} \cdot \nabla \mathbf{u} + \nabla p = 0, \\ \operatorname{div}(\mathbf{u}) = 0, \quad \mathbf{u}|_{t=0} = \bar{\mathbf{u}}. \end{cases} \quad (4.1.3)$$

We recall from chapter 1.3.5, that the issue of anomalous dissipation in turbulent flows was cast in terms of solutions of the incompressible Euler equations by Onsager in [Ons49], who observed that Hölder continuous solutions of the incompressible Euler equations $\mathbf{u} \in C^\alpha$ should conserve energy provided that $\alpha > 1/3$, but might exhibit anomalous dissipation if $\alpha < 1/3$, even in the zero viscosity limit. The existence of energy-dissipative solutions $\mathbf{u} \in C^\alpha$ for $\alpha < 1/3$, so-called *wild solutions*, has been recently shown in [Ise18, BdLSV19] for the three-dimensional case, based on pioneering work of DeLellis and Székelyhidi in [DLS09] where convex integration techniques were adapted to the study of fluid flows. However, there is an essential caveat in the construction of these wild solutions: At the outset, it is unclear if these wild solutions can be realized as vanishing viscosity limits of the Navier-Stokes equations (4.1.1). If not, their link to the questions of anomalous dissipation in turbulent flows is rather tenuous.

It is widely known that vanishing viscosity limits might exhibit additional structures that could well constrain the formation of energy dissipative solutions. This is especially true in two space dimensions, as there is a critical role played by the vorticity $\omega = \operatorname{curl}(\mathbf{u})$ of the flow. In fact, in a recent paper [CFLS16], the authors prove that if a weak solution of the incompressible Euler equations \mathbf{u} with initial data having vorticity $\bar{\omega} \in L^p$, $p > 1$, is obtained as the limit $\mathbf{u}^\nu \rightarrow \mathbf{u}$ of solutions \mathbf{u}^ν of the ν -Navier-Stokes equations (4.1.1) with the same initial data, then \mathbf{u} is energy conservative. On the other hand, $\bar{\omega} \in L^p$, $p > 1$ does not imply that $\bar{\mathbf{u}} \in C^\alpha$ for $\alpha > 1/3$.

A critical assessment of the results of the paper [CFLS16] motivate us to ask the following questions: first, can one extend the energy conservation results of [CFLS16] to even rougher initial data? In two space dimensions, Delort [Del91] (see also [VW93]) proved existence of weak solutions of the incompressible Euler equations, even when the initial vorticity $\bar{\omega} \in H^{-1} \cap \mathcal{M}$ and $\bar{\omega}$ can be written as the sum of a bounded measure of distinguished sign and a function in L^p , $1 \leq p \leq \infty$. Hence, we are interested in investigating if weak solutions of the Euler equations (realized as a vanishing viscosity limit of the Navier-Stokes equations), with measure-valued initial vorticity, are energy conservative. Such initial data correspond to interesting physical scenarios such as *vortex sheets*. In two dimensions, the vorticity of vortex sheet initial data is initially distributed along a (smooth) curve γ_0 . Classically, the dynamics of such vortex sheets has been studied by considering the evolution equation for γ_t , known as the Birkhoff-Rott equation. From the results presented in [Shv09] (pertaining to both two and higher dimensions), it follows in particular that classical vortex sheet solutions conserve energy as long as the evolving curve γ_t

remains sufficiently smooth [Shv09, Corollary 11]. Short-time existence and regularity results for γ_t are known for a suitable class of analytic initial data [SSBF81, Caf88], but in general, numerical evidence [Kra86b] indicates that global existence is precluded by the occurrence of a roll-up singularity. The energy conservation results for classical vortex sheets could thus suggest that an energy conservation result holds also in the zero-viscosity limit, at least before the occurrence of vortex sheet roll-up. Through careful numerical experiments, we will investigate the evolution of vortex sheets even well beyond the time of roll-up singularity.

In addition to the question of energy conservation in the zero-viscosity limit, we are interested in investigating if limits of other interesting approximations of the two-dimensional Euler equations, for instance numerical approximations such as the spectral viscosity method [Tad04, BT15], are energy conservative.

Another aspect of the results of [Ise18, BdLSV19, CFLS16] is the fact that they pertain only to deterministic solutions. On the other hand, most descriptions of turbulence, including the K41 theory, are probabilistic in nature, with the anomalous dissipation hypothesis being considered for ensemble averages [Fri95]. It is natural to ask if the analogous energy conservation results hold for a probabilistic description of turbulent flows.

Given these questions, the main goals and results summarized in the current chapter are:

- We prove that any weak solution \mathbf{u} of the two-dimensional incompressible Euler equations (4.1.3), which can be obtained as a strong limit $\mathbf{u}^\nu \rightarrow \mathbf{u}$ in $L_t^1([0, T]; L_x^2)$ in the zero viscosity limit of the incompressible Navier-Stokes equations (4.1.1), $\nu \rightarrow 0$, must be *energy conservative*. This implies in particular energy conservation for the large class of initial data for which strong L^2 -convergence (in $C([0, T]; L_x^2)$) has been proven in [FLT00], and extends the results of [CFLS16] to initial vorticity beyond L^p , $p > 1$.
- We consider the probabilistic framework of *statistical solutions*, proposed for the Navier-Stokes equations in [FMRT08] and references therein, and more recently for the Euler equations in [FLM17, FW18, LMPP21b] and prove analogous energy conservation results for statistical solutions of Euler equations, in particular, those that arise as limits of a spectral viscosity-Monte Carlo numerical approximation of [LMPP21b].
- For both sets of results, we express the strong compactness of approximating sequences in terms of uniform decay of the so-called *structure function* (4.2.2). The structure function appears repeatedly in the turbulence literature [Fri95] and references therein, as well as in the more recent mathematical discussions of [CG12, CV18, DN19], and it can be computed in numerical approximations and measured in experiments. Thus, characterizing energy conservation (and anomalous dissipation) in terms of the structure function is very convenient.
- The validity of the proposed theory is illustrated in terms of different numerical experiments. In particular, we consider initial data that don't necessarily belong to the class considered by Delort in [Del91] and for which no compactness/existence results are available. Numerical experiments reveal that the approximate solutions possess the desired decay of the structure function and computed energy is conserved in time.

The rest of this chapter is organized as follows: in section 4.2, we characterize energy conservation for the vanishing viscosity limit. Energy conservation for numerical approximations to statistical solutions of (4.1.3) is considered in section 4.3 and numerical experiments to illustrate and complement the theory are presented in section 4.4.

4.2 Energy conservation of vanishing viscosity limits

Our goal in this section will be to characterize the conservation of energy in weak solutions of the two-dimensional Euler equations (4.1.3), that arise as vanishing viscosity limits of the Navier-Stokes equations (4.1.1). For the convenience of the reader, we here recall the definition of approximate solutions sequences introduced in chapter 1 (cp. Definition 1.3.5):

Definition 4.2.1. *Let $\{\mathbf{u}_k\}$, $k \in \mathbb{N}$, be a uniformly bounded sequence in $L^\infty([0, T]; L^2(\mathbb{T}^2; \mathbb{R}^2))$. The sequence $\{\mathbf{u}_k\}$ is an **approximate solution sequence** for the incompressible Euler equations, if the following properties are satisfied:*

1. *The sequence $\{\mathbf{u}_k\}$ is uniformly bounded in $\text{Lip}([0, T]; H^{-L}(\mathbb{T}^2; \mathbb{R}^2))$, for some (possibly large) $L > 1$.*
2. *For any test vector field $\varphi \in C_c^\infty([0, T] \times \mathbb{T}^2; \mathbb{R}^2)$ with $\text{div}(\varphi) = 0$, we have:*

$$\lim_{k \rightarrow \infty} \int_0^T \int_{\mathbb{T}^2} \varphi_t \cdot \mathbf{u}_k + (\nabla \varphi) : (\mathbf{u}_k \otimes \mathbf{u}_k) dx dt + \int_{\mathbb{T}^2} \varphi(x, 0) \cdot \mathbf{u}_k(x, 0) dx = 0.$$

3. $\text{div}(\mathbf{u}_k) = 0$ in $\mathcal{D}'([0, T] \times \mathbb{T}^2)$.

We shall often denote (spatial) L^p spaces, such as $L^p(D; \mathbb{R}^2)$ in the abbreviated form L_x^p in the following, provided that the domain and co-domain are clear from the context. Similar notation will be used to denote time-dependent Bochner spaces $L_t^p L_x^2 := L^p([0, T]; L_x^2)$, where it is understood that the temporal domain is $[0, T]$ for some fixed $T > 0$.

Our interest is in particular approximating sequences that stem from the weak solutions of the Navier-Stokes equations. Hence, following [CFLS16], we define,

Definition 4.2.2. *A weak solution $\mathbf{u} \in L^\infty([0, T]; L_x^2)$ of the incompressible Euler equations with initial data $\bar{\mathbf{u}} \in L_x^2$ is **physically realizable**, if there exists a sequence \mathbf{u}^{ν_k} , such that each $\mathbf{u}^{\nu_k} \in C([0, T]; L_x^2)$*

1. *is a solution of (4.1.1) with viscosity $\nu_k \rightarrow 0$ ($k \rightarrow \infty$),*
2. *$\mathbf{u}^{\nu_k}(t = 0) \rightarrow \bar{\mathbf{u}}$ strongly in L_x^2 , ($k \rightarrow \infty$),*
3. *and $\mathbf{u}^{\nu_k} \rightharpoonup \mathbf{u}$ weakly in $L_t^2(L_x^2)$.*

In this case, we will refer to the sequence $\mathbf{u}^{\nu_k} \rightharpoonup \mathbf{u}$ as a **physical realisation** of \mathbf{u} .

As mentioned in the introduction, we seek to characterize compactness of approximating sequences and energy conservation in terms of the structure function. We recall the definition of the structure function. Given $\mathbf{u} \in L_x^2$, the structure function $S_2(\mathbf{u}; r)$ for $r \geq 0$ is defined as follows:

$$S_2(\mathbf{u}; r) := \left(\int_D \int_{B_r(0)} |\mathbf{u}(x+h) - \mathbf{u}(x)|^2 dh dx \right)^{1/2}. \quad (4.2.1)$$

Similarly, the time-integrated structure function $S_2^T(\mathbf{u}; r)$ for $\mathbf{u} \in L_t^2 L_x^2$, is defined by setting

$$S_2^T(\mathbf{u}; r) := \left(\int_0^T S_2(\mathbf{u}(t); r)^2 dt \right)^{1/2}. \quad (4.2.2)$$

Remark 4.2.3. As pointed out in [DN19, eq. (21), (22)], the structure function $S_2^T(\mathbf{u}^\nu; r)$ for solutions \mathbf{u}^ν of the Navier-Stokes equations at diffusive length scales $r \in [0, \nu^{1/(2-2\alpha)}]$ satisfies an a priori algebraic decay of order $\alpha \in (0, 1)$ (see also [LMPP21b, Lemma 4.5] for a corresponding statement for the spectral-viscosity scheme). Indeed, from the $L^2([0, T]; H_x^1)$ -bound, it is immediate that $S_2^T(\mathbf{u}^\nu; r) \leq Cr/\sqrt{\nu}$, where C depends only on $\|\mathbf{u}^\nu(t=0)\|_{L_x^2}$. So if $r \leq \nu^{1/(2-2\alpha)}$, then $r/\sqrt{\nu} \leq r^\alpha$ and consequently, the algebraic decay $S_2^T(\mathbf{u}^\nu; r) \leq Cr^\alpha$ is satisfied in this range. In particular, to numerically verify an algebraic decay assumption $S_2^T(\mathbf{u}^\nu; r) \leq Cr^\alpha$, it suffices to consider only a finite range, e.g. $r \in [\nu^{1/(2-2\alpha)}, 1]$.

Remark 4.2.4. A measure of regularity very similar to the structure function (4.2.1) has previously been employed in [CG12, CV18, DN19] to study the convergence of solutions of the Navier-Stokes equations to solutions of the Euler equations in the zero-viscosity limit, notably on bounded domains $D \subset \mathbb{R}^d$, $d = 2, 3$, with regular boundary. In this context, it has been shown [DN19] for both no-slip and Navier friction or slip boundary conditions, that the validity of a uniform algebraic upper bound,

$$\limsup_{\nu_k \rightarrow 0} \int_A |\mathbf{u}^{\nu_k}(x+h) - \mathbf{u}^{\nu_k}(x)|^2 dx \leq C|h|^\zeta,$$

for all $A \Subset D$ (here $C = C(A) > 0$, $\zeta = \zeta(A) \in (0, 2)$), is a sufficient condition to conclude that the weak limit $\mathbf{u}^{\nu_k} \rightharpoonup \mathbf{u}$ is a weak solution of the Euler equations on D .

In the present work, we will relate uniform (and not necessarily algebraic) decay of the structure functions to compactness properties and energy conservation of approximating sequences in the two-dimensional case. To this end, we need the following technical results: The first one follows from a simple calculation.

Lemma 4.2.5 ([LMPP21a, Lemma 2.5]). We have for any $\mathbf{u} \in H_x^1$:

$$\int_D \int_{B_r(0)} |h \cdot \nabla \mathbf{u}(x)|^2 dh dx = \frac{r^2}{4} \int_D |\nabla \mathbf{u}(x)|^2 dx.$$

The second technical inequality we will need is given in the following Lemma.

Lemma 4.2.6. There exists an absolute constant $C > 0$, such that for any $\mathbf{u} \in H_x^2$ and any $r > 0$, we have the following inequality

$$\|\omega\|_{L_x^2} \leq Cr\|\nabla\omega\|_{L_x^2} + \frac{2S_2(\mathbf{u}; r)}{r}, \quad (4.2.3)$$

where $\omega = \text{curl}(\mathbf{u})$.

Before proving Lemma 4.2.6, we remark on its significance in the present context.

Remark 4.2.7. Note that if \mathbf{u} is in H_x^α for some $0 < \alpha < 1$, then $S_2(\mathbf{u}; r) \lesssim \|\mathbf{u}\|_{H_x^\alpha} r^\alpha$ and the estimate (4.2.3) implies that

$$\|\mathbf{u}\|_{H_x^1} \lesssim r\|\mathbf{u}\|_{H_x^2} + r^{\alpha-1}\|\mathbf{u}\|_{H_x^\alpha}.$$

This estimate can also be obtained from the following interpolation inequality

$$\|\mathbf{u}\|_{H_x^1} \leq \|\mathbf{u}\|_{H_x^2}^{1-\theta} \|\mathbf{u}\|_{H_x^\alpha}^\theta \leq r\|\mathbf{u}\|_{H_x^2} + r^{(\theta-1)/\theta}\|\mathbf{u}\|_{H_x^\alpha}$$

for $r > 0$, where θ is chosen such that $1 = 2(1 - \theta) + \alpha\theta$, i.e. $\theta = 1/(2 - \alpha)$; implying once again an estimate of the form

$$\|\mathbf{u}\|_{H_x^1} \lesssim r\|\mathbf{u}\|_{H_x^2} + r^{\alpha-1}\|\mathbf{u}\|_{H_x^\alpha},$$

for any $r > 0$. Note also that with a suitable choice of r , the original interpolation estimate for $\|\mathbf{u}\|_{H_x^1}$ in terms of $\|\mathbf{u}\|_{H_x^2}$, $\|\mathbf{u}\|_{H_x^\alpha}$ can be re-obtained from the latter estimate.

In this sense, Lemma 4.2.6 can be thought to generalize such H^α -type interpolation estimates to situations where one only has uniform bounds on the structure functions, instead of an explicit H^α estimate.

Proof of Lemma 4.2.6. By an approximation argument, it is sufficient to prove the claimed inequality for $\mathbf{u} \in C^\infty \cap H_x^2$. In this case, it follows from Taylor expansion that for any x, h , we have the following equality

$$\mathbf{u}(x+h) - \mathbf{u}(x) = h \cdot \nabla \mathbf{u}(x) + \int_0^1 (1-t)(h \otimes h) : \nabla^2 \mathbf{u}(x+th) dt.$$

Let now $D(x, h) := \mathbf{u}(x+h) - \mathbf{u}(x)$, $G(x, h) := h \cdot \nabla \mathbf{u}(x)$ and

$$R(x, h) := \int_0^1 (1-t)(h \otimes h) : \nabla^2 \mathbf{u}(x+th) dt.$$

Fix $r > 0$. Define a measure m on $D \times D$ by

$$\int_{D \times D} f(x, h) dm(x, h) = \int_D \int_{B_r(0)} f(x, h) dh dx.$$

It follows from the equality $G(x, h) = D(x, h) - R(x, h)$ that

$$\|G(x, h)\|_{L_{x,h}^2(dm)} \leq \|D(x, h)\|_{L_{x,h}^2(dm)} + \|R(x, h)\|_{L_{x,h}^2(dm)}.$$

We note that by Lemma 4.2.5, we have

$$\|G(x, h)\|_{L_{x,h}^2(dm)} = \frac{r}{2} \left(\int_D |\nabla \mathbf{u}(x)|^2 dx \right)^{1/2} = \frac{r}{2} \|\omega\|_{L_x^2(dx)}.$$

Furthermore, we note that – by definition – $\|D(x, h)\|_{L_{x,h}^2(dm)} = S_2(\mathbf{u}; r)$. Finally, it is easy to see that there exists a constant C such that

$$\|R(x, h)\|_{L_{x,h}^2(dm)} \leq Cr^2 \|\nabla^2 \mathbf{u}\|_{L_x^2(dx)} \leq Cr^2 \|\nabla \omega\|_{L_x^2(dx)}.$$

Combining these expressions (and possibly enlarging the constant C), the claimed estimate follows. \square

As mentioned in the introduction, the energy conservation results of [CFLS16] are a starting point for this work. In [CFLS16], the authors characterize energy conservation in terms of uniform a priori estimates on the vorticity ω of the approximating sequences. In order to introduce the reader to our generalizations of the results of [CFLS16], we begin with the following theorem that recasts the energy conservation results of [CFLS16] in terms of the structure function.

Theorem 4.2.8. *Let \mathbf{u} be a weak solution of the incompressible Euler equations which is the physical realisation in the zero-viscosity limit of a sequence $\mathbf{u}^{\nu_k} \rightharpoonup \mathbf{u}$, as $\nu_k \rightarrow 0$. If there exist constants $C, \alpha > 0$, such that $S_2(\mathbf{u}^{\nu_k}(t); r) \leq Cr^\alpha$ for all $t \in [0, T]$, $k \in \mathbb{N}$, then \mathbf{u} is energy-conservative.*

As the proof closely follows the arguments of [CFLS16], we provide a sketch below.

Sketch of proof. Under the assumption of algebraic decay of the structure function at each $t \in [0, T]$, we have strong compactness of \mathbf{u}^{ν_k} in $C([0, T]; L_x^2)$. In particular, it follows from the weak convergence

$\mathbf{u}^{\nu_k} \rightharpoonup \mathbf{u}$ that in fact $\mathbf{u}^{\nu_k} \rightarrow \mathbf{u}$ in $C([0, T]; L_x^2)$. Thus, for any $t \in [0, T]$, we have (cp. equation (1.3.15) in chapter 1)

$$\|\mathbf{u}(t)\|_{L_x^2}^2 - \|\bar{\mathbf{u}}\|_{L_x^2}^2 = \lim_{k \rightarrow \infty} \left(\|\mathbf{u}^{\nu_k}(t)\|_{L_x^2}^2 - \|\mathbf{u}^{\nu_k}(0)\|_{L_x^2}^2 \right) = \lim_{k \rightarrow \infty} 2\nu_k \int_0^t \|\omega^{\nu_k}(s)\|_{L_x^2}^2 ds.$$

The central point of the argument is to show that under the present assumptions

$$\nu_k \int_0^T \|\omega^{\nu_k}(t)\|_{L_x^2}^2 dt \rightarrow 0, \quad (\nu_k \rightarrow 0).$$

The vorticity equation implies the following enstrophy equation

$$\frac{d}{dt} \|\omega^{\nu_k}(t)\|_{L_x^2}^2 = -2\nu_k \|\nabla \omega^{\nu_k}(t)\|_{L_x^2}^2. \quad (4.2.4)$$

We remark that $\|\omega^{\nu_k}(t)\|_{L_x^2} < \infty$ for $t > 0$ (cp. Theorem 1.3.15). By assumption and the last lemma, we can now estimate

$$\|\omega^{\nu_k}\|_{L_x^2} \leq Cr \|\nabla \omega^{\nu_k}\|_{L_x^2} + Cr^{\alpha-1}, \quad (4.2.5)$$

where $C, \alpha > 0$ are absolute constants and $r > 0$ is arbitrary. Balancing terms, we choose $r = \|\nabla \omega^{\nu_k}\|_{L_x^2}^{-1/(2-\alpha)}$. We obtain

$$\|\omega^{\nu_k}\|_{L_x^2} \leq C \|\nabla \omega^{\nu_k}\|_{L_x^2}^{(1-\alpha)/(2-\alpha)}, \quad (4.2.6)$$

implying (together with equation (4.2.4)) that there is a constant $c > 0$ such that

$$\frac{d}{dt} \|\omega^{\nu_k}(t)\|_{L_x^2}^2 \leq -c\nu_k \|\omega^{\nu_k}(t)\|_{L_x^2}^{2(2-\alpha)/(1-\alpha)} = -c\nu_k \|\omega^{\nu_k}(t)\|_{L_x^2}^{2(2+\delta)},$$

where $\delta > 0$ is chosen so that $2(2+\delta) = 2(2-\alpha)/(1-\alpha)$, i.e.

$$\delta = \frac{\alpha}{1-\alpha}. \quad (4.2.7)$$

If we now write $y_{\nu_k} = \|\omega^{\nu_k}\|_{L_x^2}^2$, then we have obtained the following inequality

$$\frac{d}{dt} y_{\nu_k} \leq -c\nu_k y_{\nu_k}^{2+\delta}. \quad (4.2.8)$$

This differential inequality is of the same form as the one that has been used in [CFLS16] to prove energy conservation provided $\bar{\omega} \in L_x^p$ ($p > 1$). Following the argument in [CFLS16], one shows that (4.2.8) implies that

$$y_{\nu_k}(t) = \|\omega^{\nu_k}(t)\|_{L_x^2}^2 \leq \frac{C(\alpha)}{(\nu_k t)^{1-\alpha}}. \quad (4.2.9)$$

Note that since $\alpha > 0$, this last estimate is an improvement over the straightforward estimate from Navier-Stokes equations (see Theorem 1.3.15), which would instead have only provided an upper bound

$$\|\omega^{\nu_k}(t)\|_{L_x^2}^2 \leq \frac{C}{\nu_k t},$$

which formally corresponds to setting $\alpha = 0$ in (4.2.9). This improved estimate is crucial to prove energy conservation, since we now find that

$$\nu_k \int_0^T \|\omega^{\nu_k}(t)\|_{L_x^2}^2 dt \leq C(\alpha) \nu_k^{1-(1-\alpha)} \int_0^T \frac{dt}{t^{1-\alpha}} = \left(\frac{C(\alpha)T^\alpha}{\alpha} \right) \nu_k^\alpha \rightarrow 0,$$

as $\nu_k \rightarrow 0$. This shows that the energy dissipation vanishes at a rate $\lesssim \nu_k^\alpha$ as $\nu_k \rightarrow 0$. Evidently, based on this estimate, the energy dissipation is expected to be larger for rough flows (corresponding to smaller values of $\alpha > 0$). Finally, in the limit $\alpha \rightarrow 0$, in which case we have no uniform control on the structure functions, nothing can be said about energy conservation. \square

The central point of the proof of Theorem 4.2.8, as outlined above, is that uniform control on the structure functions implies an improved estimate for $\|\omega^{\nu_k}(t)\|_{L_x^2}^2$ over the straightforward estimate provided by Theorem 1.3.15. Based on this improved enstrophy estimate, it can then be shown that the energy dissipation

$$\nu_k \int_0^T \|\omega^{\nu_k}(t)\|_{L_x^2}^2 dt \rightarrow 0, \quad (\nu_k \rightarrow 0),$$

converges to 0, hence implying energy conservation in the zero-viscosity limit.

More precisely, an algebraic decay of the structure functions

$$S_2(\mathbf{u}^{\nu_k}; r) \leq Cr^\alpha,$$

implies a similar bound on the energy dissipation

$$\nu_k \int_0^T \|\omega^{\nu_k}(t)\|_{L_x^2}^2 dt \leq C\nu_k^\alpha. \quad (4.2.10)$$

Remark 4.2.9. Recently, Drivas and Eyink [DE19] have obtained a similar upper bound on the energy dissipation of Leray solutions in the higher dimensional case, but under stronger assumptions on the sequence \mathbf{u}^{ν_k} . In particular, it is shown in [DE19, Lemma 1], that if $\mathbf{u}^{\nu_k} \in L^3([0, T]; B_3^{\sigma, \infty}(\mathbb{T}^d))$, $\sigma \in (0, 1]$ are uniformly bounded as $\nu_k \rightarrow 0$, then the energy dissipation is bounded for some ν_k -independent constant C by:

$$\int_0^T \int_{\mathbb{T}^d} \varepsilon[\mathbf{u}^{\nu_k}] dx dt \leq C\nu_k^{\frac{3\sigma-1}{\sigma+1}}.$$

Here, the energy dissipation measure $\varepsilon[\mathbf{u}^{\nu_k}]$ satisfies $\varepsilon[\mathbf{u}^\nu] \geq \nu|\nabla \mathbf{u}^\nu|^2$ for $d > 2$, and $\varepsilon[\mathbf{u}^\nu] = \nu|\nabla \mathbf{u}^\nu|^2$ in the two-dimensional case, $d = 2$. Above, $B_3^{\sigma, \infty}(\mathbb{T}^d)$ denotes the corresponding Besov space.

Based on the bound (4.2.10) in the two-dimensional case, it is now natural to ask whether a uniform (but not necessarily algebraic) decay such as,

$$S_2(\mathbf{u}^{\nu_k}; r) \leq \phi(r),$$

with $\phi(r)$ being a *modulus of continuity*, i.e. the function $\phi : [0, \infty) \rightarrow [0, \infty)$, such that $\phi(r) \geq 0$ for all $r \geq 0$ and $\phi(r) \rightarrow 0$, as $r \rightarrow 0$, will imply an estimate of the form,

$$\nu_k \int_0^T \|\omega^{\nu_k}(t)\|_{L_x^2}^2 dt = o_{\nu_k}(1) \rightarrow 0, \quad (\nu_k \rightarrow 0)?$$

Here, we would clearly expect the decay of $o_{\nu_k}(1) \rightarrow 0$ to depend on the properties of the modulus of continuity $\phi(r)$, as $r \rightarrow 0$.

As we will prove below, the answer to this question is positive, and the energy dissipation term can be shown to converge to zero as $\nu_k \rightarrow 0$, provided that the structure functions decay uniformly, though not necessarily algebraically. However, it turns out that a more natural way to measure the uniform decay of the sequence \mathbf{u}^{ν_k} is in terms of the *time-integrated* structure function $S_2^T(\mathbf{u}^{\nu_k}; r)$ (4.2.2), instead of $S_2(\mathbf{u}^{\nu_k}; r)$ (4.2.1). In particular, uniform decay of this structure function allows us to precisely characterize compactness of sequences in $L^p([0, T]; L_x^2)$, for $1 \leq p < \infty$, as stated in the proposition below.

Proposition 4.2.10. *Fix $1 \leq p < \infty$. Let $\{\mathbf{u}^{\nu_k}\}_{k \in \mathbb{N}}$ be an approximate solution sequence of the incompressible Euler equations. Then \mathbf{u}^{ν_k} is strongly relatively compact in $L_t^p([0, T]; L_x^2)$ if, and only if, there exists a uniform modulus of continuity $\phi(r)$, such that*

$$S_2^T(\mathbf{u}^{\nu_k}; r) \leq \phi(r), \quad \forall r > 0, \quad \forall k \in \mathbb{N}.$$

The proof of this technical proposition is provided in [LMPP21a, Appendix B]. Now, we are ready to state the main result of this section about characterizing energy conservation of approximating sequences to the Euler equations (4.1.3), in terms of the structure function. We have the following theorem:

Theorem 4.2.11. *Let $\bar{\mathbf{u}} \in L_x^2$ be initial data for the incompressible Euler equations. Let $\mathbf{u} \in L_t^\infty([0, T]; L_x^2)$ be a physically realizable solution of the incompressible Euler equations with initial data $\bar{\mathbf{u}}$. Let $\mathbf{u}^{\nu_k} \rightharpoonup \mathbf{u}$ be a physical realisation of \mathbf{u} . Then the following are equivalent:*

1. $\mathbf{u}^{\nu_k} \rightarrow \mathbf{u}$ strongly in $L^p([0, T]; L_x^2)$ for some $1 \leq p < \infty$,
2. There exists a bounded modulus of continuity $\phi(r)$, such that (uniformly in k)

$$S_2^T(\mathbf{u}^{\nu_k}; r) \leq \phi(r), \quad \forall r \geq 0, \quad \forall k \in \mathbb{N}.$$

3. \mathbf{u} is a energy conservative weak solution.

Sketch of proof. For the full details of the proof, we refer to [LMPP21a, Theorem 2.11]. Here, we will restrict attention to the core observation of the main implication (2) \Rightarrow (3): We assume that there exists a modulus of continuity $\phi(r)$, and a physical realisation $\mathbf{u}^{\nu_k} \rightharpoonup \mathbf{u}$ of \mathbf{u} , such that we have a uniform bound

$$S_2^T(\mathbf{u}^{\nu_k}; r) \leq \phi(r), \quad \forall r \geq 0, \quad \forall k \in \mathbb{N}.$$

We want to show that \mathbf{u} is energy conservative. The main ingredient is to show that for fixed $\delta > 0$, the energy dissipation term vanishes in the zero-viscosity limit:

$$\nu_k \int_\delta^T \|\omega^{\nu_k}(t)\|_{L_x^2}^2 dt \rightarrow 0, \quad \text{as } \nu_k \rightarrow 0. \quad (4.2.11)$$

To simplify the notation, we will drop the subscript k in the following, and denote the sequence $\nu_k \rightarrow 0$ instead by $\nu \rightarrow 0$. To prove (4.2.11), we observe from the vorticity transport equation that,

$$\|\omega^\nu(t)\|_{L_x^2}^2 = \|\omega^\nu(\delta)\|_{L_x^2}^2 - 2\nu \int_\delta^t \|\nabla \omega^\nu(s)\|_{L_x^2}^2 ds. \quad (4.2.12)$$

From the structure function estimate (4.2.3) it follows that we have a bound

$$\int_\delta^t \|\omega^\nu(s)\|_{L_x^2}^2 ds \leq Cr^2 \int_\delta^t \|\nabla \omega^\nu(s)\|_{L_x^2}^2 ds + C \frac{\phi(r)^2}{r^2}. \quad (4.2.13)$$

for all $r > 0$. Choosing r to balance terms on the right-hand side, we make the particular choice

$$r = \frac{\phi(\bar{r})^{1/2}}{\left(\int_{\delta}^t \|\nabla \omega^\nu(s)\|_{L_x^2}^2 ds\right)^{1/4}}, \quad \text{where } \bar{r} := \frac{\bar{\phi}^{1/2}}{\left(\int_{\delta}^t \|\nabla \omega^\nu(s)\|_{L_x^2}^2 ds\right)^{1/4}},$$

Here, $\bar{\phi} > 0$ provides an upper bound $\phi(r) \leq \bar{\phi}$. The first term of (4.2.13) is given by

$$Cr^2 \int_{\delta}^t \|\nabla \omega^\nu(s)\|_{L_x^2}^2 ds = C\phi(\bar{r}) \left(\int_{\delta}^t \|\nabla \omega^\nu(s)\|_{L_x^2}^2 ds\right)^{1/2}.$$

To estimate the second term, we note that $r \leq \bar{r}$ implies¹ $\phi(r) \leq \phi(\bar{r})$, and hence

$$C\frac{\phi(r)^2}{r^2} \leq C\phi(\bar{r}) \left(\int_{\delta}^t \|\nabla \omega^\nu(s)\|_{L_x^2}^2 ds\right)^{1/2}.$$

Estimating the right-hand side terms of (4.2.13) in this manner and taking the square of both sides, we deduce that

$$\left(\int_{\delta}^t \|\omega^\nu(s)\|_{L_x^2}^2 ds\right)^2 \leq C\phi(\bar{r})^2 \int_{\delta}^t \|\nabla \omega^\nu(s)\|_{L_x^2}^2 ds. \quad (4.2.14)$$

Let us denote $y_\nu(t) := \nu \int_{\delta}^t \|\omega^\nu(s)\|_{L_x^2}^2 ds$, and $z_\nu(t) := \int_{\delta}^t \|\nabla \omega^\nu(s)\|_{L_x^2}^2 ds$. Equation (4.2.14) can be re-written in the form

$$(y_\nu/\nu)^2 \leq C\phi\left(\beta z_\nu^{-1/4}\right) z_\nu, \quad \beta := \bar{\phi}^{1/2}. \quad (4.2.15)$$

Consider now the function $f : [0, \infty) \rightarrow [0, \infty)$, $z \mapsto f(z) := C\phi(\beta z^{-1/4})z$ for $z > 0$, and $f(0) := 0$. Since $\phi(r)$ is a bounded modulus of continuity, we have

$$\sup_{z \in (0, \infty)} f(z)/z = \sup_{r \in (0, \infty)} C\phi(r) < \infty. \quad (\text{P1})$$

Furthermore, we note that

$$\limsup_{z \rightarrow \infty} f(z)/z = \lim_{z \rightarrow \infty} C\phi(\beta z^{-1/4}) = \lim_{r \rightarrow 0} C\phi(r) = 0, \quad (\text{P2})$$

i.e. $f(z) \ll z$ has sub-linear growth. Intuitively, we would therefore expect the inverse of $f(z)$ to grow super-linearly, $f^{-1}(y) \gg y$, as $y \rightarrow \infty$. Unfortunately, there is no guarantee that $z \mapsto f(z)$ is invertible. This technical point is handled by the following lemma:

Lemma 4.2.12 (see [LMPP21a, Lemma C.1]). *Let $f : [0, \infty) \rightarrow [0, \infty)$, $z \mapsto f(z)$ be a non-negative function with the following two properties:*

(P1) $\sup_{z \in (0, \infty)} f(z)/z < \infty$, $f(0) = 0$,

(P2) $f(z)$ grows sub-linearly at infinity: $f(z) \ll z$, as $z \rightarrow \infty$, i.e. $\limsup_{z \rightarrow \infty} f(z)/z = 0$.

Then there exists a continuous, strictly monotonically increasing function $F : [0, \infty) \rightarrow [0, \infty)$, $z \mapsto F(z)$, such that $F(z) \geq f(z)$ for all $z \in [0, \infty)$. Furthermore, the inverse $F^{-1} : [0, \infty) \rightarrow [0, \infty)$, $y \mapsto F^{-1}(y)$, can be represented in the form $F^{-1}(y) = \sigma(\sqrt{y})y$, where (i) $\sigma : [0, \infty) \rightarrow [0, \infty)$ is a continuous, monotonically increasing function, and (ii) $\sigma(\sqrt{y}) \rightarrow \infty$ as $y \rightarrow \infty$.

¹By replacing $\phi(r)$ by $\Phi(r) := \sup_{s \leq r} \phi(s)$, if necessary, we may wlog assume that $r \mapsto \phi(r)$ is monotonically increasing.

Since $f(z)$ satisfies (P1) and (P2), we can construct a function $F(z) \geq f(z)$ with the properties of the last Lemma. In particular, the inverse of $F(z)$, $F^{-1} : [0, \infty) \rightarrow [0, \infty)$, $y \mapsto F^{-1}(y)$ is a monotonically increasing function which can be represented in the form

$$F^{-1}(y) = y\sigma(\sqrt{y}). \quad (4.2.16)$$

By (4.2.15), the definition of $f(z)$ and the fact that $f(z) \leq F(z)$, we have $(y_\nu/\nu)^2 \leq f(z_\nu) \leq F(z_\nu)$, uniformly for all ν . By the monotonicity of $F^{-1}(y)$, this implies that $F^{-1}((y_\nu/\nu)^2) \leq z_\nu$ for all ν and further implies that,

$$\frac{1}{\nu^2} y_\nu(t)^2 \sigma\left(\frac{y_\nu(t)}{\nu}\right) \leq z_\nu(t),$$

by our representation (4.2.16) of F^{-1} . Recalling that $z_\nu(t) := \int_\delta^t \|\nabla \omega^\nu(s)\|_{L_x^2}^2 ds$, we can equivalently write this estimate in the form

$$-\nu^2 \int_\delta^t \|\nabla \omega^\nu(s)\|_{L_x^2}^2 ds = -\nu^2 z_\nu(t) \leq -y_\nu(t)^2 \sigma\left(\frac{y_\nu(t)}{\nu}\right), \quad (4.2.17)$$

and we note that $y_\nu(t) = \nu \int_\delta^t \|\omega^\nu(s)\|_{L_x^2}^2 ds$, by definition. Making use also of the apriori inequality $\nu \|\omega^\nu(\delta)\|_{L_x^2}^2 \leq \|\bar{\mathbf{u}}\|_{L_x^2}^2 / \delta$ (cp. Theorem 1.3.15), it follows from estimate (4.2.17) and the enstrophy equation (4.2.12) that

$$\frac{d}{dt} y_\nu(t) \leq \frac{\|\bar{\mathbf{u}}\|_{L_x^2}^2}{\delta} - y_\nu(t)^2 \sigma\left(\frac{y_\nu(t)}{\nu}\right). \quad (4.2.18)$$

As a consequence of the last inequality (4.2.18), we now claim that for any $\epsilon > 0$, there exists a $\nu_0(\epsilon) > 0$ such that $y_\nu(t) \leq \epsilon$ for all $\nu \leq \nu_0(\epsilon)$. Indeed, if $y_\nu(t) \geq \epsilon$, then the differential inequality (4.2.18) above implies that

$$\frac{d}{dt} y_\nu(t) \leq \frac{\|\bar{\mathbf{u}}\|_{L_x^2}^2}{\delta} - \epsilon^2 \sigma\left(\frac{\epsilon}{\nu}\right).$$

We recall that by construction σ is a monotonically increasing function, and $\sigma(y) \rightarrow \infty$ as $y \rightarrow \infty$. Therefore, choosing $\nu_0 = \nu_0(\epsilon, \sigma, \delta, \|\bar{\mathbf{u}}\|_{L_x^2})$ sufficiently small, we can ensure that for all $\nu \leq \nu_0$ we have $\sigma\left(\frac{\epsilon}{\nu}\right) \geq \|\bar{\mathbf{u}}\|_{L_x^2}^2 / (\epsilon^2 \delta)$, or equivalently

$$\frac{\|\bar{\mathbf{u}}\|_{L_x^2}^2}{\delta} - \epsilon^2 \sigma\left(\frac{\epsilon}{\nu}\right) \leq 0.$$

This implies that $dy_\nu/dt \leq 0$ whenever $y_\nu(t) \geq \epsilon$ and $\nu \leq \nu_0$. Since $t \mapsto y_\nu(t) \geq 0$ is continuously differentiable for any $\nu > 0$ and since $y_\nu(\delta) = 0$, independently of ν , this implies that $y_\nu(t)$ cannot leave the set $\{y \in \mathbb{R} \mid 0 \leq y \leq \epsilon\}$ for any $t \in [\delta, T]$, provided that $\nu \leq \nu_0$. In particular, we conclude that for $t = T$:

$$\limsup_{\nu \rightarrow 0} \nu \int_\delta^T \|\omega^\nu(t)\|_{L_x^2}^2 dt = \limsup_{\nu \rightarrow 0} y_\nu(T) \leq \sup_{\nu \leq \nu_0} y_\nu(T) \leq \epsilon.$$

As $\epsilon > 0$ was arbitrary, this is only possible if

$$\lim_{\nu \rightarrow 0} \nu \int_\delta^T \|\omega^\nu(t)\|_{L_x^2}^2 dt = 0. \quad (4.2.19)$$

To summarize: Assuming that $S_2^T(\mathbf{u}^\nu; r) \leq \phi(r)$ is uniformly bounded by a modulus of continuity $\phi(r)$, we have shown that for any $\delta > 0$, the expression $\nu \int_\delta^T \|\omega^\nu(t)\|_{L_x^2}^2 dt$ converges to zero as $\nu \rightarrow 0$. An additional technical argument, provided in detail in [LMPP21a, Proof of Theorem 2.11], then allows us to conclude that $\|\mathbf{u}(t)\|_{L_x^2} = \|\bar{\mathbf{u}}\|_{L_x^2}$, for a.e. $t \in [0, T]$, i.e. \mathbf{u} is energy conservative. \square

Clearly Theorem 4.2.8 is a special case of the above Theorem 4.2.11. Moreover in [CFLS16], the authors have shown that physically realizable weak solutions of the two-dimensional incompressible Euler equations are energy conservative, provided that the initial vorticity $\bar{\omega}^\nu = \operatorname{curl}(\bar{\mathbf{u}}^\nu) \in L_x^p$ are uniformly bounded, for some $p > 1$. This result readily follows from the characterisation provided by Theorem 4.2.11: If \mathbf{u}^ν is the solution of (4.1.1) with viscosity $\nu > 0$, and uniformly bounded initial vorticity $\|\bar{\omega}^\nu\|_{L_x^p} \leq C$, then the vorticities $\omega^\nu = \operatorname{curl}(\mathbf{u}^\nu)$ are bounded in $C([0, T]; L_x^p)$, uniformly as $\nu \rightarrow 0$. In particular, this implies that $\{\omega^\nu\}$ is precompact in $C([0, T]; L_x^2) \hookrightarrow L_t^2([0, T]; L_x^2)$. Hence any such limit $\mathbf{u}^{\nu_k} \rightarrow \mathbf{u}$ must be energy conservative according to Theorem 4.2.11.

Next, we aim to use the characterization of energy conservation in Theorem 4.2.11 and generalize the results of [CFLS16]. To state the next lemma, we denote by $(\omega^\nu)^*$ the decreasing rearrangement of ω^ν [Lio96]. We recall that the Lorentz space $L^{(1,2)}$ is defined by

$$L^{(1,2)} = \left\{ \omega \in L^1(\mathbb{T}^2) \mid \int_0^{|\mathbb{T}^2|} \left(\int_0^s (\omega^*)^*(r) dr \right)^2 \frac{ds}{s} < \infty \right\}.$$

It is well-known that $L^{(1,2)}$ embeds continuously into H^{-1} [Lio96]. We now recall the following Lemma from [Lio96, Lemma 4.1]:

Lemma 4.2.13. *A family $\{\omega^\nu\} \subset L^{(1,2)}$ is precompact, if the following conditions hold:*

1. *There exists $C > 0$, such that $\|\omega^\nu\|_{L^{(1,2)}} \leq C$ uniformly in ν ,*
2. *$\int_0^\delta (\int_0^s (\omega^\nu)^*(r) dr)^2 \frac{ds}{s} \rightarrow 0$ as $\delta \rightarrow 0$, uniformly in ν .*

Extending the result of [CFLS16] somewhat, we note in particular the following corollary of Theorem 4.2.11:

Corollary 4.2.14. *Let \mathbf{u} be a physically realizable weak solution of the incompressible Euler equations with initial data $\bar{\mathbf{u}} \in L_x^2$, obtained in the zero-viscosity limit $\mathbf{u}^{\nu_k} \rightharpoonup \mathbf{u}$ ($\nu_k \rightarrow 0$), $\mathbf{u}^{\nu_k}(t=0) = \bar{\mathbf{u}}^{\nu_k}$. If the initial vorticities $\bar{\omega}^{\nu_k} = \operatorname{curl}(\bar{\mathbf{u}}^{\nu_k})$ satisfy the conditions of Lemma 4.2.13, then \mathbf{u} is energy conservative. In particular, the limit is energy conservative, provided that the initial vorticities ω^{ν_k} belong to a bounded subset of a rearrangement invariant space with compact embedding into H_x^{-1} .*

Proof. The conditions of Lemma 4.2.13 are preserved by the solution operator of the Navier-Stokes equations. Thus, if $\{\omega^{\nu_k} \mid k \in \mathbb{N}\}$ satisfy the conditions of Lemma 4.2.13 and hence are precompact in $L^{(1,2)}$, then also $\{\omega^{\nu_k}(t) \mid t \in [0, T], k \in \mathbb{N}\}$ belongs to a compact subset of $L^{(1,2)} \subset H_x^{-1}$, again by Lemma 4.2.13. In particular, it follows that $\{\mathbf{u}^{\nu_k}(t) \mid t \in [0, T], k \in \mathbb{N}\}$ is precompact in L_x^2 , and thus there exists a uniform modulus of continuity $\phi(r)$, such that $S_2(\mathbf{u}^{\nu_k}(t); r) \leq \phi(r)$, for all ν_k (uniformly in time). By Theorem 4.2.11, it now follows that the limit $\mathbf{u}^{\nu_k} \rightharpoonup \mathbf{u}$ is a strong limit $\mathbf{u}^{\nu_k} \rightarrow \mathbf{u}$ in $L_t^2 L_x^2$, and hence \mathbf{u} is energy conservative. \square

Remark 4.2.15. *Examples of rearrangement invariant spaces to which Corollary 4.2.14 applies have been discussed in [FLT00], and include the following: L^p ($p > 1$), Orlicz spaces contained in $L(\log L)^\alpha$ ($\alpha > 1/2$), Lorentz spaces $L^{(1,q)}$ ($1 \leq q < 2$). The result also holds, provided that e.g. the initial data for the Navier-Stokes approximations are chosen to be $\mathbf{u}^{\nu_k}(t=0) = \bar{\mathbf{u}}$ for all $k \in \mathbb{N}$, and provided that $\bar{\omega} = \operatorname{curl}(\bar{\mathbf{u}}) \in L^{(1,2)}$.*

In another direction, the following corollary is also immediate from Theorem 4.2.11:

Corollary 4.2.16. *If \mathbf{u} is a physically realizable solution with initial data $\bar{\mathbf{u}}$, and if \mathbf{u} is not energy conservative, then any physical realisation $\mathbf{u}^{\nu_k} \rightharpoonup \mathbf{u}$ develops either oscillations or concentrations in the*

limit $\nu_k \rightarrow 0$. Furthermore, if there exists a constant $C > 0$, such that the corresponding sequence of vorticities ω^{ν_k} are uniformly bounded as measures, $\|\omega^{\nu_k}(t)\|_{\mathcal{M}} \leq C$, then \mathbf{u}^{ν_k} only develops concentrations, i.e. (up to a subsequence) the measure $|\mathbf{u}^{\nu_k}(x, t)|^2 dx dt$ has a weak-* limit of the form

$$|\mathbf{u}^{\nu_k}(x, t)|^2 dx dt \xrightarrow{*} |\mathbf{u}(x, t)|^2 dx dt + \lambda_t(dx) dt,$$

where $\lambda_t \geq 0$ is a non-trivial time-parametrized, bounded measure, supported on a set of Lebesgue measure zero.

4.3 Energy conservation for numerical approximations of statistical solutions

Our aim in this section is to generalize Theorem 4.2.11 in two directions, *i.e.* first by considering other mechanisms of generating approximating sequences of the Euler equations (4.1.3). In particular, we are interested in numerical approximations of the two-dimensional Euler equations. We consider approximating the Euler equations with the following spectral viscosity method.

4.3.1 Spectral vanishing viscosity method

We again consider the spectral vanishing viscosity (SV) scheme introduced in chapter 1.4 for the incompressible Euler equations: Given $N \in \mathbb{N}$, we set $\Delta = 1/N$, and consider the following approximation of the incompressible Euler equations

$$\begin{cases} \partial_t \mathbf{u}^\Delta + \mathbb{P}_N(\mathbf{u}^\Delta \cdot \nabla \mathbf{u}^\Delta) = \epsilon_N \Delta (Q_N * \mathbf{u}^\Delta), \\ \operatorname{div}(\mathbf{u}^\Delta) = 0, \quad \mathbf{u}^\Delta|_{t=0} = \mathbb{P}_N \bar{\mathbf{u}}, \end{cases} \quad (4.3.1)$$

with periodic boundary conditions and \mathbb{P}_N is the truncated Leray projection. We will consider $\epsilon_N = \epsilon/N$, for some fixed constant $\epsilon > 0$, and m_N is to be chosen, so that $\epsilon_N m_N \rightarrow 0$, as $N \rightarrow \infty$.

Integration of the spectral vanishing viscosity method over the time-interval $[0, t]$ yields the equality

$$\|\mathbf{u}^\Delta(t)\|_{L^2}^2 = \|\mathbf{u}^\Delta(0)\|_{L^2}^2 - 2\epsilon_N \int_0^t \|\sqrt{Q_N} \omega^\Delta(s)\|_{L^2}^2 ds, \quad (4.3.2)$$

for any $t \in [0, T]$. The corresponding vorticity equation for $\omega^\Delta = \operatorname{curl}(\mathbf{u}^\Delta)$ (cp. [LM20, eq. (2.9)]), yields

$$\frac{d}{dt} \|\omega^\Delta(t)\|_{L^2}^2 = -2\epsilon_N \|\nabla \sqrt{Q_N} \omega^\Delta(s)\|_{L^2}^2$$

Then

$$\|\nabla \sqrt{Q_N} \omega^\Delta(s)\|_{L^2}^2 = (2\pi)^2 \sum_{k=1}^N \widehat{Q}_k |k|^2 |\widehat{\omega}_k|^2 \geq (2\pi)^2 \sum_{k=2m_N+1}^N |k|^2 |\widehat{\omega}_k|^2 = \|\nabla \omega^\Delta(s)\|_{L^2}^2 - \|\nabla P_{2m_N} \omega^\Delta(s)\|_{L^2}^2.$$

Employing the estimate $\|\nabla P_{2m_N} \omega^\Delta\|_{L^2}^2 \leq 4m_N^2 \|\omega^\Delta\|_{L^2}^2$, it now follows that

$$\frac{d}{dt} \|\omega^\Delta(t)\|_{L^2}^2 \leq -2\epsilon_N \|\nabla \omega^\Delta(t)\|_{L^2}^2 + 8\epsilon_N m_N^2 \|\omega^\Delta(t)\|_{L^2}^2. \quad (4.3.3)$$

This inequality will be used to analyse the energy conservation of limits obtained by the SV method, and essentially serves as the analogue of (4.2.12), which was used in the Navier-Stokes case.

Our objective will be to characterize energy conservation for the limit of solutions generated by the spectral viscosity (SV) method. Moreover, we will consider this question within the context of a more generalized, probabilistic framework of solutions of (4.1.3) that we describe below.

4.3.2 Statistical solutions

Originally introduced by Foias and Prodi in the context of Navier-Stokes equations, see [FMRT08] and references therein, statistical solutions are time-parameterized probability measures that extend weak solutions from a single function (in space-time) to a probability measure on functions. They might arise in the context of uncertainty quantification of fluid flows [FLM17, FLMW20] or to enable a probabilistic description of the dynamics of fluids. We follow the definition of statistical solutions in chapter 3, briefly recalled below:

Definition 4.3.1. A time-dependent probability measure $t \mapsto \mu_t \in \mathcal{P}(L_x^2)$ is a **statistical solution** of the incompressible Euler equations with initial data $\bar{\mu} \in \mathcal{P}(L_x^2)$, if $[0, T] \mapsto \mathcal{P}(L_x^2)$, $t \mapsto \mu_t$ is a weak-* measurable mapping, μ_t is concentrated on solenoidal (divergence-free) vector fields for almost every $t \in [0, T]$, and if the following averaged version of the Euler equations is satisfied for any $k \in \mathbb{N}$: Given any solenoidal vector fields $\varphi_1, \dots, \varphi_k \in C_c^\infty(\mathbb{T}^2 \times [0, T]; \mathbb{R}^2)$, we have

$$\begin{aligned} & \int_0^T \int_{L_x^2} \left(\frac{d}{dt} \prod_{i=1}^k \langle \mathbf{u}, \varphi_i \rangle + \sum_{i=1}^k \left[\prod_{j \neq i} \langle \mathbf{u}, \varphi_j \rangle \right] \langle (\mathbf{u} \cdot \nabla) \varphi_i, \mathbf{u} \rangle \right) d\mu_t(\mathbf{u}) dt \\ & + \int_{L_x^2} \prod_{i=1}^k \langle \mathbf{u}, \varphi_i \rangle d\bar{\mu}(\mathbf{u}) = 0. \end{aligned}$$

Here $\langle \cdot, \cdot \rangle$ denotes the following inner product between two vector fields in L_x^2 :

$$\langle \mathbf{u}, \mathbf{v} \rangle := \int_{\mathbb{T}^2} \mathbf{u}(x) \cdot \mathbf{v}(x) dx.$$

Note that setting $\mu_t = \delta_{\mathbf{u}(t)}$ for some $\mathbf{u}(t) \in L_x^2$, for almost every t , yields the definition of weak solutions of (4.1.3). Thus, statistical solutions can be thought of a probabilistic generalization of weak solutions, particularly when the initial data is a probability measure.

In chapter 3, an efficient numerical algorithm has been proposed to approximate statistical solutions of the incompressible Euler equations, using a combination of Monte-Carlo sampling of the initial measure $\bar{\mu} = \mu_t|_{t=0}$, yielding

$$\bar{\mu}^\Delta = \frac{1}{M} \sum_{i=1}^M \delta_{\bar{\mathbf{v}}_i^\Delta}, \quad \bar{\mathbf{v}}_i^\Delta \in L^2, \quad i = 1, \dots, M,$$

and then evolving the probability measure $\bar{\mu}^\Delta$ via the push-forward of the numerical solution operator $\mu_t^\Delta := (\mathcal{S}_t^\Delta)_\# \bar{\mu}^\Delta$, where $\mathcal{S}_t^\Delta : L_x^2 \rightarrow L_x^2$, $\bar{\mathbf{v}} \mapsto \mathcal{S}_t^\Delta(\bar{\mathbf{v}})$ is defined as the solution of spectral viscosity scheme with initial data $\bar{\mathbf{v}}$ computed at resolution $\Delta = 1/N$, and evaluated at time $t \in [0, T]$. Since $\bar{\mu}^\Delta$ is a convex combination of Dirac measures, this push-forward can be more concretely expressed in the form

$$\mu_t^\Delta = \frac{1}{M} \sum_{i=1}^M \delta_{\mathbf{v}_i^\Delta(t)},$$

where $\Delta = 1/N$ and $\mathbf{v}_i^\Delta(t)$ is the solution obtained from the spectral viscosity scheme (4.3.1). We recall that it has been proven in chapter 3 that μ_t^Δ converges in a suitable topology to a statistical solution μ_t , if $\bar{\mu}$ is supported on a ball $B_M = \{\mathbf{u} \in L^2 \mid \|\mathbf{u}\|_{L^2} \leq M\}$ for some $M > 0$, and provided that there exists a uniform modulus of continuity $\phi(r)$, such that the (time averaged) structure function $S_2^T(\mu_t^\Delta; r)$, given by

$$S_2^T(\mu_t^\Delta; r) := \left(\int_0^T \int_{L^2} \int_D \int_{B_r(0)} |\mathbf{u}(x+h) - \mathbf{u}(x)|^2 dh dx d\mu_t^\Delta(\mathbf{u}) dt \right)^{1/2},$$

remains uniformly bounded $S_2^T(\mu^\Delta; r) \leq \phi(r)$, as $\Delta \rightarrow 0$, for all $r > 0$. Under these conditions, there exists a subsequence $\Delta_k \rightarrow 0$ and $\mu_t \in \mathcal{P}(L^2)$, such that that

$$\int_0^T W_1(\mu_t^{\Delta_k}, \mu_t) dt \rightarrow 0, \quad (\Delta_k \rightarrow 0). \quad (4.3.4)$$

Here W_1 is the 1-Wasserstein metric defined for probability measures $\mathcal{P}(L_x^2)$ on L_x^2 . For further details, we refer to chapter 3.

Our goal in this section is to prove the following theorem:

Theorem 4.3.2. *Let $\bar{\mu} \in \mathcal{P}(L_x^2)$ be initial data for the incompressible Euler equations, such that there exists $M > 0$, s.t. $\bar{\mu}(B_M(0)) = 1$, where $B_M(0) = \{\mathbf{u} \in L_x^2 \mid \|\mathbf{u}\|_{L_x^2} < M\}$. Let μ_t^Δ be obtained from SV + MC sampling, $\Delta > 0$. If there exist constants $\bar{C} > 0$ and $0 < \alpha < 1$, such that*

$$\sup_{t \in [0, T]} S_2(\mu_t^\Delta; r) \leq \bar{C}r^\alpha, \quad \forall \Delta > 0, r > 0, \quad (4.3.5)$$

then, up to a subsequence, $\mu_t^\Delta \rightarrow \mu_t$ in $L_t^1(\mathcal{P})$, (in the sense of (4.3.4)), and μ_t is energy-conservative, in the sense that

$$t \mapsto \int_{L_x^2} \|\mathbf{u}\|_{L_x^2}^2 d\mu_t(\mathbf{u}),$$

is constant.

Remark 4.3.3. Note that the conventional (deterministic) SV scheme is a special case of the MC+SV scheme, when the initial data is given by a Dirac measure $\delta_{\bar{\mathbf{u}}}$, concentrated on the initial data $\bar{\mathbf{u}} \in L_x^2$. Therefore, 4.3.2 implies in particular the corresponding result for the conventional SV scheme.

Remark 4.3.4. Note that in Theorem 4.3.2, we have assumed a stronger bound of the form

$$\sup_{t \in [0, T]} S_2(\mu_t^\Delta; r) \leq Cr^\alpha,$$

for given $C, \alpha > 0$, rather than $S_2^T(\mu_t^\Delta; r) \leq \phi(r)$ for a fixed modulus of continuity, as was done in the characterisation of physically realizable energy conservative solutions of the incompressible Euler equations (cp. Theorem 4.2.11). This is done for two reasons: firstly it avoids certain technical difficulties in the proof, and secondly, as explained below in section 4.4, this stronger bound appears to correspond to what is observed numerically for a wide range of initial data. A slight generalization of the energy conservation statement of Theorem 4.3.2 under the assumption of a uniform decay of the time-integrated structure function $S_2^T(\mu^\Delta; r) \leq Cr^\alpha$ is straightforward.

Proof of Theorem 4.3.2. We will denote by $\mathbb{E}_t^\Delta[\dots] := \int_{L^2}(\dots) d\mu_t^\Delta$ the expected value of a quantity at time t with respect to the probability measure μ_t^Δ . Similar notation $\mathbb{E}_t[\dots]$ is used to denote the expected value of a quantity with respect to the limiting measure μ_t . To prove energy conservation, we make use of the fact that μ^Δ is a convex combination of atomic Dirac measures $\delta_{\mathbf{v}_i^\Delta(t)}$ supported on solutions of the spectral viscosity scheme at grid size $\Delta = 1/N$. This allows us directly to take expected values, by summing equation (4.3.3) over all samples $\mathbf{v}_1^\Delta, \dots, \mathbf{v}_N^\Delta$, to obtain

$$\frac{d}{dt} \mathbb{E}_t^\Delta \left[\|\omega^\Delta\|_{L_x^2}^2 \right] \leq -2\epsilon_N \mathbb{E}_t^\Delta \left[\|\nabla \omega^\Delta\|_{L_x^2}^2 \right] + 8(\epsilon_N m_N^2) \mathbb{E}_t^\Delta \left[\|\omega^\Delta\|_{L_x^2}^2 \right]. \quad (4.3.6)$$

The expected value of the "interpolation" inequality (4.2.3) yields

$$\mathbb{E}_s^\Delta \left[\|\omega^\Delta\|_{L_x^2}^2 \right] \leq Cr^2 \mathbb{E}_s^\Delta \left[\|\nabla \omega^\Delta\|_{L_x^2}^2 \right] + Cr^{-2} S_2(\mu_s^\Delta; r)^2,$$

where $C > 0$ is an absolute constant, independent of N . By the assumed uniform bound (4.3.5),

$$\mathbb{E}_s^\Delta \left[\|\omega^\Delta\|_{L_x^2}^2 \right] \leq Cr^2 \mathbb{E}_s^\Delta \left[\|\nabla \omega_n\|_{L_x^2}^2 \right] + Cr^{2(\alpha-1)}.$$

where $C = C(\bar{C})$ depends on the structure function estimate (4.3.5), but is independent of N . Choosing r to balance the two terms on the right-hand side, we set

$$r^2 = \mathbb{E}_s^\Delta \left[\|\nabla \omega^\Delta\|_{L_x^2}^2 \right]^{-1/(2-\alpha)}.$$

This choice of r yields the estimate

$$\mathbb{E}_s^\Delta \left[\|\omega^\Delta\|_{L_x^2}^2 \right] \leq C \mathbb{E}_s^\Delta \left[\|\nabla \omega^\Delta\|_{L_x^2}^2 \right]^{(1-\alpha)/(2-\alpha)}, \quad (4.3.7)$$

with $C = C(\bar{C})$. Define $\delta = \delta(\alpha)$, by $(2+\delta) = (2-\alpha)/(1-\alpha)$, i.e.

$$\delta = \frac{\alpha}{1-\alpha}. \quad (4.3.8)$$

Then (4.3.7) implies that for an absolute constant $c = c(\bar{C}, \alpha) > 0$ (depending only on \bar{C} , α in (4.3.5)):

$$c \mathbb{E}_s^\Delta \left[\|\omega^\Delta\|_{L_x^2}^2 \right]^{2+\delta} \leq \mathbb{E}_s^\Delta \left[\|\nabla \omega^\Delta\|_{L_x^2}^2 \right]. \quad (4.3.9)$$

The differential inequality (4.3.6) combined with the estimate (4.3.9) yields

$$\frac{d}{dt} \mathbb{E}_s^\Delta \left[\|\omega^\Delta\|_{L_x^2}^2 \right] \leq -c\epsilon_N \mathbb{E}_s^\Delta \left[\|\omega^\Delta\|_{L_x^2}^2 \right]^{2+\delta} + 8(\epsilon_N m_N^2) \mathbb{E}_s^\Delta \left[\|\omega^\Delta\|_{L_x^2}^2 \right]. \quad (4.3.10)$$

A short calculation, detailed in [LMPP21a], then shows that $\mathbb{E}_t^\Delta [\|\omega^\Delta\|_{L_x^2}^2] \leq C(\epsilon_N t)^{\alpha-1}$. In particular, this implies that

$$\epsilon_N \int_0^T \mathbb{E}_t^\Delta \left[\|\omega^\Delta\|_{L_x^2}^2 \right] dt \leq \frac{C(\epsilon_N T)^\alpha}{\alpha} \rightarrow 0, \quad (\text{as } N \rightarrow \infty). \quad (4.3.11)$$

Taking the expected value of (4.3.2) for a given $\Delta > 0$, we obtain

$$\left| \mathbb{E}_0^\Delta [\|\mathbf{u}\|_{L_x^2}^2] - \mathbb{E}_t^\Delta [\|\mathbf{u}\|_{L_x^2}^2] \right| \leq 2\epsilon_N \int_0^T \mathbb{E}_t^\Delta \left[\|\sqrt{Q_N} \omega^\Delta\|_{L_x^2}^2 \right] dt \leq 2\epsilon_N \int_0^T \mathbb{E}_t^\Delta \left[\|\omega^\Delta\|_{L_x^2}^2 \right] dt.$$

Employing (4.3.11), we find

$$\limsup_{\Delta \rightarrow 0} \sup_{t \in [0, T]} \left| \mathbb{E}_0^\Delta [\|\mathbf{u}\|_{L_x^2}^2] - \mathbb{E}_t^\Delta [\|\mathbf{u}\|_{L_x^2}^2] \right| \leq \limsup_{N \rightarrow \infty} 2\epsilon_N \int_0^T \mathbb{E}_t^\Delta \left[\|\omega^\Delta\|_{L_x^2}^2 \right] dt = 0, \quad (4.3.12)$$

i.e. $\lim_{\Delta \rightarrow 0} \mathbb{E}_t^\Delta [\|\mathbf{u}\|_{L_x^2}^2] = \lim_{\Delta \rightarrow 0} \mathbb{E}_0^\Delta [\|\mathbf{u}\|_{L_x^2}^2]$, uniformly for $t \in [0, T]$. Since $\mu_0^\Delta = \bar{\mu}^\Delta$ converges weakly to $\bar{\mu}$ at the initial time, and since this sequence is uniformly bounded on $B_M(0)$, we also have

$$\lim_{\Delta \rightarrow 0} \mathbb{E}_0^\Delta [\|\mathbf{u}\|_{L_x^2}^2] = \lim_{\Delta \rightarrow 0} \int_{L^2} \|\bar{\mathbf{u}}\|_{L_x^2}^2 d\bar{\mu}^\Delta(\bar{\mathbf{u}}) = \int_{L^2} \|\bar{\mathbf{u}}\|_{L_x^2}^2 d\bar{\mu}(\bar{\mathbf{u}}). \quad (4.3.13)$$

We thus conclude that for any $t \in [0, T]$:

$$\lim_{\Delta \rightarrow 0} \int_{L^2} \|\mathbf{u}\|_{L_x^2}^2 d\mu_t^\Delta(\mathbf{u}) \stackrel{(4.3.12)}{\doteq} \lim_{\Delta \rightarrow 0} \int_{L^2} \|\bar{\mathbf{u}}\|_{L_x^2}^2 d\bar{\mu}^\Delta(\bar{\mathbf{u}}) \stackrel{(4.3.13)}{\doteq} \int_{L^2} \|\bar{\mathbf{u}}\|_{L_x^2}^2 d\bar{\mu}(\bar{\mathbf{u}}).$$

On the other hand, it has been proved in Theorem 3.2.13 in chapter 3, that $\|\mathbf{u}\|_{L_x^2}^2$ is an ‘‘admissible observable’’, so that the convergence $\mu_t^\Delta \rightarrow \mu_t$ in $L_t^1(\mathcal{P})$ implies

$$\lim_{\Delta \rightarrow 0} \int_0^T \left| \mathbb{E}_t^\Delta [\|\mathbf{u}\|_{L_x^2}^2] - \mathbb{E}_t [\|\mathbf{u}\|_{L_x^2}^2] \right| dt = 0.$$

In particular, this allows us to extract a subsequence $\Delta' \rightarrow 0$ such that

$$\lim_{\Delta' \rightarrow 0} \mathbb{E}_t^{\Delta'} [\|\mathbf{u}\|_{L_x^2}^2] = \mathbb{E}_t [\|\mathbf{u}\|_{L_x^2}^2],$$

for almost every $t \in [0, T]$. Hence, we finally find that for almost all $t \in [0, T]$, we have

$$\int_{L^2} \|\mathbf{u}\|_{L_x^2}^2 d\mu_t(\mathbf{u}) = \lim_{\Delta' \rightarrow 0} \int_{L^2} \|\mathbf{u}\|_{L_x^2}^2 d\mu_t^{\Delta'}(\mathbf{u}) = \lim_{\Delta' \rightarrow 0} \int_{L^2} \|\bar{\mathbf{u}}\|_{L_x^2}^2 d\bar{\mu}^{\Delta'}(\bar{\mathbf{u}}) = \int_{L^2} \|\bar{\mathbf{u}}\|_{L_x^2}^2 d\bar{\mu}(\bar{\mathbf{u}}).$$

This concludes our proof that the limiting statistical solution μ_t is energy conservative. \square

4.4 Numerical experiments

In this section, we will present numerical experiments to illustrate and validate our theory about the precise relationship between energy conservation and uniform decay of structure functions (spectra). We start with a short summary of the numerical method and the choice of parameters for the numerical experiments.

4.4.1 Numerical method

The numerical experiments will be based on the SV method. The discretization and its implementation in SPHINX have been explained in detail in chapter 1.4. Unless otherwise indicated, for the numerical experiments reported below, we use the spectral viscosity scheme, with $\epsilon_N = \epsilon/N$, $\epsilon = 1/20$. Our choice for the Fourier multipliers Q_N is

$$\widehat{Q}_k = \begin{cases} 1 - m_N/|k|^2, & (|k| \geq m_N), \\ 0, & (\text{otherwise}), \end{cases}$$

where normally $m_N = \sqrt{N}$, except in the special case, where the added numerical viscosity mimics the form of the viscous term in the Navier-Stokes equations (4.1.1), in which we set $m_N = 0$ and $Q_N = I$ is the identity.

Given an initial probability measure $\bar{\mu} \in \mathcal{P}(L_x^2)$, a resolution $\Delta = 1/N$ and number of samples $M = M(N)$, an approximate statistical solution is obtained by the following Monte-Carlo algorithm (MC+SV):

1. Generate M i.i.d. samples $\bar{\mathbf{u}}_1, \dots, \bar{\mathbf{u}}_M \sim \bar{\mu}$,
2. Evolve each sample $\mathbf{u}_i(t) = \mathcal{S}_t^\Delta(\bar{\mathbf{u}}_i)$, where \mathcal{S}_t^Δ is the numerical solution operator obtained from the SV-scheme,
3. The approximate statistical solution at time $t \in [0, T]$ is defined as

$$\mu_t^\Delta := \frac{1}{M} \sum_{i=1}^M \delta_{\mathbf{u}_i(t)}.$$

Clearly, for convergence of the MC+SV scheme it is necessary that $M = M(N) \rightarrow \infty$ as $N \rightarrow \infty$. For our numerical experiments we have made the choice $M = N$.

4.4.2 Structure function evaluation

As indicated by the theoretical results presented in the previous sections, our main tool to determine the energy conservation of weak solutions obtained in the limit from our numerical method, will be the structure function

$$S_2(\mu_t; r) = \left(\int_{L_x^2} \int_D \int_{B_r(x)} |\mathbf{u}(y) - \mathbf{u}(x)|^2 dy dx d\mu_t(\mathbf{u}) \right)^{1/2},$$

defined for all $\mu_t \in \mathcal{P}(L_x^2)$ and for a.e. $t \in [0, T]$. We identify $\mathbf{u} \in L_x^2$ with the Dirac probability measure $\delta_{\mathbf{u}} \in \mathcal{P}(L_x^2)$, and set $S_2(\mathbf{u}; r) := S_2(\delta_{\mathbf{u}}; r)$. Note that with this definition: $S_2(\mu_t; r)^2 = \int_{L_x^2} S_2(\mathbf{u}; r)^2 d\mu_t(\mathbf{u})$.

As shown in [LMPP21a, Appendix D], there is an explicit formula for $S_2(\mathbf{u}; r)^2$ in terms of the Fourier coefficients $\hat{\mathbf{u}}(k)$ of \mathbf{u} : Namely, we have

$$S_2(\mathbf{u}; r) = \left(\sum_{k \in \mathbb{Z}^2} I_k(r) |\hat{\mathbf{u}}(k)|^2 \right)^{1/2},$$

where $I_k(r) := 2 - 4J_1(|k|r)/(|k|r)$ is expressed in terms of the Bessel function of the first kind $J_1(x)$. As discussed in [LMPP21a, Appendix D], a computationally more efficient-to-evaluate alternative to this exact expression for $S_2(\mu_t; r)$ is given by

$$\tilde{S}_2(\mathbf{u}; r) := \left(\sum_{k \in \mathbb{Z}^2} \tilde{I}_k(r) |\hat{\mathbf{u}}(k)|^2 \right)^{1/2}, \quad \tilde{I}_k(r) := \min(|k|r/2, \sqrt{2})^2. \quad (4.4.1)$$

Again, we define the corresponding statistical quantity by

$$\tilde{S}_2(\mu_t, r) := \left(\int_{L_x^2} \tilde{S}_2(\mathbf{u}; r)^2 d\mu_t(\mathbf{u}) \right)^{1/2},$$

and we recall that $\tilde{S}_2(\mu_t; r)$ is equivalent to $S_2(\mu_t; r)$, in the sense that there exists a constant $C > 0$, such that

$$\frac{1}{C} \tilde{S}_2(\mu_t; r) \leq S_2(\mu_t; r) \leq C \tilde{S}_2(\mu_t; r), \quad \forall r \geq 0, \forall \mu_t \in \mathcal{P}(L_x^2).$$

For the analysis of our numerical experiments we will use this equivalent numerical structure function instead of the exact structure function.

A second tool in our analysis will be the use of compensated energy spectra. As discussed in detail in chapter 3.4.3, an upper bound on the structure function is provided by a uniform decay of the energy spectrum. To this end, we define the numerical energy spectrum of a vector field $\mathbf{u} \in L_x^2$ as

$$E(\mathbf{u}; K) := \frac{1}{2} \sum_{|k|_\infty = K} |\hat{\mathbf{u}}(k)|^2, \quad \forall K \in \mathbb{N}_0, \quad (4.4.2)$$

where $|k|_\infty = \max(|k_1|, |k_2|)$ is the maximum norm of $k \in \mathbb{Z}^2$. We extend this definition to arbitrary $\mu_t \in \mathcal{P}(L_x^2)$ by setting

$$E(\mu_t; K) := \int_{L_x^2} E(\mathbf{u}; K) d\mu_t(\mathbf{u}).$$

Note again that $E(\mathbf{u}; K) = E(\delta_{\mathbf{u}}; K)$. It can be shown (cp. (3.4.6) on page 63) that for any $1 < \lambda < 3$:

$$K^\gamma E(\mu_t^\Delta; K) \leq C, \forall K \Rightarrow S_2(\mu_t^\Delta; r) \leq C' r^\alpha, \forall r \geq 0, \forall \Delta > 0, \quad (4.4.3)$$

where $\alpha = (\lambda - 1)/2$, and $C, C' > 0$ are constants. Given $\lambda \in (1, 3)$, we will refer to the function $K \mapsto K^\gamma E(\mu_t^\Delta; K)$ as the compensated energy spectrum with exponent γ , in the following.

Owing to Theorem 4.3.2, a uniform algebraic bound on the structure function implies that the limiting solution generated by our numerical method is energy conservative. Thus, the evolution of the numerical structure function $\tilde{S}_2(r)$ and the compensated energy spectra will be our main tools to investigate the energy conservation of the limits of our numerical approximations. A convenient measure for the uniform algebraic decay of the structure functions $S_2(\mu_t^\Delta; r)$ is the best-decay-constant $C_{\max}^\Delta(\alpha, t)$, which we define

$$C_{\max}^\Delta(\alpha; t) := \sup_{r>0} r^{-\alpha} \tilde{S}_2(\mu_t^\Delta; r), \quad (4.4.4)$$

i.e. the best constant C , such that $\tilde{S}_2(\mu_t^\Delta; r) \leq Cr^\alpha$ for all $r > 0$. Note that for any given resolution $\Delta > 0$, the structure function $\tilde{S}_2(\mu_t^\Delta; r)$ decays like $\sim r$ on the subgrid scale, *i.e.* for $r \ll \Delta$. Therefore, given $0 < \alpha < 1$, the best-decay-constant $C_{\max}^\Delta(\alpha; t)$ is well-defined and finite, for any fixed numerical resolution Δ . Furthermore, if there exists α , for which $C_{\max}^\Delta(\alpha; t)$ remains uniformly bounded in time, and with increasing resolution, then this is sufficient to ensure (strong) compactness, and hence energy conservation in the limit $\Delta \rightarrow 0$, by Theorem 4.3.2.

Similarly, we define a constant $D_{\max}^\Delta(\lambda; t)$ as the best upper bound on the compensated energy spectrum with exponent λ :

$$D_{\max}^\Delta(\lambda; t) := \sup_{K>0} K^\lambda E(\mu_t^\Delta; K). \quad (4.4.5)$$

Finally, we will also compute the evolution of energy directly, *i.e.*

$$t \mapsto \int_{L_x^2} \|\mathbf{u}\|_{L_x^2}^2 d\mu_t(\mathbf{u}),$$

for each numerical experiment. For the latter, it is important to keep in mind that there are several sources of errors for each numerical approximation, which may affect the results obtained from this direct computation of the energy evolution: Firstly, each approximate statistical solution is obtained by Monte-Carlo sampling (with N samples). As is well-known, the evaluation of the dissipated energy by Monte-Carlo sampling is associated with a sampling error that scales like $\sim 1/\sqrt{N}$. Secondly, in addition to the statistical error, the initial data has also to be approximated, for instance by mollification, and subsequent truncation of the Fourier spectrum. These procedures induce numerical error that propagates into the solution. Finally, there are errors on account of the space-time discretization. All of these sources of numerical errors should be taken into account, when directly evaluating the energy dissipation.

4.4.3 A Sinusoidal vortex sheet

Deterministic case

The first case we consider is the case of initial data for the incompressible Euler equations which is a Dirac measure, concentrated on a vortex sheet, *i.e.* $\bar{\mu} = \delta_{\bar{\mathbf{u}}}$, where $\bar{\mathbf{u}}$ is a sinusoidal vortex sheet initial data. This initial data has previously been studied in [LM20, LMPP21b]. Let us first recall the construction.

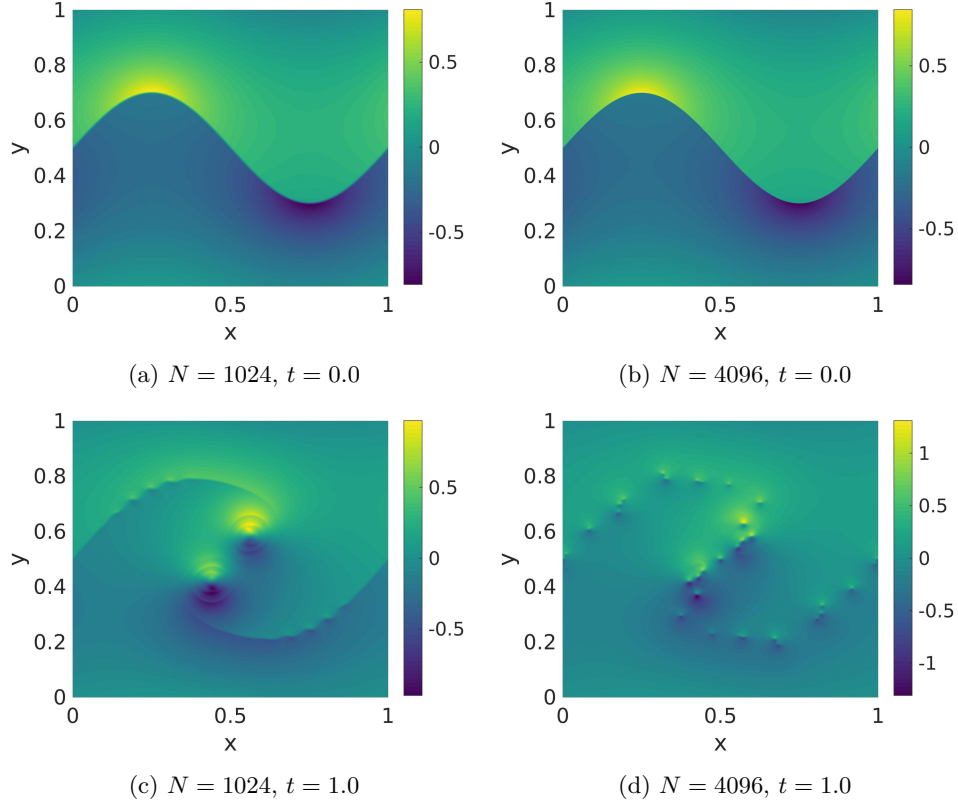


Figure 4.1: Deterministic evolution of sinusoidal vortex sheet with Navier-Stokes-like diffusion (viscosity parameter $\epsilon = 0.01$). Horizontal x -component of velocity at initial time and final time, for resolutions $N = 1024$ and $N = 4096$.

We consider a vorticity distributed uniformly along the graph

$$\Gamma = \{x = (x_1, x_2) \in T^2 \mid x_2 = 0.2 \sin(2\pi x_1)\},$$

and we recall that in the numerical implementation in SPHINX, the torus T^2 is identified with $[0, 1]^2$. The vorticity is given by

$$\bar{\omega}(x) = \delta(x - \Gamma) - \int_{T^2} d\Gamma.$$

The second term in the definition of $\bar{\omega}$ is a constant which serves to ensure that $\int_{T^2} \bar{\omega} dx = 0$, *i.e.* it enforces the vanishing of the 0-th Fourier coefficient. The initial velocity field $\bar{\mathbf{u}} \in L_x^2$ is chosen so that $\text{div}(\bar{\mathbf{u}}) = 0$, $\text{curl}(\bar{\mathbf{u}}) = \bar{\omega}$. Given a grid size N , our numerical approximation $\bar{\mathbf{u}}^\Delta \approx \bar{\mathbf{u}}$ is obtained by mollification $\bar{\mathbf{u}}^\Delta = \psi_{\rho_N} * \bar{\mathbf{u}}$ against a mollifier $\psi_{\rho_N}(x) := \rho_N^{-2} \psi(x/\rho_N)$, with $\psi(x)$ a third-order B-spline. The smoothing parameter ρ_N is chosen of the form $\rho_N = \rho/N$ for a fixed constant $\rho > 0$. For the present simulation, we have set $\rho = 10$. Further details on the construction of this initial data can be found in chapter 3.5.2, on page 71.

We point out that this initial data belongs to the so-called *Delort class* [Del91]. It was recently shown in [LM20] that the numerical approximations, generated by the spectral viscosity method, converge on increasing the resolution and up to a subsequence, to a weak solution of the incompressible Euler

equations. Given this context, we have computed the numerical solution up to final time $T = 1$, and for resolutions $N \in \{128, 256, \dots, 8192\}$. The numerical diffusion operator was chosen so as to mimic the form of the diffusion term in the underlying Navier-Stokes equations (4.1.1) by setting $m_N = 0$ and consequently, $Q_N = I$ in (4.3.1). For these computations, we set $\epsilon_N = \epsilon/N$, $\epsilon = 0.01$. A representative illustration of the initial data and evolution of the computed approximate solutions at different resolutions $N = 1024$, $N = 4096$ can be found in Figure 4.1. From this figure, we observe that the initial vortex sheet breaks up into smaller and smaller vortices, on increasing resolution.

Our objective is to validate our theory on the connection between the uniform decay of the structure function and the conservation of energy. To this end, we first consider the temporal evolution of the numerical structure function (4.4.1) (cp. Figure 4.2). Indicated in Figure 4.2 are representative plots of the numerical structure functions evaluated at different times $t = 0.0, 0.4, 1.0$ during the evolution of the vortex sheet, and at the various resolutions considered. In addition, we indicate as a black dashed line the graph of $r \mapsto C_{\max}^{\Delta} r^{1/2}$, where $C_{\max}^{\Delta} = C_{\max}^{\Delta}(\alpha = 1/2; t = 0)$ is determined from (4.4.4), at resolution $\Delta = 1/8192$. At the initial time $t = 0$, the expected scaling $S_2(r) \sim r^{1/2}$ of the structure function of the vortex sheet at resolved scales is clearly visible. For a fixed resolution $\Delta = 1/N$, it is straightforward to observe that the resulting numerical approximation cannot represent non-smooth features on scales $r \lesssim \Delta$ and the structure function scales as $S_2(r) \sim r$, for $r \lesssim \Delta$ in Figure 4.2.

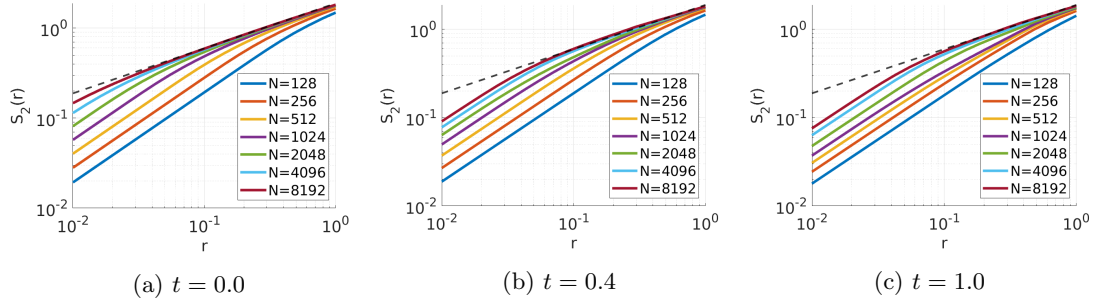


Figure 4.2: Temporal evolution of structure function for deterministic sinusoidal vortex sheet initial data, for different resolutions $\Delta = 1/N$. The black dashed line indicates the best upper bound $C_{\max}^{\Delta} r^{\alpha}$ computed at $t = 0$, with exponent $\alpha = 1/2$, and at the finest resolution considered, $\Delta = 1/8192$.

Figures 4.2 (A)-(C) clearly indicate a uniform decay of the structure function over time, and uniformly in N , with a decay exponent that is the same as the decay exponent of the structure function initially.

This uniform decay of the structure functions is further confirmed by considering the evolution of the compensated energy spectra $K \mapsto K^{\lambda} E(K)$, where we choose the exponent $\lambda = 2$. This choice is consistent with a $S_2(r) \leq Cr^{\alpha}$, where $\alpha = (\lambda - 1)/2 = 1/2$, decay of the structure function.

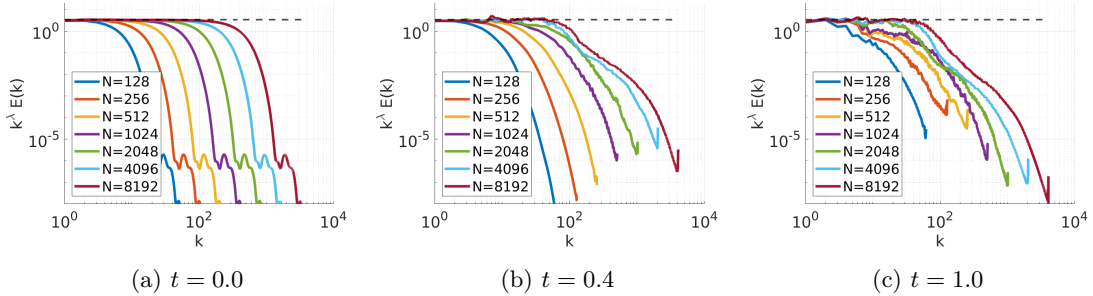


Figure 4.3: Temporal evolution of compensated energy spectra $K^\lambda E(K)$ for deterministic sinusoidal vortex sheet initial data, with $\lambda = 2$.

As can be seen from Figure 4.3 (A), the initial data follow the expected scaling $E(K) \sim K^{-2}$. This scaling appears to be mostly preserved at later times, cp. Figure 4.3 (B), (C), with only some small fluctuations in the compensated spectra. These fluctuations might imply $E(K) \leq CK^{-2+\epsilon}$ for a small $\epsilon > 0$, incorporating *intermittent* corrections to the structure function. Nevertheless, this form of the energy spectrum clearly implies the compactness required for energy conservation.

Since the above numerical results strongly suggest a decay of the structure function as $S_2(r) \leq Cr^\alpha$, with $\alpha = 1/2$, we consider the temporal evolution of the best-decay constant $C_{\max}^\Delta(\alpha = 1/2; t)$ (cp. (4.4.4)), which is displayed in Figure 4.4, as well as its energy spectral counterpart $D_{\max}^\Delta(\lambda = 2; t)$, evaluated according to (4.4.5).

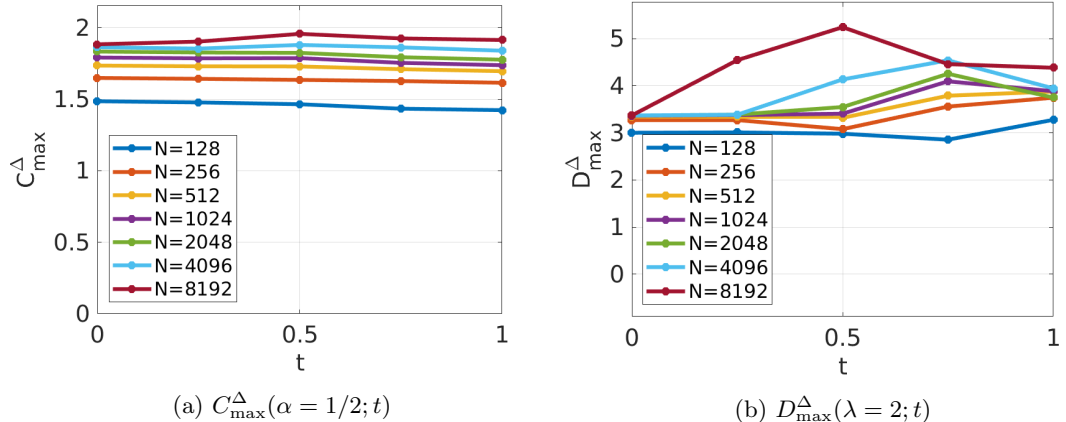


Figure 4.4: Temporal evolution of C_{\max}^Δ (eq. (4.4.4)) and D_{\max}^Δ (eq. (4.4.5)) for deterministic sinusoidal vortex sheet.

Figure 4.4 strongly indicates that $C_{\max}^\Delta(\alpha = 1/2; t)$ remains uniformly bounded in time $t \in [0, T]$, as $\Delta \rightarrow 0$. Thus, from the above figures, we clearly infer that the structure functions (and spectra) converge on increasing resolution. This *saturation* of structure functions, with increasing resolution, is reminiscent of similar observations of convergence of structure functions, but with increasing Reynolds number, for homogeneous isotropic 3D turbulent flows, reported for instance in the recent paper [ISY20].

Finally, we consider directly the evolution of the energy. Here, we are faced with the difficulty that the initial values of the numerical approximations converge at the same time as the viscosity parameter

$\epsilon_N \rightarrow 0$. Keeping this in mind, we consider the *relative energy dissipation*,

$$\frac{\Delta E}{E} := \frac{E_t^\Delta - \bar{E}_0}{\bar{E}_0},$$

which depends on Δ and the time t , as well as a reference value \bar{E}_0 for the initial energy in the limit $\Delta \rightarrow 0$. We obtain this reference value by extrapolation of the initial energy E_0^Δ for the resolutions $\Delta \in \{1/8192, 1/4096, \dots, 1/128\}$, considered. We have chosen the second-order (Richardson-)extrapolation ansatz

$$E_0^\Delta = \bar{E}_0 + c_1 \Delta + c_2 \Delta^2 + O(\Delta^3),$$

where the constants \bar{E}_0 , c_1 and c_2 can be estimated from the values of E_0^Δ , for the highest resolutions $\Delta = 1/8192, 1/4096, 1/2048$ considered. Other, higher-order choices for the extrapolation have been checked to lead to very similar results.

The temporal evolution of $\Delta E/E$ is shown in Figure 4.5 (A), for these $\Delta = 1/N$. Figure 4.5 (B) compares $\Delta E/E$ at time $t = 0$ and $t = T$, at the final time $T = 1$, as a function of the resolution Δ . In this figure, we plot both the numerical error in the approximation of the initial data (represented by the blue curve), as well as the numerical energy dissipation (difference between the blue and the red curves). As $\Delta \rightarrow 0$, there is a clear indication that $\Delta E/E$, evaluated at both the initial and final times, converges to 0. Extrapolation of the red curve to $\Delta = 0$ yields a very small value of $\Delta E/E \approx -0.00035$, consistent with a true limiting value of $\Delta E/E = 0$ at $\Delta = 0$. The direct evaluation of the energy is thus consistent with the uniform decay of the structure functions, and a uniform bound on the energy spectra observed above.

Thus, in this particular case, the theoretical predictions of energy conservation resulting from uniform decay of structure function (spectra) is completely validated. It is worth pointing out that the theory of Delort in [Del91] (and its numerical analogue in [LMPP21b]) only indicate weak compactness of the approximating sequences. On the other hand, all the numerical evidence points to a strong compactness of the limit solution, hinting at more regularity of the limit.

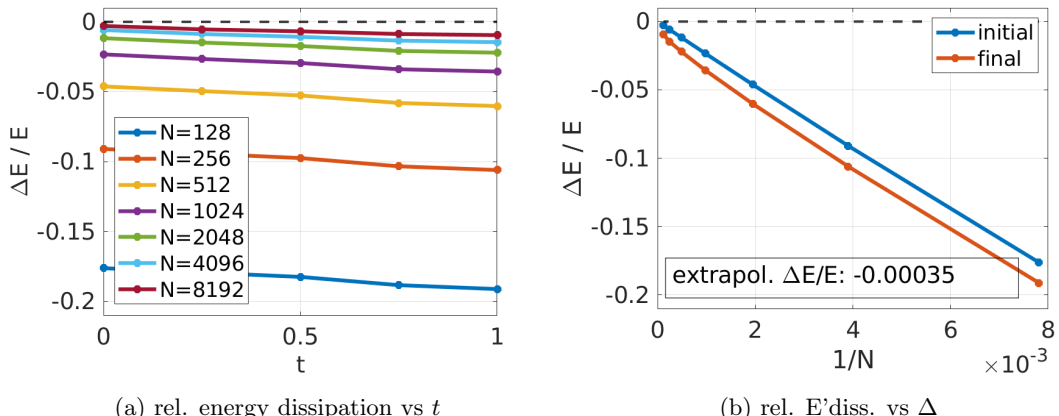


Figure 4.5: Deterministic sinusoidal vortex sheet with Navier-Stokes-like diffusion: Relative energy dissipation as a function of t (left), and as a function of $\Delta = 1/N$ at the final time $t = 1$ (right).

Statistical initial data

Next, we consider an example of the initial data $\bar{\mu} \in \mathcal{P}(L_x^2)$, with $\bar{\mu}$ not being a Dirac measure. To this end, we take the numerical initial data $\bar{\mathbf{u}}^\Delta(x) \in L_x^2$ of the previous section (with smoothing parameter $\rho_N = \rho/N$, $\rho = 5$), and define a random perturbation as

$$\bar{\mathbf{u}}^\Delta(x; \omega) := \mathbb{P}(\bar{\mathbf{u}}^\Delta(x_1, x_2 + \sigma_\alpha(x_1; \omega))),$$

where \mathbb{P} denotes the Leray projection onto divergence-free vector fields, followed by a projection onto the first N Fourier modes, and $\sigma_\alpha(x, \omega)$ is a random function which is used to randomly perturb the vortex sheet: Fix $q \in \mathbb{N}$ and a perturbation size $\alpha > 0$. Given $\omega = (\alpha_1, \dots, \alpha_q, \beta_1, \dots, \beta_q)$, we define

$$\sigma_\alpha(x_1; \omega) := \sum_{k=1}^q \alpha_k \sin(k2\pi x_1 - \beta_i),$$

where $\alpha_1, \dots, \alpha_q \in [0, \alpha]$, and $\beta_1, \dots, \beta_q \in [0, 2\pi]$ are i.i.d., uniformly distributed random variables. The initial data $\bar{\mu}^\Delta \in \mathcal{P}(L_x^2)$ is defined as the law of the random fields $\bar{\mathbf{u}}^\Delta(x; \omega)$. For our numerical experiment, we have chosen $q = 10$, and $\alpha = 1/320$. The numerical diffusion parameter is $\epsilon_N = \epsilon/N$, with $\epsilon = 0.01$. Figure 4.6 shows the x -component of the velocity of a typical individual random sample $\bar{\mathbf{u}}^\Delta$, as well as the mean and variance of this component at the initial time $t = 0.0$. The mean and variance at the final time $t = 1.0$ are shown in Figure 4.7.

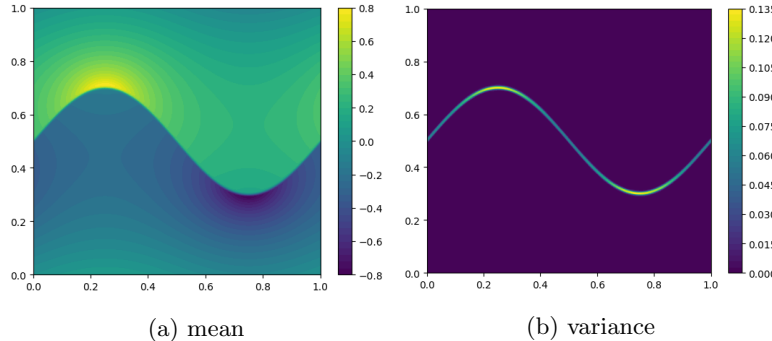


Figure 4.6: Perturbed sinusoidal vortex sheet: Mean (A) and variance (B) at the initial $t = 0.0$, $N = 1024$.

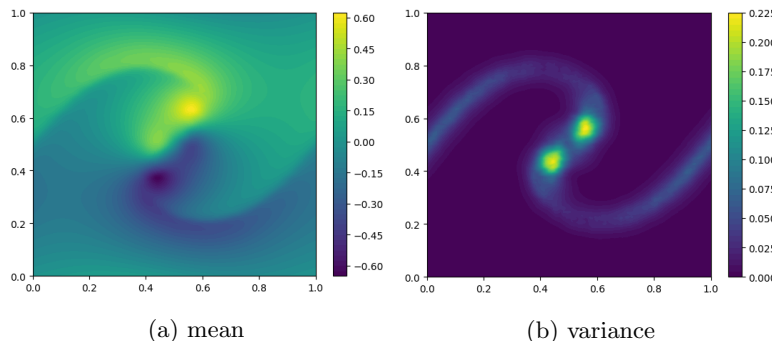


Figure 4.7: Perturbed sinusoidal vortex sheet: Mean (A) and variance (B) at the final time $t = 1.0$, $N = 1024$.

We consider the temporal evolution of the structure functions computed from the approximate statistical solution obtained at various resolutions $N \in \{128, 256, 512, 1024\}$. Plots for the numerical structure function (4.4.1) at $t = 0, 0.5, 1$ are shown in Figure 4.8 (A)-(C). Again, we indicate by a black dashed line the best upper bound of the form $C_{\max}^{\Delta} r^{1/2}$, with C_{\max}^{Δ} given by (4.4.4) fixed at time $t = 0$, and for the highest considered resolution of $\Delta = 1/1024$.

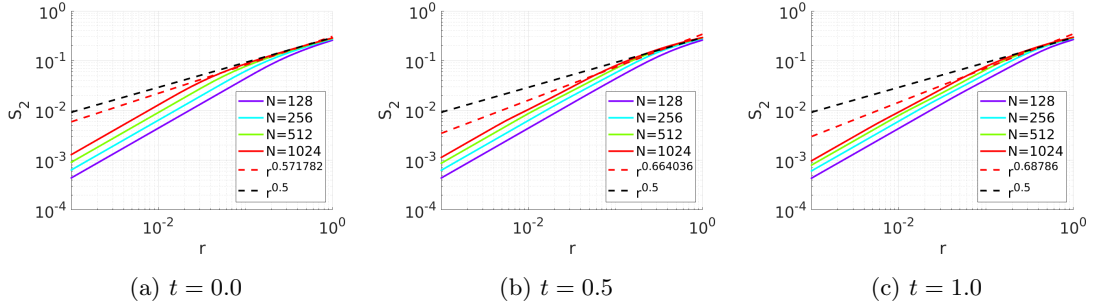


Figure 4.8: Temporal evolution of structure function for randomly perturbed sinusoidal vortex sheet initial data, for different resolutions $\Delta = 1/N$. The black dashed line indicates the best upper bound $C_{\max}^{\Delta} r^{\alpha}$ computed at $t = 0$, with exponent $\alpha = 1/2$, and at the finest resolution considered, $\Delta = 1/1024$.

Similarly to Figure 4.2 in the last section, these plots of the structure function at different t and N indicate a uniform bound $S_2(\mu_t^{\Delta}; r) \leq Cr^{1/2}$. To complement these plots of the structure function, we again analyse the (compensated) energy spectra (4.4.2), with exponent $\lambda = 2$. Again, the choice of this value for λ is motivated by the relation (4.4.3), according to which a value of $\alpha = 1/2$ is expected to correspond to $\lambda = 2$. The resulting energy spectra are shown in Figure 4.9.

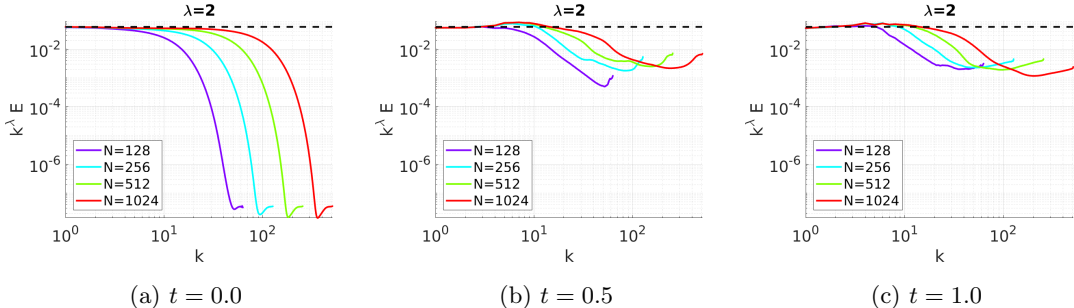


Figure 4.9: Temporal evolution of compensated energy spectra $K^{\lambda} E(K)$ for randomly perturbed sinusoidal vortex sheet initial data, with $\lambda = 2$.

Again, we observe an exact scaling of the compensated energy spectra for μ_t^{Δ} at $t = 0$ (cp. Figure 4.9 (A)). Also at later times, this scaling is approximately preserved, as shown in Figure 4.9 (B),(C), indicated a uniform bound on compensated energy spectra.

A more quantitative evaluation of the uniform boundedness of the structure function is obtained by tracking the temporal evolution of the best-upper-bound constants $C_{\max}^{\Delta}(\alpha; t)$ for the structure function (4.4.4) with exponent $\alpha = 1/2$, and $D_{\max}^{\Delta}(\lambda; t)$ for the compensated energy spectra (4.4.5), with corresponding exponent $\lambda = 2$. This is shown in Figure 4.10.

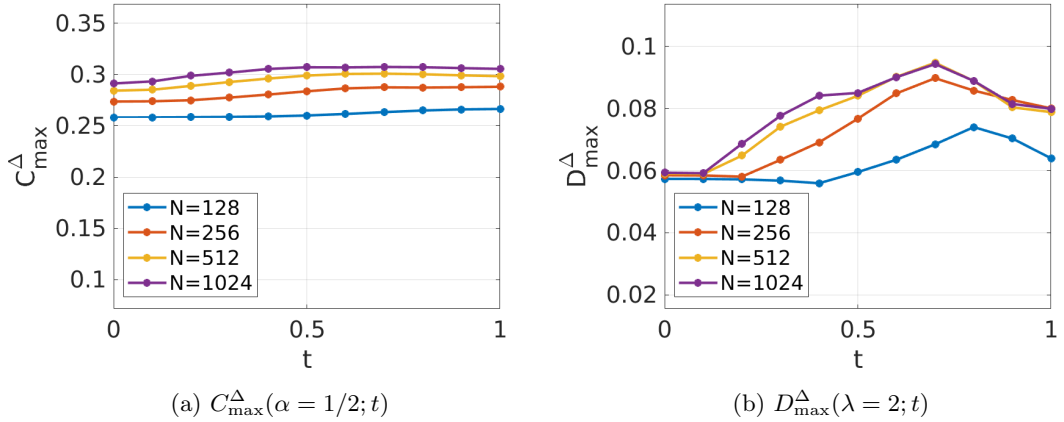


Figure 4.10: Temporal evolution of C_{\max}^{Δ} (eq. (4.4.4)) and D_{\max}^{Δ} (eq. (4.4.5)) for randomly perturbed sinusoidal vortex sheet.

Figure 4.10 strongly indicates that the structure function does indeed exhibit a uniform scaling $S_2(\mu_t^{\Delta}; r) \leq Cr^{1/2}$, implying energy conservation of the limiting statistical solution.

We finally consider the direct evaluation of the energy evolution of the approximate statistical solutions. In addition to the sources of error in the energy evolution for the deterministic initial data, we also have to consider another source of error in the Monte-Carlo approximation of the approximate statistical solution μ_t^{Δ} . Our Monte-Carlo sampling at resolution N is based on N samples. As is well-known, the typical Monte-Carlo error is

$$\left| \mathbb{E}[\Delta E/E] - \frac{1}{N} \sum_{i=1}^N \frac{\Delta E_i}{E_i} \right| \lesssim \frac{\text{Std}[\Delta E/E]}{\sqrt{N}}, \quad (4.4.6)$$

where $\text{Std}[\Delta E/E]$ is the standard deviation computed based on the N MC-samples $(\Delta E/E)_1, \dots, (\Delta E/E)_N$. For the statistical solutions considered, we will display this MC error by error bars and a shaded region.

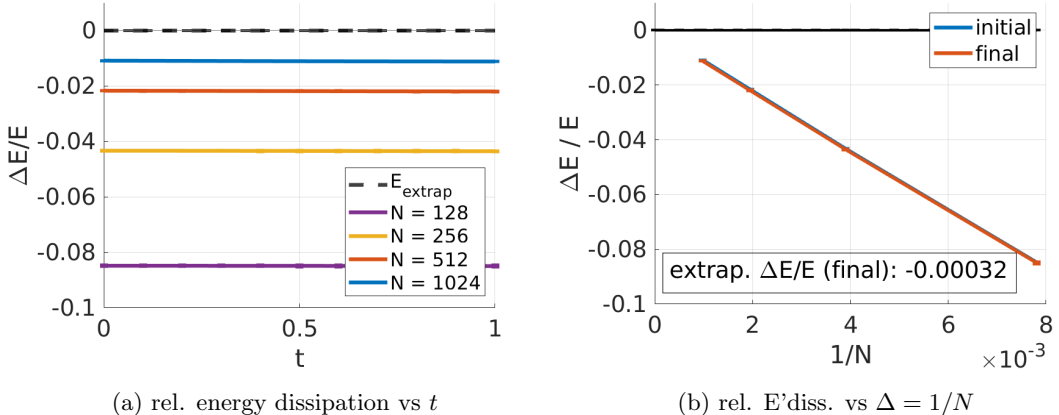


Figure 4.11: Randomly perturbed sinusoidal vortex sheet: Relative energy dissipation $\mathbb{E}[\Delta E/E]$ as a function of t (left), and as a function of $\Delta = 1/N$ at the final time $t = 1$ (right).

It turns out that for the current initial data, the MC error in the energy is very small, so that the shaded regions are almost invisible. In this case, the numerical error in the approximation of the initial data dominates. We plot the computed $\Delta E/E$ in Figure 4.11. As in the last section, the reference value \bar{E}_0 is determined by a second-order Richardson-extrapolation of the computed initial energy E_0^Δ to $\Delta = 0$.

Figure 4.11 clearly indicates that the energy dissipation is very small for this case, for all resolutions considered, and $\Delta E/E$ appears to converge to 0, as $N \rightarrow \infty$, again indicating energy conservation in the limit. We have also indicated the value of $\Delta E/E$ at the final time $t = T$, and (second-order) extrapolated to $\Delta = 0$, based on the available values of E_T^Δ for $\Delta = 1/1024, 1/512$ and $1/256$. This extrapolation suggests that $\Delta E/E \approx 0.00032$, which is orders of magnitude smaller than the error of $\Delta E/E$ at the initial time (whose limit $\Delta \rightarrow 0$ is exactly 0), which is also visible in Figure 4.11 (B). Thus, also for the randomly perturbed sinusoidal vortex sheet, the limiting statistical solution is expected to be energy conservative.

Finally, comparing figures 4.11 for the SV scheme and 4.5 for Navier-Stokes-like diffusion clearly shows that the Navier-Stokes-like diffusion is much more diffusive. This highlights the better approximation properties of the (formally) spectrally accurate SV scheme, as opposed to a similar scheme with diffusion applied to all Fourier modes.

4.4.4 Vortex sheet without distinguished sign

The previous numerical experiment considered a vortex sheet of (essentially) distinguished sign. For this type of initial data, the existence of solutions has been proven rigorously by compensated compactness methods, in the celebrated work of Delort [Del91]. When the vortex sheet initial data is not necessarily of distinguished sign, then no existence results for weak solutions are known. Based on numerical experiments by Krasny [Kra87], which have shown that vortex sheets develop a much more complex roll-up without a sign-restriction, it has in fact been conjectured [Maj88], [MB01, p.447] that approximate solution sequences for initial data without distinguished sign might not converge to a weak solution, and instead exhibit the phenomenon of concentrations in the limit, thus necessitating a more general concept of measure-valued solutions. Our next numerical experiment therefore considers the case of a vortex sheet without distinguished sign.

We start with unperturbed vorticity $\bar{\omega} \in \mathcal{M}$ a bounded measure, given by

$$\bar{\omega}(x) = s(t)\delta(x - \gamma(t)) - \int_0^{2\pi} s(t) d\gamma(t),$$

where $\gamma(t) = (t, 0.2 \sin(Kt)) \in T^2$ defines the curve along which the vorticity is distributed, with $K = 10$, and the vortex strength $s(t)$ along $\gamma(t)$ is given by $s(t) = \sin(Kt)$. The numerical approximation $\bar{\omega}^\Delta$ is obtained as the convolution $\bar{\omega}^\Delta(x) := \bar{\omega} * \psi_{\rho_N}$, where $\rho_N = \rho/N$, $\rho = 5$, and ψ_{ρ_N} is the B-spline mollifier already considered in section 4.4.3. We let $\bar{\mathbf{u}}^\Delta$ denote the corresponding divergence-free velocity field. Finally, we define the perturbed initial data for given $\alpha > 0$, by setting

$$\bar{\mathbf{u}}^\Delta(x; \omega) := \mathbb{P}(\bar{\mathbf{u}}^\Delta(x_1, x_2 + \sigma_\alpha(x_1; \omega))),$$

where $x_1 \mapsto \sigma_\alpha(x_1, \omega)$ is the random perturbation already introduced in section 4.4.3. We have chosen $\alpha = 0.025$ for our numerical simulation. Again, we let $\bar{\mu}^\Delta \in \mathcal{P}(L_x^2)$ be the law of the random field $\bar{\mathbf{u}}^\Delta$. Figure 4.12 shows the x -component of the velocity of a typical individual random sample $\bar{\mathbf{u}}^\Delta$, as well as the mean and variance of this component at the initial time $t = 0.0$. For comparison, the mean and variance at the final time $t = 2.0$ are shown in Figure 4.13. The viscosity parameter in the SV scheme was chosen as $\epsilon_N = \epsilon/N$, for $\epsilon = 0.05$.

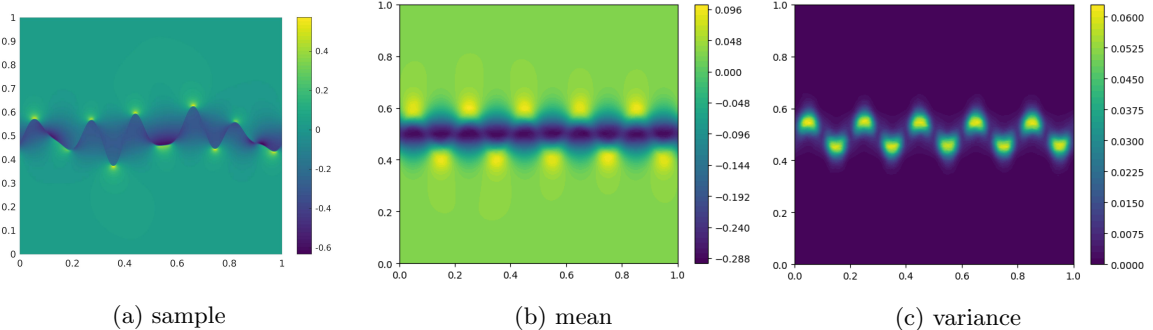


Figure 4.12: Perturbed vortex sheet without distinguished sign: Individual sample (A), mean (B) and variance (C) at the initial $t = 0.0$, $N = 1024$.

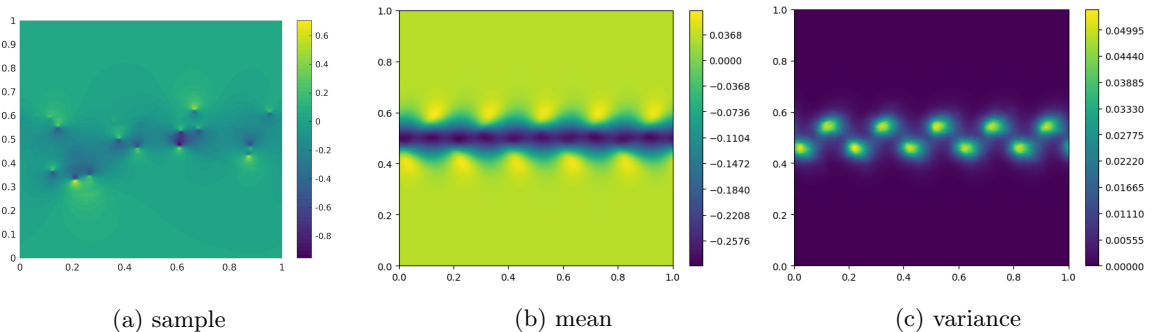


Figure 4.13: Perturbed vortex sheet without distinguished sign: Individual sample (A), mean (B) and variance (C) at the final time $t = 2.0$, $N = 1024$.

We start by considering the temporal evolution of the structure functions computed from the approximate statistical solution obtained at various resolutions $N \in \{128, 256, 512, 1024\}$.

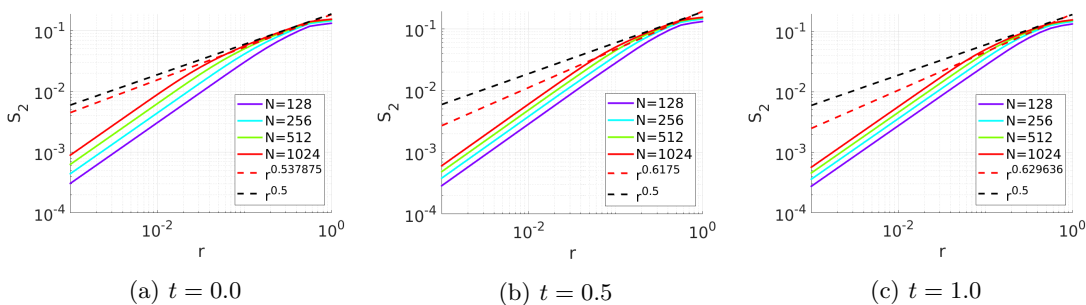


Figure 4.14: Temporal evolution of structure function for randomly perturbed vortex sheet initial data without distinguished sign, for different resolutions $\Delta = 1/N$. The black dashed line indicates the best upper bound $C_{\max}^{\Delta} r^{\alpha}$ computed at $t = 0$, with exponent $\alpha = 1/2$, and at the finest resolution considered, $\Delta = 1/1024$.

Perhaps unexpectedly, the structure functions shown in Figure 4.14 exhibit a uniform bound for

$t = 0, 1, 2$, also without the sign restriction on the vorticity; similar to the bound on the structure function observed for the distinguished vortex sheet case in section 4.4.3. Again, the bound on the structure function indicates that $S_2(\mu_t^\Delta; r) \leq Cr^{1/2}$, for some constant $C > 0$.

We next consider the evolution of the compensated energy spectra $K \mapsto K^\lambda E(\mu_t^\Delta; K)$ with exponent $\lambda = 2$ (which corresponds to the exponent $\alpha = 1/2$ of the structure function), in Figure 4.15.

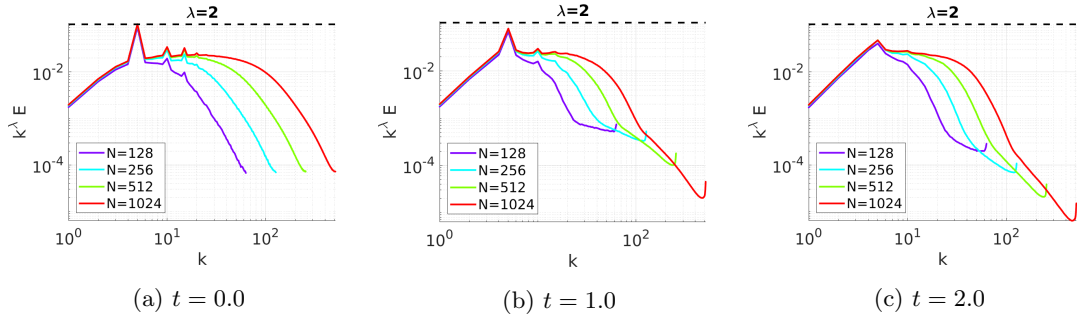


Figure 4.15: Temporal evolution of compensated energy spectra $K^\lambda E(K)$ for randomly perturbed sinusoidal vortex sheet initial data, with $\lambda = 2$.

The compensated energy spectra confirm the observed uniform bound on the structure function, indicating that $E(\mu_t^\Delta; K) \leq DK^{-2}$, for some constant $D > 0$. To analyse this qualitative observation at a more quantitative level, we track the best-upper-bounds C_{\max}^Δ (4.4.4) and D_{\max}^Δ (4.4.5) in Figure 4.16.

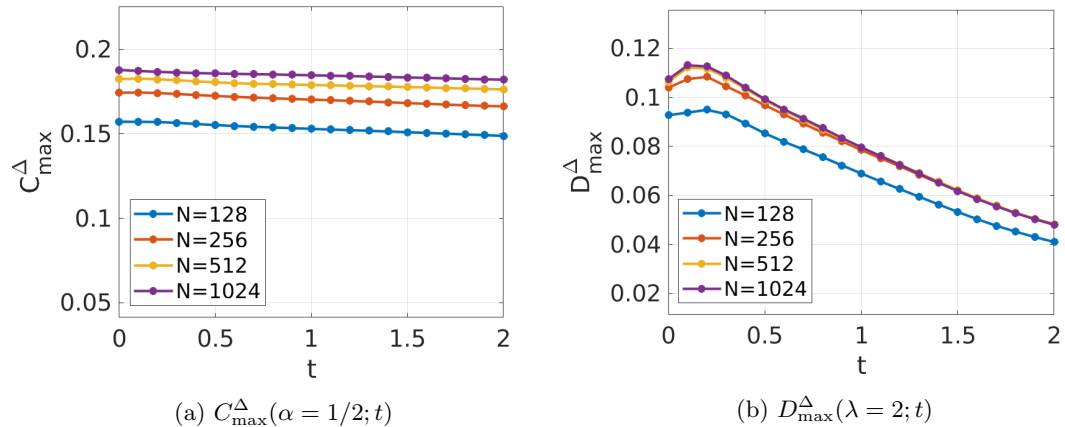


Figure 4.16: Temporal evolution of C_{\max}^Δ (eq. (4.4.4)) and D_{\max}^Δ (eq. (4.4.5)) for randomly perturbed vortex sheet without distinguished sign.

Figure 4.16 clearly indicates that the structure function remains uniformly bounded over time and with respect to resolution also for this signed vortex sheet case.

Finally, we consider the evolution of the numerically obtained energy dissipation, directly. Again, we consider the temporal evolution of the quantity

$$\frac{\Delta E}{E} = \frac{E^\Delta(t) - \bar{E}_0}{\bar{E}_0},$$

where $E^\Delta(t) = \int_{L_x^2} \|u\|_{L_x^2}^2 d\mu_t^\Delta(u)$. The estimate for the Monte-Carlo error of this quantity is indicated by the shaded regions. The reference value \bar{E}_0 has been determined by second-order Richardson-extrapolation of the given data $E^\Delta(0)$ for $\Delta \in \{1/1024, 1/512, 1/256\}$ to $\Delta = 0$.

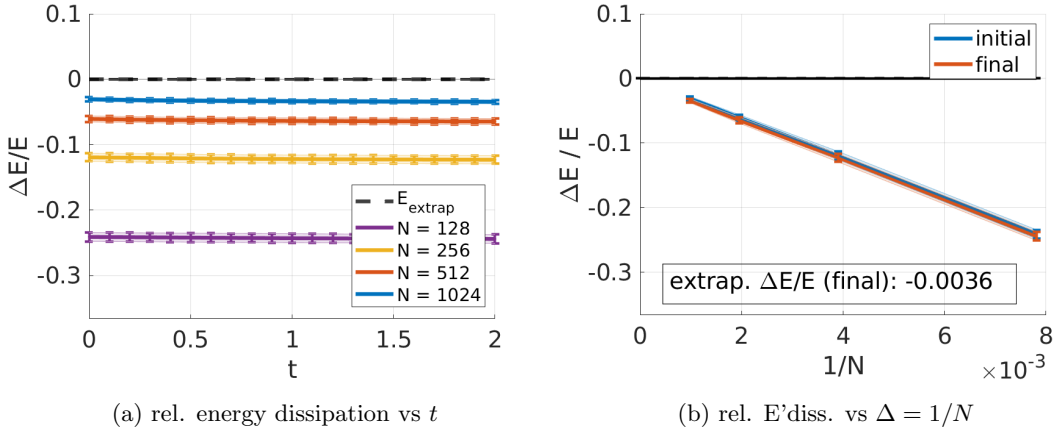


Figure 4.17: Vortex sheet without distinguished sign: Relative energy dissipation as a function of t (left), and as a function of $\Delta = 1/N$ at the final time $t = 1$ (right).

Unexpectedly, also for this initial data, where the individual random realisations of the initial data have vorticity $\bar{\omega}^\Delta \in \mathcal{M}$, i.e. a bounded measure, *without a distinguished sign*, our numerical experiments indicate that the energy dissipation converges to zero as $\Delta \rightarrow 0$ (at least over the time interval $[0, T]$ with $T = 2$ considered), implying that the limiting statistical solution is energy conservative, and confirming our observed bounds on the structure function.

4.5 Discussion

A characteristic feature of fluids described by the incompressible Euler equations is turbulence, marked by the appearance of energy containing eddies at ever smaller scales. Energy conservation and anomalous dissipation are very interesting elements of physical theories of turbulence such as those of Kolmogorov and Onsager.

In this chapter, we consider the questions of energy conservation and dissipation of solutions of the incompressible Euler equations in two space dimensions, following the original publication [LMPP21a]. We prove in Theorem 4.2.11 that weak solutions of the incompressible Euler equations, realized as strong (in the topology of $L^1([0, T]; L_x^2)$) vanishing viscosity limits of the underlying Navier-Stokes equations conserve energy (in time). This result allows us to extend the results of [CFLS16] on energy conservation to a larger class of admissible initial data, for which strong compactness of approximate solutions is known. The proof relies on control of the underlying vorticity and an essential role is played by uniform decay of the so-called *structure function* (4.2.2).

Next, we also investigate the question of energy conservation for statistical solutions of the incompressible Euler equations. As discussed in chapter 3, statistical solutions are time-parameterized probability measures on L_x^2 , whose time evolution is constrained in terms of moment equations, consistent with and derived from the incompressible Euler equations. They were proposed as a suitable probabilistic solution framework for the Euler equations in order to describe unstable and turbulent fluid flows in

[LMPP21b, FW18]. We prove in Theorem 4.3.2 that statistical solutions of the Euler equations, generated as limits of numerical approximations with a Monte Carlo (MC)- Spectral viscosity (SV) method of [LMPP21b], conserve energy as long as the structure function decays uniformly (in numerical resolution). This result is of great practical utility as these statistical solutions can be computed [LMPP21b] and the assertions of the theory validated in numerical experiments.

To this end, we presented a suite of numerical experiments with both deterministic and stochastic initial data, focusing on vortex sheets. From the numerical experiments, we observed that the structure functions (and the energy spectra) were indeed uniformly decaying and energy conservation of the limit solutions was clearly demonstrated.

This chapter only considered two-dimensional flows. Future work could aim to carry out a similar programme for examining the questions of conservation/anomalous dissipation of energy for three-dimensional incompressible flows.

Chapter 5

Limitations of the approach

In the previous chapters, we have presented numerical evidence which demonstrates that approximate solutions of the incompressible Euler equations computed by state-of-the-art numerical methods, such as spectral methods, may not converge *deterministically* to a unique limit, if the underlying solution has low regularity. This is consistent with available theoretical results, which only guarantee the uniqueness of solutions under more restrictive (Lipschitz) regularity assumptions (cp. the weak-strong uniqueness theorem 1.3.11). In our numerical experiments a marked contrast was observed between the non-convergence in any “traditional” deterministic sense, versus the apparent stability and convergence of *statistical quantities* at increasing numerical resolution. These observations are in line with similar results in the context of hyperbolic conservation laws [FMT16, FKMT17, FLMW20], which partially motivated the present work. We furthermore expect that similar conclusions will apply more generally to PDEs exhibiting features of “turbulence”. These results clearly indicate the practical need to efficiently approximate apparently more stable and robustly computable *statistical solutions* for high to very high Reynolds number flows.

The difficulties in predicting the behaviour of turbulent or chaotic dynamical systems is particularly well-known for numerical weather forecasting, where the high sensitivity to perturbations in the initial data [Lor63] is sometimes referred to as the “butterfly effect”. Despite this high sensitivity, weather forecasts have seen a steady increase of forecast skill over the last decades [BTB15]. This is in some part due to improvements in computational resources, but to a large extent reflects the increased availability of measurement data and the increased sophistication of methods to combine this data with the underlying mathematical model to increase prediction accuracy [MH12, LSZ15, RC15]. In the formulation of statistical solutions of the preceding chapters, it is not clear how such measurement data should be incorporated in the model. We thus identify our first main limitation:

- The **first limitation** of the statistical solutions discussed in the previous chapters of the present thesis is that *available measurement data*, which is crucial in practical applications, is not explicitly reflected by this solution concept.

Statistical solutions as described in chapter 3 are also natural to consider in the context of uncertainty quantification: In practice, the initial state of the system has to be inferred from measurements. These measurements are usually noisy and incomplete, and therefore do not allow the initial state to be reconstructed to arbitrary accuracy. Since the equations of fluid dynamics are very sensitive to perturbations, small errors in the initial data are strongly amplified by the non-linear dynamics. Thus, in large-scale applications including weather forecasting and climate science, predictions based on a single forward solve, relying on the most likely initial state cannot be expected to be reliable. Instead, the

uncertainty in our knowledge of the initial data and the corresponding predictions has to be explicitly taken into account. Such uncertainty is naturally represented by a probability measure $\bar{\mu}$ on the (infinite-dimensional) state space. The prediction of the future state, including an estimate of the *uncertainties* in this prediction, thus requires the computation of the corresponding statistical solution, allowing for principled uncertainty quantification. While the need for such systematic uncertainty quantification is widely appreciated, a major obstacle for its implementation in large-scale applications is the fact that the computation of the relevant statistical quantities via Monte-Carlo or Markov-chain Monte-Carlo methods can require up to $O(10^5)$ forward model evaluations of the underlying PDE [Gey11]. The computational cost of a single solve is typically very high for relevant applications, *e.g.* requiring millions of node hours of computation time on HPC facilities, for a single forward solve of the Navier-Stokes equations in realistic engineering geometries [Alf11]. Hence, systematic uncertainty quantification based on fully resolved simulations cannot be carried out routinely, at present. This leads to the second main limitation of statistical solutions discussed so far:

- The **second limitation** of the approach to statistical solutions, and in particular their computation via Monte-Carlo and Markov chain Monte-Carlo sampling, is their *high computational cost*, requiring many (costly) forward solves of the underlying forward model.

It has been observed in many numerical experiments (cp. chapters 3, 4), that, while individual solutions (samples) can exhibit features on very fine scales, statistics computed by taking an average over many such individual realizations are much smoother. Even though the precise mechanism behind this “statistical smoothing” remains poorly understood from the theoretical perspective at present, this empirical observation might nevertheless point to alternative representations of statistical solutions, which might take advantage of such statistical smoothness properties.

In the remaining two chapters 6 and 7 of the present thesis, we will propose two approaches to overcoming the limitations identified above, based on the recent works [LMW21, LMK21, KLM21]: In chapter 6, we consider approximate statistical solutions obtained by blending available measurement data with numerical approximations of an underlying mathematical model, following a Bayesian point of view. In particular, we will be interested in the stability and compactness properties of approximate solutions computed from a numerical discretization for *ill-posed* problems, for which the convergence to a unique limit cannot be guaranteed, in the limit of infinite resolution $\Delta \rightarrow 0$. Then, in chapter 7, we analyse the approximation of operators by neural networks-based surrogate models, and propose an alternative representation of approximate statistical solutions relying on these methods. In contrast to the (expensive) evaluation of the forward operator by traditional numerical methods, such surrogate models are orders of magnitude faster to evaluate. While surrogate models are not necessarily expected to achieve the (machine) accuracy of traditional methods, they are ideally suited for tasks in which the *fast* evaluation of the underlying operator is of central importance, and a reasonable accuracy (*e.g.* less than 1% relative error) is sufficient. This makes neural network-based surrogate models ideal candidates to complement more traditional numerical methods in many-query problems, such as (Bayesian) uncertainty quantification.

Chapter 6

Bayesian inversion for fluid flows

6.1 Introduction

Many problems in engineering and the natural sciences seek to identify the underlying (unseen) state of a physical system. Such a reconstruction is usually based on two ingredients: The first ingredient is the information encoded in our knowledge of the underlying physical laws, resulting in a mathematical model of the system. The second ingredient consists of observational data gathered from physical measurements. The problem of determining the state of the underlying system by combining measurements with a mathematical model of the system is referred to as an *inverse problem*. The present chapter connects the statistical solutions introduced in chapter 3, with a *Bayesian* approach to inverse problems in Banach spaces, thus providing a first step towards overcoming one of the limitations of the statistical solutions approach pointed out in the last chapter: We will show how available measurement data can be combined with statistical solutions in a principled manner and will study the convergence of *numerical approximations* in the presence of data, with applications to the incompressible Euler and Navier-Stokes equations. The present chapter is based on the recent work [LMW21].

6.1.1 Inverse problems

Inverse problems arise in a variety of areas of technological, engineering and scientific interest: examples include fields such as the atmospheric sciences, geophysics, oceanography, hydrology, materials science, chemistry and biochemistry, image processing and signal processing [Stu10]. Inverse problems generally seek to determine the underlying unknown state of a system, or certain parameters characterizing that system, by combining a mathematical model with available measurement data. The measurements may be noisy and often provide only partial information on the underlying state. In the presence of such partial observations, the deterministic problem of finding the state from measurements is generally ill-posed. While a common approach for solving the resulting ill-posed deterministic inverse problem proceeds by regularization, a statistical approach based on Bayesian inference has gained increased attention in recent years [Tar05, KS06, Stu10]. Following the Bayesian approach, prior (domain) knowledge of the system state, in the absence of measurements, is encoded by a prior probability measure. The additional information provided by the measurements is used to improve this prior estimate by Bayes' rule; the solution of the Bayesian inverse problem, the *posterior measure*, is the conditional prior probability of the underlying state given the measurements. The Bayesian inverse problem thus can be seen as a mapping from measurements to the posterior measure, the latter providing the sought-after (probabilistic) estimate of the underlying system state. In contrast to the generic situation for deterministic inverse problems, it

has been shown that the corresponding Bayesian inverse problem is often *well-posed* in suitable metrics [Stu10, Lat20, Spr20]. Furthermore, Bayesian inverse problems provide a different point of view on the deterministic formulation of regularized ill-posed inverse problems: As shown in [Stu10], the latter can often be viewed as the maximum a posteriori (MAP) estimator of a Bayesian inverse problem with a suitable choice of prior.

The mapping from system state u to the corresponding measurement y is usually referred to as the forward problem. Previous discussions of the well-posedness of Bayesian inverse problems have focused on mathematical models defining a well-posed (Lipschitz continuous) forward problem, establishing stability results for the posterior with respect to measurements with respect to the Hellinger distance under suitable assumptions [Stu10]. More recently, the assumptions on the forward mapping have been considerably relaxed [Lat20, Spr20]. In [Lat20, Spr20], the well-posedness of abstract Bayesian inverse problems has been investigated in a variety of metrics (total variation, Wasserstein, Kullback-Leibler). As observed in [Lat20], under suitable assumptions on the measurement noise, the Bayesian inverse problem is well-posed (continuity with respect to measurements) even if the forward mapping is merely a measurable map. The general continuity properties of the posteriors with respect to perturbations in the prior and the log-likelihood have been considered in [Spr20]. A main conclusion that can be drawn from [Lat20, Spr20] is a remarkable stability of the measurement-to-posterior mapping with only minimal regularity assumptions on the forward problem.

6.1.2 Ill-posed forward problems

For many problems of physical interest, in particular in the context of fluid dynamics, we are confronted with forward problems which are not known to be well-posed in a mathematical sense (existence, uniqueness, continuous dependence on initial data). Indeed, there are many fundamental open questions surrounding the mathematical theory of well-posedness for partial differential equations (PDEs) of physical interest, such as the incompressible or compressible Euler equations. From the numerical practitioner's point of view, it is well-known that solutions to such PDEs may depend very sensitively on small perturbations in the initial data and that, even upon mesh refinement, numerical approximations may either not converge at all or converge only very slowly [FKMT17, FLMW20, LM20, LMPP21b]. Hence, we pose that many of the equations of fluid dynamics may safely be considered as *ill-posed*, in any practical sense of the word. In general, we are thus faced with the following situation: For a given discretization with “grid spacing” $\Delta > 0$, we have a well-defined discretized forward model possessing a unique solution operator \mathcal{S}_t^Δ mapping initial data \bar{u} to the solution $u(t) = \mathcal{S}_t^\Delta(\bar{u})$ at time $t \geq 0$. Furthermore, this solution operator \mathcal{S}_t^Δ defines a continuous mapping $\bar{u} \mapsto \mathcal{S}_t^\Delta(\bar{u})$, albeit with a modulus of continuity that depends on Δ , and may deteriorate as $\Delta \rightarrow 0$. It is not known whether there exists a well-defined limiting solution operator \mathcal{S}_t , such that $\mathcal{S}_t(\bar{u}) = \lim_{\Delta \rightarrow 0} \mathcal{S}_t^\Delta(\bar{u})$ for all initial data \bar{u} . For many models, the only available a priori estimates provide control on the physical energy, or entropy, of the solution, in the form of an a priori estimate of the form $\|\mathcal{S}_t^\Delta(\bar{u})\| \leq C\|\bar{u}\|$ for a suitable norm $\|\cdot\|$ and some constant $C > 0$. This is the general setting we shall consider in the present chapter.

6.1.3 Contributions and outline

We can summarize the main contributions of the work presented in this chapter as follows:

- We investigate the well-posedness of Bayesian inversion for problems for which the forward mapping may be ill-posed; in particular our discussion applies to equations obtained in singular limits (*e.g.* zero-viscosity limit).

- As a main contribution of this work, we show that under very general conditions, the existence of a suitable notion of limiting posterior, of *e.g.* numerical approximations of the Bayesian inverse problem, can be proven *a priori*.
- While uniqueness of such a limiting posterior is not guaranteed in general, this existence result opens up the possibility of finding/defining suitable selection criteria, which may identify the physically correct posterior solution of the Bayesian inverse problem among a set of candidate solutions.
- In addition, we discuss the implications of these compactness and stability results for the data assimilation/filtering problem associated with measurements of time-dependent (infinite dimensional) dynamical systems.
- Applications to the incompressible Navier-Stokes and Euler equations are presented.

The rest of the chapter is organized as follows, we start with some notation and preliminaries in Section 7.2. The Bayesian inverse problem, with an ill-posed forward map is considered in Section 6.2 and the corresponding data assimilation (filtering) problem is presented in Section 6.3. We apply the abstract results of sections 6.2 and 6.3 to the fundamental equations of fluid dynamics in Section 6.4. Some relevant background on measure theory, including basic results on the Wasserstein distance, are briefly summarized in Appendix B.

6.2 Bayesian inverse problem

6.2.1 Problem setting

The goal of the present section is to investigate the general stability, compactness and consistency of the Bayesian inverse problem (BIP) for PDEs for which the forward problem is potentially ill-posed. The setting is as follows: We are given a sequence of observables $\mathcal{L}^\Delta(u)$, as $\Delta \rightarrow 0$. We assume that for each $\Delta > 0$, the mapping

$$\mathcal{L}^\Delta : X \rightarrow \mathbb{R}^d, \quad u \mapsto \mathcal{L}^\Delta(u), \quad (6.2.1)$$

is well-defined and measurable. We think of $\mathcal{L}^\Delta(u)$ as either a discretized observable arising from a numerical discretization of an underlying PDE model, or from a regularization – *e.g.* by adding a small amount of viscosity – of such a PDE model. We consider the Bayesian inverse problem of finding the probability distribution $\text{Prob}[u|y]$ for the underlying data u , given a finite-dimensional measurement $y \in \mathbb{R}^d$ of the form

$$y = \mathcal{L}^\Delta(u) + \eta, \quad \eta \sim \rho(y) dy. \quad (6.2.2)$$

The noise $\eta \in \mathbb{R}^d$ is here assumed to have a distribution $\rho(y)$ which is absolutely continuous with respect to Lebesgue measure dy on \mathbb{R}^d , $\int_{\mathbb{R}^d} \rho(y) dy = 1$, and $\rho(y) > 0$ for all $y \in \mathbb{R}^d$. As shown in [Lat20, Thm. 2.5], under these conditions on $\rho(y)$, the measurability of $\mathcal{L}^\Delta(u)$ is sufficient to guarantee the existence of a solution to the BIP to (6.2.2) given an arbitrary prior $\mu \in \mathcal{P}(X)$. This solution is given by the posterior

$$d\mu^{\Delta,y}(u) = \frac{1}{Z^\Delta(y)} \exp(-\Phi^{\Delta,y}(u)) d\mu(u), \quad (6.2.3)$$

where

$$\Phi^{\Delta,y}(u) := -\log \rho(y - \mathcal{L}^\Delta(u)) \quad (6.2.4)$$

denotes the log-likelihood function, and

$$Z^\Delta(y) = \int_X \exp(-\Phi^{\Delta,y}(u)) d\mu(u), \quad (6.2.5)$$

is the required normalization constant. We note that the condition that $\rho(y) > 0$ implies that the log-likelihood $\Phi^{\Delta,y}$ is finite, i.e., $\Phi^{\Delta,y}(u) < \infty$ for all $u \in X$.

As is customary, we will denote the Radon-Nikodym derivative of $\mu^{\Delta,y}$ with respect to μ by $d\mu^{\Delta,y}/d\mu$, i.e.

$$\frac{d\mu^{\Delta,y}}{d\mu}(u) = \frac{1}{Z^\Delta(u)} \exp(-\Phi^{\Delta,y}(u)). \quad (6.2.6)$$

The solution of the BIP (6.2.3) can be characterized as the unique minimizer $\mu^{\Delta,y} = \operatorname{argmin}_{\nu \in \mathcal{P}(X)} J^{\Delta,y}(\nu)$ of the following functional $J^{\Delta,y} : \mathcal{P}(X) \rightarrow \mathbb{R}$ (cp. e.g. [DE11, Prop. 1.4.2]):

$$J^{\Delta,y}(\nu) := \mathcal{D}_{\text{KL}}(\nu || \mu) + \int_X \Phi^{\Delta,y}(u) d\nu(u), \quad (6.2.7)$$

where $\mathcal{D}_{\text{KL}}(\nu || \mu)$ denotes the Kullback-Leibler divergence (B.0.6). Furthermore, the minimum of $J^{\Delta,y}$ is explicitly given by [DE11, eq. (1.15)],

$$-\log \left(\int_X e^{-\Phi^{\Delta,y}(u)} d\mu(u) \right) = \inf_{\nu \in \mathcal{P}(X)} J^{\Delta,y}(\nu). \quad (6.2.8)$$

Taking into account (6.2.5), we can write the last equation equivalently as follows:

$$Z^\Delta(y) = \exp \left(- \inf_{\nu \in \mathcal{P}(X)} J^{\Delta,y}(\nu) \right). \quad (6.2.9)$$

While the existence of a solution to the BIP is ensured by the non-negativity of the noise distribution $\rho(y)$, the stability and compactness results of the present work will be based on following additional assumptions on the noise:

Assumption 6.2.1. Fix a symmetric, positive definite matrix $\Gamma \in \mathbb{R}^{d \times d}$, and denote by $|\cdot|_\Gamma$ the corresponding norm on \mathbb{R}^d given by

$$|y|_\Gamma = \sqrt{\langle y, y \rangle_\Gamma}, \quad \langle y, y' \rangle_\Gamma = \langle \Gamma^{-1/2} y, \Gamma^{-1/2} y' \rangle = \langle y, \Gamma^{-1} y' \rangle, \quad (6.2.10)$$

with $\langle \cdot, \cdot \rangle$ the standard Euclidean inner product on \mathbb{R}^d . We assume that the noise $\eta \sim \rho(y) dy$ in (6.2.2) possesses a distribution that is absolutely continuous with respect to Lebesgue measure dy on \mathbb{R}^d with probability density $\rho(y)$, satisfying the following conditions:

- [regularity] $y \mapsto \rho(y)$ is Lipschitz continuous with respect to $|\cdot|_\Gamma$,¹
- [boundedness] $y \mapsto \rho(y)$ is bounded from above,
- [tail-condition] there exists a constant $C > 0$, such that

$$\rho(y) \geq \frac{\exp(-\frac{1}{2}|y|_\Gamma^2)}{C}, \quad \forall y \in \mathbb{R}^d. \quad (6.2.11)$$

¹Although all norms on the finite-dimensional space \mathbb{R}^d are equivalent, measurement noise such as Gaussian noise is naturally associated with the norm $|\cdot|_\Gamma$ induced by the covariance matrix Γ .

Remark 6.2.2. Note that if, instead of (6.2.11), $\rho(y)$ satisfies a tail-condition of the form $\rho(y) \geq \exp(-C|y|_\Gamma^2)/C$, then upon simply rescaling $\tilde{\Gamma} := \sqrt{2/C}\Gamma$, we have $\rho(y) \geq \exp(-\frac{1}{2}|y|_\Gamma^2)/C$. Hence $\rho(y)$ satisfies assumption 6.2.1 with a rescaled matrix $\Gamma \rightarrow \tilde{\Gamma}$ in this case. Therefore, the precise constant $\frac{1}{2}$ in the tail-condition (6.2.11) can be assumed without loss of generality. The factor of $1/2$ turns out to be particularly convenient.

Assumption (6.2.1) is clearly fulfilled for normally distributed measurement noise η . This is the main application we have in mind. However, it is worth pointing out that the assumption is satisfied for a much wider class of measurement noise: In particular, since the tail-condition requires only a lower bound, our results apply to situations in which one encounters noise *with a heavy tail*.

Remark 6.2.3 (Gaussian noise). If the noise $\eta \sim \mathcal{N}(0, \Gamma)$ is normally distributed (Gaussian), then (up to an unimportant additive constant)

$$\Phi^{\Delta, y}(u) = \frac{1}{2}|y - \mathcal{L}^\Delta(u)|_\Gamma^2,$$

where the natural Γ -norm is given by (6.2.10). In this case, we have

$$\frac{d\mu^{\Delta, y}}{d\mu}(u) = \frac{1}{Z^\Delta(y)} \exp\left(-\frac{1}{2}|y - \mathcal{L}^\Delta(u)|_\Gamma^2\right). \quad (6.2.12)$$

Let us note the following immediate observations from assumption 6.2.1:

Lemma 6.2.4. If the noise $\eta \sim \rho(y)dy$ satisfies assumption 6.2.1, then there exists a constant $L > 0$, such that for all $y, y' \in \mathbb{R}^d$, and $\Delta, \Delta' > 0$

$$\left|e^{-\Phi^{\Delta, y}(u)} - e^{-\Phi^{\Delta, y'}(u)}\right| \leq L|y - y'|_\Gamma, \quad (6.2.13)$$

and

$$\left|e^{-\Phi^{\Delta, y}(u)} - e^{-\Phi^{\Delta', y}(u)}\right| \leq L|\mathcal{L}^\Delta(u) - \mathcal{L}^{\Delta'}(u)|_\Gamma. \quad (6.2.14)$$

The log-likelihood $\Phi^{\Delta, y}$ is bounded from below, uniformly in $\Delta > 0$ and $y \in \mathbb{R}^d$: there exists a constant $C \geq 0$ depending only on $\sup_{y \in \mathbb{R}^d} \rho(y) < \infty$, such that

$$\text{ess inf}_{u \in X} \Phi^{\Delta, y}(u) \geq -C, \quad \forall \Delta > 0, y \in \mathbb{R}^d. \quad (6.2.15)$$

There exists a constant $C' \geq 0$, such that

$$\Phi^{\Delta, y}(u) \leq C' + \frac{1}{2}|y - \mathcal{L}^\Delta(u)|_\Gamma^2. \quad (6.2.16)$$

In particular, we have

$$\Phi^{\Delta, y}(u) \leq C' + |y|_\Gamma^2 + |\mathcal{L}^\Delta(u)|_\Gamma^2. \quad (6.2.17)$$

Given a sequence of observables $\mathcal{L}^\Delta(u)$ ($\Delta \rightarrow 0$) arising for example from numerical discretizations at grid scale Δ , it is now natural to ask what can be said about the limiting behaviour of the corresponding sequence of posteriors $\mu^{\Delta, y}$. For many problems arising in the context of fluid dynamics very limited information is available on the stability and convergence of the observables $\mathcal{L}^\Delta(u) \rightarrow \mathcal{L}(u)$ to a well-defined limit. Indeed, even the existence of a limiting observable $\mathcal{L}(u)$ is often not guaranteed, due to

the (potential) ill-posedness of the forward model. It is thus important to study the behaviour of the sequence $\mu^{\Delta,y}$ under minimal assumptions on the observables $\mathcal{L}^\Delta(u)$. We pose that these assumption should either be *rigorously provable* for models of practical interest, or at least numerically *verifiable and routinely observed* in numerical experiments. In the remainder of this section, we will follow this programme for abstract Bayesian inverse problems. We will in particular consider

- the **stability** of the posteriors $\mu^{\Delta,y}$ with respect to the measurements y with respect to the Wasserstein distance, obtaining estimates which hold uniformly as $\Delta \rightarrow 0$,
- the general **compactness** properties of the sequence $\mu^{\Delta,y}$ in the Wasserstein distance, and
- the **consistency** of $\mu^{\Delta,y}$ with the posterior μ^y corresponding to the limiting measurement $\mathcal{L}^\Delta(u) \rightarrow \mathcal{L}(u)$, provided that the latter exists.

In particular, as a consequence of our discussion, we will prove the existence of a set of candidate solutions of the BIP in the limit $\Delta \rightarrow 0$, under mild boundedness assumptions on the observables $\mathcal{L}^\Delta(u)$. While of some independent interest, the present section on the abstract Bayesian inverse problem can also be viewed as preparing the stage our subsequent discussion of the data assimilation or filtering problem in section 6.3. In particular, we will prove several crucial lemmas below, on which we will build in section 6.3. In the applications presented in section 6.4, we will show that the assumed bounds in the abstract results of the present section can be established by a priori estimates for models of practical importance.

6.2.2 Stability with respect to measurements

We first discuss the stability of the posterior $\mu^{\Delta,y}$ with respect to the measurement y . As a natural measure of the distance between two posteriors $\mu^{\Delta,y}$, $\mu^{\Delta,y'}$, we consider the 1-Wasserstein distance $W_1(\mu^{\Delta,y}, \mu^{\Delta,y'})$. Our goal is to prove an explicit upper bound on $W_1(\mu^{\Delta,y}, \mu^{\Delta,y'})$ in terms of $|y - y'|_\Gamma$. We note that our discussion of stability for the BIP overlaps in part with a similar discussion contained in [Lat20, Spr20]. In particular, [Spr20] contains a general discussion of the stability of posteriors with respect to both the log-likelihood and priors, and with respect to a number of distance metrics between probability measures. Since some needed estimates have not appeared in [Lat20, Spr20], at least in the precise form needed for our purposes, we have decided to include detailed proofs in this manuscript.

We begin our discussion of the stability properties of the BIP with the following lemma, proving that the sequence of densities $d\mu^{\Delta,y}/d\mu$ is uniformly bounded in $L^\infty(\mu)$, provided that $\sup_{\Delta>0} \|\mathcal{L}^\Delta(u)\|_{L^2(\mu)} < \infty$; here we define the $L^2(\mu)$ -norm of the observables $\mathcal{L}^\Delta(u)$ as follows

Remark 6.2.5. *The $L^2(\mu)$ -norm of $\mathcal{L}^\Delta(u)$ is defined by*

$$\|\mathcal{L}^\Delta(u)\|_{L^2(\mu)} := \left(\int_X |\mathcal{L}^\Delta(u)|_\Gamma^2 d\mu(u), \right)^{1/2}$$

where Γ is the covariance matrix of the additive noise η .

We now state the following

Lemma 6.2.6. *Let $d\mu^{\Delta,y}/d\mu$ be given by (6.2.6), and $Z^\Delta(y)$ be defined as in (6.2.5). Then*

$$Z^\Delta(y) \geq \exp \left(- \int_X \Phi^{\Delta,y}(u) d\mu(u) \right), \quad (6.2.18)$$

and

$$\frac{d\mu^{\Delta,y}}{d\mu}(u) \leq \exp \left(\int_X \Phi^{\Delta,y}(u) d\mu(u) - \operatorname{ess\,inf}_{u \in X} \Phi^{\Delta,y}(u) \right), \quad \forall u \in X, \quad (6.2.19)$$

In particular, if the noise $\eta \sim \rho(y)dy$ satisfies the standing assumption 6.2.1, then there exists a constant $C > 0$ depending only on the noise distribution $\rho(y)$, such that

$$Z^\Delta(y) \geq \frac{1}{C} \exp\left(-|y|_\Gamma^2 - \|\mathcal{L}^\Delta\|_{L^2(\mu)}^2\right), \quad (6.2.20)$$

and

$$\frac{d\mu^{\Delta,y}}{d\mu}(u) \leq C \exp\left(|y|_\Gamma^2 + \|\mathcal{L}^\Delta\|_{L^2(\mu)}^2\right), \quad \forall u \in X. \quad (6.2.21)$$

Proof. Since the exponential (Gaussian-like) factor in the definition of $d\mu^{\Delta,y}/d\mu$, eq. (6.2.6), is bounded from above by $\exp(-\text{ess inf}_{u \in X} \Phi^{\Delta,y}(u))$, it suffices to prove the lower bound on $Z^\Delta(y)$. We recall that by (6.2.9), we can write

$$Z^\Delta(y) = \exp\left(-\inf_{\nu \in \mathcal{P}(X)} J^{\Delta,y}(\nu)\right),$$

where $J^{\Delta,y}(\nu) = \mathcal{D}_{\text{KL}}(\nu||\mu) + \int_X \Phi^{\Delta,y}(u) d\nu(u)$. In particular, it follows that

$$\inf_{\nu \in \mathcal{P}(X)} J^{\Delta,y}(\nu) \leq J^{\Delta,y}(\mu) = \int_X \Phi^{\Delta,y}(u) d\mu(u).$$

Thus, we conclude that

$$Z^\Delta(y) \geq \exp\left(-\int_X \Phi^{\Delta,y}(u) d\mu(u)\right).$$

This implies the first two estimates (6.2.18) and (6.2.19) of this lemma.

Under the noise assumption 6.2.1, by (6.2.17), there exists $C' > 0$ depending only on the noise distribution $\rho(y)$, such the last term can be bounded from below, yielding

$$Z^\Delta(y) \geq \exp\left(-C' - |y|_\Gamma^2 - \int_X |\mathcal{L}^\Delta(u)|_\Gamma^2 d\mu(u)\right),$$

and thus the claimed inequality (6.2.20) for $Z^\Delta(y)$ with $C = \exp(C')$. Furthermore, by (6.2.15), there exists C'' , such that

$$\text{ess inf}_{u \in X} \Phi^{\Delta,y}(u) \geq -C''.$$

Thus the claimed inequality (6.2.21) holds with $C = \exp(C' + C'')$. \square

We next discuss the stability of $d\mu^{\Delta,y}/d\mu$ with respect to y . The following Lemma shows that the map $y \mapsto d\mu^{\Delta,y}/d\mu$ is locally Lipschitz continuous with respect to the L^∞ -norm.

Lemma 6.2.7. *Under assumption 6.2.1. Let $\mathcal{L}^\Delta(u) \in L^2(\mu)$. There exists a constant $C > 0$ (depending only on the noise distribution), such that*

$$\left\| \frac{d\mu^{\Delta,y}}{d\mu} - \frac{d\mu^{\Delta,y'}}{d\mu} \right\|_{L^\infty(\mu)} \leq C|y - y'|_\Gamma \exp\left(|y|_\Gamma^2 + |y'|_\Gamma^2 + 2\|\mathcal{L}^\Delta\|_{L^2(\mu)}^2\right). \quad (6.2.22)$$

Proof. Fix $u \in X$ for the moment. Denote $e(y) := e(y; u) = \exp(-\Phi^{\Delta,y}(u))$, so that

$$\begin{aligned} \frac{d\mu^{\Delta,y}}{d\mu} - \frac{d\mu^{\Delta,y'}}{d\mu} &= \frac{e(y)}{Z^\Delta(y)} - \frac{e(y')}{Z^\Delta(y')} \\ &= \frac{e(y) - e(y')}{Z^\Delta(y)} + \frac{e(y')}{Z^\Delta(y')} \frac{(Z^\Delta(y') - Z^\Delta(y))}{Z^\Delta(y)}. \end{aligned}$$

By (6.2.13), we can estimate $|e(y) - e(y')| \leq C|y - y'|_\Gamma$. Next, we note that this bound for $e(y)$ also implies that

$$|Z^\Delta(y) - Z^\Delta(y')| \leq \int_X |e(y; u) - e(y'; u)| d\mu(u) \leq C|y - y'|_\Gamma \underbrace{\int_X 1 d\mu(u)}_{=1}.$$

Hence,

$$\left| \frac{d\mu^y}{d\mu} - \frac{d\mu^{y'}}{d\mu} \right| \leq \frac{C|y - y'|_\Gamma}{Z^\Delta(y)} + \frac{e(y')}{Z^\Delta(y')} \frac{C|y - y'|_\Gamma}{Z^\Delta(y)}.$$

Finally, from Lemma 6.2.6, we can estimate

$$\frac{1}{Z^\Delta(y)} \leq Ce^{|y|_\Gamma^2 + \|\mathcal{L}^\Delta\|_{L^2(\mu)}^2} \leq Ce^{|y|_\Gamma^2 + |y'|_\Gamma^2 + 2\|\mathcal{L}^\Delta\|_{L^2(\mu)}^2},$$

and

$$\frac{e(y')}{Z^\Delta(y')} \frac{1}{Z^\Delta(y)} \leq Ce^{|y|_\Gamma^2 + |y'|_\Gamma^2 + 2\|\mathcal{L}^\Delta\|_{L^2(\mu)}^2}.$$

Combining these estimates, we conclude that

$$\left| \frac{d\mu^y}{d\mu} - \frac{d\mu^{y'}}{d\mu} \right| \leq 2C|y - y'|_\Gamma \exp\left(|y|_\Gamma^2 + |y'|_\Gamma^2 + 2\|\mathcal{L}^\Delta\|_{L^2(\mu)}^2\right).$$

Since $u \in X$ was arbitrary, the claimed inequality follows by taking the supremum over $u \in X$ on the left. \square

Let us also remark in passing the following Lemma, whose proof is analogous to the proof of Lemma 6.2.7.

Lemma 6.2.8. *Under assumption 6.2.1. Let $\mathcal{L}^\Delta(u), \mathcal{L}(u) \in L^2(\mu)$, and $y \in \mathbb{R}^d$. There exists a constant $C > 0$ (depending only on the noise distribution), such that for any $p \in [1, \infty]$, we have*

$$\left\| \frac{d\mu^{\Delta,y}}{d\mu} - \frac{d\mu^y}{d\mu} \right\|_{L^p(\mu)} \leq C \|\mathcal{L}^\Delta(u) - \mathcal{L}(u)\|_{L^p(\mu)} \exp\left(2|y|_\Gamma^2 + \|\mathcal{L}^\Delta\|_{L^2(\mu)}^2 + \|\mathcal{L}\|_{L^2(\mu)}^2\right),$$

for all u for which $\mathcal{L}^\Delta(u), \mathcal{L}(u)$ is defined.

Proof. The proof is an almost verbatim repetition of the proof of Lemma 6.2.7, with the roles of y, y' and $\mathcal{L}^\Delta(u), \mathcal{L}(u)$ interchanged. \square

Using Lemma 6.2.7, we can now state the following theorem on the stability of the measurement-to-posteriors map:

Theorem 6.2.9. *We make the assumption 6.2.1 on the noise $\eta \sim \rho(y) dy$. Fix a prior $\mu \in \mathcal{P}_1(X)$. Given a measurement $y \in \mathbb{R}^d$, $\Delta > 0$ with observable $\mathcal{L}^\Delta(u)$ and prior μ , let $\mu^{\Delta,y}$ denote the corresponding posterior (6.2.3). Assume that*

$$M := \sup_{\Delta > 0} \|\mathcal{L}^\Delta\|_{L^2(\mu)} < \infty.$$

Then the family of posteriors $\{\mu^{\Delta,y}\}$ is uniformly bounded in $\text{Lip}_{\text{loc}}(\mathbb{R}^d; \mathcal{P}_1(X))$ and hence locally equicontinuous: There exists a constant $C = C(\rho, \Gamma, M, \mu)$, independent of $\Delta > 0$ and y, y' , such that

$$W_1(\mu^{\Delta,y}, \mu^{\Delta,y'}) \leq C|y - y'|_\Gamma e^{|y|_\Gamma^2 + |y'|_\Gamma^2}. \quad (6.2.23)$$

Proof. Fix $\Phi \in \text{Lip}(X)$ with semi-norm $\|\Phi\|_{\text{Lip}} \leq 1$. Then

$$\begin{aligned} \int_X \Phi(u)(d\mu^{\Delta,y}(u) - d\mu^{\Delta,y'}(u)) &= \int_X [\Phi(u) - \Phi(0)](d\mu^{\Delta,y}(u) - d\mu^{\Delta,y'}(u)) \\ &\leq \int_X \|u\|_X \left| \frac{d\mu^{\Delta,y}}{d\mu} - \frac{d\mu^{\Delta,y'}}{d\mu} \right| d\mu(u) \\ &\leq \left\| \frac{d\mu^{\Delta,y}}{d\mu} - \frac{d\mu^{\Delta,y'}}{d\mu} \right\|_{L^\infty(\mu)} \left(\int_X \|u\|_X d\mu(u) \right). \end{aligned}$$

Estimating the last term using Lemma 6.2.7 and taking the supremum over all such Lipschitz continuous Φ on the left-hand side, we obtain by Kantorovich duality:

$$W_1(\mu^{\Delta,y}, \mu^{\Delta,y'}) \leq \bar{C} \|u\|_{L^1(\mu)} |y - y'|_\Gamma e^{|y|^2_\Gamma + |y'|^2_\Gamma},$$

where \bar{C} is independent of Δ . In fact, we can choose

$$\bar{C} = \sup_{\Delta > 0} C e^{2\|\mathcal{L}^\Delta(u)\|_{L^2(\mu)}^2} = C e^{2M^2},$$

with C the constant from Lemma 6.2.7. \square

Remark 6.2.10. *The previous stability result only depends on the continuity properties of the noise distribution ρ , and is independent of any continuity properties of the observable $\mathcal{L}(u)$. In the same spirit, if $d\mu^y/d\mu = 1/Z(y) \exp(-\frac{1}{2}|y - \mathcal{L}(u)|^2_\Gamma)$ is a posterior with Gaussian noise, and if $\|\mathcal{L}(u)\|_{L^2(\mu)} < \infty$, then we can show that for any $\phi(u) \in L^1(\mu)$ (i.e. $\phi(u)$ is integrable with respect to the prior μ), we have that*

$$\mathbb{R}^d \rightarrow \mathbb{R}, \quad y \mapsto \mathbb{E}^y[\phi] := \frac{1}{Z(y)} \int_X \phi(u) d\mu^y(u),$$

is real analytic; this follows from [HSZ20, Lemma 4.5]. In particular, this result is independent of any smoothness properties of $\mathcal{L}(u)$. In section 6.3, we will show that the conclusion remains true even for the time-dependent data assimilation (filtering) problem (cp. Remark 6.3.10).

6.2.3 Compactness properties

Having established the uniform equicontinuity of the measurement-to-posterior mapping, we next wish to show that the posteriors $\mu^{\Delta,y}$, for fixed $y \in \mathbb{R}^d$, form a compact sequence as $\Delta \rightarrow 0$ in (\mathcal{P}_1, W_1) , and that all limit points are absolutely continuous with respect to the prior μ . The proof of compactness of $\mu^{\Delta,y}$ will be based on the variational characterization of the posteriors to the BIP, in terms of the Kullback-Leibler divergence with respect to the prior.

We now show pointwise compactness of the posteriors $\mu^{\Delta,y}$ for fixed $y \in \mathbb{R}^d$.

Theorem 6.2.11. *Fix a prior $\mu \in \mathcal{P}_1(X)$. Fix $y \in \mathbb{R}^d$. Assume that the log-likelihood $\Phi^{\Delta,y} \geq -C$ is uniformly bounded from below, and that $\int_X \Phi^{\Delta,y}(u) d\mu(u) \leq C$ are uniformly bounded from above for $\Delta > 0$. Then the family of posteriors $\{\mu^{\Delta,y}\}_{\Delta>0}$ is pre-compact in $\mathcal{P}_1(X)$, and any limit point $\mu^{*,y} = \lim_{\Delta_k \rightarrow 0} \mu^{\Delta_k,y}$ is absolutely continuous with respect to the prior μ .*

Proof. As remarked in the introduction to this section, the posterior $\mu^{\Delta,y}$ can be characterized as the unique minimizer $\mu^{\Delta,y} = \operatorname{argmin}_{\nu \in \mathcal{P}_1(X)} J^{\Delta,y}(\nu)$ of the functional $J^{\Delta,y}$ (6.2.7). In particular, this vari-

ational characterization implies that

$$\begin{aligned}\mathcal{D}_{\text{KL}}(\mu^{\Delta,y} \parallel \mu) &= J^{\Delta,y}(\mu^{\Delta,y}) - \int_X \underbrace{\Phi^{\Delta,y}(u)}_{\geq -C} d\mu^{\Delta,y}(u) \leq J^{\Delta,y}(\mu^{\Delta,y}) + C \\ &\leq J^{\Delta,y}(\mu) + C = \int_X \Phi^{\Delta,y}(u) d\mu(u) + C \leq 2C.\end{aligned}$$

It follows that

$$\{\mu^{\Delta,y}\}_{\Delta>0} \subset \{\nu \in \mathcal{P}_1(X) \mid \mathcal{D}_{\text{KL}}(\nu \parallel \mu) \leq 2C\}.$$

From the coercivity property of the Kullback-Leibler divergence \mathcal{D}_{KL} , the sublevel set $\{\nu \in \mathcal{P}_1(X) \mid \mathcal{D}_{\text{KL}}(\nu \parallel \mu) \leq 2C\}$ is compact with respect to the topology of weak convergence of probability measures. Furthermore, any weak limit point $\mu^{*,y} = w - \lim_{\Delta_k \rightarrow 0} \mu^{\Delta_k,y}$ satisfies $\mathcal{D}_{\text{KL}}(\mu^{*,y} \parallel \mu) \leq 2C < \infty$, and hence is absolutely continuous with respect to μ . This shows that $\{\mu^{\Delta,y}\}_{\Delta>0}$ is precompact with respect to the weak topology on $\mathcal{P}(X)$. We finally want to show that if $\mu^{*,y} = w - \lim_{\Delta_k \rightarrow 0} \mu^{\Delta_k,y}$ is a weak limit of the family $\{\mu^{\Delta,y}\}_{\Delta>0}$, then in fact $W_1(\mu^{*,y}, \mu^{\Delta_k,y}) \rightarrow 0$ converges with respect to the 1-Wasserstein distance. As a consequence, we conclude that $\{\mu^{\Delta,y}\}_{\Delta>0}$ is also pre-compact in the metric space (\mathcal{P}_1, W_1) .

To this end, suppose we are given a weakly convergent subsequence $\mu^{\Delta_k,y} \rightharpoonup \mu^{*,y}$. By (B.0.5), in order to show that $W_1(\mu^{*,y}, \mu^{\Delta_k,y}) \rightarrow 0$, it suffices to prove that

$$\int_X \|u\|_X d\mu^{\Delta_k,y}(u) \rightarrow \int_X \|u\|_X d\mu^{*,y}(u).$$

Let $\epsilon > 0$ be arbitrary. We want to show that

$$\limsup_{k \rightarrow \infty} \left| \int_X \|u\|_X d\mu^{\Delta_k,y}(u) - \int_X \|u\|_X d\mu^{*,y}(u) \right| \leq \epsilon.$$

By Lemma 6.2.6, and the assumed uniform upper bound on $\int \Phi^{\Delta,y}(u) d\mu(u)$, there exists a constant $C > 0$, such that

$$\frac{d\mu^{\Delta,y}}{d\mu} \leq C, \quad \forall \Delta > 0.$$

As $\int_X \|u\|_X d\mu(u) < \infty$, we can choose $M > 0$ sufficiently large, so that

$$\int_{\|u\|_X \geq M} \|u\|_X d\mu(u) < \epsilon/(2C).$$

Then, clearly

$$\int_{\|u\|_X \geq M} \|u\|_X d\mu^{\Delta_k,y}(u) = \int_{\|u\|_X \geq M} \|u\|_X \frac{d\mu^{\Delta_k,y}}{d\mu} d\mu(u) \leq C \int_{\|u\|_X \geq M} \|u\|_X d\mu(u) < \epsilon/2, \quad (6.2.24)$$

for all $k \in \mathbb{N}$, and by the lower semi-continuity of weak limits, a similar inequality holds for $\mu^{*,y}$:

$$\int_{\|u\|_X \geq M} \|u\|_X d\mu^{*,y}(u) \leq \liminf_{k \rightarrow \infty} \int_{\|u\|_X \geq M} \|u\|_X d\mu^{\Delta_k,y}(u) \leq \epsilon/2. \quad (6.2.25)$$

Define $F_M(u) := \min(\|u\|_X, M) \in C_b(X)$. Then,

$$\begin{aligned} & \limsup_{k \rightarrow \infty} \left| \int_X \|u\|_X d\mu^{\Delta_k, y} - \int_X \|u\|_X d\mu^{*, y} \right| \\ & \leq \limsup_{k \rightarrow \infty} \left| \int_X F_M(u) [d\mu^{\Delta_k, y} - d\mu^{*, y}] \right| \\ & + \limsup_{k \rightarrow \infty} \int_{\|u\|_X \geq M} \|u\|_X d\mu^{\Delta_k, y}(u) + \int_{\|u\|_X \geq M} \|u\|_X d\mu^{*, y}(u) \\ & \leq 0 + \epsilon/2 + \epsilon/2 = \epsilon. \end{aligned}$$

To pass to the last line, we used the upper bounds (6.2.24), (6.2.25) and the fact that

$$\int_X F_M(u) d\mu^{\Delta_k, y}(u) \rightarrow \int_X F_M(u) d\mu^{*, y}(u),$$

since $F_M \in C_b(X)$ and $\mu^{\Delta_k, y} \rightharpoonup \mu^{*, y}$. Since $\epsilon > 0$ was arbitrary, we conclude that

$$\int_X \|u\|_X d\mu^{\Delta_k, y}(u) \rightarrow \int_X \|u\|_X d\mu^{*, y}(u),$$

and hence $W_1(\mu^{\Delta_k, y}, \mu^{*, y}) \rightarrow 0$ (cp. (B.0.5)). In particular, this shows that any weak limit point of $\{\mu^{\Delta, y}\}_{\Delta > 0}$ is also a limit point in $\mathcal{P}_1(X)$ with respect to the 1-Wasserstein metric W_1 . Since $\{\mu^{\Delta, y}\}_{\Delta > 0}$ is weakly pre-compact, it follows that it is also pre-compact in $\mathcal{P}_1(X)$ with respect to the W_1 -metric. \square

Finally, we can combine the uniform equicontinuity result of Theorem 6.2.9 with the point-wise compactness established in Theorem 6.2.11 to prove the following general compactness theorem for posteriors, now considered as mappings $y \mapsto \mu^{\Delta, y}$:

Theorem 6.2.12. *We make assumption 6.2.1 on the noise distribution. Fix a prior $\mu \in \mathcal{P}_1(X)$. Let $\{\mathcal{L}^\Delta\}_{\Delta > 0}$ be a uniformly $L^2(\mu_0)$ -bounded family of measurable mappings $\mathcal{L}^\Delta : X \rightarrow \mathbb{R}^d$. Then the corresponding family of posterior measures $y \mapsto \mu^{\Delta, y}$ is pre-compact with respect to the topology of locally uniform convergence on $\text{Lip}_{\text{loc}}(\mathbb{R}^d; \mathcal{P}_1(X))$: For any sequence $\Delta \rightarrow 0$, there exists a subsequence $\Delta_k \rightarrow 0$ and a y -parametrized probability measure $y \mapsto \mu^{*, y} \in \text{Lip}_{\text{loc}}(\mathbb{R}^d; \mathcal{P}_1(X))$, such that for any $R > 0$, there exists $C = C(R, \Gamma, \mu)$, such that*

$$W_1(\mu^{*, y}, \mu^{*, y'}) \leq C|y - y'|_\Gamma, \quad \forall y, y' \in B_R(0),$$

and we have

$$\sup_{|y|_\Gamma \leq R} W_1(\mu^{\Delta_k, y}, \mu^{*, y}) \rightarrow 0, \quad \text{as } k \rightarrow \infty.$$

Furthermore, any such limit $\mu^{*, y}$ is absolutely continuous with respect to the prior μ , and can be written in the form $d\mu^{*, y}(u) = Z(y)^{-1} \exp(-\Phi^*(u; y)) d\mu(u)$.

Proof. This theorem is a direct consequence of the Arzelà-Ascoli Theorem A.2.1, the pointwise compactness Theorem 6.2.11 and the uniform equicontinuity Theorem 6.2.9. \square

Remark 6.2.13. *The last theorem shows that under quite general conditions, we can assign a set of “solutions” of a BIP (or at least candidate solutions) to a family of posteriors $\mu^{\Delta, y}$ solving the discretized BIP at resolution $\Delta > 0$. This set of candidate solutions of the BIP in the limit $\Delta \rightarrow 0$ is given by*

$$\mathcal{S} = \left\{ \mu^{*, y} \mid \exists \Delta_k \rightarrow 0, \text{ s.t. } \mu^{*, y} = \lim_{k \rightarrow \infty} \mu^{\Delta_k, y} \right\},$$

or equivalently, we can write

$$\mathcal{S} = \bigcap_{\overline{\Delta} > 0} \text{cl}(\{y \mapsto \mu^{\Delta,y} \mid \Delta \leq \overline{\Delta}\}),$$

where cl denotes the closure in $\text{Lip}_{\text{loc}}(\mathbb{R}^d; P_p(X))$. We note that the set \mathcal{S} is non-empty: This follows from the fact that finite intersections are clearly non-empty and that each of the sets is a compact subset of $\text{Lip}_{\text{loc}}(\mathbb{R}^d; P_p(X))$ (finite intersection property of compact sets). So under these very general assumptions, there always exists at least one candidate solution.

One possible selection criterion to find the “best” solution among the candidate solutions \mathcal{S} of Remark 6.2.13 is by minimizing the Kullback-Leibler divergence with respect to the prior μ (with the idea of this being the most conservative estimate):

$$\mu^{*,y} = \underset{\nu \in \mathcal{S}}{\operatorname{argmin}} \mathcal{D}_{\text{KL}}(\nu || \mu).$$

6.2.4 Consistency with the canonical posterior

In the previous section, we have shown that under very general assumptions on the observables $\mathcal{L}^\Delta(u)$, we can define a set of candidate solutions \mathcal{S} for the BIP in the limit $\Delta \rightarrow 0$. In this section, we show that if $\mathcal{L}^\Delta(u) \rightarrow \mathcal{L}(u)$ converges to a unique limit (even in an average sense), then $\mu^{\Delta,y} \rightarrow \mu^y$ converges to the unique solution of the BIP with measurement $\mathcal{L}(u)$ with respect to the Wasserstein distance W_1 . In particular, the set of candidate solutions \mathcal{S} identified in Remark 6.2.13 is in this case given by $\mathcal{S} = \{\mu^y\}$.

Theorem 6.2.14. *Under the noise assumption 6.2.1. Fix a prior $\mu \in \mathcal{P}_2(X)$. Let $\mu^{\Delta,y}$ and μ^y denote the posteriors for the BIP with observables \mathcal{L}^Δ and \mathcal{L} , respectively. Assume that there exists a constant $M > 0$, such that*

$$\|\mathcal{L}^\Delta(u)\|_{L^2(\mu)}, \|\mathcal{L}(u)\|_{L^2(\mu)} \leq M. \quad \forall \Delta > 0.$$

Then, we have the estimate

$$W_1(\mu^{\Delta,y}, \mu^y) \leq C \|\mathcal{L}^\Delta(u) - \mathcal{L}(u)\|_{L^2(\mu)},$$

where $C = C(\Gamma, \mu, y, M)$ depends on the prior μ , the measurement $y \in \mathbb{R}^d$ and the upper bound M , but is independent of Δ .

Proof. For any $\Phi \in \text{Lip}$, such that $\|\Phi\|_{\text{Lip}} \leq 1$, we find

$$\begin{aligned} \int_X \Phi(u) [d\mu^{\Delta,y}(u) - d\mu^y(u)] &= \int_X [\Phi(u) - \Phi(0)] [d\mu^{\Delta,y}(u) - d\mu^y(u)] \\ &= \int_X [\Phi(u) - \Phi(0)] \left[\frac{d\mu^{\Delta,y}}{d\mu} - \frac{d\mu^y}{d\mu} \right] d\mu(u) \\ &\leq \int_X \|u\|_X \left| \frac{d\mu^{\Delta,y}}{d\mu} - \frac{d\mu^y}{d\mu} \right| d\mu(u) \\ &\leq \|u\|_{L^2(\mu)} \left\| \frac{d\mu^{\Delta,y}}{d\mu} - \frac{d\mu^y}{d\mu} \right\|_{L^2(\mu)}. \end{aligned}$$

By Lemma 6.2.8, we have

$$\begin{aligned} \left\| \frac{d\mu^{\Delta,y}}{d\mu} - \frac{d\mu^y}{d\mu} \right\|_{L^2(\mu)} &\leq C \|\mathcal{L}^\Delta(u) - \mathcal{L}(u)\|_{L^2(\mu)} e^{|y|^2 + \|\mathcal{L}^\Delta(u)\|_{L^2(\mu)}^2 + \|\mathcal{L}(u)\|_{L^2(\mu)}^2} \\ &\leq C \|\mathcal{L}^\Delta(u) - \mathcal{L}(u)\|_{L^2(\mu)} e^{|y|^2 + 2M^2}, \end{aligned}$$

for a constant $C = C(\Gamma)$. Using this estimate, we can now bound

$$\int_X \Phi(u) [d\mu^{\Delta,y}(u) - d\mu^y(u)] \leq \bar{C} \|\mathcal{L}^\Delta(u) - \mathcal{L}(u)\|_{L^2(\mu)},$$

where $\bar{C} = Ce^{|y|^2+2M^2} (\int_X \|u\|_X^2 d\mu(u))^{1/2}$. Taking the supremum over all Lipschitz continuous $\Phi(u)$, with Lipschitz semi-norm $\|\Phi\|_{\text{Lip}} \leq 1$ on the left, we obtain the claimed estimate. \square

6.3 Data assimilation

6.3.1 Problem setting

In the context of time-evolution equations, one is often not only interested in obtaining an estimate for the (initial) state given individual measurements y , but to track the temporal evolution of a system, given measurements y_1, y_2, \dots acquired over time. The data assimilation problem seeks to provide a best estimate for the state u of the system at time t , expressed in terms of a posterior probability measure $\nu_t^y(u)$, given the available measurements y_1, y_2, \dots . There are at least two types of data assimilation problems: Following standard terminology, we call *filtering*, the problem of determining the posterior $\nu_t^y(u)$ at time $t \in [0, T]$ from the measurements available up to time t , *i.e.* from measurements in the time-interval $[0, t)$. The filtering problem thus provides the best prediction given a set of past measurements. On the other hand, if the posterior $\nu_t^y(u)$ at $t \in [0, T]$ is obtained “after the fact”, *i.e.* given a set of measurements acquired during the whole time-interval $[0, T]$, then we speak of the *smoothing* problem. The generic data assimilation problem is schematically illustrated in Figure 6.1.

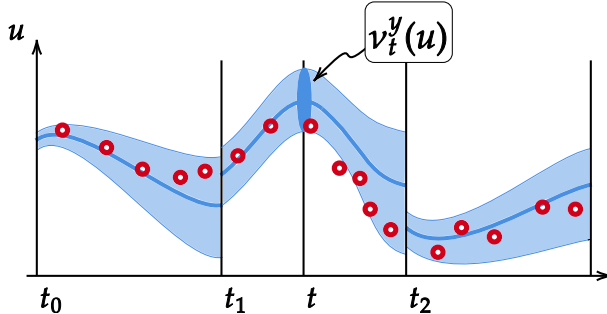


Figure 6.1: Schematic illustration of the data assimilation problem: Measurements (red circles) are used at times $t = t_0, t_1, \dots$, to periodically update the posterior measure ν_t^y (indicated by its confidence interval in blue), combining all available information from the deterministic evolution and noisy measurements.

In the following, we will focus on the filtering problem, for which we provide a precise formulation below; however, most of the results should apply mutatis mutandis also to the smoothing problem. Due to the weak temporal and spatial regularity properties of the fluid dynamics applications of interest in the present work, simple pointwise measurements of the form $\mathcal{L}(u) = u(x_k, t_k)$ are not well-defined. Thus, we will first discuss an appropriate notion of observables. We make the following definition

Definition 6.3.1 (Eulerian Observables). *A mapping $\mathcal{G} : L^1(0, T; L_x^2) \rightarrow \mathbb{R}^d$, $u(x, t) \mapsto \mathcal{G}(u) = (\mathcal{G}^1(u), \dots, \mathcal{G}^d(u))$, with $\mathcal{G}^k(u)$ of the form*

$$\mathcal{G}^k(u) = \int_0^T \int_D \phi^{(k)}(x, t) g^{(k)}(u(x, t)) dx dt, \quad (6.3.1)$$

for $u(x, t) \in L^1(0, T; L_x^2)$, is called an **Eulerian observable** (or simply observable), provided that, for all $k = 1, \dots, d$, we have $\phi^{(k)}(x, t) \in L^\infty(D \times [0, T])$ and $g^{(k)}(u)$ is Lipschitz continuous with

$$|g^{(k)}(u) - g^{(k)}(u')| \leq C|u - u'|. \quad (6.3.2)$$

To simplify notation in the following, instead of (6.3.1) we shall simply write

$$\mathcal{G}(u) = \int_0^T \int_D \phi(x, t) g(u(x, t)) dx dt, \quad (6.3.3)$$

where $\phi(x, t) := (\phi^{(1)}(x, t), \dots, \phi^{(d)}(x, t))$, $g(u) = (g^{(1)}(u), \dots, g^{(d)}(u))$, and it is understood that the multiplication in (6.3.3) is carried out componentwise.

It is then straightforward to prove the following result.

Proposition 6.3.2. *An Eulerian observable $\mathcal{G}(u)$ is Lipschitz continuous on $L_t^1([0, T]; L_x^2)$, i.e., there exists a constant $C > 0$, such that*

$$|\mathcal{G}(u) - \mathcal{G}(u')| \leq C \int_0^T \|u - u'\|_{L_x^2} dt, \quad \forall u, u' \in L^1([0, T]; L_x^2).$$

Proof. This follows immediately from the definition (6.3.3) of $\mathcal{G}(u)$ and the assumed bound (6.3.2). \square

Assumption 6.3.3 (standing assumption). *In the present section, we will make the standing assumption that the approximate solution operators $\mathcal{S}_t^\Delta : L_x^2 \rightarrow L_x^2$ (as well as a possible limit $\mathcal{S}_t : L_x^2 \rightarrow L_x^2$, if it exists) satisfy uniform bounds of the following form:*

- *Energy admissibility: For any $u \in L_x^2$, we have*

$$\|\mathcal{S}_t^\Delta(u)\|_{L_x^2} \leq C\|u\|_{L_x^2}, \quad \forall u \in L_x^2,$$

- *Weak time-regularity: There exist constants $L, C > 0$, such that*

$$\|\mathcal{S}_t^\Delta(u) - \mathcal{S}_{t'}^\Delta(u)\|_{H_x^{-L}} \leq C|t - t'|, \quad \forall u \in L_x^2, t, t' \in [0, T],$$

i.e. $t \mapsto \mathcal{S}_t^\Delta(u)$ is Lipschitz continuous with values in some negative index Sobolev space.

Given a sequence of measurement times $0 = t_0 < t_1 < t_2 < \dots < t_N = T$ for $N \in \mathbb{N}$, we denote $\delta t_j = t_j - t_{j-1}$. Given observables of the form

$$\mathcal{G}_j : L_t^1([0, \delta t_j]; L_x^2) \rightarrow \mathbb{R}, \quad \mathcal{G}_j(u) = \int_0^{\delta t_j} \int_D \phi_j(x, t) g_j(u(x, t)) dx dt \quad (6.3.4)$$

the filtering problem at grid scale $\Delta > 0$ is described as follows: The temporal evolution of the system state $u(x, t)$ is modeled by the approximate solution operator \mathcal{S}_t^Δ , i.e. $u(x, t) = \mathcal{S}_t^\Delta(\bar{u})$, where $\bar{u} = u(x, 0)$. We fix a prior $\mu_{\text{prior}} \in \mathcal{P}(L_x^2)$ at the initial time $t = t_0$, representing our best estimate of the state of the system in the absence of measurements. For a sequence of measurements y_1, \dots, y_N , we denote $Y_j = (y_1, \dots, y_j)$ the vector of partial measurements up to time t_j . We wish to find a sequence of probability measures $\nu_{t_1}^{\Delta, Y_1}, \nu_{t_2}^{\Delta, Y_2}, \dots, \nu_{t_N}^{\Delta, Y_N}$, where $\nu_{t_j}^{\Delta, Y_j}$ provides a best (probabilistic) estimate of the state of the system at times t_j , given the measurements $Y_j = (y_1, \dots, y_j)$ available up to that time. The measurements are modeled as

$$y_j = \mathcal{L}_j^\Delta(\bar{u}) + \eta_j, \quad \eta_j \sim \rho_j(y) dy, \quad (6.3.5)$$

where for each j , the noise distribution ρ_j is required to satisfy the assumption 6.2.1 with a matrix $\Gamma_j \in \mathbb{R}^{d \times d}$ and observable $\mathcal{L}_j^\Delta(\bar{u}) = \mathcal{G}_j(\mathcal{S}_{t_{j-1}+t}^\Delta(\bar{u}))$, i.e.,

$$\mathcal{L}_j^\Delta(\bar{u}) = \int_0^{\delta t_j} \int_D \phi_j(x, t) g_j(u(x, t_{j-1} + t)) dx dt, \quad (6.3.6)$$

where $u(x, t) = \mathcal{S}_t^\Delta(\bar{u})$ is the approximate solution corresponding to \mathcal{S}_t^Δ , with initial data $\bar{u} = u(x, 0)$.

Remark 6.3.4. More generally, given all measurements $Y_j = (y_1, \dots, y_j)$ obtained in the time interval $[0, t_j]$, we might be interested in ν_t^{Δ, Y_j} , the best probabilistic Bayesian estimate of the state u at arbitrary time $t \in [0, T]$, i.e. we can formally consider the conditional probabilities

$$\nu_t^{\Delta, Y_j}(du) = \text{Prob}[u(\cdot, t) \in du | Y_j] = \text{Prob}[u(\cdot, t) \in du | y_1, \dots, y_j],$$

for $t \in [0, T]$. The filtering problem thus considers the case for which all available information at time $t = t_j$ is incorporated in $\nu_{t_j}^{\Delta, Y_j}$, providing the best prediction of the state u at time t_j , given all measurements made during the time-interval $[0, t_j]$.

We note that, under assumption 6.3.3, Proposition 6.3.2 implies in particular that

$$\begin{aligned} \|\mathcal{L}_j^\Delta(u)\|_{L^2(\mu_{\text{prior}})} &\leq C(1 + \|u\|_{L^2(\mu_{\text{prior}})}), \\ \|\mathcal{L}_j^\Delta(u) - \mathcal{L}_j^{\Delta'}(u)\|_{L^2(\mu_{\text{prior}})} &\leq C \int_{t_{j-1}}^{t_j} \|\mathcal{S}_t^\Delta(u) - \mathcal{S}_t^{\Delta'}(u)\|_{L^2(\mu_{\text{prior}})} dt, \end{aligned} \quad (6.3.7)$$

where $C = C(\mathcal{G}_j, T) > 0$.

We will denote the log-likelihood function corresponding to the observable $\mathcal{G}_j(u)$ on the j -th time interval $[t_{j-1}, t_j]$ by

$$\Phi_j^{\Delta, y_j}(u) = -\log \rho_j(y_j - \mathcal{G}_j(\mathcal{S}_t^\Delta(u))), \quad \forall u \in L_x^2. \quad (6.3.8)$$

We formalize the filtering problem as follows:

Definition 6.3.5 (Filtering). At the initial time $t = 0$, we fix a prior measure μ_{prior} , and define

$$\nu_{t_0}^{\Delta, Y_0} := \mathcal{S}_{0,\#}^\Delta \mu_{\text{prior}}. \quad (6.3.9)$$

We note that $\mathcal{S}_0^\Delta \approx \text{Id}$ is an approximation to the identity. Given times $0 = t_0 < t_1 < \dots < t_N = T$ and measurements y_1, \dots, y_N , the **filtering problem** involves the following two recursive steps.

1. **Correction step:** Given $\nu_{t_{j-1}}^{\Delta, Y_{j-1}}$ as a prior at time t_{j-1} , solve the Bayesian inverse problem with new measurement $y_j = \mathcal{G}_j(\mathcal{S}_t^\Delta(u)) + \eta_j$, for $t \in [0, \delta t_j]$, to obtain a corrected Bayesian estimate

$$d\nu_{t_{j-1}}^{\Delta, Y_j}(u) = \frac{1}{Z_j^\Delta(y_j)} \exp\left(-\Phi_j^{\Delta, y_j}(u)\right) d\nu_{t_{j-1}}^{\Delta, Y_{j-1}}(u). \quad (6.3.10)$$

2. **Prediction step:** Based on this corrected estimate, predict the probability distribution at time t_j , as the push-forward:

$$\nu_{t_j}^{\Delta, Y_j} = \mathcal{S}_{\delta t_j, \#}^\Delta \nu_{t_{j-1}}^{\Delta, Y_j}, \quad (6.3.11)$$

where we recall that $\delta t_j = t_j - t_{j-1}$.

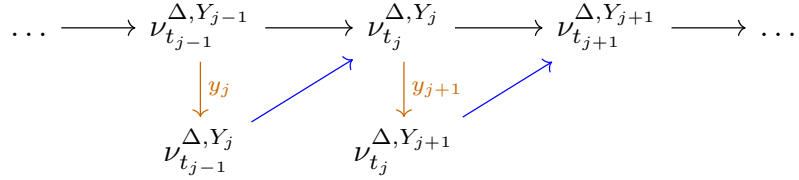


Figure 6.2: Schematic for the filtering problem: (orange) the correction step incorporates the measurement $y_j = \mathcal{L}_j^\Delta(\bar{u}) + \eta_j$ to update the current best estimate, (blue) the updated estimate is used to predict the next state.

Remark 6.3.6. Informally, we can write the correction step (6.3.10) of the filtering problem as follows:

$$\begin{aligned} \text{Prob}[u(t_{j-1}) \in du | Y_j] &= \text{Prob}[y_j = \mathcal{G}_j(\mathcal{S}_t^\Delta(u(t_{j-1}))) | u(t_{j-1})] \\ &\quad \times \text{Prob}[u(t_{j-1}) \in du | Y_{j-1}], \end{aligned}$$

The prediction step (6.3.11) can be expressed intuitively as

$$\begin{aligned} \text{Prob}[u(t_j) \in du | Y_j] &= \text{Prob}\left[\mathcal{S}_{\delta t_j}^\Delta(u(t_{j-1})) \in du | Y_j\right] \\ &= \mathcal{S}_{\delta t_j, \#} \text{Prob}[u(t_{j-1}) \in du | Y_{j-1}]. \end{aligned}$$

The filtering problem is thus defined by recursion, and provides a sequence of best-estimates $\nu_{t_j}^{\Delta, Y_j}$ given the time sequence $0 = t_0, t_1, \dots, t_N$ and measurements y_1, \dots, y_N , and based on a fixed prior μ_{prior} at the initial time $t = 0$.

Although the filtering problem is most naturally expressed in terms of the above recursive prediction/correction scheme, it turns out to be beneficial for the analysis of this problem to discuss an equivalent alternative formulation. To this end, we consider $\mu^{\Delta, Y_j} \in \mathcal{P}(L_x^2)$ for $j = 0, \dots, N$, informally given by

$$\mu^{\Delta, Y_j}(du) = \text{Prob}[u(\cdot, 0) \in du | Y_j], \quad (6.3.12)$$

i.e. the probability of the initial state $u(\cdot, 0) \in du$, given the measurements $Y_j = (y_1, \dots, y_j)$. More precisely, we define $\mu^{\Delta, Y_j}(du)$ as the solution of the BIP with prior μ_{prior} and given the measurement

$$Y_j = (\mathcal{L}_1^\Delta(u), \mathcal{L}_2^\Delta(u), \dots, \mathcal{L}_j^\Delta(u)) + (\eta_1, \eta_2, \dots, \eta_j),$$

and $(\eta_1, \eta_2, \dots, \eta_j)$ the measurement noise. For simplicity, we will assume that the random variables η_1, \dots, η_j at different time-steps are independent. In this case, the law of (η_1, \dots, η_j) is a simple product,

$$(\eta_1, \dots, \eta_j) \sim \rho_1(y_1) dy_1 \otimes \dots \otimes \rho_j(y_j) dy_j,$$

and the solution of the above BIP with prior μ_{prior} is given by

$$d\mu^{\Delta, Y_j}(u) = \frac{1}{Z_j^\Delta(Y_j)} \exp\left(-\sum_{k=1}^j \Phi_k^{\Delta, y_k} \circ \mathcal{S}_{t_{k-1}}^\Delta(u)\right) d\mu_{\text{prior}}(u), \quad (6.3.13)$$

where we note that, by (6.3.8) and the definition of $\mathcal{L}_k^\Delta(u) = \mathcal{G}_k(\mathcal{S}_{t_{k-1}+t}^\Delta(u))$, we have that

$$\begin{aligned} \Phi_k^{\Delta, y_k} \circ \mathcal{S}_{t_{k-1}}^\Delta(u) &= -\log \rho_k(y_k - \mathcal{G}_k(\mathcal{S}_{t_{k-1}}^\Delta(u))) \\ &= -\log \rho_k(y_k - \mathcal{L}_k^\Delta(u)), \quad \forall u \in L_x^2, \end{aligned} \quad (6.3.14)$$

i.e. $\Phi_k^{\Delta, y_k} \circ \mathcal{S}_{t_{k-1}}^\Delta$ is the log-likelihood function corresponding to the measurement $y_k = \mathcal{L}_k(u) + \eta_k$, and starting from the initial data $u \in L_x^2$ at time $t = 0$. In (6.3.13), $\mathcal{Z}_j^\Delta(Y_j)$ is a suitable normalization constant, defined by

$$\mathcal{Z}_j^\Delta(Y_j) = \int_{L_x^2} \exp \left(- \sum_{k=1}^j \Phi_k^{\Delta, y_k} \circ \mathcal{S}_{t_{k-1}}^\Delta(u) \right) d\mu_{\text{prior}}(u),$$

for $Y_j = (y_1, \dots, y_j)$. We note that $\mathcal{L}_k^\Delta(u) = \mathcal{G}_j(\mathcal{S}_{t_{k-1}+t}^\Delta(u))$ (cp. equation (6.3.6)) can be written as

$$\mathcal{L}_k^\Delta(u) = \int_{t_{k-1}}^{t_k} \int_D \phi_k(x, t - t_{k-1}) g_k(\mathcal{S}_t^\Delta(u)) dx dt,$$

i.e. \mathcal{L}_k provides a measurement of the solution $\mathcal{S}_t^\Delta(u)$ with initial data u (at $t = 0$) over the time interval $[t_{k-1}, t_k]$. Consistent with the above identity for μ^{Δ, Y_j} (which is valid for $j \geq 1$), we define

$$\mu^{\Delta, Y_0} := \mu_{\text{prior}}, \quad (6.3.15)$$

corresponding to the empty sum in (6.3.13).

We can now state the following proposition, providing an alternative formulation of the filtering problem. We refer to [LMW21, Proposition 4.7] for the detailed proof.

Proposition 6.3.7. *Let $\nu_{t_j}^{\Delta, Y_j}$ denote the recursively computed sequence of probability measures in the filtering problem (cp. Definition 6.3.5). Let μ^{Δ, Y_j} be given by (6.3.13). Then, we have the identity*

$$\nu_{t_j}^{\Delta, Y_j} = \mathcal{S}_{t_j, \#}^\Delta \mu^{\Delta, Y_j}, \quad (6.3.16)$$

i.e. $\nu_{t_j}^{\Delta, Y_j}$ is given by the push-forward of μ^{Δ, Y_j} to time $t = t_j$.

Remark 6.3.8. *The content of Proposition 6.3.7 is intuitively clear: The measure $\mu^{\Delta, Y_j}(u)$ provides the best Bayesian estimate for the initial state $u(\cdot, t)$ at $t = 0$ given the measurements $Y_j = (y_1, \dots, y_j)$ acquired over the interval $[0, t_j]$. Proposition 6.3.7 expresses the fact that the best Bayesian estimate for the state $u(x, t_j)$ at time t_j should simply be given by evolving the best initial estimate μ^{Δ, Y_j} (given Y_j), forward in time to $t = t_j$, via the solution operator $\mathcal{S}_{t_j}^\Delta$.*

Remark 6.3.9. *Proposition 6.3.7 also indicates a consistent definition of ν_t^{Δ, Y_j} for any $t \in [0, T]$. Indeed, the best Bayesian estimate for $u(\cdot, t)$ given the measurements Y_j is simply given by*

$$\nu_t^{\Delta, Y_j} = \mathcal{S}_{t, \#}^\Delta \mu^{\Delta, Y_j}, \quad (6.3.17)$$

Remark 6.3.10. *We recall that by Remark 6.2.10, for any $\phi \in L^1(\mu_{\text{prior}})$, the mapping*

$$Y_j \mapsto \int_{L_x^2} \phi(u) d\mu^{\Delta, Y_j}(u),$$

is analytic in Y_j , for Gaussian measurement noise. As a consequence of Proposition 6.3.7, it follows that also

$$Y_j \mapsto \int_{L_x^2} \phi(u) d\nu_t^{\Delta, Y_j}(u) = \int_{L_x^2} \phi(\mathcal{S}_t^\Delta(u)) d\mu^{\Delta, Y_j}(u),$$

is analytic in Y_j , independently of the smoothness of the solution operator \mathcal{S}_t^Δ .

6.3.2 Stability with respect to measurements

In this section, we investigate the stability properties of the solution of the filtering problem with respect to the measurements y_1, \dots, y_N . Our analysis will be based on the representation (6.3.13) of the previous section and the stability results for the BIP in section 6.2. Due to the low a priori time-regularity of the time-dependent mapping $t \mapsto \nu_t^{\Delta, Y_j}$, we will formulate the stability in the space $L_t^1(\mathcal{P}) = L^1([0, T]; \mathcal{P}(L_x^2))$, defined as the set of all weak-* measurable mappings $[0, T] \rightarrow \mathcal{P}(L_x^2)$, $t \mapsto \nu_t$, such that

$$\int_0^T \|u\|_{L_x^2} d\nu_t(u) dt < \infty,$$

with metric

$$d_T(\nu_t, \nu'_t) := \int_0^T W_1(\nu_t, \nu'_t) dt, \quad \forall \nu_t, \nu'_t \in L^1([0, T]; \mathcal{P}(L_x^2)).$$

This space has been introduced in chapter 3, Definition 3.2.3; it is not difficult to prove that $(L_t^1(\mathcal{P}), d_T)$ is a complete metric space (cp. Proposition 3.2.4).

We can now state the following lemma:

Lemma 6.3.11. *Let $T > 0$. Let $\mu_{\text{prior}} \in \mathcal{P}_1(L_x^2)$ be a prior such that $\|u\|_{L^1(\mu_{\text{prior}})} < \infty$. Let ν_t^{Δ, Y_j} be given by (6.3.17) for $t \in [0, T]$, so that, formally, $\nu_t^{\Delta, Y_j}(du) = \text{Prob}[u(\cdot, t) \in du | Y_j]$. Then for any $R > 0$, there exists $C = C(R) > 0$, such that for any $t, \delta t \geq 0$, we have*

$$\int_t^{t+\delta t} W_1\left(\nu_\tau^{\Delta, Y_j}, \nu_\tau^{\Delta, Y_j'}\right) d\tau \leq C\delta t \left(\sum_{k=1}^j |y_k - y'_k|_{\Gamma_k}^2\right)^{1/2}, \quad (6.3.18)$$

for all $Y_j = (y_1, \dots, y_j)$, $Y'_j = (y'_1, \dots, y'_j)$ such that $\sqrt{\sum_{k=1}^j |y_k|_{\Gamma_k}^2} \leq R$, $\sqrt{\sum_{k=1}^j |y'_k|_{\Gamma_k}^2} \leq R$.

Proof. To simplify the notation in the following, we set

$$|Y_j|_\Gamma := \left(\sum_{k=1}^j |y_k|_{\Gamma_k}^2\right)^{1/2}.$$

By (6.3.17), we have $\nu_t^{\Delta, Y_j} = \mathcal{S}_{t, \#}^\Delta \mu^{\Delta, Y_j}$, where μ^{Δ, Y_j} solves a BIP and is given by (6.3.13). Since μ^{Δ, Y_j} is the solution of a standard BIP with noise $\eta = (\eta_1, \dots, \eta_j)$ satisfying assumption 6.2.1, then by Lemma 6.2.7, we obtain

$$\left\| \frac{d\mu^{\Delta, Y_j}}{d\mu_{\text{prior}}} - \frac{d\mu^{\Delta, Y'_j}}{d\mu_{\text{prior}}} \right\|_{L^\infty(\mu_{\text{prior}})} \leq C|Y_j - Y'_j|_\Gamma. \quad (6.3.19)$$

Let $\Phi(u) \in \text{Lip}(L_x^2)$ be a function with Lipschitz constant ≤ 1 . Then there exists $g(u)$ such that

$$\Phi(u) - \Phi(0) = g(u)\|u\|_{L_x^2}, \quad |g(u)| \leq 1.$$

Now note that

$$\begin{aligned}
\int_{L_x^2} \Phi(u) [d\nu_t^{\Delta, Y_j} - d\nu_t^{\Delta, Y'_j}] &= \int_{L_x^2} [\Phi(u) - \Phi(0)] [d\nu_t^{\Delta, Y_j} - d\nu_t^{\Delta, Y'_j}] \\
&= \int_{L_x^2} g(u) \|u\|_{L_x^2} \mathcal{S}_{t,\#}^\Delta [d\mu^{\Delta, Y_j} - d\mu^{\Delta, Y'_j}] \\
&= \int_{L_x^2} g(\mathcal{S}_t^\Delta(u)) \|\mathcal{S}_t^\Delta(u)\|_{L_x^2} \left[\frac{d\mu^{\Delta, Y_j}}{d\mu_{\text{prior}}} - \frac{d\mu^{\Delta, Y'_j}}{d\mu_{\text{prior}}} \right] d\mu_{\text{prior}}(u) \\
&\leq \int_{L_x^2} |g(\mathcal{S}_t^\Delta(u))| \|\mathcal{S}_t^\Delta(u)\|_{L_x^2} \left| \frac{d\mu^{\Delta, Y_j}}{d\mu_{\text{prior}}} - \frac{d\mu^{\Delta, Y'_j}}{d\mu_{\text{prior}}} \right| d\mu_{\text{prior}}(u).
\end{aligned}$$

Using the fact that $|g(u)| \leq 1$, and that $\|\mathcal{S}_t^\Delta(u)\|_{L_x^2} \leq C\|u\|_{L_x^2}$, by assumption 6.3.3, we can further estimate the last expression

$$\begin{aligned}
&\int_{L_x^2} |g(\mathcal{S}_t^\Delta(u))| \|\mathcal{S}_t^\Delta(u)\|_{L_x^2} \left| \frac{d\mu^{\Delta, Y_j}}{d\mu_{\text{prior}}} - \frac{d\mu^{\Delta, Y'_j}}{d\mu_{\text{prior}}} \right| d\mu_{\text{prior}}(u) \\
&\leq C \int_{L_x^2} \|u\|_{L_x^2} \left| \frac{d\mu^{\Delta, Y_j}}{d\mu_{\text{prior}}} - \frac{d\mu^{\Delta, Y'_j}}{d\mu_{\text{prior}}} \right| d\mu_{\text{prior}}(u) \\
&\leq C \left(\int_{L_x^2} \|u\|_{L_x^2} d\mu_{\text{prior}}(u) \right) \left\| \frac{d\mu^{\Delta, Y_j}}{d\mu_{\text{prior}}} - \frac{d\mu^{\Delta, Y'_j}}{d\mu_{\text{prior}}} \right\|_{L^\infty(\mu_{\text{prior}})}.
\end{aligned}$$

Taking the supremum over all $\Phi(u)$ such that $\|\Phi\|_{\text{Lip}} \leq 1$ on the left, and noting the upper bound (6.3.19) on the last term, we find

$$W_1 \left(\nu_t^{\Delta, Y_j}, \nu_t^{\Delta, Y'_j} \right) \leq C|Y_j - Y'_j|_\Gamma,$$

where the constant $C > 0$ is independent of Y_j, Y'_j . Integrating in time, we obtain the claimed inequality

$$\int_t^{t+\delta t} W_1 \left(\nu_t^{\Delta, Y_j}, \nu_t^{\Delta, Y'_j} \right) dt \leq C\delta t|Y_j - Y'_j|_\Gamma.$$

□

We will finally state a general stability theorem for the solution of the filtering problem. To this end, we introduce the following notation

Definition 6.3.12. Given times $0 = t_0 < t_1 < \dots < t_N = T$, and measurements y_1, \dots, y_N , we denote by $\nu^{\Delta, \mathbf{y}}$, with $\mathbf{y} = (y_1, \dots, y_N)$ the solution of the associated filtering problem, i.e.,

$$\nu_t^{\Delta, \mathbf{y}} := \begin{cases} \nu_t^{\Delta, Y_0}, & t \in [0, t_1), \\ \nu_t^{\Delta, Y_1}, & t \in [t_1, t_2), \\ \vdots \\ \nu_t^{\Delta, Y_{N-1}}, & t \in [t_{N-1}, t_N), \\ \nu_t^{\Delta, Y_N}, & t \geq t_N, \end{cases} \quad (6.3.20)$$

Theorem 6.3.13. *Let $\nu_t^{\Delta, \mathbf{y}}$ denote the solution of the filtering problem with prior $\mu_{\text{prior}} \in \mathcal{P}_1(L_x^2)$, and measurements $\mathbf{y} = (y_1, \dots, y_N)$. Then for any $R > 0$, there exists $C = C(R, T)$, such that*

$$\int_0^T W_1(\nu_t^{\Delta, \mathbf{y}}, \nu_t^{\Delta, \mathbf{y}'}) dt \leq C |\mathbf{y} - \mathbf{y}'|_\Gamma, \quad (6.3.21)$$

for all \mathbf{y}, \mathbf{y}' such that $|\mathbf{y}|_\Gamma, |\mathbf{y}'|_\Gamma \leq R$. Here, we use the norm

$$|\mathbf{y}|_\Gamma := \left(\sum_{k=1}^N |y_k|_{\Gamma_k}^2 \right)^{1/2}.$$

Proof. The claimed stability estimate follows readily from Lemma 6.3.11: Indeed, $\nu_t^{\Delta, \mathbf{y}}$ is defined piecewise in time, for $t \in [0, T) = [t_0, t_N)$, as

$$\nu_t^{\Delta, \mathbf{y}} = \sum_{k=1}^N 1_{[t_{k-1}, t_k)}(t) \nu_t^{\Delta, Y_{k-1}}.$$

Thus, by the estimate of Lemma 6.3.11, we find for some $C = C(R)$:

$$\begin{aligned} \int_0^T W_1(\nu_t^{\Delta, \mathbf{y}}, \nu_t^{\Delta, \mathbf{y}'}) dt &= \sum_{k=1}^N \int_{t_{k-1}}^{t_k} W_1(\nu_t^{\Delta, Y_{k-1}}, \nu_t^{\Delta, Y'_{k-1}}) dt \\ &\leq C \sum_{k=1}^N \delta t_k |Y_{k-1} - Y'_{k-1}|_\Gamma \\ &\leq CT |\mathbf{y} - \mathbf{y}'|_\Gamma. \end{aligned}$$

□

6.3.3 Compactness properties

Our second main result for the filtering problem is a conditional compactness result, motivated by the study of statistical solutions of the compressible and incompressible Euler equations in chapters 3 and 4 (see also [FLMW20]). In chapter 3, we have studied the forward problem for statistical initial data $\bar{\mu}$ a probability measure on L_x^2 . We proved that under Assumption 6.3.3, the sequence of discretized approximate solutions $\mu_t^\Delta := (\mathcal{S}_t^\Delta)_\# \bar{\mu}$ (push-forward by the discretized solution operator) is compact in $\mathcal{P}_1(L_x^2)$, provided that the following measure of average two-point correlations

$$S_2^T(\mu_t^\Delta; r) := \left(\int_0^T \int_{L_x^2} S_2(u; r)^2 d\mu_t^\Delta(u) dt \right)^{1/2}, \quad (6.3.22)$$

are uniformly bounded as $\Delta \rightarrow 0$, where

$$S_2(u; r) := \left(\int_D \int_{B_r(0)} |u(x+h) - u(x)|^2 dh dx \right)^{1/2}, \quad (6.3.23)$$

measures the average of two-point correlations of u : More precisely, if μ_t^Δ is of the form $\mu_t^\Delta = \mathcal{S}_{t,\#}^\Delta \mu_0$, $\mu_0 \in \mathcal{P}_2(L_x^2)$, with $\mathcal{S}_t^\Delta : L_x^2 \rightarrow L_x^2$ satisfying assumption 6.3.3, and if we have $S_2^T(\mu_t^\Delta; r) \leq \phi(r)$, for some modulus of continuity $\phi(r)$ uniformly in Δ , then μ_t^Δ is compact in $L_t^1(\mathcal{P})$. The quantity $r \mapsto S_2^T(\mu_t^\Delta; r)$

is referred to as the (time-integrated) structure function of μ_t^Δ . For simplicity, we will state the following results in the periodic setting with domain $D = \mathbb{T}^d$. Numerical evidence for the uniform boundedness of these structure functions for the statistical forward problem has been presented for a variety of initial probability measures μ supported on rough initial data of the two-dimensional incompressible Euler equations in [LMPP21b, LMPP21a], and in the context of hyperbolic conservation laws in [FLMW20].

We formulate this observation motivated by the numerical experiments in [FLMW20, LMPP21b, LMPP21a] abstractly as the following assumption:

Assumption 6.3.14. *The prior μ_{prior} has finite second moments,*

$$\int_{L_x^2} \|u\|_{L_x^2}^2 d\mu_{\text{prior}}(u) < \infty,$$

and there exists a modulus of continuity $\phi(r)$, such that

$$S_2^T(\mathcal{S}_{t,\#}^\Delta \mu_{\text{prior}}; r) \leq \phi(r), \quad \forall r > 0, t \in [0, T], \quad (6.3.24)$$

uniformly for all $\Delta > 0$. Here $\mathcal{S}_{t,\#}^\Delta \mu_{\text{prior}}$ denotes the push-forward measure of the prior μ_{prior} by the discretized solution operator \mathcal{S}_t^Δ .

Remark 6.3.15. Let $\bar{\mu} = \mu_{\text{prior}} \in \mathcal{P}(L_x^2)$ be a probability measure with finite second moments. We note that under our standing Assumption 6.3.3 on the uniform boundedness of the \mathcal{S}_t^Δ , and if \mathcal{S}_t^Δ converges to \mathcal{S}_t in $L^1([0, T]; L^1(\bar{\mu}))$, then Assumption 6.3.14 is automatically satisfied. Indeed, for any $\Phi \in \text{Lip}(L_x^2)$ with $\|\Phi\|_{\text{Lip}} \leq 1$, we have

$$\begin{aligned} \int_{L_x^2} \Phi(u) [d(\mathcal{S}_{t,\#}^\Delta \bar{\mu}) - d(\mathcal{S}_{t,\#} \bar{\mu})] &= \int_{L_x^2} [\Phi(\mathcal{S}_t^\Delta(u)) - \Phi(\mathcal{S}_t(u))] d\bar{\mu}(u) \\ &\leq \int_{L_x^2} \|\mathcal{S}_t^\Delta(u) - \mathcal{S}_t(u)\|_{L_x^2} d\bar{\mu}(u). \end{aligned}$$

Taking the supremum over all such Φ and integrating over $[0, T]$, we obtain

$$\int_0^T W_1(\mathcal{S}_{t,\#}^\Delta \bar{\mu}, \mathcal{S}_{t,\#} \bar{\mu}) dt \leq \int_{L_x^2} \int_0^T \|\mathcal{S}_t^\Delta(u) - \mathcal{S}_t(u)\|_{L_x^2} dt d\bar{\mu}(u).$$

Thus, the assumption that $\mathcal{S}_t^\Delta(u) \rightarrow \mathcal{S}_t(u)$ in $L^1([0, T]; L^1(\bar{\mu}))$ implies that

$$\int_0^T W_1(\mathcal{S}_{t,\#}^\Delta \bar{\mu}, \mathcal{S}_{t,\#} \bar{\mu}) dt \rightarrow 0, \quad (\Delta \rightarrow 0),$$

i.e., that $\mathcal{S}_{t,\#}^\Delta \bar{\mu} \rightarrow \mathcal{S}_{t,\#} \bar{\mu}$ in $L_t^1(\mathcal{P}) = L^1([0, T]; \mathcal{P}(L_x^2))$. In particular, $\mathcal{S}_{t,\#}^\Delta \bar{\mu}$ is compact in $L_t^1(\mathcal{P})$, from which it follows (cp. [LMW21, Prop. A.2]) that there exists a modulus of continuity $\phi(r)$, such that $S_2^T(\mathcal{S}_{t,\#}^\Delta \bar{\mu}; r) \leq \phi(r)$.

We also note that if there exists a set $A \subset L_x^2$, such that $\bar{\mu}(A) = 1$, and $\mathcal{S}_t^\Delta(u) \rightarrow \mathcal{S}_t(u)$ point-wise for all $u \in A$, and almost all $t \in [0, T]$, then $\mathcal{S}_t^\Delta(u) \rightarrow \mathcal{S}_t(u)$ in $L^1([0, T]; L^1(\bar{\mu}))$. Indeed, this follows from the point-wise bound

$$\|\mathcal{S}_t^\Delta(u) - \mathcal{S}_t(u)\|_{L_x^2} \leq \|\mathcal{S}_t^\Delta(u)\|_{L_x^2} + \|\mathcal{S}_t(u)\|_{L_x^2} \leq 2\|u\|_{L_x^2},$$

the fact that $\int \|u\|_{L_x^2} d\bar{\mu}(u) < \infty$, and the dominated convergence theorem.

Conditional on Assumption 6.3.14, we can prove a compactness result for the filtering problem:

Lemma 6.3.16. *Let $\nu_t^{\Delta, \mathbf{y}}$ be the solution of the filtering problem with prior $\mu_{\text{prior}} \in \mathcal{P}_2(L_x^2)$, such that $\|u\|_{L^2(\mu_{\text{prior}})} < \infty$, and measurements $\mathbf{y} = (y_1, \dots, y_N)$. If assumption 6.3.14 holds, then $\nu_t^{\Delta, \mathbf{y}}$ is a compact sequence in $L_t^1(\mathcal{P})$, as $\Delta \rightarrow 0$.*

The proof of this lemma is based on proving a uniform upper bound on the structure function $S_2^T(\nu_t^{\Delta, \mathbf{y}}; r) \leq CS_2^T(\mathcal{S}_{t,\#}^\Delta \mu_{\text{prior}}; r) \leq \phi(r)$. For the details of the argument, we refer to [LMW21, Lemma 4.6]. Combining the uniform stability result, Theorem 6.3.13 with the point-wise compactness result, Lemma 6.3.16, we can formulate the following theorem:

Theorem 6.3.17. *Fix a prior $\mu_{\text{prior}} \in \mathcal{P}_1(L_x^2)$, such that $\|u\|_{L^2(\mu_{\text{prior}})} < \infty$. Let $0 = t_0 < t_1 < \dots < t_N = T$ be a strictly increasing sequence of times for fixed $N \in \mathbb{N}$. Let $\mathbf{y} = (y_1, y_2, \dots, y_N) \in \mathbb{R}^{d \times N}$ be a sequence of measurements. Let $\nu_t^{\Delta, \mathbf{y}}$, $j = 0, \dots, N$, be the solution of the associated filtering problem. If assumption 6.3.14 holds, then the sequence $\nu_t^{\Delta, \mathbf{y}}$ is pre-compact in $C_{\text{loc}}(\mathbb{R}^{d \times N}; L_t^1(\mathcal{P}))$, as $\Delta \rightarrow 0$. In fact, there exists a subsequence $\Delta_k \rightarrow 0$, and $\mu_t^{*, \mathbf{y}}$ with*

$$\mathbf{y} \mapsto \nu_t^{*, \mathbf{y}} \in \text{Lip}_{\text{loc}}(\mathbb{R}^{N \times d}; L_t^1(\mathcal{P})),$$

such that

$$d_T(\nu_t^{\Delta_k, \mathbf{y}}, \nu_t^{*, \mathbf{y}}) = \int_0^T W_1(\nu_t^{\Delta_k, \mathbf{y}}, \nu_t^{*, \mathbf{y}}) dt \rightarrow 0,$$

converges locally uniformly in \mathbf{y} .

Proof. By Theorem 6.3.13, the mapping

$$\mathbb{R}^{d \times N} \ni \mathbf{y} \mapsto \nu_t^{\Delta, \mathbf{y}} \in L_t^1(\mathcal{P}),$$

is uniformly bounded on any compact subset $K \subset \mathbb{R}^{d \times N}$ and uniformly equicontinuous on K . By Lemma 6.3.16, the sets

$$\left\{ \nu_t^{\Delta, \mathbf{y}} \mid \Delta > 0 \right\} \subset L_t^1(\mathcal{P}),$$

are pre-compact for any fixed $\mathbf{y} \in \mathbb{R}^{d \times N}$ (pointwise compactness). By the Arzelá-Ascoli Theorem A.2.1, the claimed compactness result follows. \square

Remark 6.3.18. *In practice, a very popular choice of priors are Gaussian priors $\mu_{\text{prior}} \sim \mathcal{N}(m, \Gamma)$ on function spaces, i.e. priors μ_{prior} such that each finite-dimensional projection is Gaussian. We point out in passing that Theorems 6.2.9, 6.2.12, 6.3.13 and 6.3.17 on the stability and compactness properties of approximate posteriors apply in particular, when the prior is Gaussian.*

6.3.4 Consistency with the canonical solution

We finally discuss the consistency of the above convergence result for the approximate filtering problems based on the discretized solution operator \mathcal{S}_t^Δ , and the limiting filtering problem with solution operator \mathcal{S}_t . More precisely, we show that if $\mathcal{S}_t^\Delta(u) \rightarrow \mathcal{S}_t(u)$ converges in a suitable sense, then $\nu_t^{\Delta, \mathbf{y}} \rightarrow \nu_t^{\mathbf{y}}$ in $L_t^1(\mathcal{P})$, where $\nu_t^{\mathbf{y}}$ denotes the solution of the limiting filtering problem.

Theorem 6.3.19. *Assume that $\mu_{\text{prior}} \in \mathcal{P}_1(L_x^2)$ is such that $\|u\|_{L^2(\mu_{\text{prior}})} < \infty$. Then there exists a constant $C > 0$, independent of Δ , such that*

$$\int_0^T W_1(\nu_t^{\Delta, \mathbf{y}}, \nu_t^{\mathbf{y}}) dt \leq C \int_0^T \|\mathcal{S}_t^\Delta(u) - \mathcal{S}_t(u)\|_{L^2(\mu_{\text{prior}})} dt.$$

In particular, if $\mathcal{S}_t^\Delta(u) \rightarrow \mathcal{S}_t(u)$ in $L^1([0, T]; L^2(\mu_{\text{prior}}))$, then $\nu_t^{\Delta, \mathbf{y}} \rightarrow \nu_t^{\mathbf{y}}$ in $L_t^1(\mathcal{P})$.

Proof. Fix $t \in [0, T]$ and $j \in \{0, \dots, N-1\}$, such that $t \in [t_j, t_{j+1}]$. Then, by the definition of $\nu_t^{\Delta, \mathbf{y}}$, we have

$$\nu_t^{\Delta, \mathbf{y}} = \nu_t^{\Delta, Y_j} = \mathcal{S}_{t, \#}^\Delta \mu^{\Delta, Y_j},$$

where the last equality follows from (6.3.17). Given $\Phi \in \text{Lip}$, with $\|\Phi\|_{\text{Lip}} \leq 1$ and $\Phi(0) = 0$, we find

$$\begin{aligned} \int_{L_x^2} \Phi(u) \left[d\nu_t^{\Delta, \mathbf{y}}(u) - d\nu_t^{\mathbf{y}}(u) \right] &= \int_{L_x^2} \Phi(u) \left[\mathcal{S}_{t, \#}^\Delta d\mu^{\Delta, Y_j}(u) - \mathcal{S}_{t, \#} d\mu^{Y_j}(u) \right] \\ &= \int_{L_x^2} \Phi(u) \left[\mathcal{S}_{t, \#}^\Delta d\mu^{\Delta, Y_j}(u) - \mathcal{S}_{t, \#} d\mu^{Y_j}(u) \right] \\ &\quad + \int_{L_x^2} \Phi(u) \left[\mathcal{S}_{t, \#} d\mu^{Y_j}(u) - \mathcal{S}_{t, \#}^\Delta d\mu^{Y_j}(u) \right] \\ &=: (I) + (II). \end{aligned}$$

We can estimate the two last terms individually as follows: For the first term, we obtain

$$\begin{aligned} (I) &= \int_{L_x^2} \Phi(u) \left[\mathcal{S}_{t, \#}^\Delta d\mu^{\Delta, Y_j}(u) - \mathcal{S}_{t, \#} d\mu^{Y_j}(u) \right] \\ &= \int_{L_x^2} \Phi(\mathcal{S}_t^\Delta(u)) \left[\frac{d\mu^{\Delta, Y_j}}{d\mu_{\text{prior}}} - \frac{d\mu^{Y_j}}{d\mu_{\text{prior}}} \right] d\mu_{\text{prior}}(u) \\ &\leq C \int_{L_x^2} \|u\|_{L_x^2} \left| \frac{d\mu^{\Delta, Y_j}}{d\mu_{\text{prior}}} - \frac{d\mu^{Y_j}}{d\mu_{\text{prior}}} \right| d\mu_{\text{prior}}(u) \\ &\leq C \|u\|_{L^2(\mu_{\text{prior}})} \left\| \frac{d\mu^{\Delta, Y_j}}{d\mu_{\text{prior}}} - \frac{d\mu^{Y_j}}{d\mu_{\text{prior}}} \right\|_{L^2(\mu_{\text{prior}})}. \end{aligned}$$

The last term can be estimated using Lemma 6.2.8, recalling that μ^{Δ, Y_j} is defined as the posterior with prior μ_{prior} and given the measurements $(\mathcal{L}_1^\Delta, \dots, \mathcal{L}_j^\Delta)$ of the form (6.3.6). Lemma 6.2.8 therefore yields

$$\left\| \frac{d\mu^{\Delta, Y_j}}{d\mu_{\text{prior}}} - \frac{d\mu^{Y_j}}{d\mu_{\text{prior}}} \right\|_{L^2(\mu_{\text{prior}})} \leq C \left(\sum_{\ell=1}^j \|\mathcal{L}_\ell^\Delta(u) - \mathcal{L}_\ell(u)\|_{L^2(\mu_{\text{prior}})}^2 \right)^{1/2},$$

for some constant $C > 0$ depending only on the prior μ_{prior} ; here, we have used the fact that Y_j is fixed, and that $\|\mathcal{L}_\ell^\Delta(u)\|_{L^2(\mu_{\text{prior}})}, \|\mathcal{L}_\ell(u)\|_{L^2(\mu_{\text{prior}})} \leq C(1 + \|u\|_{L^2(\mu_{\text{prior}})}) < \infty$ are bounded independently of $\Delta > 0$, which allows us to bound the additional exponential factor in Lemma 6.2.8 uniformly in Δ . Continuing, we note that the observables are Lipschitz continuous by assumption; Indeed, by (6.3.7), we have

$$\|\mathcal{L}_\ell^\Delta(u) - \mathcal{L}_\ell(u)\|_{L^2(\mu_{\text{prior}})} \leq C \int_{t_{\ell-1}}^{t_\ell} \|\mathcal{S}_t^\Delta(u) - \mathcal{S}_t(u)\|_{L^2(\mu_{\text{prior}})} dt.$$

It follows that

$$(I) \leq C \left(\sum_{\ell=1}^j \left[\int_{t_{\ell-1}}^{t_\ell} \|\mathcal{S}_t^\Delta(u) - \mathcal{S}_t(u)\|_{L^2(\mu_{\text{prior}})} dt \right]^2 \right)^{1/2}.$$

Denoting $F(t, \ell) := 1_{[t_{\ell-1}, t_\ell]}(t) \|\mathcal{S}_t^\Delta(u) - \mathcal{S}_t(u)\|_{L^2(\mu_{\text{prior}})}$, we can estimate the last term as follows, using Minkowski's integral inequality:

$$\left(\sum_{\ell=1}^j \left[\int_0^T F(t, \ell) dt \right]^2 \right)^{1/2} \leq \int_0^T \left(\sum_{\ell=1}^j |F(t, \ell)|^2 \right)^{1/2} dt.$$

Finally, recalling that all $F(t, \ell)$, $\ell = 1, \dots, j$, have *disjoint* supports in t , we conclude that

$$\begin{aligned} (I) &\leq C \int_0^T \left(\sum_{\ell=1}^j |F(t, \ell)|^2 \right)^{1/2} dt = C \sum_{\ell=1}^j \int_{t_{\ell-1}}^{t_\ell} |F(t, \ell)| dt \\ &\leq C \int_0^T \|\mathcal{S}_t^\Delta(u) - \mathcal{S}_t(u)\|_{L^2(\mu_{\text{prior}})} dt. \end{aligned}$$

To estimate the second term, we note that

$$\begin{aligned} \int_{L_x^2} \Phi(u) [\mathcal{S}_{t,\#}^\Delta d\mu^{Y_j}(u) - \mathcal{S}_{t,\#} d\mu^{Y_j}(u)] &= \int_{L_x^2} [\Phi(\mathcal{S}_t^\Delta(u)) - \Phi(\mathcal{S}_t(u))] d\mu^{Y_j}(u) \\ &\leq \int_{L_x^2} \|\mathcal{S}_t^\Delta(u) - \mathcal{S}_t(u)\|_{L_x^2} d\mu^{Y_j}(u) \\ &\leq C \int_{L_x^2} \|\mathcal{S}_t^\Delta(u) - \mathcal{S}_t(u)\|_{L_x^2} d\mu_{\text{prior}}(u) \\ &\leq C \|\mathcal{S}_t^\Delta(u) - \mathcal{S}_t(u)\|_{L^2(\mu_{\text{prior}})}. \end{aligned}$$

Thus, employing the above estimates for (I) and (II), we conclude that for any $\Phi \in \text{Lip}$, $\|\Phi\|_{\text{Lip}} \leq 1$, and for any $t \in [0, T]$, we have

$$\begin{aligned} \int_{L_x^2} \Phi(u) [d\nu_t^{\Delta,y}(u) - d\nu_t^y(u)] &\leq C \|\mathcal{S}_t^\Delta(u) - \mathcal{S}_t(u)\|_{L^2(\mu_{\text{prior}})} \\ &\quad + C \int_0^T \|\mathcal{S}_t^\Delta(u) - \mathcal{S}_t(u)\|_{L^2(\mu_{\text{prior}})} dt. \end{aligned}$$

Taking the supremum over all such Φ on the left, and integrating over $t \in [0, T]$, it follows that

$$\int_0^T W_1(\nu_t^{\Delta,y}, d\nu_t^y) dt \leq C \int_0^T \|\mathcal{S}_t^\Delta(u) - \mathcal{S}_t(u)\|_{L^2(\mu_{\text{prior}})} dt,$$

where $C > 0$ is independent of Δ . \square

6.4 Applications

In the present section, we discuss several concrete applications of the abstract results obtained in the previous sections.

6.4.1 Incompressible Euler

The incompressible Euler equations model the motion of an ideal inviscid fluid, and are given by the following system of PDEs for the fluid velocity field $\mathbf{u} = \mathbf{u}(x, t)$:

$$\begin{cases} \partial_t \mathbf{u} + \operatorname{div}(\mathbf{u} \otimes \mathbf{u}) + \nabla p = 0, \\ \operatorname{div}(\mathbf{u}) = 0, \quad \mathbf{u}(\cdot, 0) = \bar{\mathbf{u}}. \end{cases} \quad (6.4.1)$$

Here, $p = p(x, t)$ is the scalar pressure, which can be determined from $\mathbf{u}(x, t)$ via solution of the elliptic equation, $-\Delta p = \operatorname{div}(\operatorname{div}(\mathbf{u} \otimes \mathbf{u}))$.

In the following, we will focus on the periodic case with domain $D = \mathbb{T}^d$, and dimension $d \in \{2, 3\}$. Physically meaningful solutions of (6.4.1) are required to satisfy an energy admissibility constraint of the form $\|\mathbf{u}(t)\|_{L_x^2} \leq \|\bar{\mathbf{u}}\|_{L^2}$ for all $t \in [0, T]$, so that $\mathbf{u}(t) \in L_x^2(\mathbb{T}^d; \mathbb{R}^d)$ is uniformly bounded in time. In particular, we consider solutions in the space $\mathbf{u} \in L_t^\infty([0, T]; L_x^2)$.

Spectral viscosity scheme

Popular numerical discretizations of the forward problem for the incompressible Euler equations on periodic domains are spectral methods [DGO84, Cho68, KK00, Gho96]. We briefly recall the spectral (hyper-)viscosity method, originally proposed by Tadmor [Tad89] in the context of scalar conservation laws, and further detailed in chapter 1.4, in the context of the incompressible Euler equations.

Writing $\mathbf{u}^\Delta(x, t) = \sum_{|k|_\infty \leq N} \hat{\mathbf{u}}_k^\Delta(t) e^{ik \cdot x}$, where $\Delta = 1/N$, we consider the following discretization:

$$\begin{cases} \partial_t \mathbf{u}^\Delta + \mathbb{P}_N(\mathbf{u}^\Delta \cdot \nabla \mathbf{u}^\Delta) = -\epsilon_N |\nabla|^{2s} (Q_N * \mathbf{u}^\Delta), \\ \operatorname{div}(\mathbf{u}^\Delta) = 0, \quad \mathbf{u}^\Delta|_{t=0} = \mathbb{P}_N \bar{\mathbf{u}}. \end{cases} \quad (6.4.2)$$

Here \mathbb{P}_N is the truncated Leray projection operator onto divergence-free vector fields (1.4.3), introduced in chapter 1.4, $s \geq 1$ is the hyperviscosity parameter, and Q_N is a Fourier multiplier. The choice of parameters $m_N \rightarrow \infty$, $\epsilon_N \rightarrow 0$, and Fourier multiplier, and the intuition behind this scheme, are further described in chapter 1.4.

A priori estimates and consistency for the SV scheme

Multiplying the evolution equation (6.4.2) by \mathbf{u}^Δ and integrating by parts, we recall the following energy balance from chapter 1.4,

$$\|\mathbf{u}^\Delta(t)\|_{L_x^2}^2 + 2\epsilon_N (2\pi)^d \sum_{|k|_\infty \leq N} \int_0^t \widehat{Q}_k |k|^{2\sigma} |\hat{\mathbf{u}}_k^\Delta(\tau)|^2 d\tau \leq \|\bar{\mathbf{u}}\|_{L_x^2}^2.$$

In particular, for any admissible choice of the parameters of the SV scheme, we obtain the a priori energy bound

$$\|\mathbf{u}^\Delta(t)\|_{L_x^2} \leq \|\bar{\mathbf{u}}\|_{L_x^2}, \quad \forall t \in [0, T]. \quad (6.4.3)$$

We also recall [LM15, Lemma 3.2] that the SV scheme is consistent with the incompressible Euler equations, in the sense that for any initial data $\bar{\mathbf{u}} \in L_x^2$, the sequence \mathbf{u}^Δ converges (up to a subsequence) in the sense of Young measures to an energy admissible measure-valued solution [LM15], as $\Delta \rightarrow 0$. In fact, we have the following simple Lemma:

Lemma 6.4.1. *The approximate solution operator $\mathcal{S}_t^\Delta : L_x^2 \rightarrow L_x^2$ obtained from the SV scheme (6.4.2) at grid scale $\Delta = 1/N$ satisfies assumption 6.3.3.*

Proof. Energy admissibility has already been derived preceding (6.4.3). The simple argument to show temporal Lipschitz continuity with values in a sufficiently negative Sobolev space H_x^{-L} has e.g. been provided in [LM15, Remark 3.3]. \square

It is known (cp. the weak-strong uniqueness Theorem 1.3.11) that if there exists a strong solution $\mathbf{u} \in C([0, T]; L_x^2)$ for given initial data $\bar{\mathbf{u}}$, such that

$$\int_0^T \|\nabla \mathbf{u}(t)\|_{L_x^\infty} dt < \infty, \quad (6.4.4)$$

then this strong solution \mathbf{u} is unique in the class of energy admissible measure-valued solutions. As a consequence of this weak-strong uniqueness result and the convergence to measure-valued solutions of the SV scheme 6.4.2, we conclude that $\mathbf{u}^\Delta \rightarrow \mathbf{u}$ converges e.g. in $L_t^2([0, T]; L_x^2)$ (in fact, $L_t^p([0, T]; L_x^2)$ for all $p < \infty$), if \mathbf{u} is a strong (Lipschitz) solution. We collect this observation in the following proposition.

Proposition 6.4.2. *Let $\bar{\mathbf{u}} \in L_x^2$ be given initial data for the incompressible Euler equations. If there exists a unique strong solution $\mathbf{u} = \mathcal{S}_t(\bar{\mathbf{u}})$ of (6.4.1) with initial data $\bar{\mathbf{u}}$ and such that (6.4.4) holds, then the approximate solution $\mathbf{u}^\Delta = \mathcal{S}_t^\Delta(\bar{\mathbf{u}})$ computed by the SV scheme converges to $\mathcal{S}_t(\bar{\mathbf{u}})$. More precisely, we have*

$$\int_0^T \|\mathcal{S}_t^\Delta(\bar{\mathbf{u}}) - \mathcal{S}_t(\bar{\mathbf{u}})\|_{L_x^2}^2 dt \rightarrow 0, \quad \text{as } \Delta \rightarrow 0.$$

In the two-dimensional case, $d = 2$, the vorticity is known to be advected by the flow, implying that, at least formally, L^p -norms of $\omega = \operatorname{curl}(\mathbf{u})$ can be controlled. The SV scheme ensures L^p -control on the vorticity $\omega^\Delta = \operatorname{curl}(\mathbf{u}^\Delta)$ for $p = 2$: In the *two-dimensional case*, we have the following enstrophy bound (see e.g. [LM20, Proposition 4.2])

$$\|\omega^\Delta(t)\|_{L_x^2} \leq \|\bar{\omega}\|_{L_x^2}, \quad \forall t \in [0, T], \quad (6.4.5)$$

where $\bar{\omega} = \operatorname{curl}(\bar{\mathbf{u}})$ is the vorticity of the initial data. If the initial vorticity $\bar{\omega} \in L_x^\infty$ is bounded, it has been shown by Yudovich [Yud63], that there exists a solution $\mathbf{u} = \mathcal{S}_t(\bar{\mathbf{u}})$ of the incompressible Euler equations with uniformly bounded vorticity $\|\operatorname{curl}(\mathbf{u})\|_{L_x^\infty} \leq \|\bar{\omega}\|_{L_x^\infty}$. Furthermore, this solution $\mathcal{S}_t(\mathbf{u})$ is unique in the class of solution with bounded vorticity [Yud63]. Later, it has been pointed out by Liu and Xin [LX95], that the proof of uniqueness in [Yud63, Yud95] actually extends to provide a weak-strong uniqueness result in a wider class: If \mathbf{v} is another weak solution of the incompressible Euler equations with vorticity bound $\|\operatorname{curl}(\mathbf{v}(t))\|_{L_x^p} \leq C$, for any $p > 4/3$, then $\mathbf{v} \equiv \mathbf{u}$ is the unique Yudovich solution.² As a consequence of this weak-strong uniqueness result and the enstrophy bound (6.4.5), we obtain

Proposition 6.4.3. *If $\bar{\mathbf{u}}$ is initial data for the two-dimensional incompressible Euler equations with bounded vorticity, $\|\bar{\omega}\|_{L_x^\infty} < \infty$, then the approximate solutions $\mathbf{u}^\Delta = \mathcal{S}_t^\Delta(\bar{\mathbf{u}})$ converge strongly in $L_t^2([0, T]; L_x^2)$ to the unique Yudovich solution $\mathcal{S}_t(\bar{\mathbf{u}})$, i.e.*

$$\int_0^T \|\mathcal{S}_t^\Delta(\bar{\mathbf{u}}) - \mathcal{S}_t(\bar{\mathbf{u}})\|_{L_x^2}^2 dt \rightarrow 0, \quad \text{as } \Delta \rightarrow 0.$$

A second consequence of the enstrophy bound (6.4.5) is a uniform estimate on the structure function:

Proposition 6.4.4. *If $\bar{\mathbf{u}} \in L_x^2$ is initial data for the two-dimensional incompressible Euler equations with bounded enstrophy, $\|\bar{\omega}\|_{L_x^2} < \infty$ with $\bar{\omega} = \operatorname{curl}(\bar{\mathbf{u}})$, then there exists a constant $C > 0$, such that for any $\Delta > 0$, the structure function obeys the bound*

$$S_2(\mathcal{S}_t^\Delta(\bar{\mathbf{u}}); r) \leq Cr\|\bar{\omega}\|_{L_x^2}, \quad \forall t \in [0, T], r \geq 0.$$

Proof. By definition, we have for any $\mathbf{u} \in H_x^1$:

$$S_2(\mathbf{u}; r)^2 = \int_{B_r(0)} \int_D |\mathbf{u}(x+h) - \mathbf{u}(x)|^2 dx dh = \int_{B_r(0)} \|\mathbf{u}(\cdot + h) - \mathbf{u}(\cdot)\|_{L_x^2}^2 dh.$$

The estimate $\|\mathbf{u}(\cdot + h) - \mathbf{u}(\cdot)\|_{L_x^2} \leq C\|\nabla \mathbf{u}\|_{L_x^2}|h|$ is classical. Furthermore, it follows from the incompressibility of \mathbf{u} that $\|\nabla \mathbf{u}\|_{L_x^2} = \|\operatorname{curl}(\mathbf{u})\|_{L_x^2}$. Hence,

$$S_2(\mathbf{u}; r)^2 = \int_{B_r(0)} \|\mathbf{u}(\cdot + h) - \mathbf{u}(\cdot)\|_{L_x^2}^2 dh \leq \int_{B_r(0)} C\|\operatorname{curl}(\mathbf{u})\|_{L_x^2}^2 |h|^2 dh \leq C\|\operatorname{curl}(\mathbf{u})\|_{L_x^2}^2 r^2.$$

²In fact, the Yudovich-class weak-strong uniqueness result of [LX95] can be slightly extended to prove that Yudovich solutions are unique in the class of weak solutions with a L_x^p vorticity bound for *any* $p > 1$. Since this extension is not necessary in the present case, we do not provide a detailed proof here.

Setting $\mathbf{u} = \mathcal{S}_t^\Delta(\bar{\mathbf{u}})$, we thus find

$$S_2(\mathcal{S}_t^\Delta(\bar{\mathbf{u}}); r) \leq Cr\|\operatorname{curl}(\mathcal{S}_t^\Delta(\mathbf{u}))\|_{L_x^2} \leq Cr\|\bar{\omega}\|_{L_x^2},$$

where the last inequality follows from (6.4.5). \square

The well-posed case

Combining the general results for the Bayesian inverse and filtering problems in sections 6.2 and 6.3, and the above convergence results for the spectral viscosity scheme, we can now prove:

Theorem 6.4.5. *If $\mu_{\text{prior}} \in \mathcal{P}(L_x^2)$ is a prior, and if there exists $M > 0$, $s > d/2 + 2$, such that $\mu_{\text{prior}}(B_M^s) = 1$, where*

$$B_M^s := \{\bar{\mathbf{u}} \in L_x^2 \cap H_x^s \mid \|\bar{\mathbf{u}}\|_{H_x^s} \leq M\} \subset L_x^2,$$

then there exists a time interval $[0, T]$ with $T = T(M, s) > 0$, such that the BIP and filtering problems for the incompressible Euler equations are well-posed on $[0, T]$: Given measurements in the time-interval $[0, T]$, there exists a unique solution μ^y for the BIP and ν_t^y for the filtering problem. The posteriors μ^y and ν_t^y are W_1 -stable with respect to measurements, in the sense of (6.2.23) and (6.3.21), respectively. Furthermore, the approximations $\mu^{\Delta, y}$ and $\nu_t^{\Delta, y}$ obtained by the numerical discretization with the SV scheme converge to this solution as $\Delta \rightarrow 0$, in the 1-Wasserstein norm W_1 .

Proof. We first observe that there exists a $T > 0$, such that the initial value problem for the incompressible Euler equations is well-posed on $[0, T]$, for all initial data $\bar{\mathbf{u}} \in B_M^s$. In fact, by Sobolev embedding, there exists $T > 0$ such that the quantity (6.4.4) is finite. In particular, by Proposition 6.4.2, $\mathcal{S}_t^\Delta(\bar{\mathbf{u}}) \rightarrow \mathcal{S}_t(\bar{\mathbf{u}})$ converges to the unique solution for all initial data $\bar{\mathbf{u}} \in B_M^s$ and $t \in [0, T]$. From this point-wise convergence and the following uniform bound on the measurements

$$|\mathcal{L}^\Delta(\bar{\mathbf{u}})|_\Gamma = |\mathcal{G}(\mathcal{S}_t^\Delta(\bar{\mathbf{u}}))|_\Gamma \leq C\|\mathcal{S}_t^\Delta(\bar{\mathbf{u}})\|_{L_x^2}^2 \leq C\|\bar{\mathbf{u}}\|_{L_x^2}^2 \leq CM^2,$$

for all $\bar{\mathbf{u}} \in B_M^s$, it now follows from dominated convergence that

$$\|\mathcal{L}^\Delta(\bar{\mathbf{u}}) - \mathcal{L}(\bar{\mathbf{u}})\|_{L^2(\mu_{\text{prior}})} \rightarrow 0, \quad (\Delta \rightarrow 0).$$

In particular, by the consistency Theorem 6.2.14 for the BIP, it follows that the approximate posterior of the BIP $\mu^{\Delta, y} \rightarrow \mu^y$ converges wrt. to the 1-Wasserstein metric to the unique solution in the limit $\Delta \rightarrow 0$. Furthermore, by Theorem 6.2.9, the posteriors $\mu^{\Delta, y}$ are uniformly stable with respect to the measurements y (cp. equation (6.2.23)).

We next discuss the filtering problem. By Lemma 6.4.1, the SV scheme satisfies Assumption 6.3.3. Theorem 6.3.13 implies that the posteriors ν_t^y are uniformly stable with respect to the measurements y . Due to the pointwise convergence $\mathcal{S}_t^\Delta(\bar{\mathbf{u}}) \rightarrow \mathcal{S}_t(\bar{\mathbf{u}})$ for all $\bar{\mathbf{u}} \in B_M^s$ and the uniform bound

$$\|\mathcal{S}_t^\Delta(\bar{\mathbf{u}}) - \mathcal{S}_t(\bar{\mathbf{u}})\|_{L_x^2} \leq 2M,$$

Lebesgue's dominated convergence theorem implies that

$$\lim_{\Delta \rightarrow 0} \int_0^T \|\mathcal{S}_t^\Delta(\bar{\mathbf{u}}) - \mathcal{S}_t(\bar{\mathbf{u}})\|_{L^2(\mu_{\text{prior}})} dt = 0.$$

The consistency Theorem 6.3.19 therefore shows that $\nu_t^{\Delta, y} \rightarrow \nu_t^y$ in $L^1(\mathcal{P})$. \square

In the two-dimensional case, the above result can be improved:

Theorem 6.4.6. *If $\mu_{\text{prior}} \in \mathcal{P}(L_x^2)$ is a prior for the two-dimensional incompressible Euler equations, such that*

$$\int \|\operatorname{curl}(\bar{\mathbf{u}})\|_{L_x^\infty}^2 d\mu_{\text{prior}}(\bar{\mathbf{u}}) < \infty,$$

then the BIP and filtering problems for the incompressible Euler equations are well-posed and the numerical solutions converge as in the conclusion of Theorem 6.4.5 on $[0, T]$, for any $T > 0$.

Proof. The condition

$$\int \|\operatorname{curl}(\bar{\mathbf{u}})\|_{L_x^\infty}^2 d\mu_{\text{prior}}(\bar{\mathbf{u}}) < \infty,$$

implies that μ_{prior} is concentrated on Yudovich initial data. The strong convergence $\mathcal{S}_t^\Delta(\bar{\mathbf{u}}) \rightarrow \mathcal{S}_t(\bar{\mathbf{u}})$ to the unique Yudovich solution for such initial data $\bar{\mathbf{u}}$ has been shown in Proposition 6.4.3. The remainder of the proof follows verbatim as in the proof of Theorem 6.4.5. \square

The ill-posed case

Beyond the short-time existence, uniqueness and stability results for the incompressible Euler equations with smooth initial data there are currently no general a priori well-posedness results for the forward problem in the three-dimensional case. In the two-dimensional case, existence results are known for initial data with vorticity $\bar{\omega} \in L^p$, $p \geq 1$, as well as for less regular initial data with a essential sign restriction, of the form $\bar{\omega} = \bar{\omega}_0 + \bar{\omega}_1$, such that $\bar{\omega}_0 \in \mathcal{M}_+$, $\bar{\omega}_0 \geq 0$ a bounded Radon measure and $\bar{\omega}_1 \in L^1$ [Del91, VW93]. Uniqueness remains unknown for such rough flows beyond the class considered by Yudovich, even if $\bar{\omega} \in L^p$, for $p < \infty$.

Thus, the forward problem may be ill-posed for general initial data $u \in L_x^2$ for the incompressible Euler equations, in both two and three dimensions. Despite this possible lack of stability and compactness for the forward problem, the general results of Section 6.2 imply that the Bayesian inverse problem is stable with respect to measurements and compact in the 1-Wasserstein norm for approximations obtained from the SV scheme.

Theorem 6.4.7. *If $\mu_{\text{prior}} \in \mathcal{P}_1(L_x^2)$ is any prior for the incompressible Euler equations in either two or three dimensions, then the posteriors $\mu^{\Delta,y}$ of the BIP (6.2.3) for the incompressible Euler equations are uniformly stable in y , in the sense of (6.2.23), for any $\Delta > 0$. Furthermore, the posteriors $\mu^{\Delta,y}$ form a compact sequence in \mathcal{P}_1 , as $\Delta \rightarrow 0$.*

For the filtering problem, we have the following result:

Theorem 6.4.8. *If $\mu_{\text{prior}} \in \mathcal{P}_1(L_x^2)$ is a prior for the incompressible Euler equations for $d = 2$ or $d = 3$, then the approximate solutions $v_t^{\Delta,y}$ of the filtering problem computed by the SV scheme are uniformly stable with respect to the measurements y , in the sense of (6.3.21), for any $\Delta > 0$. In addition, if either*

- (a) *there exists a modulus of continuity such that*

$$S_2^T(\mathcal{S}_{t,\#}^\Delta \mu_{\text{prior}}; r) \leq \phi(r), \quad \forall \Delta > 0, r \geq 0,$$

or

- (b) *$d = 2$ and μ_{prior} satisfies*

$$\int \|\operatorname{curl}(\bar{\mathbf{u}})\|_{L_x^2}^2 d\mu_{\text{prior}}(\bar{\mathbf{u}}) < \infty,$$

then the posteriors $\nu_t^{\Delta, \mathbf{y}}$ form a compact sequence in $L_t^1(\mathcal{P})$.

Remark 6.4.9. Numerical evidence that assumption (a) of Theorem 6.4.8 is verified for a large range of priors supported on rough initial data, at least in the two-dimensional case, has been presented in [LMPP21b, LMPP21a].

Remark 6.4.10. We emphasize that the proof of the uniform local Lipschitz-stability

$$d_T\left(\nu_t^{\Delta, \mathbf{y}}, \nu_t^{\Delta, \mathbf{y}'}\right) \leq C|\mathbf{y} - \mathbf{y}'|_F,$$

has been rigorously established from a priori estimates, and is not conditional on any assumptions on the structure functions. We believe this stability result to be of particular importance to practitioners in data assimilation.

6.4.2 Incompressible Navier-Stokes

We consider the incompressible Navier-Stokes equations (cp. (1.2.3) in chapter 1), with viscosity $\nu > 0$. For simplicity we shall again focus on the case of periodic boundary conditions. It is well-known that in the two-dimensional case, the Navier-Stokes are well-posed on L_x^2 , for any fixed value of the viscosity $\nu > 0$ (cp. Theorem 1.3.13). In the three-dimensional case, it has been shown in the celebrated work of Leray [Ler34] that energy admissible solutions exist, but their uniqueness remains an open challenge. Again, we consider the numerical approximation by spectral methods, analogous to (6.4.2), leading now to the discretized system

$$\begin{cases} \partial_t \mathbf{u}^\Delta + \mathbb{P}_N(\mathbf{u}^\Delta \cdot \nabla \mathbf{u}^\Delta) = \nu \Delta \mathbf{u}^\Delta, \\ \operatorname{div}(\mathbf{u}^\Delta) = 0, \mathbf{u}^\Delta|_{t=0} = \mathbb{P}_N \bar{\mathbf{u}}. \end{cases} \quad (6.4.6)$$

Multiplying the first equation of (6.4.6) by \mathbf{u}^Δ and integrating over space and the time interval $[0, t]$, we find the a priori energy estimate

$$\frac{1}{2} \|\mathbf{u}^\Delta(t)\|_{L_x^2}^2 + \nu \int_0^t \|\nabla \mathbf{u}^\Delta\|_{L_x^2}^2 dt = \frac{1}{2} \|\mathbf{u}^\Delta(0)\|_{L_x^2}^2 \leq \frac{1}{2} \|\bar{\mathbf{u}}\|_{L_x^2}^2. \quad (6.4.7)$$

Furthermore, from (6.4.6), we have

$$\partial_t \mathbf{u}^\Delta = -\mathbb{P}_N \operatorname{div}(\mathbf{u}^\Delta \otimes \mathbf{u}^\Delta) + \nu \Delta \mathbf{u}^\Delta.$$

Due to the uniform L^2 -bound $\|\mathbf{u}^\Delta\|_{L_x^2} \leq \|\bar{\mathbf{u}}\|_{L_x^2}$, it is not hard to see that the terms on the right hand side are uniformly bounded in H_x^{-L} for sufficiently large $L > 0$, with an upper bound depending only on $\|\bar{\mathbf{u}}\|_{L_x^2}$ (cp. the corresponding derivation for the SV scheme on page 19). Thus, it follows that $\mathbf{u}^\Delta(t) = \mathcal{S}_t^\Delta(\bar{\mathbf{u}}) \in \operatorname{Lip}([0, T]; H_x^{-L})$ for some $L > 0$. In particular, we conclude that assumption 6.3.3 is satisfied for the spectral numerical approximants of the Navier-Stokes equations. Owing to the energy estimate (6.4.7), and in particular, the a priori estimate $\int_0^T \|\nabla \mathbf{u}\|_{L_x^2}^2 dt \leq \nu^{-1} \|\bar{\mathbf{u}}\|_{L_x^2}^2$, one can also show (cp. [LMW21, Lemma 5.12]):

Lemma 6.4.11. Let $\mu_{\text{prior}} \in \mathcal{P}(L_x^2)$ be a prior for the incompressible Navier-Stokes equations (7.3.5), such that $\int_{L_x^2} \|\bar{\mathbf{u}}\|_{L_x^2}^2 d\mu_{\text{prior}}(\bar{\mathbf{u}}) < \infty$. Let $\mathcal{S}_t^\Delta : L_x^2 \rightarrow L_x^2$ denote the approximate solution operator obtained from the spectral scheme (6.4.6). Then we have the following structure function estimate:

$$S_2^T(\mathcal{S}_{t,\#}^\Delta \mu_{\text{prior}}; r) \leq \frac{r}{\sqrt{2\nu}} \left(\int_{L_x^2} \|\bar{\mathbf{u}}\|_{L_x^2}^2 d\mu_{\text{prior}}(\bar{\mathbf{u}}) \right)^{1/2}.$$

In particular, $S_2^T(\mathcal{S}_{t,\#}^\Delta \mu_{\text{prior}}; r) \leq Cr$ is uniformly bounded by a modulus of continuity as $\Delta \rightarrow 0$.

As a result of these a priori estimates for the incompressible Navier-Stokes equations and the general compactness results for Bayesian inverse problems derived in the present work, we can now state:

Theorem 6.4.12. *If $\mu_{\text{prior}} \in \mathcal{P}_1(L_x^2)$ is any prior for the incompressible Navier-Stokes equations with viscosity $\nu > 0$, then the posteriors $\mu^{\Delta,y}$ of the BIP (6.2.3) are uniformly stable in y , in the sense of (6.2.23), for any $\Delta > 0$. Furthermore, the posteriors $\mu^{\Delta,y}$ form a compact sequence in \mathcal{P}_1 and any limit point $\mu^{*,y}$ is absolutely continuous with respect to the prior μ_{prior} .*

For the filtering problem, we obtain the following result:

Theorem 6.4.13. *If $\mu_{\text{prior}} \in \mathcal{P}_1(L_x^2)$ is a prior for the incompressible Navier-Stokes equations (7.3.5) with fixed viscosity $\nu > 0$ (for $d = 2$ or $d = 3$), and if μ_{prior} has finite second moment*

$$\int \|\bar{\mathbf{u}}\|_{L_x^2}^2 d\mu_{\text{prior}}(\bar{\mathbf{u}}) < \infty,$$

then the approximate solutions $\nu_t^{\Delta,y}$ of the filtering problem for the Navier-Stokes equations computed by the spectral scheme (6.4.6) are uniformly stable with respect to the measurements y , in the sense of (6.3.21) and the posteriors $\nu_t^{\Delta,y}$ form a compact sequence in $L_t^1(\mathcal{P}_1)$.

6.5 Discussion

Inverse problems are usually considered for models with a well-posed forward problem, for which existence, uniqueness and stability can be shown. However, *ill-posed* forward PDEs arise in a wide variety of contexts of central importance to physics and engineering, including turbulent dynamics encountered in fluid dynamics, oceanography and meteorology. For many of the PDEs encountered in this context, proofs of existence and uniqueness, or indeed stability, of the forward problem are still unresolved issues. Intimately related to these many outstanding problems in analysis are open questions in the numerical approximation of solutions for such PDEs. Indeed, from the numerical point of view, many models in fluid dynamics are known to exhibit a very strong sensitivity to perturbations in the initial data, and thus cannot be stably approximated, at least in a deterministic sense. As shown in a number of numerical experiments [FKMT17, FLMW20, GGL⁺01, LM15, Leo18, LMPP21b], as well as in chapters 2 and 3 of the present thesis, the high sensitivity and the formation of ever smaller scales due to turbulence precludes the convergence of state-of-the-art numerical schemes to a limiting solution upon mesh refinement. The observed lack of convergence of numerical approximants could be termed as a *practical ill-posedness*, *i.e.* the convergence of numerical approximations is not observed (at presently attainable mesh sizes).

Due to the importance of inverse problems in engineering and physics, and confronted with the practical ill-posedness of the forward problem for many models, it is then natural to ask, whether the numerical approximation of the inverse or data assimilation problem suffers from a similar ill-posedness. Of particular relevance in this context are the general stability properties with respect to perturbations in the measurements and the compactness and convergence properties of numerical approximations. In the present work, we have investigated these questions from the point of view of Bayesian inverse problems. While several general results for abstract Bayesian inverse problems were discussed in Section 6.2, a particular focus and the main motivation for the present work stem from the data assimilation (filtering) problem in the context of fluid mechanics, presented in Section 6.3.

For the numerical approximation of the abstract Bayesian inverse problem in the limit of infinite mesh refinement $\Delta \rightarrow 0$, the main results of this work concern the approximate posteriors $\mu^{\Delta,y}$ at grid size $\Delta > 0$ with finite-dimensional measurement y . We prove:

- (stability) uniform in $\Delta > 0$ stability of $\mu^{\Delta,y}$ with respect to the measurements y in the 1-Wasserstein norm,
- (compactness) compactness of the approximate solution sequence $\{\mu^{\Delta,y}\}_{\Delta>0}$ in the space of probability measures $\mathcal{P}_1(X)$ with respect to the Wasserstein norm,
- (consistency) convergence in $\mathcal{P}_1(X)$ to the canonical posterior $\mu^{*,y}$, provided that the observables converge in an average L^2 -sense.

All of these results are obtained under only mild boundedness assumptions on the approximate observables and on the measurement noise (*e.g.* satisfied by Gaussian noise). The general compactness properties allow us to define a set of candidate solutions to the BIP, generated by the numerical scheme. As this set can be shown to be non-empty a priori, this potentially opens up the possibility of identifying the correct solution among these candidates by a suitable selection criterion (cf. Remark 6.2.13).

Building upon these general considerations for the abstract BIP, a derivation of similar stability, compactness and consistency properties for the filtering problem has been given in Section 6.3. In this case, the approximate posterior measures $t \mapsto \mu_t^{\Delta,y}$ are time-dependent, and are updated at discrete times to incorporate information obtained from measurements. In contrast to the abstract BIP, the filtering problem as formulated in Section 6.3 involves a recursive process, alternating between evolving the current posterior to the next discrete time step, where it serves as a prior for the new measurements, and using the new measurements to obtain the next posterior. In a suitable space of time-parametrized probability measures, we show that a similar uniform stability result with respect to the measurements as for the abstract BIP also holds for this formulation of the filtering problem. Perhaps astonishingly, even though perturbations to the measurement y perturb $\mu_{t_i}^{\Delta,y}$ at each time-step and the filtering problem involves a successive application of a push-forward $\mathcal{S}_{t,\#}^{\Delta} \mu_{t_i}^{\Delta,y}$ by the discretized solution operator \mathcal{S}_t^{Δ} , our stability result holds under a mere boundedness assumption on \mathcal{S}_t^{Δ} , and *does not require* any uniform continuity of the mapping $\mu \mapsto \mathcal{S}_t^{\Delta} \mu$. In practice, the boundedness assumption usually corresponds to a discrete energy or entropy inequality, which is satisfied by suitably designed numerical schemes. In addition to this general stability result, we prove compactness of the approximate solution sequence $\mu_t^{\Delta,y}$ for the filtering problem, under the assumption of a uniform bound on the second-order structure function. The structure function measures two point-correlations in the flow, and is a very natural quantity in the study of turbulence. If the solution of the forward problem possesses unique solutions almost surely with respect to the prior, then we prove that the numerically obtained solutions of the filtering problem (obtained by a consistent numerical scheme) converge to expected canonical solution of the filtering problem.

The applicability of the abstract results of sections 6.2 and 6.3 to the numerical approximation of Bayesian inverse problems encountered in practice is discussed in Section 6.4. We consider two model problems: the incompressible Euler equations (in 2d and 3d) and the incompressible Navier-Stokes equations (in 3d). For the incompressible Euler equations, we consider the numerical approximation by spectral schemes and verify the sufficient conditions for stability, compactness and consistency by a priori analysis for a class of priors in 2d. In 3d, the general stability and consistency properties continue to hold by the same a priori considerations; the compactness property holds under the additional assumption of a physically motivated bound on the structure functions. For the incompressible Navier-Stokes equations (in 3d), we prove the conditions for stability and compactness by a priori analysis, for numerical solutions obtained by spectral schemes. We point out that numerical evidence that the required bound on the structure function holds, has been demonstrated by numerical experiments for a number initial priors in [FLMW20, LMPP21b, LMPP21a], and is further motivated by physical considerations.

The (partial) well-posedness results in the context of Bayesian inversion presented in this work, even for models for which the forward problem may be ill-posed, have been derived under mild assumptions

and are applicable to a wide range of models encountered in practice. The stability results should be of particular significance to practitioners, as they demonstrate that under mild conditions on the numerical scheme, the approximate solutions of the BIP and data assimilation problems are stable with respect to perturbations of the measurements, *independently of the numerical resolution*. The general compactness results presented in this work could be of importance in determining suitable selection criteria to single out a “canonical” posterior amongst the set of candidate solutions.

Chapter 7

Surrogate models and operator learning for fluid flows

In the previous chapter, we have discussed a Bayesian approach to state estimation, and have shown that this approach exhibits remarkable robustness and stability properties, even under very minimal assumptions on the underlying forward model. In the time-dependent setting, this approach combines measurement data with prior (domain) knowledge specified via the prior $\mu_{\text{prior}} \in \mathcal{P}(L_x^2)$, to provide an estimate of the current state of the physical system at time t in the form of a probability measure $\nu_t^y \in \mathcal{P}(L_x^2)$ (the filtering distribution). In practice, computing relevant statistical quantities from this probability measure ν_t^y is a difficult task, requiring many (costly) forward solves of the underlying model when employing Markov chain Monte-Carlo methods. In large-scale fluid dynamics applications such as weather prediction and climate science, the high computational cost often rules out a principled Bayesian approach to state estimation, at present. To overcome these present limitations, a new approach to many query problems, employing neural network based surrogate models has recently been proposed by a number of authors [LJK19, BHKS21, LKA⁺20, LKA⁺21]. In this approach, suitable neural network architectures have been proposed to approximate *operators*, such as the solution operator of a PDE. In this context, the task of approximating an operator is referred to as “operator learning”. Numerical experiments have shown empirically that the resulting “neural operator networks” can be successfully trained to approximate operators arising in a variety of contexts, including Darcy flow [BHKS21], the Navier-Stokes equations [LKA⁺21], high-speed boundary layers [DLLM⁺21], electro-convection [CWL⁺21] and hypersonics applications [MLM⁺20]. Neural operator networks are thus promising candidates to complement more traditional numerical methods in the form of surrogate models in many-query problems such as Bayesian data assimilation. The problem is here split into an (expensive) offline phase, where a conventional numerical solver is used to generate data and the neural operator is trained, and a (cheap) online phase, where the trained neural operator is used for the sampling of the posterior. First numerical results based on such a surrogate model approach have been reported in [LKA⁺21], considering the 2D Navier-Stokes equations as a model problem. The results based on the surrogate were shown to have comparable accuracy to results obtained with a spectral solver. However, the online phase of the computation via the surrogate model was orders of magnitude (x500) faster than the spectral solver. In fact, even including the offline training phase, the surrogate approach was found to significantly speed up the computation. In the present chapter, we will discuss first results on the *theoretical foundations* of the surrogate model approach proposed in [LKA⁺21]. This chapter is based on the recent work [KLM21].

7.1 Introduction

Deep neural networks have been extremely successful in diverse fields of science and engineering including image classification, speech recognition, natural language understanding, autonomous systems, game intelligence and protein folding, [LBH15] and references therein. Moreover, deep neural networks are being increasingly used successfully in scientific computing, particular in simulating physical and engineering systems modeled by partial differential equations (PDEs). Examples include the use of physics informed neural networks [RK18, RPK19, MM20a, MM20b] for solving forward and inverse problems for PDEs and supervised learning algorithms for high-dimensional parabolic PDEs [EHJ17] and parametric elliptic [KPS19, SZ19] and hyperbolic [LMR20, LMCR20] PDEs, among others.

The success of deep neural networks at a wide variety of learning tasks can be attributed to a confluence of several factors such as the availability of massive labeled data sets, the design of novel architectures and training algorithms as well as the abundance of high-end computing platforms such as GPUs [GBC16]. Still, it is fair to surmise that this edifice of success partly rests on the foundation of *universal approximation* [Bar93, Cyb89, HSW89], *i.e.*, the ability of neural networks to approximate any continuous (even measurable) function, mapping a finite-dimensional input space into another finite-dimensional output space, to arbitrary accuracy.

However, many interesting learning tasks entail learning *operators* *i.e.*, mappings between an infinite-dimensional input Banach space and (possibly) an infinite-dimensional output space. A prototypical example in scientific computing is provided by nonlinear operators that map the initial datum into the (time series of) solution of a nonlinear time-dependent PDE such as the Navier-Stokes equations of fluid dynamics. *A priori*, it is unclear if neural networks can be successfully employed for learning such operators from data, given that their universality only pertains to finite-dimensional functions.

The first successful use of neural networks in the context of such *operator learning* was provided in [CC95], where the authors proposed a novel neural network based learning architecture, which they termed as *operator networks* and proved that these operator networks possess a surprising universal approximation property for infinite-dimensional nonlinear operators. Operator networks are based on two different neural networks, a *branch net* and a *trunk net*, which are trained concurrently to learn from data. More recently, the authors of [LJK19] have proposed using deep, instead of shallow, neural networks in both the trunk and branch net and have christened the resulting architecture as a *DeepOnet*. In a recent article [LMK21], the universal approximation property of DeepOnets was extended, making it completely analogous to universal approximation results for finite-dimensional functions by neural networks. The authors of [LMK21] were also able to show that DeepOnets can break the curse of dimensionality for a large variety of PDE learning tasks. Hence, in spite of the underlying infinite-dimensional setting, DeepOnets are capable to approximating a large variety of nonlinear operators efficiently. This is further validated by the success of DeepOnets in many interesting examples in scientific computing [MLM⁺20, CWL⁺21, LLL⁺21] and references therein.

An alternative operator learning framework is provided by the concept of *neural operators*, first proposed in [AAB⁺20]. Just as canonical artificial neural networks are a concatenated composition of multiple hidden layers, with each hidden layer composing an affine function with a scalar nonlinear activation function, neural operators also compose multiple hidden layers, with each hidden layer composing an affine *operator* with a local, scalar nonlinear activation operator. The infinite-dimensional setup is reflected in the fact that the affine operator can be significantly more general than in the finite-dimensional case, where it is represented by a weight matrix and bias vector. On the other hand, for neural operators, one can even use *non-local* linear operators, such as those defined in terms of an integral kernel. The evaluation of such integral kernels can be performed either with graph kernel networks [AAB⁺20] or with multipole expansions [LKA⁺20].

More recently, the authors of [LKA⁺21] have proposed using convolution-based integral kernels within neural operators. Such kernels can be efficiently evaluated in the Fourier space, leading to the resulting neural operators being termed as *Fourier Neural Operators* (FNOs). In [LKA⁺21], the authors discuss the advantages, in terms of computational efficiency, of FNOs over the other neural operators mentioned above. Moreover, they present several convincing numerical experiments to demonstrate that FNOs can very efficiently approximate a variety of operators that arise in simulating PDEs.

However, the theoretical basis for neural operators has not yet been properly investigated. In particular, it is unclear if neural operators such as FNOs are *universal* *i.e.*, if they can approximate a large class of nonlinear infinite-dimensional operators. Moreover in this infinite-dimensional setting, universality does not suffice to indicate computational viability or efficiency as the size of the underlying neural networks might grow exponentially with respect to increasing accuracy, see discussion in [LMK21] on this issue. Hence in addition to universality, it is natural to ask if neural operators can *efficiently* approximate a large class of operators, such as those arising in the simulation of parametric PDEs.

The investigation of these questions is the main rationale for the work summarized in the current chapter. We focus our attention here on FNOs as they appear to be the most promising of the neural operator based operator learning frameworks. The main result of this work is to show that FNOs are *universal* in possessing the ability to approximate a very large class of continuous nonlinear operators. This result highlights the potential of FNOs in operator learning.

As argued before, a universality result is only a first step and by itself, does not constitute evidence for efficient approximation by FNOs. In fact, we show that in the worst case, the network size might grow exponentially with respect to accuracy, when approximating general operators. Hence, there is a need to derive explicit bounds on the network size in terms of the desired error tolerance. In this context, we consider a concrete computational realization of FNOs, that we term as *pseudospectral FNO* or Ψ -FNO (for short). In addition to proving universality for Ψ -FNOs, we will suggest a mechanism through which Ψ -FNOs can approximate operators arising from PDEs, efficiently. We also derive explicit error bounds for this architecture in approximating PDEs: the incompressible Navier-Stokes and Euler equations of fluid dynamics. In particular, we prove that the size of Ψ -FNOs in approximating the underlying operators for both these PDEs, under suitable regularity hypotheses, only scales polynomially (log-linearly) in the error. A similar analysis for another PDE, the stationary Darcy flow equations can be found in [KLM21]. Thus, FNOs can approximate these operators efficiently and these results validate some of the computational findings of [LKA⁺21]. Together, these results constitute the first theoretical justification for the use of FNOs.

The rest of this chapter is organized as follows: in section 7.2, we introduce FNOs and state the universality result. We also introduce Ψ -FNOs in this section. In section 7.3, we show that Ψ -FNOs can efficiently approximate operators, stemming from the incompressible Navier-Stokes and Euler equations. In section 7.4, we will provide a rationale for the use of (Ψ)-FNOs in the approximation of statistical solutions. Since the contents of the present chapter concern neural networks and hence are somewhat distinct from the remainder of this thesis, we refer the reader to Appendix A, where the notation employed in the current chapter is reviewed in detail, and the list of mathematical symbols on page 175, for a handy reference.

7.2 Approximation by Fourier Neural Operators

In this section, we present Fourier Neural Operators (FNOs) and discuss their approximation of a class of nonlinear operators specified below:

7.2.1 Setting for Operator Learning

Setting 7.2.1. We fix a spatial dimension $d \in \mathbb{N}$, and denote by $D \subset \mathbb{R}^d$ a domain in \mathbb{R}^d . We consider the approximation of operators $\mathcal{G} : \mathcal{A}(D; \mathbb{R}^{d_a}) \rightarrow \mathcal{U}(D; \mathbb{R}^{d_u})$, $a \mapsto u := \mathcal{G}(a)$, where the input $a \in \mathcal{A}(D; \mathbb{R}^{d_a})$, $d_a \in \mathbb{N}$, is a function $a : D \rightarrow \mathbb{R}^{d_a}$ with d_a components, and the output $u \in \mathcal{U}(D; \mathbb{R}^{d_u})$, $d_u \in \mathbb{N}$, is a function $u : D \rightarrow \mathbb{R}^{d_u}$ with d_u components. Here $\mathcal{A}(D; \mathbb{R}^{d_a})$ and $\mathcal{U}(D; \mathbb{R}^{d_u})$ are Banach spaces (or suitable subsets of Banach spaces). Typical examples of \mathcal{A} and \mathcal{U} include the space of continuous functions $C(D; \mathbb{R}^{d_u})$, or Sobolev spaces $H^s(D; \mathbb{R}^{d_u})$ of order $s \geq 0$ (see Appendix A for definitions.).

Concrete examples for operators \mathcal{G} , involving solution operators of PDEs, are given in section 7.3.

7.2.2 Neural Operators

With the above setting 7.2.1 and as defined in [AAB⁺20], a neural operator $\mathcal{N} : \mathcal{A}(D; \mathbb{R}^{d_a}) \rightarrow \mathcal{U}(D; \mathbb{R}^{d_u})$, $a \mapsto \mathcal{N}(a)$ is a mapping of the form

$$\mathcal{N}(a) = \mathcal{Q} \circ \mathcal{L}_L \circ \mathcal{L}_{L-1} \circ \cdots \circ \mathcal{L}_1 \circ \mathcal{R}(a),$$

for a given depth $L \in \mathbb{N}$, where $\mathcal{R} : \mathcal{A}(D; \mathbb{R}^{d_a}) \rightarrow \mathcal{U}(D; \mathbb{R}^{d_v})$, $d_v \geq d_u$, is a *lifting* operator (acting locally), of the form

$$\mathcal{R}(a)(x) = Ra(x), \quad R \in \mathbb{R}^{d_v \times d_a}, \tag{7.2.1}$$

and $\mathcal{Q} : \mathcal{U}(D; \mathbb{R}^{d_v}) \rightarrow \mathcal{U}(D; \mathbb{R}^{d_u})$ is a local *projection* operator, of the form

$$\mathcal{Q}(v)(x) = Qv(x), \quad Q \in \mathbb{R}^{d_u \times d_v}. \tag{7.2.2}$$

Remark 7.2.2. In practice, it has been found that improved results can be obtained if the simple linear lifting and projection operators \mathcal{R} (7.2.1) and \mathcal{Q} (7.2.2) are replaced instead by non-linear mappings of the form

$$\widehat{\mathcal{R}}(a)(x) = \widehat{R}(a(x), x), \quad \widehat{\mathcal{Q}}(v)(x) = \widehat{Q}(v(x), x),$$

where $\widehat{R} : \mathbb{R}^{d_a} \times D \rightarrow \mathbb{R}^{d_v}$ and $\widehat{Q} : \mathbb{R}^{d_v} \times D \rightarrow \mathbb{R}^{d_u}$ are neural networks with activation function σ . Our error estimates will rely on the (more restrictive) linear choice of lifting and projection operators, given by (7.2.1), (7.2.2). The linear choice has the theoretical benefit of ensuring compositionality, i.e. that a composition of neural operators can again be represented by a neural operator (cf. [KLM21, Lemma D.4]). Despite this technical distinction, we emphasize that all of our error and complexity estimates continue to hold also for neural operators with non-linear lifting and projections, since linear operators can always be approximated by non-linear ones (cp. [KLM21, Lemma C.1]). In fact, in the non-linear case, our results imply that \widehat{Q} , \widehat{R} can be chosen to be shallow networks.

In analogy with canonical finite-dimensional neural networks, the layers $\mathcal{L}_1, \dots, \mathcal{L}_L$ are non-linear operator layers, $\mathcal{L}_\ell : \mathcal{U}(D; \mathbb{R}^{d_v}) \rightarrow \mathcal{U}(D; \mathbb{R}^{d_v})$, $v \mapsto \mathcal{L}_\ell(v)$, which we assume to be of the form

$$\mathcal{L}_\ell(v)(x) = \sigma \left(W_\ell v(x) + b_\ell(x) + (\mathcal{K}(a; \theta_\ell)v)(x) \right), \quad \forall x \in D.$$

Here, the weight matrix $W_\ell \in \mathbb{R}^{d_v \times d_v}$ and bias $b_\ell(x) \in \mathcal{U}(D; \mathbb{R}^{d_v})$ define an affine pointwise mapping $W_\ell v(x) + b_\ell(x)$. The richness of linear operators in the infinite-dimensional setting can partly be realized by defining the following *non-local* linear operator,

$$\mathcal{K} : \mathcal{A} \times \Theta \rightarrow L(\mathcal{U}(D; \mathbb{R}^{d_v}), \mathcal{U}(D; \mathbb{R}^{d_v})),$$

that maps the input field a and a parameter $\theta \in \Theta$ in the parameter-set Θ to a bounded linear operator $\mathcal{K}(a, \theta) : \mathcal{U}(D; \mathbb{R}^{d_v}) \rightarrow \mathcal{U}(D; \mathbb{R}^{d_v})$, and the non-linear activation function $\sigma : \mathbb{R} \rightarrow \mathbb{R}$ is applied component-wise. As proposed in [AAB⁺20], the linear operators $\mathcal{K}(a, \theta)$ are integral operators of the form

$$(\mathcal{K}(a; \theta)v)(x) = \int_D \kappa_\theta(x, y; a(x), a(y))v(y) dy, \quad \forall x \in D. \quad (7.2.3)$$

Here, the integral kernel $\kappa_\theta : \mathbb{R}^{2(d+d_a)} \rightarrow \mathbb{R}^{d_v \times d_v}$ is a neural network parametrized by $\theta \in \Theta$. Specific examples of the integral kernel (7.2.3) include those evaluated with a graph kernel network as in [AAB⁺20] or with a multipole expansion [LKA⁺20].

7.2.3 Fourier Neural Operators

As defined in [LKA⁺21], Fourier Neural operators (FNOs) are special cases of general neural operators (7.2.3), in which the kernel $\kappa_\theta(x, y; a(x), a(y))$ is of the form $\kappa_\theta = \kappa_\theta(x - y)$. In this case, (7.2.3) can be written as a convolution

$$(\mathcal{K}(\theta)v)(x) = \int_D \kappa_\theta(x - y)v(y) dy, \quad \forall x \in D. \quad (7.2.4)$$

For concreteness, we consider the periodic domain $D = \mathbb{T}^d$ (which we identify with the standard torus $\mathbb{T}^d = [0, 2\pi]^d$), although non-periodic, rectangular domains D can also be handled in a straightforward manner.

Given this periodic framework, the convolution operator in (7.2.4) can be computed using the Fourier transform \mathcal{F} and the inverse Fourier transform \mathcal{F}^{-1} (see Appendix A (A.1.1) and (A.1.2) for notation and definitions), resulting in the following equivalent representation of the kernel (7.2.3),

$$(\mathcal{K}(\theta)v)(x) = \mathcal{F}^{-1}\left(P_\theta(k) \cdot \mathcal{F}(v)(k)\right)(x), \quad \forall x \in \mathbb{T}^d. \quad (7.2.5)$$

Here, $P_\theta(k) \in \mathbb{C}^{d_v \times d_v}$ is a full matrix indexed by $k \in \mathbb{Z}^d$, and is related to the integral kernel $\kappa_\theta(x)$ in (7.2.4) via the Fourier transform, $P_\theta(k) = \mathcal{F}(\kappa_\theta)(k)$. Note that we must impose that $P_\theta(-k) = P_\theta(k)^\dagger$ coincides with the Hermitian transpose for all $k \in \mathbb{Z}^d$, to ensure that the image function $(\mathcal{K}(\theta)v)(x)$ is a real-valued function for real-valued $v(x)$. Consequently, the form of Fourier neural operators (FNOs) for the periodic domain \mathbb{T}^d is that of a mapping $\mathcal{N} : \mathcal{A}(D; \mathbb{R}^{d_a}) \rightarrow \mathcal{U}(D; \mathbb{R}^{d_u})$, of the form

$$\mathcal{N}(a) := \mathcal{Q} \circ \mathcal{L}_L \circ \mathcal{L}_{L-1} \circ \cdots \circ \mathcal{L}_1 \circ \mathcal{R}(a), \quad (7.2.6)$$

where the lifting and projection operators \mathcal{R} and \mathcal{Q} are given by (7.2.1) and (7.2.2), respectively, and where the non-linear layers \mathcal{L}_ℓ are of the form

$$\mathcal{L}_\ell(v)(x) = \sigma\left(W_\ell v(x) + b_\ell(x) + \mathcal{F}^{-1}\left(P_\ell(k) \cdot \mathcal{F}(v)(k)\right)(x)\right). \quad (7.2.7)$$

Here, $W_\ell \in \mathbb{R}^{d_v \times d_v}$ and $b_\ell(x)$ define a pointwise affine mapping (corresponding to weights and biases), and $P_\ell : \mathbb{Z}^d \rightarrow \mathbb{C}^{d_v \times d_v}$ defines the coefficients of a non-local, linear mapping via the Fourier transform.

Remark 7.2.3. *The simplest example for a FNO, as defined by (7.2.6),(7.2.4) is as follows; let $\widehat{\mathcal{N}} : \mathbb{R}^{d_a} \rightarrow \mathbb{R}^{d_u}$ be a canonical finite-dimensional neural network with activation function σ . We can associate to $\widehat{\mathcal{N}}$ the mapping $\mathcal{N} : L^2(\mathbb{T}^d; \mathbb{R}^{d_a}) \rightarrow L^2(\mathbb{T}^d; \mathbb{R}^{d_u})$, given by $a(x) \mapsto \widehat{\mathcal{N}}(a(x))$. We easily observe that \mathcal{N} is a FNO as we can write it in the form,*

$$\widehat{\mathcal{N}} = \widehat{\mathcal{Q}} \circ \widehat{\mathcal{L}}_L \circ \cdots \circ \widehat{\mathcal{L}}_1 \circ \widehat{\mathcal{R}},$$

where $\widehat{\mathcal{R}}(y) = Ry$ with $R \in \mathbb{R}^{d_v \times d_a}$, and each layer $\widehat{\mathcal{L}}_\ell$ is of the form $\widehat{\mathcal{L}}_\ell(y) = \sigma(W_\ell y + b_\ell)$ for some $W_\ell \in \mathbb{R}^{d_v \times d_v}$, $b_\ell \in \mathbb{R}^{d_v}$, with $\widehat{\mathcal{Q}}$ being an affine output layer of the form $\widehat{\mathcal{Q}}(y) = Qy + q$ with $Q \in \mathbb{R}^{d_u \times d_v}$, $q \in \mathbb{R}^{d_u}$. Replacing the input y by a function $v(x)$, these layers clearly are a special case of the FNO lifting layer (7.2.1), the non-linear layers (7.2.7) (with $P_\ell \equiv 0$ and constant bias $b_\ell(x) \equiv b_\ell$), and the projection layer (7.2.2). Thus, any finite-dimensional neural network can be identified with a FNO as defined above.

For the remainder of this work, we make the following

Assumption 7.2.4 (Activation function). *Unless explicitly stated otherwise, the activation function $\sigma : \mathbb{R} \rightarrow \mathbb{R}$ in (7.2.7) is assumed to be non-polynomial, (globally) Lipschitz continuous and $\sigma \in C^3$.*

7.2.4 Universal Approximation by FNOs

Next, we will show that FNOs (7.2.6) are *universal* i.e., given a large class of operators, as defined in setting 7.2.1, one can find an FNO that approximates it to desired accuracy. To be more precise, we have the following theorem,

Theorem 7.2.5 (Universal approximation). *Let $s, s' \geq 0$. Let $\mathcal{G} : H^s(\mathbb{T}^d; \mathbb{R}^{d_a}) \rightarrow H^{s'}(\mathbb{T}^d; \mathbb{R}^{d_u})$ be a continuous operator. Let $K \subset H^s(\mathbb{T}^d; \mathbb{R}^{d_a})$ be a compact subset. Then for any $\epsilon > 0$, there exists a FNO $\mathcal{N} : H^s(\mathbb{T}^d; \mathbb{R}^{d_a}) \rightarrow H^{s'}(\mathbb{T}^d; \mathbb{R}^{d_u})$, of the form (7.2.6), continuous as an operator $H^s \rightarrow H^{s'}$, such that*

$$\sup_{a \in K} \|\mathcal{G}(a) - \mathcal{N}(a)\|_{H^{s'}} \leq \epsilon.$$

Sketch of proof. The detailed proof of this universal approximation theorem is provided in [KLM21, Thm. 2.5]. We only provide an outline here. For notational simplicity, we set $d_a = d_u = 1$, and first observe the following lemma, proved in [KLM21, Appendix D.1]:

Lemma 7.2.6. *Assume that the universal approximation Theorem 7.2.5 holds for $s' = 0$. Then it holds for arbitrary $s' \geq 0$.*

The main objective is thus to prove Theorem 7.2.5 for the special case $s' = 0$; i.e. given a continuous operator $\mathcal{G} : H^s(\mathbb{T}^d) \rightarrow L^2(\mathbb{T}^d)$, $K \subset H^s(\mathbb{T}^d)$ compact, and $\epsilon > 0$, we wish to construct a FNO $\mathcal{N} : H^s(\mathbb{T}^d) \rightarrow L^2(\mathbb{T}^d)$, such that $\sup_{a \in K} \|\mathcal{G}(a) - \mathcal{N}(a)\|_{L^2} \leq \epsilon$.

To this end, we start by defining the following operator,

$$\mathcal{G}_N : H^s(\mathbb{T}^d) \rightarrow L^2(\mathbb{T}^d), \quad \mathcal{G}_N(a) := P_N \mathcal{G}(P_N a), \quad (7.2.8)$$

with P_N being the orthogonal Fourier projection operator onto Fourier modes $|k|_\infty \leq N$. Thus, \mathcal{G}_N can be thought of loosely as the *Fourier projection* of the continuous operator \mathcal{G} .

Next, we can show that for any given $\epsilon > 0$, there exists $N \in \mathbb{N}$, such that

$$\|\mathcal{G}(a) - \mathcal{G}_N(a)\|_{L^2} \leq \epsilon, \quad \forall a \in K. \quad (7.2.9)$$

Thus, the proof boils down to finding a FNO (7.2.6) that can approximate the operator \mathcal{G}_N to any desired accuracy.

To this end, we introduce a set of Fourier wavenumbers $k \in \mathcal{K}_N$, by

$$\mathcal{K}_N := \{k \in \mathbb{Z}^d \mid |k|_\infty \leq N\}, \quad (7.2.10)$$

and define a *Fourier conjugate* or *Fourier dual* operator of the form $\widehat{\mathcal{G}}_N : \mathbb{C}^{\mathcal{K}_N} \rightarrow \mathbb{C}^{\mathcal{K}_N}$,

$$\widehat{\mathcal{G}}_N(\widehat{a}_k) := \mathcal{F}_N (\mathcal{G}_N (\text{Re} (\mathcal{F}_N^{-1}(\widehat{a}_k)))) , \quad (7.2.11)$$

such that the identity

$$\mathcal{G}_N(a) = \mathcal{F}_N^{-1} \circ \widehat{\mathcal{G}}_N \circ \mathcal{F}_N(P_N a), \quad (7.2.12)$$

holds for all *real-valued* $a \in L^2(\mathbb{T}^d)$. Here, \mathcal{F}_N is the discrete Fourier transform and \mathcal{F}_N^{-1} is the discrete inverse Fourier transform.

The next steps in the proof are to leverage the natural decomposition of the projection \mathcal{G}_N in (7.2.12) in terms of the discrete Fourier transform $\mathcal{F}_N \circ P_N$, the discrete inverse Fourier transform \mathcal{F}_N^{-1} and the Fourier conjugate operator $\widehat{\mathcal{G}}_N$ and approximate each of these operators by Fourier neural operators.

We start by denoting,

$$\mathbb{R}^{2\mathcal{K}_N} = (\mathbb{R}^2)^{\mathcal{K}_N} (\simeq \mathbb{C}^{\mathcal{K}_N}), \quad (7.2.13)$$

as the set consisting of coefficients $\{(v_{1,k}, v_{2,k})\}_{k \in \mathcal{K}_N}$, where $v_{\ell,k} \in \mathbb{R}$ are indexed by a tuple (ℓ, k) , $\ell \in \{1, 2\}$, $k \in \mathcal{K}_N$, and interpreting the operator $\mathcal{F}_N \circ P_N$ as a mapping $\mathcal{F}_N \circ P_N : a \mapsto \{(\text{Re}(\widehat{a}_k), \text{Im}(\widehat{a}_k))\}_{|k| \leq N}$, with input $a \in L^2(\mathbb{T}^d)$ and the output $\{\text{Re}(\widehat{a}_k), \text{Im}(\widehat{a}_k)\}_{|k| \leq N} \in \mathbb{R}^{2\mathcal{K}_N}$ is viewed as a *constant* function in $L^2(\mathbb{T}^d; \mathbb{R}^{2\mathcal{K}_N})$. The approximation of this operator is a straightforward consequence of the following Lemma, proved in [KLM21, Appendix D.2],

Lemma 7.2.7. *Let $B > 0$ and $N \in \mathbb{N}$ be given. For all $\epsilon > 0$, there exists a FNO $\mathcal{N} : L^2(\mathbb{T}^d) \rightarrow L^2(\mathbb{T}^d; \mathbb{R}^{2\mathcal{K}_N})$, $v \mapsto \{\mathcal{N}(v)_{\ell,k}\}$, with constant output functions (constant as a function of $x \in \mathbb{T}^d$), and such that*

$$\left. \begin{aligned} \|\text{Re}(\widehat{v}_k) - \mathcal{N}(v)_{1,k}\|_{L^\infty} &\leq \epsilon \\ \|\text{Im}(\widehat{v}_k) - \mathcal{N}(v)_{2,k}\|_{L^\infty} &\leq \epsilon \end{aligned} \right\} \quad \forall k \in \mathbb{Z}^d, |k|_\infty \leq N,$$

for all $\|v\|_{L^2} \leq B$, and where $\widehat{v}_k \in \mathbb{C}$ denotes the k -th Fourier coefficient of v .

In the next step, we approximate the (discrete) inverse Fourier transform \mathcal{F}_N^{-1} by an FNO. We recall that FNOs act on functions rather than on constants. Therefore, to connect \mathcal{F}_N^{-1} and FNOs, we are going to interpret the mapping

$$\mathcal{F}_N^{-1} : [-R, R]^{2\mathcal{K}_N} \subset \mathbb{R}^{2\mathcal{K}_N} \rightarrow L^2(\mathbb{T}^d),$$

as a mapping

$$\mathcal{F}_N^{-1} : \begin{cases} L^2(\mathbb{T}^d; [-R, R]^{2\mathcal{K}_N}) \rightarrow L^2(\mathbb{T}^d), \\ \{\text{Re}(\widehat{v}_k), \text{Im}(\widehat{v}_k)\}_{|k| \leq N} \mapsto v(x), \end{cases}$$

where the input $\{\text{Re}(\widehat{v}_k), \text{Im}(\widehat{v}_k)\}_{|k| \leq N} \in [-R, R]^{2\mathcal{K}_N}$ is identified with a *constant* function in $L^2(\mathbb{T}^d; [-R, R]^{2\mathcal{K}_N})$. The existence of a FNO of the form (7.2.6) that can approximate the inverse discrete Fourier transform to desired accuracy is a consequence of the following lemma, proved in [KLM21, Appendix D.3],

Lemma 7.2.8. *Let $B > 0$ and $N \in \mathbb{N}$ be given. For all $\epsilon > 0$, there exists a FNO $\mathcal{N} : L^2(\mathbb{T}^d; \mathbb{R}^{2\mathcal{K}_N}) \rightarrow L^2(\mathbb{T}^d)$, such that for any $v \in L_N^2(\mathbb{T}^d)$ with $\|v\|_{L^2} \leq B$, we have*

$$\|v - \mathcal{N}(w)\|_{L^2} \leq \epsilon,$$

where $w(x) := \{(\text{Re}(\widehat{v}_k), \text{Im}(\widehat{v}_k))\}_{k \in \mathcal{K}_N}$, i.e. $w \in L^2(\mathbb{T}^d; \mathbb{R}^{2\mathcal{K}_N})$ is a *constant* function collecting the real and imaginary parts of the Fourier coefficients \widehat{v}_k of v .

Finally, by setting $\widehat{K} := \mathcal{F}_N(P_N K) \subset \mathbb{C}^{\mathcal{K}_N}$ as the (compact) image of K under the continuous mapping $\mathcal{F}_N \circ P_N : L^2(\mathbb{T}^d) \rightarrow \mathbb{C}^{\mathcal{K}_N}$ and identifying $\mathbb{C}^{\mathcal{K}_N} \simeq \mathbb{R}^{2\mathcal{K}_N}$, where $\widehat{v}_{1,k} := \text{Re}(\widehat{v}_k)$ and $\widehat{v}_{2,k} := \text{Im}(\widehat{v}_k)$ for $k \in \mathcal{K}_N$, we can view $\widehat{\mathcal{G}}_N$ as a continuous mapping

$$\widehat{\mathcal{G}}_N : \widehat{K} \subset \mathbb{R}^{2\mathcal{K}_N} \rightarrow \mathbb{R}^{2\mathcal{K}_N},$$

on a compact subset. Hence, by the universal approximation theorem for finite-dimensional neural networks [Bar93, HSW89], one can readily show that there exists an FNO, with only *local* weights (see remark 7.2.3), which will approximate this continuous mapping $\widehat{\mathcal{G}}_N$ on compact subsets to desired accuracy.

Hence, each of the component operators of the decomposition (7.2.12) can be approximated to desired accuracy by FNOs and the universal approximation theorem follows by composing these FNOs and estimating the resulting error, with details provided in [KLM21, Appendix D.4]. \square

In the following theorem, we will show that the universal approximation Theorem 7.2.5 can be extended to include operators defined on function spaces with Lipschitz domains. In fact, the Lipschitz condition can be relaxed to include all locally uniform domains using ideas from [Rog06]; we will, however, not pursue this for simplicity of the exposition. We show that one can construct a period extension of the input function and a FNO so that the restriction of the FNO's periodic output to the domain of interest gives a suitable approximation to any continuous operator. Similar ideas have been pursued in the design of numerical algorithms for solving PDEs and usually go by the name of *Fourier continuations* [BL10, LB10]. A major challenge for these methods is designing a suitable periodic function whose restriction gives the solution if interest. We show that FNOs can learn the output representation automatically.

Theorem 7.2.9. *Let $s, s' \geq 0$ and $\Omega \subset [0, 2\pi]^d$ be a domain with Lipschitz boundary. Let $\mathcal{G} : H^s(\Omega; \mathbb{R}^{d_a}) \rightarrow H^{s'}(\Omega; \mathbb{R}^{d_u})$ be a continuous operator. Let $K \subset H^s(\Omega; \mathbb{R}^{d_a})$ be a compact subset. Then there exists a continuous, linear operator $\mathcal{E} : H^s(\Omega; \mathbb{R}^{d_a}) \rightarrow H^s(\mathbb{T}^d; \mathbb{R}^{d_a})$ such that $\mathcal{E}(a)|_{\Omega} = a$ for all $a \in H^s(\Omega; \mathbb{R}^{d_a})$. Furthermore, for any $\epsilon > 0$, there exists a FNO $\mathcal{N} : H^s(\mathbb{T}^d; \mathbb{R}^{d_a}) \rightarrow H^{s'}(\mathbb{T}^d; \mathbb{R}^{d_u})$ of the form (7.2.6), such that*

$$\sup_{a \in K} \|\mathcal{G}(a) - \mathcal{N} \circ \mathcal{E}(a)\|_{H^{s'}} \leq \epsilon.$$

Proof. Since Ω is open we have that $\text{dist}(\Omega, \partial[0, 2\pi]^d) > 0$ hence the conclusion of [KLM21, Lemma B.3] follows with the hypercube $B = [0, 2\pi]^d$, in particular, there exists a continuous, linear operator $\mathcal{E} : H^s(\Omega; \mathbb{R}^{d_a}) \rightarrow H^s([0, 2\pi]^d; \mathbb{R}^{d_a})$ such that $\mathcal{E}(a)|_{\Omega} = a$ and $\mathcal{E}(a)$ is periodic on $[0, 2\pi]^d$ for all $a \in H^s(\Omega; \mathbb{R}^{d_a})$, i.e. under the identification $[0, 2\pi]^d \simeq \mathbb{T}^d$, we have a continuous mapping $\mathcal{E} : H^s(\Omega; \mathbb{R}^{d_a}) \rightarrow H^s(\mathbb{T}^d; \mathbb{R}^{d_a})$. Similarly, we can construct an extension operator $\mathcal{E}' : H^{s'}(\Omega; \mathbb{R}^{d_u}) \rightarrow H^{s'}(\mathbb{T}^d; \mathbb{R}^{d_u})$.

We can then associate to $\mathcal{G} : H^s(\Omega; \mathbb{R}^{d_a}) \rightarrow H^{s'}(\Omega; \mathbb{R}^{d_u})$ another continuous operator $\overline{\mathcal{G}} : H^s(\mathbb{T}^d; \mathbb{R}^{d_a}) \rightarrow H^{s'}(\mathbb{T}^d; \mathbb{R}^{d_u})$, by defining $\overline{\mathcal{G}}(a) := \mathcal{E}' \circ \mathcal{G} \circ \mathcal{R}(a)$. Here $\mathcal{R}(a) := a|_{\Omega}$ denotes the restriction to Ω which is clearly linear and continuous. By the continuity of \mathcal{E} , we have that $K' := \mathcal{E}(K)$ is compact in $H^s(\mathbb{T}^d; \mathbb{R}^{d_a})$. By the universal approximation Theorem 7.2.5, for any $\epsilon > 0$, there exists a FNO $\overline{\mathcal{N}} : H^s(\mathbb{T}^d; \mathbb{R}^{d_a}) \rightarrow H^{s'}(\mathbb{T}^d; \mathbb{R}^{d_u})$, such that

$$\sup_{a' \in K'} \|\overline{\mathcal{G}}(a') - \overline{\mathcal{N}}(a')\|_{H^{s'}} \leq \epsilon.$$

But then, using the fact that $\mathcal{R} \circ \mathcal{E} = \text{Id}$, $\mathcal{R} \circ \mathcal{E}' = \text{Id}$, the mapping $\mathcal{N} : H^s(\Omega; \mathbb{R}^{d_a}) \rightarrow H^{s'}(\Omega; \mathbb{R}^{d_u})$, given

by $\mathcal{N} := \mathcal{R} \circ \bar{\mathcal{N}} \circ \mathcal{E}$, satisfies

$$\begin{aligned} \sup_{a \in K} \|\mathcal{G}(a) - \mathcal{N}(a)\|_{H^{s'}} &= \sup_{a \in K} \|\mathcal{R} \circ \mathcal{E}' \circ \bar{\mathcal{G}} \circ \mathcal{R} \circ \mathcal{E}(a) - \mathcal{R} \circ \bar{\mathcal{N}} \circ \mathcal{E}(a)\|_{H^{s'}} \\ &= \sup_{a \in K} \|\mathcal{R} \circ \bar{\mathcal{G}} \circ \mathcal{E}(a) - \mathcal{R} \circ \bar{\mathcal{N}} \circ \mathcal{E}(a)\|_{H^{s'}} \\ &\leq \sup_{a \in K} \|\bar{\mathcal{G}} \circ \mathcal{E}(a) - \bar{\mathcal{N}} \circ \mathcal{E}(a)\|_{H^{s'}} \\ &= \sup_{a' \in K'} \|\bar{\mathcal{G}}(a') - \bar{\mathcal{N}}(a')\|_{H^{s'}} \\ &\leq \epsilon. \end{aligned}$$

□

Remark 7.2.10. *The form of the universal approximation Theorem 7.2.5 stated above, shows that any continuous operator $\mathcal{G} : H^s \rightarrow L^2$ can be approximated to arbitrary accuracy by a FNO, on a given compact subset $K \subset H^s$. The restriction to compact subsets may not always be very natural. For example, to train FNOs in practice, it might be more convenient to draw training samples from a measure μ such as the law of a Gaussian random field, which does not have compact support. Furthermore, the operator \mathcal{G} may not always be continuous. To address these issues, one can follow the recent paper [LMK21], where the authors prove a more general version for the universal approximation of operators for DeepOnets; for any input measure μ , and a Borel measurable operator \mathcal{G} , such that $\int \|\mathcal{G}(a)\|_{L^2}^2 d\mu(a) < \infty$, it is shown that for any $\epsilon > 0$, there exists a DeepOnet $\mathcal{N}(a) \approx \mathcal{G}(a)$ such that*

$$\int \|\mathcal{G}(a) - \mathcal{N}(a)\|_{L^2}^2 d\mu(a) < \epsilon.$$

In particular, there are no restrictions on the topological support of μ . The result of [LMK21] was for the alternative operator learning framework of DeepOnets, but the ideas and the proof can be analogously extended to FNOs.

7.2.5 Ψ -Fourier neural operators

In practice, one needs to compute the FNO, of form (7.2.6), both during training as well as for the evaluation of the neural operator. Thus, given any input function a , one should be able to readily calculate the FNO $\mathcal{N}(a)$, requiring the efficient computation of the Fourier transform \mathcal{F} (A.1.1) and the inverse Fourier transform \mathcal{F}^{-1} (A.1.2). In general, this is not possible as evaluating the Fourier transform (A.1.1) entails computing an integral exactly. Therefore, approximations are necessary to realize the action of FNOs on functions. Following [LKA⁺21], one can efficiently approximate the Fourier transform and its inverse by the discrete Fourier transform (A.1.14) and the discrete inverse Fourier transform (A.1.15), respectively. This amounts to performing a pseudo(Ψ)-spectral Fourier projection between successive layers of the FNO and leading to the following precise definition,

Definition 7.2.11 (Ψ -FNO). *A Ψ -FNO (or Ψ -spectral FNO) is a mapping*

$$\mathcal{N} : \mathcal{A}(\mathbb{T}^d; \mathbb{R}^{d_a}) \rightarrow \mathcal{U}(\mathbb{T}^d; \mathbb{R}^{d_u}), \quad a \mapsto \mathcal{N}(a),$$

of the form

$$\mathcal{N}(a) = \mathcal{Q} \circ \mathcal{I}_N \circ \mathcal{L}_L \circ \mathcal{I}_N \circ \cdots \circ \mathcal{L}_1 \circ \mathcal{I}_N \circ \mathcal{R}(a), \tag{7.2.14}$$

where \mathcal{I}_N denotes the pseudo-spectral Fourier projection onto trigonometric polynomials of degree $N \in \mathbb{N}$ (A.1.11), the lifting operator $\mathcal{R} : \mathcal{A}(\mathbb{T}^d; \mathbb{R}^{d_a}) \rightarrow \mathcal{U}(\mathbb{T}^d; \mathbb{R}^{d_v})$, the projection $\mathcal{Q} : \mathcal{U}(\mathbb{T}^d; \mathbb{R}^{d_v}) \rightarrow \mathcal{U}(\mathbb{T}^d; \mathbb{R}^{d_u})$ are defined as in (7.2.1), (7.2.2), and the non-linear layers \mathcal{L}_ℓ , for $\ell = 1, \dots, N$, are of the form

$$\mathcal{L}_\ell(v)(x) = \sigma \left(W_\ell v(x) + b_\ell(x) + \mathcal{F}^{-1} \left(P_\ell(k) \cdot \mathcal{F}(v)(k) \right)(x) \right).$$

Here, $W_\ell \in \mathbb{R}^{d_v \times d_v}$ and $b_\ell(x) \in \mathcal{U}(\mathbb{T}^d; \mathbb{R}^{d_v})$ define a pointwise affine mapping $v \mapsto W_\ell v(x) + b_\ell(x)$, and the coefficients $P_\ell(k) \in \mathbb{R}^{d_v \times d_v}$ ($k \in \mathcal{K}_N$) define a (non-local) convolution operator via the Fourier transform.

Note that a Ψ -FNO \mathcal{N} is uniquely defined, as an operator, by its restriction to the finite-dimensional subspace $L_N^2(\mathbb{T}^d; \mathbb{R}^{d_a}) \subset \mathcal{A}(\mathbb{T}^d; \mathbb{R}^{d_a})$ (see Appendix A for the definition of L_N^2). Furthermore, we have that the image $\text{Im}(\mathcal{N}) \subset L_N^2(\mathbb{T}^d; \mathbb{R}^{d_u})$. To indicate that a Ψ -FNO is of the form 7.2.14, for some $N \in \mathbb{N}$, we shall thus more simply say that “ $\mathcal{N} : L_N^2(\mathbb{T}^d; \mathbb{R}^{d_a}) \rightarrow L_N^2(\mathbb{T}^d; \mathbb{R}^{d_u})$ is a Ψ -FNO”.

At the level of numerical implementation, a Ψ -FNO can be naturally identified with a *finite-dimensional* mapping

$$\hat{\mathcal{N}} : \mathbb{R}^{d_a \times \mathcal{J}_N} \rightarrow \mathbb{R}^{d_u \times \mathcal{J}_N}, \quad \mathbf{a} \mapsto \mathcal{N}(\mathbf{a}),$$

with input $\mathbf{a} = \{a_j\}_{j \in \mathcal{J}_N} \in \mathbb{R}^{d_a \times \mathcal{J}_N}$ corresponding to the point-values $a_j = a(x_j)$ on the grid $\{x_j\}_{j \in \mathcal{J}_N}$, and $\mathcal{J}_N := \{0, \dots, 2N\}^d$. Here, $\hat{\mathcal{N}}$ is of the form

$$\hat{\mathcal{N}}(\mathbf{a}) = \hat{\mathcal{Q}} \circ \hat{\mathcal{L}}_L \circ \hat{\mathcal{L}}_{L-1} \circ \dots \circ \hat{\mathcal{L}}_1 \circ \hat{\mathcal{R}}(\mathbf{a}),$$

where the lifting operator $\hat{\mathcal{R}} : \mathbb{R}^{d_a \times \mathcal{J}_N} \rightarrow \mathbb{R}^{d_v \times \mathcal{J}_N}$, $\mathbf{a} \mapsto \hat{\mathcal{R}}(\mathbf{a})$, the projection $\hat{\mathcal{Q}} : \mathbb{R}^{d_v \times \mathcal{J}_N} \rightarrow \mathbb{R}^{d_u \times \mathcal{J}_N}$, $\mathbf{v} \mapsto \hat{\mathcal{Q}}(\mathbf{v})$, are given by

$$\begin{aligned} \hat{\mathcal{R}}(\mathbf{a}) &= \{Ra_j\}_{j \in \mathcal{J}_N}, \quad (R \in \mathbb{R}^{d_v \times d_a}), \\ \hat{\mathcal{Q}}(\mathbf{v}) &= \{Qv_j\}_{j \in \mathcal{J}_N}, \quad (Q \in \mathbb{R}^{d_u \times d_v}), \end{aligned}$$

and the non-linear layers $\hat{\mathcal{L}}_\ell$, for $\ell = 1, \dots, N$, are of the form

$$\hat{\mathcal{L}}_\ell(\mathbf{v})_j = \sigma \left(W_\ell v_j + b_{\ell,j} + \mathcal{F}_N^{-1} \left(P_\ell(k) \cdot \mathcal{F}_N(\mathbf{v})(k) \right)_j \right) \quad (7.2.15)$$

for $j \in \mathcal{J}_N$. Here, $W_\ell \in \mathbb{R}^{d_v \times d_v}$, $b_{\ell,j} = b_\ell(x_j) \in \mathbb{R}^{d_v \times \mathcal{J}_N}$ defines a pointwise affine mapping $W_\ell v_j + b_{\ell,j}$, the coefficients $P_\ell(k) \in \mathbb{R}^{d_v \times d_v}$, ($k \in \mathcal{K}_N$) define a (non-local) convolution operator via the discrete Fourier transform, and the non-linear activation function $\sigma : \mathbb{R} \rightarrow \mathbb{R}$ is extended componentwise to a function $\mathbb{R}^{d_v \times \mathcal{J}_N} \rightarrow \mathbb{R}^{d_v \times \mathcal{J}_N}$. Comparing \mathcal{N} with the corresponding discretization $\hat{\mathcal{N}}$, it is easy to see that

$$\hat{\mathcal{N}}(\{a(x_j)\}_{j \in \mathcal{J}_N})_j = \mathcal{N}(a)(x_j), \quad \forall j \in \mathcal{J}_N.$$

In particular, this implies that $\mathcal{N}(a)(x)$ can in practice be computed for any $x \in \mathbb{T}^d$ via the Fourier interpolation of the grid values $\hat{\mathcal{N}}(\{a(x_j)\})_{j \in \mathcal{J}_N}$. In contrast to general FNOs, Ψ -FNOs therefore allow for efficient numerical implementation. Furthermore, the discrete (inverse) Fourier transforms in each hidden layer in (7.2.15) can be very efficiently computed using the fast Fourier transform (FFT).

The above discussion also leads to a very natural definition of the size of a Ψ -FNO below:

Definition 7.2.12 (Depth, width, lift and size). *The **depth** and **width** of a Ψ -FNO \mathcal{N} (cp. Definition 7.2.11), are defined by*

$$\text{depth}(\mathcal{N}) := L, \quad \text{width}(\mathcal{N}) := d_v |\mathcal{J}_N| = d_v |\mathcal{K}_N| = (2N + 1)^d d_v.$$

We refer to the dimension d_v , as the *lift* of \mathcal{N} , i.e. we set

$$\text{lift}(\mathcal{N}) := d_v.$$

The *size* of a Ψ -FNO \mathcal{N} is defined as the total number of degrees of freedom in a Ψ -FNO. A simple calculation shows that

$$\text{size}(\mathcal{N}) = \underbrace{d_u d_v}_{\text{size}(\mathcal{Q})} + L \underbrace{(d_v^2 + d_v |\mathcal{J}_N| + d_v^2 |\mathcal{J}_N|)}_{\text{size}(\mathcal{L}_\ell)} + \underbrace{d_a d_v}_{\text{size}(\mathcal{R})}.$$

The precise size of a Ψ -FNO will not be of any particular relevance for our asymptotic complexity estimates. Instead, we will usually content ourselves with the simple estimate

$$\text{size}(\mathcal{N}) \lesssim \text{depth}(\mathcal{N}) \text{width}(\mathcal{N}) \text{lift}(\mathcal{N}),$$

where we assume that $\max(d_a, d_u) \leq d_v$; under this condition, the above estimate follows from the fact that $\text{size}(\mathcal{N}) \sim L d_v^2 |\mathcal{J}_N|$.

Given our discussion, it is natural to ask whether any FNO $\widehat{\mathcal{N}} = \mathcal{Q} \circ \mathcal{L}_L \circ \mathcal{L}_{L-1} \circ \dots \circ \mathcal{L}_1 \circ \mathcal{R}$ can be approximated to arbitrary accuracy by an associated Ψ -FNO $\mathcal{N} : L_N^2 \rightarrow L_N^2$,

$$\mathcal{N} = \mathcal{Q} \circ \mathcal{I}_N \circ \mathcal{L}_L \circ \mathcal{I}_N \circ \dots \circ \mathcal{L}_1 \circ \mathcal{I}_N \circ \mathcal{R},$$

for sufficiently large $N \in \mathbb{N}$? An affirmative answer can be given for a natural class of FNOs of *finite width*, defined as follows.

Definition 7.2.13. A FNO $\widehat{\mathcal{N}} : \mathcal{A}(\mathbb{T}^d; \mathbb{R}^{d_a}) \rightarrow \mathcal{U}(\mathbb{T}^d; \mathbb{R}^{d_u})$ is said to be **of finite width**, if $\widehat{\mathcal{N}}$ is a composition $\widehat{\mathcal{N}} = \mathcal{Q} \circ \mathcal{L}_L \circ \dots \circ \mathcal{L}_1 \circ \mathcal{R}$, with layers \mathcal{L}_ℓ of the form (7.2.7), and for which there exists a “width” $W \in \mathbb{N}$, such that the Fourier multiplier $P_\ell(k) \equiv 0$, for $|k|_\infty > W$.

We can now state the following theorem, which shows that Ψ -FNOs \mathcal{N} provide an arbitrarily close approximation of a given FNO $\widehat{\mathcal{N}}$:

Theorem 7.2.14. Assume that the activation function $\sigma \in C^\infty$ is globally Lipschitz continuous. Let $\widehat{\mathcal{N}} : H^s(\mathbb{T}^d; \mathbb{R}^{d_a}) \rightarrow L^2(\mathbb{T}^d; \mathbb{R}^{d_u})$ be a FNO of finite width, with $s > d/2$. Then for any $\epsilon, B > 0$, there exists $N \in \mathbb{N}$ and a Ψ -FNO $\mathcal{N} : L_N^2(\mathbb{T}^d; \mathbb{R}^{d_a}) \rightarrow L_N^2(\mathbb{T}^d; \mathbb{R}^{d_u})$, such that

$$\sup_{\|a\|_{H^s} \leq B} \|\widehat{\mathcal{N}}(a) - \mathcal{N}(a)\|_{L^2} \leq \epsilon.$$

For the proof, we refer to [KLM21, Appendix D.5]. In particular, the last theorem implies an extension of the universal approximation Theorem 7.2.5 to Ψ -FNOs, provided that the input functions have sufficient regularity for the pseudo-spectral projection \mathcal{I}_N to be well-defined:

Theorem 7.2.15 (Universal approximation for Ψ -FNOs). Let $s > d/2$, and let $s' \geq 0$. Let $\mathcal{G} : H^s(\mathbb{T}^d; \mathbb{R}^{d_a}) \rightarrow H^{s'}(\mathbb{T}^d; \mathbb{R}^{d_u})$ be a continuous operator. And let $K \subset H^s(\mathbb{T}^d; \mathbb{R}^{d_a})$ be a compact subset. Then for any $\epsilon > 0$, there exists $N \in \mathbb{N}$ and a Ψ -FNO $\mathcal{N} : L_N^2(\mathbb{T}^d; \mathbb{R}^{d_a}) \rightarrow L_N^2(\mathbb{T}^d; \mathbb{R}^{d_u})$, such that

$$\sup_{a \in K} \|\mathcal{G}(a) - \mathcal{N}(a)\|_{H^{s'}} \leq \epsilon.$$

Proof. Similar to the proof of the universal approximation theorem for FNOs, we again note that the general case $s' \geq 0$ can be deduced from the statement of Theorem 7.2.15 for the special case $s' = 0$. This is the content of the following lemma, whose proof is provided in [KLM21, Appendix D.6]:

Lemma 7.2.16. *Assume that Theorem 7.2.15 holds for $s' = 0$. Then it holds for arbitrary $s' \geq 0$.*

The special case $s' = 0$ follows immediately from Theorem 7.2.14 and the observation that the FNO approximation constructed in the proof of the universal approximation theorem for FNOs, Theorem 7.2.5, has finite width. \square

Structure and properties of Ψ -FNOs

We conclude this section by pointing out some aspects of the structure of Ψ -FNOs (7.2.14) that will be relevant in the following. To start with, we can simplify Ψ -FNOs by viewing them in terms of two types of layers, which we will refer to as σ - and \mathcal{F} -layers, respectively. A **σ -layer** $\mathcal{L} = \mathcal{L}_\sigma$ of a Ψ -FNO is a **local, non-linear** layer of the form $\mathcal{L}_\sigma(v)(x) = \mathcal{I}_N \sigma(A\mathcal{I}_N v(x) + b)$, or, in the numerical implementation (cp. (7.2.15))

$$\mathcal{L}_\sigma(v)_j = \sigma(Av_j + b_j), \quad \forall j \in \mathcal{J}_N,$$

with $A \in \mathbb{R}^{d_v \times d_v}$, and $b_j \in \mathbb{R}^{\mathcal{J}_N \times d_v}$ defining an affine mapping. A **\mathcal{F} -layer** $\mathcal{L} = \mathcal{L}_{\mathcal{F}}$ of a Ψ -FNO is a **non-local, linear** layer of the form $\mathcal{L}_{\mathcal{F}}(v)(x) = \mathcal{F}^{-1}(P(k) \cdot \mathcal{F}(\mathcal{I}_N v)(k))(x)$, which in a practical implementation corresponds to

$$\mathcal{L}_{\mathcal{F}}(v)_j = \mathcal{F}_N^{-1}\left(P(k) \cdot \mathcal{F}_N(v)(k)\right)_j, \quad \forall j \in \mathcal{J}_N,$$

where $P : \mathcal{K}_N \rightarrow \mathbb{C}^{d_v \times d_v}$ is a collection of complex weights, with $P(-k) = P(k)^\dagger$ the Hermitian transpose of $P(k)$, and \mathcal{F}_N (\mathcal{F}_N^{-1}) denotes the discrete (inverse) Fourier transform.

The main point of these definitions is that each Ψ -FNO can be decomposed into a finite number of σ -layers and \mathcal{F} -layers, and that the converse is also true; *i.e.* any composition of σ -layers and \mathcal{F} -layers can be represented by a Ψ -FNO. These statements are made precise in a series of technical Lemmas, which are stated and proved in [KLM21, Appendix D.7].

7.3 Approximation of PDEs by Ψ -FNOs

We have shown in the previous section that FNOs (7.2.6) as well as their computational realizations (Ψ -FNOs (7.2.14)) are universal *i.e.*, they approximate any continuous operator, defined in the setting 7.2.1, to desired accuracy. However, as repeatedly discussed in the introduction, universality alone does not suffice to claim that FNOs can approximate operators efficiently. In particular, it could happen that the size of the FNO is unfeasibly large to ensure a given accuracy of the approximation. That this is indeed the case is made precise in the following remark.

Remark 7.3.1. *We observe from the proof of Theorem 7.2.5 that the desired FNO, approximating the operator \mathcal{G} , is constructed as $\mathcal{N}_{\text{IFT}} \circ \widehat{\mathcal{N}} \circ \mathcal{N}_{\text{FT}}$, with $\mathcal{N}_{\text{FT}}, \mathcal{N}_{\text{IFT}}$ approximating the Fourier and Inverse Fourier transforms, respectively, whereas $\widehat{\mathcal{N}} : \mathbb{R}^{2\mathcal{K}_N} \rightarrow \mathbb{R}^{2\mathcal{K}_N}$ is a canonical finite-dimensional neural network approximation of the ‘‘Fourier conjugate operator’’ (7.2.11): $\widehat{\mathcal{G}}_N : \mathbb{R}^{2\mathcal{K}_N} \rightarrow \mathbb{R}^{2\mathcal{K}_N}$. We note that N herein has to be chosen sufficiently large in order to yield the desired error tolerance of ϵ . By Theorem A.1.3, this depends on the smoothness of the input space, *i.e.*, if the input $a \in K \subset H^s$, for some $s > 0$, then we need to choose N such that $N^{-s} \sim \epsilon$. Further assuming that the mapping \mathcal{G} is Lipschitz continuous, implies that the Fourier conjugate operator $\widehat{\mathcal{G}}$ is also Lipschitz continuous as a mapping from $\mathbb{R}^{2\mathcal{K}_N}$ to $\mathbb{R}^{2\mathcal{K}_N}$. Hence, neural network approximation results, such as those of [Yar17] for ReLU activations or [DLM21] for tanh activations, yield that the width of the approximating neural*

network $\widehat{\mathcal{N}}$ scales as $\text{width}(\widehat{\mathcal{N}}) \gtrsim \epsilon^{-D}$, where D is the dimension of the domain of $\widehat{\mathcal{G}}_N$. In the present case, we have $D = |\mathcal{K}_N| \sim N^d \sim \epsilon^{-d/s}$, yielding that

$$\text{width}(\widehat{\mathcal{N}}) \gtrsim \epsilon^{-\epsilon^{-d/s}}. \quad (7.3.1)$$

This scaling represents a super-exponential growth in the size of the FNO \mathcal{N} , with respect to the error ϵ , incurred in approximating the underlying operator \mathcal{G} .

Given the above remark, we infer that in the worst case, a FNO approximating a generic Lipschitz continuous operator \mathcal{G} , can require extremely large sizes to achieve the desired accuracy, making it unfeasible in practice. The same holds for Ψ -FNOs of the form (7.2.14). This super-exponential growth appears as a form of *curse of dimensionality* i.e., exponential growth of complexity (measured here in the size of the FNO), with respect to the error.

Hence, it is reasonable to ask how these extremely pessimistic complexity bounds on FNOs (Ψ -FNOs), can be reconciled to their robust numerical performance for approximating PDEs, as reported in [LKA⁺21]. The rest of the section investigates this fundamental question.

The starting point of our explanation for the robustness of FNOs in approximating PDEs is the observation that operators which arise in the context of PDEs have a special structure and are not merely generic continuous operators mapping one infinite-dimensional function space to another. To see this, we point out that many time-dependent PDEs arising in physics can be written in the general abstract form,

$$\partial_t u + \nabla \cdot F(u, \nabla u) = 0, \quad (7.3.2)$$

where for any $(t, x) \in [0, T] \times D \subset \mathbb{R}^d$, $u(t, x) \in \mathbb{R}^{d_u}$ is a vector of physical quantities, describing e.g. density, velocity or temperature of a fluid or other material at a given point $x \in D$ in the domain D and at time $t \in [0, T]$. Equation (7.3.2) describes the general form of a conservation law for the physical quantities u with a flux function $F(u, \nabla u)$, which is typically *non-linear*, and can e.g. represent advection or diffusion terms. The flux function $F(u, \nabla u)$ may also depend on u in a *non-local* manner. For example, for the incompressible Navier-Stokes equations in \mathbb{R}^d , we have $u \equiv \mathbf{u} : \mathbb{T}^d \rightarrow \mathbb{R}^d$, where

$$\mathbf{u}(x, t) = (u_1(x, t), \dots, u_d(x, t)) \in \mathbb{R}^d,$$

represent the fluid velocity at (x, t) , and the flux is defined by

$$F(\mathbf{u}, \nabla \mathbf{u}) = -\mathbf{u} \otimes \mathbf{u} - p + \nu \nabla \mathbf{u},$$

where $p = p(\mathbf{u})$ depends on \mathbf{u} in a non-local manner:

$$p = \mathcal{R} : (\mathbf{u} \otimes \mathbf{u}), \quad \mathcal{R} := (-\Delta)^{-1}(\nabla \otimes \nabla),$$

where \mathcal{R} is a (non-local) Riesz transform.

A popular numerical method for time-dependent PDEs, of the form (7.3.2), particularly on periodic domains $D = \mathbb{T}^d$, is the *pseudo-spectral method* [CHQZ07], wherein (7.3.2) is discretized as,

$$\partial_t u_N + \nabla \cdot \mathcal{I}_N F(u_N, \nabla u_N) = 0, \quad (7.3.3)$$

where $u_N \in L_N^2$ is a trigonometric polynomial of degree $\leq N$.

The resulting system of ODEs (7.3.3) can be further discretized in time using a time-marching scheme. For simplicity, the forward Euler discretization with time step τ leads to,

$$u_N^{n+1} = u_N^n - \tau \nabla \cdot \mathcal{I}_N F(u_N^n, \nabla u_N^n). \quad (7.3.4)$$

One might prove that the system (7.3.4) provides a convergent approximation for the underlying time-dependent PDE (7.3.2) for many different choices of the flux F . In order to connect the approximation (7.3.4) with FNOs, we decompose the right hand side of (7.3.4) as,

$$\begin{aligned} u_N^n &\xrightarrow{\mathcal{R}} \begin{Bmatrix} u_N^n \\ u_N^n \end{Bmatrix} \xrightarrow{\mathcal{F}} \begin{Bmatrix} u_N^n \\ \nabla u_N^n \end{Bmatrix} \\ &\xrightarrow{\sigma} \dots \xrightarrow{\sigma} \begin{Bmatrix} u_N^n \\ F_N^\sigma(u_N^n, \nabla u_N^n) \end{Bmatrix} \\ &\xrightarrow{\mathcal{F}} \begin{Bmatrix} u_N^n \\ \nabla \cdot F_N^\sigma(u_N^n, \nabla u_N^n) \end{Bmatrix} \longmapsto u_N^n - \tau \nabla \cdot F_N^\sigma(u_N^n, \nabla u_N^n). \end{aligned}$$

Here, \mathcal{R} is the lifting operator and σ , \mathcal{F} are the σ - and \mathcal{F} -layers, respectively, of a Ψ -FNO, that are defined in section 7.2.5. The above representation suggests that the Fourier \mathcal{F} -layers of a Ψ -FNO allow us to take *exact* derivatives, and a composition of σ -layers of a Ψ -FNO allows us to approximate continuous functions to any desired accuracy (via the standard universal approximation theorem for finite-dimensional neural networks); in particular, a composition of σ -layers can provide an approximation

$$(u, \nabla u) \mapsto F_N^\sigma(u, \nabla u) \approx \mathcal{I}_N F(u, \nabla u).$$

Thus, by a suitable composition of σ - and \mathcal{F} -layers, Ψ -FNOs can *emulate* pseudo-spectral methods, providing a mechanism by which such neural operators can approximate solution operators for a large class of PDEs efficiently.

We will make this intuition precise for the incompressible Navier-Stokes and Euler equations, the following.

7.3.1 Incompressible Euler and Navier-Stokes equations

The motion of a viscous, incompressible Newtonian fluid is modeled by the incompressible Navier-Stokes equations,

$$\begin{cases} \partial_t \mathbf{u} + \mathbf{u} \cdot \nabla \mathbf{u} + \nabla p = \nu \Delta \mathbf{u}, \\ \operatorname{div}(\mathbf{u}) = 0, \quad \mathbf{u}(t=0) = \bar{\mathbf{u}}, \end{cases} \quad (7.3.5)$$

For simplicity, we assume periodic boundary conditions in the domain \mathbb{T}^d . The viscosity is denoted by $\nu \geq 0$ and we would like to state that the subsequent analysis also applies for $\nu = 0$, where (7.3.5) reduces to the incompressible Euler equations modeling an ideal fluid.

We recall that if the initial data $\bar{\mathbf{u}}$ of (7.3.5) belongs to $\dot{L}^2(\mathbb{T}^d; \mathbb{R}^d)$, *i.e.* if

$$\int_{\mathbb{T}^d} \bar{\mathbf{u}}(x) dx = 0,$$

then we also have that the corresponding solution $\mathbf{u}(x, t) \in \dot{L}^2(\mathbb{T}^d; \mathbb{R}^d)$ (reflecting momentum conservation). Next, we recall that the Leray-projection operator $\mathbb{P} : L^2(\mathbb{T}^d; \mathbb{R}^d) \rightarrow \dot{L}^2(\mathbb{T}^d; \operatorname{div})$, is defined as the L^2 -orthogonal projection onto the subspace $\dot{L}^2(\mathbb{T}^d; \operatorname{div}) \subset \dot{L}^2(\mathbb{T}^d; \mathbb{R}^d)$, consisting of divergence-free vector fields; *i.e.* we have $\mathbf{u} \in \dot{L}^2(\mathbb{T}^d; \operatorname{div})$ if, and only if, $\mathbf{u} \in \dot{L}^2(\mathbb{T}^d; \mathbb{R}^d)$ and

$$\int_{\mathbb{T}^d} \mathbf{u}(x) \cdot \nabla \varphi(x) dx = 0, \quad \forall \varphi \in C^\infty(\mathbb{T}^d).$$

In terms of Fourier series, the Leray projection $\mathbb{P} : \dot{L}^2(\mathbb{T}^d; \mathbb{R}^d) \rightarrow \dot{L}^2(\mathbb{T}^d; \text{div})$ is explicitly given by

$$\mathbb{P} \left(\sum_{k \in \mathbb{Z}^d} \hat{\mathbf{u}}_k e^{ik \cdot x} \right) = \sum_{k \in \mathbb{Z}^d \setminus \{0\}} \left(1 - \frac{k \otimes k}{|k|^2} \right) \hat{\mathbf{u}}_k e^{ik \cdot x}. \quad (7.3.6)$$

In terms of the Leray projection \mathbb{P} , we can now equivalently write the incompressible Navier-Stokes equations (7.3.5) as the following equation on the Hilbert space $\dot{L}^2(\mathbb{T}^d; \text{div})$ as,

$$\begin{cases} \partial_t \mathbf{u} = -\mathbb{P}(\mathbf{u} \cdot \nabla \mathbf{u}) + \nu \Delta \mathbf{u}, \\ \mathbf{u}(t=0) = \bar{\mathbf{u}}. \end{cases} \quad (7.3.7)$$

Given this background, our main objective in this section is to construct a Ψ -FNO that will approximate the operator \mathcal{G} which maps the initial data $\bar{\mathbf{u}}$ to the solution $\mathbf{u}(\cdot, T)$ (at the final time T) of the incompressible Navier-Stokes equations (7.3.5), (7.3.7). To this end, we will follow the general program outlined at the beginning of this section and introduce a suitable pseudo-spectral method for approximating the Navier-Stokes equations. Then, we construct a Ψ -FNO that can efficiently emulate this pseudo-spectral method.

A fully-discrete Ψ -spectral approximation of the Navier-Stokes equations (7.3.5)

The form of the Leray-projected Navier-Stokes equations (7.3.7) naturally suggests the following fully-discrete approximation of (7.3.5):

$$\begin{cases} \frac{\mathbf{u}^{\Delta, n+1} - \mathbf{u}^{\Delta, n}}{\tau} + \mathbb{P}_N(\mathbf{u}^{\Delta, n} \cdot \nabla \mathbf{u}^{\Delta, n+1}) = \nu \Delta \mathbf{u}^{\Delta, n+1}, \\ \mathbf{u}^{\Delta, 0} = \mathcal{I}_N \mathbf{u}(t=0). \end{cases} \quad (7.3.8)$$

Here, we fix $\Delta = 1/N$, $N \in \mathbb{N}$ and introduce the space, $\dot{L}_N^2(\mathbb{T}^d; \text{div}) := \dot{L}^2(\mathbb{T}^d; \text{div}) \cap \dot{L}_N^2(\mathbb{T}^d; \mathbb{R}^d)$. We fix a time-step $\tau > 0$ and let $\mathbf{u}^{\Delta, n} \in \dot{L}_N^2(\mathbb{T}^d; \text{div})$, for all $n = 0, \dots, n_T$, with n_T such that $\tau n_T = T$. Moreover, we use the following *truncated* Leray-Fourier projection operator $\mathbb{P}_N : L^2(\mathbb{T}^d) \rightarrow \dot{L}_N^2(\mathbb{T}^d; \text{div})$ in analogy with (7.3.6):

$$\mathbb{P}_N \left(\sum_{k \in \mathbb{Z}^d} \hat{\mathbf{u}}_k e^{ik \cdot x} \right) := \sum_{0 < |k|_\infty \leq N} \left(1 - \frac{k \otimes k}{|k|^2} \right) \hat{\mathbf{u}}_k e^{ik \cdot x}, \quad (7.3.9)$$

to complete the description of the scheme (7.3.8).

We observe that the scheme (7.3.8) is *implicit i.e.*, at each time step n , one has to solve an operator equation to compute the velocity field $\mathbf{u}^{\Delta, n+1}$ at the next time step. Thus, one needs to show the solvability of this operator equation in order to ensure that the scheme (7.3.8) is *well-defined*. Under the following CFL condition for choosing a small enough time step τ ,

$$\tau \|\mathbf{u}^{\Delta, n}\|_{L^\infty} N \leq \frac{1}{2}, \quad (7.3.10)$$

it has been proved in [KLM21, Appendix F.1] that the scheme (7.3.8) is well-defined.

Next, in practice, one has to numerically approximate the solutions of the implicit equation (7.3.8) for evaluating the velocity field $\mathbf{u}^{\Delta, n+1}$, at the next time-step. We choose to do so by recasting the solution of the implicit equation (7.3.8) to finding a *fixed point* for the mapping,

$$\mathbf{w}_N \mapsto F(\mathbf{w}_N) := (1 - \nu \tau \Delta)^{-1} \mathbf{u}^{\Delta, n} - \tau (1 - \nu \tau \Delta)^{-1} \mathbb{P}_N(\mathbf{u}^{\Delta, n} \cdot \nabla \mathbf{w}_N). \quad (7.3.11)$$

In [KLM21, Appendix F.1, Lemma F.4], it is shown that a standard Picard-type iteration converges to a fixed point for the map (7.3.11). This suggests the following numerical algorithm for approximating strong solutions of the incompressible Navier-Stokes equations (7.3.5),

Algorithm 7.3.2 (Pseudo-spectral approximation of the Navier-Stokes equations (7.3.5)).

Input: $U > 0, N \in \mathbb{N}, T > 0, a time-step \tau > 0, such that n_T = T/\tau \in \mathbb{N}, and \tau U N^{d/2+1} \leq \frac{1}{2e}, initial data \mathbf{u}^{\Delta,0} \in L_N^2(\mathbb{T}^d; \text{div}), such that \|\mathbf{u}^{\Delta,0}\|_{L^2} \leq U.$

Output: $\mathbf{u}^{\Delta,n_T} \in L_N^2(\mathbb{T}^d; \text{div}) an approximation of the solution \mathbf{u}^{\Delta,n_T} \approx \mathbf{u}(t = T) of (7.3.5) at time t = T.$

(1) Set

$$\kappa_0 := \left\lceil \frac{\log(T^2/\tau^2)}{\log(2)} \right\rceil \in \mathbb{N}.$$

(2) For $n = 0, \dots, n_T - 1$:

- (i) Set $\mathbf{w}_N^{n,0} := 0,$
- (ii) For $k = 1, \dots, \kappa_0$: Compute

$$\mathbf{w}_N^{n,k} := (1 - \nu \tau \Delta)^{-1} \mathbf{u}^{\Delta,n} - \tau (1 - \nu \tau \Delta)^{-1} \mathbb{P}_N \left(\mathbf{u}^{\Delta,n} \cdot \nabla \mathbf{w}_N^{n,k-1} \right),$$

- (iii) Set $\mathbf{u}^{\Delta,n+1} := \mathbf{w}_N^{n,\kappa_0},$

□

The convergence of the algorithm 7.3.2, together with a convergence rate, to the strong solution of the Navier-Stokes equations is summarized in the following theorem,

Theorem 7.3.3. *Let $U, T > 0$. Consider the Navier-Stokes equations on \mathbb{T}^d , for $d \geq 2$. Assume that $r \geq d/2 + 2$, and let $\mathbf{u} \in C([0, T]; H^r) \cap C^1([0, T]; H^{r-2})$ be a solution of the Navier-Stokes equations (7.3.5), such that $\|\mathbf{u}\|_{L^2} \leq U$. Choose a time-step τ , such that $\tau U N^{d/2+1} \leq (2e)^{-1}$. There exists a constant*

$$C = C(T, d, r, \|\mathbf{u}\|_{C_t(H_x^r)}, \|\mathbf{u}\|_{C_t^1(H_x^{r-2})}) > 0,$$

such that with $\mathbf{u}^{\Delta,0} := \mathcal{I}_N \mathbf{u}(0)$, and for the sequence $\mathbf{u}^{\Delta,1}, \dots, \mathbf{u}^{\Delta,n_T} \in L_N^2(\mathbb{T}^d; \text{div})$ generated by Algorithm 7.3.2, we have

$$\max_{n=0, \dots, n_T} \|\mathbf{u}^{\Delta,n} - \mathbf{u}(t^n)\|_{L^2} \leq C (\tau + N^{-r}),$$

where $n_T \tau = T$. In particular, choosing $\tau \sim N^{-r}$, we have

$$\max_{n=0, \dots, n_T} \|\mathbf{u}^{\Delta,n} - \mathbf{u}(t^n)\|_{L^2} \leq CN^{-r},$$

with $n_T \sim N^r$ (and enlarging the constant $C > 0$ by a constant factor).

The proof of this theorem relies on several techniques from numerical analysis and has been presented in detail in [KLM21, Appendix F.2].

Approximation of algorithm 7.3.2 by Ψ -FNOS

Next, we are going to construct a Ψ -FNO of the form (7.2.14), which can efficiently emulate the pseudo-spectral algorithm 7.3.2. To this end, we have the following result (proved in [KLM21, Appendix F.3]) on the efficient approximation of the non-linear term in the Navier-Stokes equations by FNOS,

Lemma 7.3.4. *Assume that the activation function $\sigma \in C^3$ is three times continuously differentiable and non-linear. There exists a constant $C > 0$, such that for any $N \in \mathbb{N}$, and for any $\epsilon, B > 0$, there exists a Ψ -FNO $\mathcal{N} : L_{2N}^2(\mathbb{T}^d; \mathbb{R}^d) \times L_{2N}^2(\mathbb{T}^d; \mathbb{R}^d) \rightarrow L_{2N}^2(\mathbb{T}^d; \mathbb{R}^d)$, with*

$$\text{depth}(\mathcal{N}), \text{lift}(\mathcal{N}) \leq C, \quad \text{width}(\mathcal{N}) \leq CN^d,$$

such that we have

$$\|\mathbb{P}_N(\mathbf{u}_N \cdot \nabla \mathbf{w}_N) - \mathcal{N}(\mathbf{u}_N, \mathbf{w}_N)\|_{L_N^2} \leq \epsilon,$$

for all trigonometric polynomials $\mathbf{u}_N, \mathbf{w}_N \in L_N^2(\mathbb{T}^d; \mathbb{R}^d) \subset L_{2N}^2(\mathbb{T}^d; \mathbb{R}^d)$ of degree $|k|_\infty \leq N$, satisfying the bound $\|\mathbf{u}_N\|_{L^2}, \|\mathbf{w}_N\|_{L^2} \leq B$.

Thus, from the preceding Lemma, we have that the nonlinearities in algorithm 7.3.2 can be efficiently approximated by Ψ -FNOS. This paves the way for the following theorem on the emulation of the pseudo-spectral algorithm 7.3.2 by Ψ -FNOS,

Theorem 7.3.5. *Let $U, T > 0$ and viscosity $\nu \geq 0$. Consider the Navier-Stokes equations on \mathbb{T}^d , for $d \geq 2$. Assume that $r \geq d/2 + 2$, and let $\mathcal{V} \subset C([0, T]; H^r) \cap C^1([0, T]; H^{r-2})$ be a set of solutions of the Navier-Stokes equations (7.3.5), such that $\sup_{\mathbf{u} \in \mathcal{V}} \|\mathbf{u}\|_{L^2} \leq U$, and*

$$\overline{U} := \sup_{\mathbf{u} \in \mathcal{V}} \left\{ \|\mathbf{u}\|_{C_t(H_x^r)} + \|\mathbf{u}\|_{C_t^1(H_x^{r-2})} \right\} < \infty.$$

For $t \in [0, T]$, denote $\mathcal{V}_t := \{\mathbf{u}(t) \mid \mathbf{u} \in \mathcal{V}\}$. Let $\mathcal{G} : \mathcal{V}_0 \rightarrow \mathcal{V}_T$ denote the solution operator of (7.3.5), mapping initial data $\bar{\mathbf{u}} = \mathbf{u}(t=0)$, to the solution $\mathbf{u}(T)$ at $t = T$ of the incompressible Navier-Stokes equations. There exists a constant

$$C = C(d, r, U, \overline{U}, T) > 0,$$

such that for $N \in \mathbb{N}$ there exists a Ψ -FNO $\mathcal{N} : L_N^2(\mathbb{T}^d; \mathbb{R}^d) \rightarrow L_N^2(\mathbb{T}^d; \mathbb{R}^d)$, such that

$$\sup_{\mathbf{u} \in \mathcal{V}_0} \|\mathcal{G}(\mathbf{u}) - \mathcal{N}(\mathbf{u})\|_{L^2} \leq CN^{-r},$$

and such that

$$\text{width}(\mathcal{N}) \leq CN^d, \quad \text{depth}(\mathcal{N}) \leq CN^r \log(N), \quad \text{lift}(\mathcal{N}) \leq C.$$

The proof of this theorem relies on standard ideas from numerical analysis and is provided in detail in [KLM21, Appendix F.2].

Remark 7.3.6. *It is straightforward to observe from Theorem 7.3.5 that the size of a Ψ -FNO to achieve a desired error tolerance $\epsilon > 0$, scales (neglecting log-terms) as*

$$\text{size}(\mathcal{N}) \leq C\epsilon^{-(1+\frac{d}{r})}, \tag{7.3.12}$$

Given that we need $r \geq d/2 + 2$, we observe from (7.3.12) that the size of the Ψ -FNO, approximating the initial data to solution operator \mathcal{G} , for the Navier-Stokes equations (7.3.5), scales at most sub-quadratically with respect to the error tolerance ϵ for the physically relevant values $d = 2, 3$. This polynomial scaling should be compared with the super-exponential growth (see Remark 7.3.1) of the size of FNOS in approximating a generic Lipschitz-continuous operator. Thus, we are able to demonstrate that Ψ -FNOS can approximate the solutions of Navier-Stokes equations far more efficiently than what the universal approximation Theorem 7.2.15 suggests.

Remark 7.3.7. From the convergence Theorem 7.3.3, we observe that the underlying scheme (7.3.8) is first-order in time. This low accuracy of the scheme necessitates a large number of time steps and affects the overall complexity. We describe a second-order accurate time discretized version of the pseudo-spectral method for approximating the Navier-Stokes equations (7.3.5) in [KLM21] and in complete analogy with Theorem 7.3.5, we can construct a Ψ -FNO to emulate this second-order in time pseudo-spectral scheme, resulting in a Ψ -FNO of

$$\text{size}(\mathcal{N}) \leq C\epsilon^{-(\frac{1}{2} + \frac{d}{r})}, \quad (7.3.13)$$

to obtain a desired accuracy of ϵ . Thus, we can obtain a more efficient approximation of the underlying operator than Ψ -FNO emulating the first-order time scheme (7.3.8). In particular for $r \geq 2d$, we obtain that the size of a Ψ -FNO only grows sub-linearly in terms of the desired accuracy.

For use in the next section, we note that Theorem 7.3.5 is based on the following precise emulation result for Algorithm 7.3.2 by Ψ -FNOs:

Proposition 7.3.8. Let $N \in \mathbb{N}$, define $\Delta \equiv 1/N$, and let $\mathcal{S}_T^\Delta : L_N^2(\mathbb{T}^d; \mathbb{R}^d) \rightarrow L_N^2(\mathbb{T}^d; \mathbb{R}^d)$, $\mathbf{u}^{\Delta,0} \mapsto \mathcal{S}_T^\Delta(\mathbf{u}^{\Delta,0}) = \mathbf{u}^{\Delta,n_T}$ be the approximate solution operator defined by Algorithm 7.3.2. There exists a constant $C > 0$, such that for any $\epsilon, B > 0$, there exists a Ψ -FNO $\mathcal{N} : L_{2N}^2(\mathbb{T}^d; \mathbb{R}^d) \rightarrow L_{2N}^2(\mathbb{T}^d; \mathbb{R}^d)$, with

$$\text{width}(\mathcal{N}) \leq CN^d, \quad \text{depth}(\mathcal{N}) \leq Cn_T \log(n_T), \quad \text{lift}(\mathcal{N}) \leq C,$$

such that

$$\sup_{\|\mathbf{u}\|_{L^2} \leq B} \|\mathcal{S}_T^\Delta(\mathbf{u}) - \mathcal{N}(\mathbf{u})\|_{L^2} \leq \epsilon,$$

where the supremum is taken over $\{\mathbf{u} \in L_N^2 \mid \|\mathbf{u}\|_{L^2} \leq B\}$.

7.4 Approximation of statistical solutions via surrogates

We now consider the problem of approximating a statistical solution $t \mapsto \mu_t$ of the incompressible Euler equations based on surrogates. The previous section shows that FNOs can efficiently emulate spectral methods; in practice, and based on the encouraging initial results of numerical experiments in [LKA⁺21] and similar work [LJK19, DLLM⁺21, CWL⁺21, MLM⁺20], we expect FNOs of much smaller size to be able to provide accurate approximations of the solution operator of the incompressible Euler equations. Hence, it is natural to attempt to replace the (costly) forward evaluation by spectral methods in the computation of statistical solutions (cp. Algorithm 3.4.1, in chapter 3), by FNOs, whose evaluation is computationally much cheaper. To this end, we propose the following (prototypical) algorithm:

Algorithm 7.4.1 (Statistical solution surrogate). Given an initial probability measure $\bar{\mu} \in \mathcal{P}(L_x^2)$, a resolution $N \in \mathbb{N}$ and a number of samples $M \in \mathbb{N}$, we obtain a statistical solution surrogate μ_t^* for $t \geq 0$:

- (1) Draw M iid samples $\bar{\mathbf{u}}_1, \dots, \bar{\mathbf{u}}_M \sim \bar{\mu}$,
- (2) For $j = 1, \dots, M$, evaluate the corresponding solution based on the numerical discretization 7.3.8 of the previous section, $\mathbf{u}_j^\Delta(t) := \mathcal{S}_t^\Delta(\bar{\mathbf{u}}_j)$, where $\Delta = 1/N$,
- (3) Minimize the empirical loss $\hat{\mathcal{L}}$ over parameters $\theta \in \Theta$ of the Ψ -FNO $\mathcal{S}_t^\theta : L_N^2 \rightarrow L_N^2$, where

$$\hat{\mathcal{L}} = \frac{1}{M} \sum_{j=1}^M \|\mathcal{S}_t^\theta(\bar{\mathbf{u}}_j) - \mathbf{u}_j^\Delta(t)\|_{L_x^2}^2,$$

to obtain $\mathcal{S}_t^* := \mathcal{S}_t^{\theta^*} : L_N^2 \rightarrow L_N^2$, where $\theta^* \in \Theta$ is the optimized parameter,

- (4) Define $\mu_t^* := \mathcal{S}_{t,\#}^* \bar{\mu}$ as the push-forward measure under \mathcal{S}_t^* .

□

Remark 7.4.2. Note that we are considering a surrogate approximation of the initial data-to-solution mapping at a fixed $t \in [0, T]$, in Algorithm 7.4.1. This allows us to directly refer to the error and complexity analysis carried out in the preceding section. In some cases, especially in the Bayesian context, one might be interested in a time-parametrized approximation $t \mapsto \mathcal{S}_t^*$, for all $t \in [0, T]$. In this case, we propose to add a time-interval parameter $\Delta t > 0$ to the input, which we assume to be small relative to the time-scales of the evolution of statistical quantities, and train the surrogate recurrently to provide a mapping

$$\bar{\mathbf{u}} \mapsto \mathcal{S}_{\Delta t}^*(\bar{\mathbf{u}}) \mapsto \mathcal{S}_{2\Delta t}^*(\bar{\mathbf{u}}) \mapsto \dots \mapsto \mathcal{S}_{n\Delta t}^*(\bar{\mathbf{u}}),$$

where $T = n\Delta t$, and where $\mathcal{S}_{k\Delta t}^* = \mathcal{S}_{\Delta t}^* \circ \dots \circ \mathcal{S}_{\Delta t}^*$ is the k -fold composition of $\mathcal{S}_{\Delta t}^*$. Values at $t \in (k\Delta t, (k+1)\Delta t)$ can then be obtained by conventional interpolation.

From Proposition 7.3.8, we can now deduce the following error and complexity estimate for statistical solution surrogates:

Theorem 7.4.3 (Error estimate for statistical solution surrogates). Let $\mathcal{S}_t^\Delta : L_N^2 \rightarrow L_N^2$ denote the solution operator defined by Algorithm 7.3.2, where $\Delta \equiv 1/N$ and with $n_T \sim N^{d/2+1}$ timesteps. Let $\bar{\mu} \in \mathcal{P}(L_x^2)$ be statistical initial data for the incompressible Navier-Stokes or Euler equations. Assume that:

- There exists $M > 0$, such that $\bar{\mu}$ is concentrated on $B_M^s(0) := \{\bar{\mathbf{u}} \in H^s(\mathbb{T}^d; \mathbb{R}^d) \mid \|\bar{\mathbf{u}}\|_{H_x^s} \leq M\}$, for some $s > d/2$, so that the point-evaluation $\text{ev}_x : \bar{\mathbf{u}} \mapsto \bar{\mathbf{u}}(x)$ is well-defined, $\bar{\mu}$ -almost surely.
- There exist constants $C, \alpha > 0$, and a statistical solution $\mu_t \in C([0, T]; \mathcal{P}(L_x^2))$, such that the approximate statistical solution $\mu_t^\Delta := \mathcal{S}_{t,\#}^\Delta \bar{\mu}$ satisfies

$$W_1(\mu_T, \mu_T^\Delta) \leq C\Delta^\alpha,$$

i.e. that $\mu_T^\Delta \rightarrow \mu_T$ converges at a convergence rate $\alpha > 0$.

Then there exists a constant $\tilde{C} > 0$, such that for any $\epsilon > 0$, there exists a Ψ -FNO $\mathcal{S}_T^* : L_N^2 \rightarrow L_N^2$, with

$$\text{width}(\mathcal{S}_T^*) \leq \tilde{C}\epsilon^{-d/\alpha}, \quad \text{depth}(\mathcal{S}_T^*) \leq \tilde{C}\epsilon^{(d+2)/2\alpha} \log(\epsilon^{-1}), \quad \text{lift}(\mathcal{S}_T^*) \leq \tilde{C},$$

and such that the statistical solution surrogate $\mu_T^* := \mathcal{S}_{T,\#}^* \bar{\mu}$ satisfies,

$$W_1(\mu_T, \mu_T^*) \leq \epsilon.$$

Proof. Fix $N \in \mathbb{N}$, N even, for the moment, so that $N/2 \in \mathbb{N}$. To derive a suitable estimate, we compare the surrogate model with the corresponding approximation by the numerical scheme of Algorithm 7.3.2, at resolution $2\Delta = 2/N$. We note that $W_1(\mu_T, \mu_T^*) \leq W_1(\mu_T, \mu_T^{2\Delta}) + W_1(\mu_T^{2\Delta}, \mu_T^*)$. By assumption, the first term is bounded by

$$W_1(\mu_T, \mu_T^{2\Delta}) \leq CN^{-\alpha}. \tag{7.4.1}$$

To estimate the second term, we note that for any 1-Lipschitz continuous function $\Phi : L_x^2 \rightarrow \mathbb{R}$, we have

$$\begin{aligned} \int_{L_x^2} \Phi(\mathbf{u}) [d\mu_T^{2\Delta}(\mathbf{u}) - d\mu_T^*(\mathbf{u})] &= \int_{L_x^2} \Phi(\mathbf{u}) [d(\mathcal{S}_T^{2\Delta} \bar{\mu})(\mathbf{u}) - d(\mathcal{S}_{T,\#}^* \bar{\mu})(\mathbf{u})] \\ &= \int_{L_x^2} [\Phi(\mathcal{S}_T^{2\Delta}(\mathbf{u})) - \Phi(\mathcal{S}_T^*(\mathbf{u}))] d\bar{\mu}(\mathbf{u}) \\ &\leq \int_{L_x^2} \|\mathcal{S}_T^{2\Delta}(\mathbf{u}) - \mathcal{S}_T^*(\mathbf{u})\|_{L_x^2} d\bar{\mu}(\mathbf{u}). \end{aligned}$$

Taking the supremum over all such Φ , we conclude that

$$W_1(\mu_T^{2\Delta}, \mu_T^*) \leq \int_{L_x^2} \|\mathcal{S}_T^{2\Delta}(\mathbf{u}) - \mathcal{S}_T^*(\mathbf{u})\|_{L_x^2} d\bar{\mu}(\mathbf{u}).$$

Since we clearly have $\mathcal{S}_T^{2\Delta}(\mathbf{u}) = \mathcal{S}_T^{2\Delta}(\mathcal{I}_N \mathbf{u})$, $\mathcal{S}_T^*(\mathbf{u}) = \mathcal{S}_T^*(\mathcal{I}_N \mathbf{u})$, where \mathcal{I}_N denotes the pseudo-spectral projection, we can further estimate this by

$$W_1(\mu_T^{2\Delta}, \mu_T^*) \leq \sup_{\mathbf{u} \in \text{supp}(\bar{\mu})} \|\mathcal{S}_T^{2\Delta}(\mathcal{I}_N \mathbf{u}) - \mathcal{S}_T^*(\mathcal{I}_N \mathbf{u})\|_{L_x^2}.$$

Next, since $\bar{\mu}$ is concentrated on $B_M^s(0)$ by assumption, and since $\mathcal{I}_N : H_x^s \rightarrow L_x^2$ is a bounded operator for $s > d/2$ (cp. Theorem A.1.3 in Appendix A), it follows that there exists $B > 0$, such that

$$\|\mathcal{I}_N \mathbf{u}\|_{L_x^2} \leq B, \quad \forall \mathbf{u} \in \text{supp}(\bar{\mu}).$$

We can thus estimate

$$W_1(\mu_T^{2\Delta}, \mu_T^*) \leq \sup_{\|\mathbf{u}_N\|_{L_x^2} \leq B} \|\mathcal{S}_T^{2\Delta}(\mathbf{u}_N) - \mathcal{S}_T^*(\mathbf{u}_N)\|_{L_x^2},$$

where the supremum is over the (finite-dimensional) ball $\{\mathbf{u}_N \in L_N^2 \mid \|\mathbf{u}_N\|_{L_x^2} \leq B\}$. By Proposition 7.3.8 and the fact that $n_T \sim N^{d/2+1}$, there thus exists a constant $C_0 > 0$, such that for any $\tilde{\epsilon}, B > 0$, there exists a Ψ -FNO $\mathcal{N} : L_N^2 \rightarrow L_N^2$, with $\text{width}(\mathcal{N}) \leq C_0 N^d$, $\text{depth}(\mathcal{N}) \leq C_0 N^{d/2+1} \log(N)$, $\text{lift}(\mathcal{N}) \leq C_0$, and such that

$$\sup_{\|\mathbf{u}_N\| \leq B} \|\mathcal{S}_T^{2\Delta}(\mathbf{u}_N) - \mathcal{N}(\mathbf{u}_N)\|_{L_x^2} \leq \tilde{\epsilon}.$$

Applying this result for $\tilde{\epsilon} = N^{-\alpha}$, and defining $\mathcal{S}_T^* := \mathcal{N}$, we conclude that there exists a Ψ -FNO $\mathcal{S}_T^* : L_N^2 \rightarrow L_N^2$, such that $\text{width}(\mathcal{S}_T^*) \leq C_0 N^d$, $\text{depth}(\mathcal{S}_T^*) \leq C_0 N^{d/2+1} \log(\epsilon^{-1})$, $\text{lift}(\mathcal{S}_T^*) \leq C_0$, and such that

$$W_1(\mu_T^{2\Delta}, \mu_T^*) \leq \sup_{\|\mathbf{u}_N\| \leq B} \|\mathcal{S}_T^{2\Delta}(\mathbf{u}_N) - \mathcal{N}(\mathbf{u}_N)\|_{L_x^2} \leq N^{-\alpha}.$$

By (7.4.1), this implies that

$$W_1(\mu_T, \mu_T^*) \leq (C + 1)N^{-\alpha}.$$

In particular, we can choose $N := \lceil (\epsilon/(C + 1))^{-1/\alpha} \rceil$, to conclude that there exists a constant $\tilde{C} > 0$, independent of ϵ , and a Ψ -FNO $\mathcal{S}_T^* : L_N^2 \rightarrow L_N^2$, such that $\text{width}(\mathcal{S}_T^*) \leq \tilde{C} \epsilon^{-d/\alpha}$, $\text{depth}(\mathcal{S}_T^*) \leq \tilde{C} \epsilon^{-(d+2)/2\alpha} \log(N)$, $\text{lift}(\mathcal{S}_T^*) \leq \tilde{C}$, and

$$W_1(\mu_T, \mu_T^*) \leq \epsilon.$$

This concludes the proof. \square

Remark 7.4.4. *Theorem 7.4.3 shows that, assuming that the spectral scheme 7.3.2 converges to a statistical solution μ_t , then with a sufficiently high resolution, there exists a Ψ -FNO \mathcal{S}_T^* , for which the corresponding statistical solution surrogate $\mu_T^* = \mathcal{S}_{T,\#}^* \bar{\mu}$ provides an accurate approximation of μ_T in the Wasserstein distance. Unfortunately, even if a surrogate \mathcal{S}_T^* can be proven to exist, no theoretical guarantees are currently available that a machine-learning (optimization) algorithm such as Algorithm 7.4.1 will actually find a good approximation. In the absence of such a priori guarantees, extensive numerical experiments will be required to demonstrate the viability of Algorithm 7.4.1, in practice. We will leave this interesting topic for future investigations.*

In practice, one is usually interested in *statistical quantitites* computed from the underlying statistical solution μ_t . Following the general observation from chapter 3 that typical statistical quantities computed from μ_t are generally very smooth, we will assume that the mapping $t \mapsto \int_{L_x^2} \mathcal{G}(\mathbf{u}) d\mu_t(\mathbf{u})$ is *continuous* for all considered observables, in the following; and hence that point-wise evaluation of these quantitites in time is well-defined. Algorithm 7.4.1 then naturally leads to the following algorithm for the estimation of statistical quantities:

Algorithm 7.4.5 (Surrogate estimation of statistical quantitites). *Given an initial probability measure $\bar{\mu} \in \mathcal{P}(L_x^2)$ for which there exists a unique statistical solution μ_t , given an observable $\mathcal{G} : L_x^2 \rightarrow \mathbb{R}^K$, a resolution $\Delta = 1/N$, $N \in \mathbb{N}$, and numbers $M, \tilde{M} \in \mathbb{N}$, corresponding to*

- M surrogate training samples, and
- \tilde{M} Monte-Carlo samples,

respectively, the following algorithm computes an approximation of the expected values with respect to the statistical solution μ_t , i.e. of $\mathbb{E}_t[\mathcal{G}(\mathbf{u})] := \int_{L_x^2} \mathcal{G}(\mathbf{u}) d\mu_t(\mathbf{u})$.

- ① Compute the statistical solution surrogate μ_t^* by Algorithm 7.4.1, with initial data $\bar{\mu}$, resolution $\Delta = 1/N$, and based on M empirical samples.
- ② Draw \tilde{M} iid samples $\bar{\mathbf{u}}_1^*, \dots, \bar{\mathbf{u}}_{\tilde{M}}^* \sim \bar{\mu}$ from the initial measure $\bar{\mu}$.
- ③ For each $j = 1, \dots, \tilde{M}$, compute $\mathcal{G}(\mathbf{u}_j^*(t)) \in \mathbb{R}^K$, where $\mathbf{u}_j^*(t) := \mathcal{S}_t^*(\bar{\mathbf{u}}_j^*)$, and estimate $\mathbb{E}_t^*[\mathcal{G}(\mathbf{u})] \approx \mathbb{E}_t[\mathcal{G}(\mathbf{u})]$ by

$$\mathbb{E}_t^*[\mathcal{G}(\mathbf{u})] := \frac{1}{\tilde{M}} \sum_{j=1}^{\tilde{M}} \mathcal{G}(\mathbf{u}_j^*(t)).$$

□

We next estimate the error of the output of Algorithm 7.4.5, for a Lipschitz continuous observable $\mathcal{G} : L_x^2 \rightarrow \mathbb{R}^K$. To this end, let $\mathcal{S}_t^\Delta : L_x^2 \rightarrow L_x^2$ denote the solution operator associated with scheme (7.3.8), and we assume that the approximate statistical solution $\mu_t^\Delta := \mathcal{S}_{t,\#}^\Delta \bar{\mu}$, converges $\mu_t^\Delta \rightarrow \mu_t$ with respect to the 1-Wasserstein distance to the limiting statistical solution μ_t (cp. chapter 3). We can then decompose the error

$$\begin{aligned} \hat{\mathcal{E}}_{\text{total}} &= \left| \mathbb{E}_t[\mathcal{G}(\mathbf{u})] - \mathbb{E}_t^*[\mathcal{G}(\mathbf{u})] \right| = \left| \int_{L_x^2} \mathcal{G}(\mathbf{u}) d\mu_t(\mathbf{u}) - \frac{1}{\tilde{M}} \sum_{j=1}^{\tilde{M}} \mathcal{G}(\mathbf{u}_j^*(t)) \right| \\ &\leq \left| \int_{L_x^2} \mathcal{G}(\mathbf{u}) d\mu_t(\mathbf{u}) - \int_{L_x^2} \mathcal{G}(\mathbf{u}) d\mu_t^\Delta(\mathbf{u}) \right| \\ &\quad + \left| \int_{L_x^2} \mathcal{G}(\mathbf{u}) d\mu_t^\Delta(\mathbf{u}) - \int_{L_x^2} \mathcal{G}(\mathbf{u}) d\mu_t^*(\mathbf{u}) \right| \\ &\quad + \left| \int_{L_x^2} \mathcal{G}(\mathbf{u}) d\mu_t^*(\mathbf{u}) - \frac{1}{\tilde{M}} \sum_{j=1}^{\tilde{M}} \mathcal{G}(\mathbf{u}_j^*(t)) \right| \\ &=: \hat{\mathcal{E}}_{\text{discretization}} + \hat{\mathcal{E}}_{\text{emulation}} + \hat{\mathcal{E}}_{\text{MC}}, \end{aligned}$$

into the discretization error, the surrogate emulation error and the Monte-Carlo sampling error. An upper bound for the discretization error is given by

$$\hat{\mathcal{E}}_{\text{discretization}} \leq \text{Lip}(\mathcal{G})W_1(\mu_t, \mu_t^\Delta).$$

In particular, if we assume that $\mu_t^\Delta \rightarrow \mu_t$ converges with respect to the 1-Wasserstein distance at a convergence rate $\alpha > 0$, then we have

$$\hat{\mathcal{E}}_{\text{discretization}} \lesssim \Delta^\alpha.$$

Due to the still ill-understood convergence theory of neural network approximations obtained via an optimization algorithm, such as Algorithm 7.4.1, a precise quantification of the emulation error appears out of reach at present. Clearly, this emulation error should decay as a function of the number of training samples M , and by Proposition 7.3.8, we also know that errors arbitrarily close to 0 can be obtained in theory, provided that the Ψ -FNO neural network exceeds a certain minimal size. We will thus make the *assumption* that we have an estimate of the form

$$\hat{\mathcal{E}}_{\text{emulation}} \lesssim \frac{1}{M^\gamma},$$

for some convergence rate $\gamma > 0$. Extensive numerical experiments for model problems in [LJK19, Fig. 10] for a related neural operator architecture (“DeepONets”) have found convergence rates $\gamma \in [1, 4]$, albeit for simpler operators. Based on these early results, we will assume that $\gamma > 1/2$, in the following discussion.

Finally, the Monte-Carlo error is expected (on average) to be of size

$$\hat{\mathcal{E}}_{\text{MC}} \lesssim \frac{1}{\sqrt{M}},$$

yielding an expected total error estimate $\hat{\mathcal{E}}_{\text{total}} \lesssim \Delta^\alpha + M^{-\gamma} + (\tilde{M})^{-1/2}$. If $\gamma > 1/2$ as may be expected based on the results of [LJK19], then clearly, we must choose $\tilde{M} \gg M$ to achieve a given accuracy $\hat{\mathcal{E}}_{\text{total}} \lesssim \epsilon$, *i.e.* the number of Monte-Carlo samples required is much greater than the number of training samples for the surrogate model. More precisely, the above estimate indicates a scaling $\tilde{M} \sim \epsilon^{-2}$, $M \sim \epsilon^{-1/\gamma}$. Denoting by $C^* > 0$ the cost of a single forward evaluation of the surrogate model, $C_{\text{train}}^* > 0$ the training cost per training sample, and by C^Δ a single forward solve of the numerical discretization, the total computational cost to achieve an error of size $\sim \epsilon$, is thus estimated as follows:

Method	Computational cost
direct sampling	$C^\Delta \epsilon^{-2}$
surrogate sampling	$\underbrace{(C^\Delta + C_{\text{train}}^*) \epsilon^{-1/\gamma}}_{\text{training}} + \underbrace{C^* \epsilon^{-2}}_{\text{sampling}}$

Table 7.1: Estimated computational cost for direct Monte-Carlo sampling based on traditional numerical method, and surrogate sampling employing a Ψ -FNO surrogate – split into a training phase, followed by a MC sampling phase.

Table 7.1 illustrates that surrogate sampling is expected to be more efficient than a direct sampling approach, provided that the training convergence rate $\gamma > 1/2$: Indeed, it is reasonable to assume that $C_{\text{train}}^* \lesssim C^\Delta$, since in practice, the neural network representing the Ψ -FNO should involve (considerably) fewer neurons than the number of arithmetic operations required for one forward solve of the corresponding numerical algorithm, resulting in the bound on the computational cost. Hence, we expect

that $C^\Delta \epsilon^{-2} \sim (C^\Delta + C^*)\epsilon^{-2} \gg (C^\Delta + C_{\text{train}}^*)\epsilon^{-1/\gamma}$ for small $\epsilon \rightarrow 0$. Furthermore, the evaluation of the surrogate model, once trained, is in practice *many orders of magnitude faster* than the evaluation of the numerical algorithm, *i.e.* we have $C^* \ll C^\Delta$, and hence also $C^*\epsilon^{-2} \ll C^\Delta\epsilon^{-2}$. In particular, this indicates that surrogate sampling might achieve a saving in computational resources, compared to direct sampling via “traditional” methods.

Thus, the (non-rigorous) estimates summarized in Table 7.1 provide a clear rationale for the potential benefits of statistical solution surrogates based on operator learning, over straight-forward methods based on direct sampling using traditional numerical solvers for uncertainty quantification tasks. This is also in line with empirical observations from numerical experiments in [LMR20] and [LMCR20], where neural network-based surrogate models (in a finite-dimensional setting) have been used successfully to speed up similar many-query problems in uncertainty quantification and optimization, respectively.

7.5 Discussion

Many learning tasks, particularly, but not exclusively, in scientific computing, are naturally formulated as learning operators mapping one infinite-dimensional space to another. Neural operators have recently been proposed as a framework for operator learning. A particular form, the so-called Fourier Neural Operators (FNOs) (7.2.6), have been shown to be efficient in approximating a wide variety of operators that arise in PDEs [LKA⁺21]. Our main aim in the present work was to analyze FNOs and Ψ -FNOs (7.2.14), which is a concrete computational realization of FNOs. To this end, we have presented the following results, following [KLM21]:

- We showed in Theorem 7.2.5 and Theorem 7.2.15 that FNOs (resp. Ψ -FNOs) are *universal* *i.e.*, they can approximate any continuous operator to desired accuracy. Our proof relies heavily on the ability of FNOs to approximate the Fourier transform and its inverse, together with the neural network approximation of the finite-dimensional Fourier conjugate operator (7.2.11). Thus, FNOs have the same universal approximation property as canonical neural networks for finite-dimensional functions and DeepOnets for operators [LMK21]. This universality result paves the way for the widespread use of FNOs in the context of operator learning.
- However as stated in remark 7.3.1, in the worst case, the size of a FNO can grow *super-exponentially* in terms of the desired error for approximating a general Lipschitz continuous operator. This might inhibit the use of FNOs. On the other hand, we argue in the beginning of section 7.3 that Ψ -FNOs, which are a concrete computational realization of FNOs, can approximate the nonlinearities and differential operators that define PDEs, very efficiently. Hence, one can think of Ψ -FNOs as a new form of pseudo-spectral methods for PDEs, which in practice are adapted to, and optimized based on the given training data. Thus, one can expect that Ψ -FNOs can approximate PDEs efficiently.
- We consider the incompressible Navier-Stokes and Euler equations for fluid dynamics, and prove rigorously that there exists a Ψ -FNO which can approximate the underlying nonlinear operators efficiently, as we can show that the size of the Ψ -FNO only needs to grow polynomially in terms of the error. A second application of Ψ -FNOs to the stationary Darcy flow is given in [KLM21]. These two prototypical examples show that FNOs can approximate these widely used PDEs efficiently, corroborating the empirical results presented in [LKA⁺21].
- We propose an algorithm for the approximation of statistical solutions, and the computation of statistical quantities, based on neural network-based surrogate models. And we provide a clear rationale for the benefits of the resulting *statistical solution surrogates* versus the straight-forward Monte-Carlo evaluation of statistical quantities based on traditional numerical methods.

Hence, our analysis provides very strong theoretical evidence that FNOs are an effective framework for operator learning, and for their potential benefits in applications. Extending the analysis summarized in this chapter to other neural operators can be readily envisaged. The use of FNOs for more general operators, particularly those arising in non-scientific computing settings, such as images, text and speech, also needs to be investigated.

Chapter 8

Conclusions and further research

The present thesis has focused on the approximation of the incompressible Euler equations (1.1.1), from both a deterministic and a statistical point of view. Physically, these equations can be seen as an idealized model of high Reynolds-number flows, in which effects due to viscosity are small compared to the typical flow speeds and length scales. In such flows, non-linear terms describing the transport of momentum dominate over regularizing terms due to viscosity, often leading to a very complex, turbulent behaviour. Physical theories of turbulence predict that typical solutions in this regime possess very low (Hölder) regularity. The mathematical theory for such rough solutions of the incompressible Euler equations is still very far from complete, and many open questions regarding well-posedness and stability remain. At the level of numerical approximations, the lack of stability with respect to perturbations in the initial data results in a lack of rigorous convergence proofs. Furthermore, an absence of (strong) convergence in any conventional *deterministic sense* is empirically observed in numerical experiments for initial data with low regularity.

The first main result of this work is a (weak) convergence result for the approximation of rough solutions of the two-dimensional Euler equations by the SV scheme, presented in chapter 2. This result is based on compensated compactness methods, and its proof follows the most general available existence result for solutions of the two-dimensional incompressible Euler equations, for initial data in the so-called “*Delort class*”. The work summarized in chapter 2 closes a long-standing gap between available existence theory and convergence results for general purpose numerical schemes. Despite these provable compactness properties, numerical experiments reviewed in chapter 2 show that in practice, even for carefully tuned parameters of the numerical scheme, the *strong* convergence of the SV scheme for such rough initial data is prevented by the appearance of small-scale instabilities at high resolutions, which are strongly amplified by the flow. This is in line with earlier computations of vortex sheets [FMT16, LM15, Leo18]. These earlier investigations have found that while each *deterministic* simulation may be unstable and cannot be robustly computed by state-of-the-art numerical schemes, *statistical quantities* are much more stable and can be reliably approximated when considering *ensembles* of solutions.

The second main result of this thesis is the introduction and study of a *statistical solution* concept for the incompressible Euler equations, presented in chapter 3. While a general (a priori) mathematical well-posedness theory of statistical solutions remains out of reach at present, we study the convergence of numerical approximations to a statistical solution and derive theoretical convergence criteria which can be verified *a posteriori* from numerical experiments. These convergence criteria are either formulated as uniform bounds (in resolution $\Delta > 0$) on the structure functions, or are based on a dual (Fourier transformed) description, in terms of a uniform decay of the energy spectra of the flow. Both of these quantities are closely related to physical theories of turbulence [Fri95], based on which the required

uniform bounds would be expected to be satisfied in practice. Extensive numerical experiments carried out for the two-dimensional Euler equations provide empirical evidence that the convergence criteria are indeed satisfied for a wide range of initial data, and indicate the convergence of numerical approximations to a well-defined limiting statistical solution.

The observed well-behaved evolution of structure functions in chapter 3, provides the motivation for the detailed study of uniform bounds on these structure functions, in chapter 4. In particular, we are interested in the question of anomalous energy dissipation in the zero-viscosity limit of the Navier-Stokes equations. This research direction has lead to the third main result of the present thesis, which shows that, in two spatial dimensions, *any* uniform bound on the second-order structure functions (in the zero-viscosity limit) implies energy conservation of the limiting solution of the incompressible Euler equations. The results summarized in chapter 4 go considerably beyond the well-known critical regularity threshold identified by Onsager, which predicts energy-conservation for solutions with α -Hölder regularity for $\alpha > 1/3$, and clearly shows that solutions obtained in the zero-viscosity limit possess additional fine properties which are not shared by general (energy-admissible) solutions.

Finally, in chapters 6 and 7, we make first steps towards addressing two limitations of statistical solutions. The first limitation concerns the blending of statistical solutions with observational data; combining the underlying mathematical model with observational data has proven pivotal in real-world applications, such as numerical weather forecasting. In chapter 6, we thus study a statistical Bayesian approach to state estimation for PDEs for which the forward problem is (potentially) ill-posed. We prove compactness and uniform stability results for numerical approximations of Bayesian inverse problems and data assimilation, under very mild assumptions, and show the existence of a limiting posterior obtained in the high resolution limit ($\Delta \rightarrow 0$). Furthermore, we show convergence to the canonical posterior, provided that the approximate solution operator $\mathcal{S}_t^\Delta(u) \rightarrow \mathcal{S}_t(u)$, $\Delta \rightarrow 0$, merely converges *almost everywhere* with respect to the prior probability measure $\mu_{\text{prior}}(du)$.

Finally, in chapter 7 we summarize approximation results for a recently proposed operator learning framework termed *Fourier neural operators* (FNOs) [LKA⁺21], based on neural networks. We discuss the first universal approximation theorems for this architecture, showing that FNOs can approximate operators $\mathcal{G} : H^s \rightarrow H^{s'}, s, s' \geq 0$, to arbitrary accuracy. Employing ideas from spectral methods, we furthermore derive explicit complexity and error estimates for the FNO approximation of the solution operator of the incompressible Euler and Navier-Stokes equations, proving that this infinite-dimensional approximation task can be solved *efficiently*, and more precisely, that the overall complexity scales at most algebraically in the desired approximation accuracy. These results provide the first theoretical justification for the use of FNOs in applications. Based on this FNO architecture, we propose a surrogate model approach for the evaluation of statistical quantities, by the use of a so-called *statistical solution surrogate*. We provide empirical complexity estimates for the computation of statistical quantities based on this surrogate approach, and show that they compare favourably in comparison with a direct evaluation based on traditional numerical methods.

The results presented in the present thesis thus lay the mathematical foundations for statistical solutions of the incompressible Euler equations and their numerical approximation, emphasizing the central role played by structure functions in their convergence theory, as well as making initial steps toward the incorporation of observational data in a Bayesian approach, and addressing the theoretical underpinnings of a novel neural network based approach to many-query problems, within the general framework of “operator learning” architectures.

Future research directions

While the theoretical results on statistical solutions presented in chapter 3 apply also to the three-dimensional Euler equations, more numerical experiments are needed to investigate whether the obser-

vations presented for the two-dimensional case also apply in the three-dimensional case. Corresponding work on statistical solutions of the compressible Euler equations and related hyperbolic conservation laws strongly indicates that similar conclusions will apply also in three spatial dimensions. Due to the high computational cost of three-dimensional simulations, to render such numerical experiments feasible, further developments will be required in the numerical implementation, taking full advantage of accelerated computing capabilities based on GPUs. In particular, these experiments can numerically investigate the more intricate question of three-dimensional anomalous energy dissipation, and will allow for a direct comparison of two- and three-dimensional turbulence.

The rigorous theoretical justification for many of the empirical observations presented in the present work remains unknown. For example, more work is needed to explain the observed stability of statistical quantities and the apparently well-defined evolution of statistical solutions, even in situations where the underlying deterministic evolution is very unstable, and potentially ill-posed. Progress in the understanding of this distinction between the stability of statistical quantities versus the instability of deterministic predictions, possibly in the context of simpler model equations, would mark a major contribution towards the understanding of high Reynolds number flows, in the opinion of the present author.

In this context, we point out a potentially interesting analogy that can be made between the theory of statistical solutions investigated in the present thesis and related work [FW18, LMS16, FLMW20, VF77, FRT10, PP21], and the well-posedness theory of finite-dimensional ODEs with rough coefficients initiated by DiPerna and Lions [DL89]: The authors of [DL89] studied solutions of ODEs of the form

$$\frac{dX}{dt} = \mathbf{b}(X), \quad X(t=0) = \bar{x} \in \mathbb{R}^d, \quad (8.0.1)$$

for vector-fields \mathbf{b} which possess only Sobolev regularity, *e.g.* for $\mathbf{b} \in W^{1,1}(\mathbb{R}^d; \mathbb{R}^d)$, with distributional divergence $\text{div}(\mathbf{b}) = 0$ (in fact, much more general vector fields are considered in [DL89]). Classical existence and uniqueness results for (8.0.1) require considerably more regularity on the vector field \mathbf{b} , such as Lipschitz continuity, to guarantee well-posedness for solutions of (8.0.1). The main idea of [DL89] is that while the ODE (8.0.1) is generally ill-posed, the associated transport equation (PDE)

$$\partial_t \rho + \mathbf{b} \cdot \nabla \rho = 0, \quad \rho(t=0) = \bar{\rho} \in L^1(\mathbb{R}^d), \quad (8.0.2)$$

can nevertheless be well-posed; in fact, it can be used to study and shed light on the initial value problem (8.0.1), and can be used to define a unique flow $X \in C(\mathbb{R}; L^1(\mathbb{R}^d; \mathbb{R}^d))$ providing solutions of the ODE.

DiPerna-Lions theory		Statistical solutions
$\begin{cases} \frac{dX}{dt} = \mathbf{b}(X), \\ X(t=0) = \bar{x}. \end{cases}$	\longleftrightarrow	$\begin{cases} \partial_t \mathbf{u} = -\mathbb{P}\text{div}(\mathbf{u} \otimes \mathbf{u}), \\ \mathbf{u}(t=0) = \bar{\mathbf{u}}. \end{cases}$
$\begin{cases} \partial_t \rho + \mathbf{b} \cdot \nabla \rho = 0, \\ \rho(t=0) = \bar{\rho}. \end{cases}$	\longleftrightarrow	$\begin{cases} (\text{Statistical sol. } \mu_t), \\ \mu_t _{t=0} = \bar{\mu}. \end{cases}$

Table 8.1: Analogy between DiPerna-Lions theory [DL89] and statistical solutions.

To make the analogy to statistical solutions apparent, we now interpret non-negative initial data $\bar{\rho} \in L^1$ of (8.0.2) as a probability distribution $\bar{\mu}$ on initial data \bar{x} to the ODE (8.0.1), so that for

measurable $A \subset \mathbb{R}^d$, we have

$$\bar{\mu}(A) = \text{Prob}[\bar{x} \in A] = \frac{\int_A \bar{\rho}(x) dx}{\int_{\mathbb{R}^d} \bar{\rho}(x) dx}.$$

In this analogy, the solution $t \mapsto \rho(\cdot, t)$ of the transport PDE (8.0.2) corresponds to a “statistical solution”,

$$\mu_t(A) = \frac{\int_A \bar{\rho}(x, t) dx}{\int_{\mathbb{R}^d} \bar{\rho}(x, t) dx} \in \mathcal{P}(\mathbb{R}^d),$$

describing the evolution of the uncertain (statistical) initial data $\bar{\mu}$ to (8.0.1). By the results of the DiPerna-Lions theory, there thus exists a class of “statistical initial data” for which the evolution of the corresponding statistical solution is well-defined, even though the *deterministic problem* (8.0.1) (corresponding to Dirac initial data $\bar{\mu} = \delta_x$) is *ill-posed*.

Extensive numerical experiments conducted in the context of statistical solutions for PDEs arising in fluid dynamics suggest that there might exist a similar class of statistical initial data for which the (infinite-dimensional) statistical evolution is well-posed, even though the problem at the level of deterministic solutions is ill-posed. We have summarized this analogy in Table 8.1. Future work could attempt to make progress towards making this analogy more precise. A key element that is currently missing in the PDE context is a better understanding of the well-posedness theory for the infinite-dimensional analogue of the transport equation (8.0.2), describing the evolution of statistical solutions $\mu_t \in \mathcal{P}(L_x^2)$. We have proposed a description of the evolution of μ_t in Definition 3.3.1, formulated in terms of a hierarchy of equations, relying on the duality between the probability measure $\mu_t \in \mathcal{P}(L_x^2)$ and the corresponding correlation marginals $\nu_{t,x}^k \in \mathcal{P}(U^k)$, $k \in \mathbb{N}$, on state-space U .

The theoretical benefit of this hierarchy of equations for statistical solutions is its linearity, similar to (8.0.2); the main drawback is the formulation as a infinite hierarchy of coupled PDEs. Currently, it is not clear to what extent this hierarchy is amenable to direct mathematical analysis, and future work is needed to better understand the mathematical properties of this hierarchy, and to what extent it might allow to make the analogy with finite-dimensional transport equations, indicated in Table 8.1, precise.

In chapter 6, we have presented a theoretical discussion of the numerical approximation of Bayesian inversion and data assimilation for prototypical models of fluid dynamics, the incompressible Euler and Navier-Stokes equations. The theoretical results of chapter 6 should be complemented by numerical experiments, investigating the practical convergence of approximate posteriors obtained by numerical discretizations, as $\Delta \rightarrow 0$.

The approximation theory developed in chapter 7 for Fourier neural operators represents the first steps in the analysis of neural network architectures for operator learning, with potential for applications to many-query problems including uncertainty quantification, Bayesian inversion and PDE constrained optimization. Many open questions and challenges remain in establishing the mathematical foundations of this emerging field; Open research directions include the numerical investigation and comparison of different operator learning frameworks, demonstrating the practical viability of neural network based surrogate models, as well as extensions of the approximation theory, in particular for statistical solutions.

The author hopes that the work presented in this thesis may serve as a starting point for future work in a variety of interesting and fruitful research directions, with potential for impact on problems in science and engineering.

List of symbols

Throughout this work, we follow the convention that constants C appearing in estimates may change their value from line to line. The dependency of the constant C on the given data (e.g. parameters α, β, γ) should usually be clear from the context and will be indicated by writing $C = C(\alpha, \beta, \gamma)$. For the convenience of the reader, we provide a list of the most common symbols used in this work, below:

Frequently used symbols

\mathbb{T}^d	periodic torus, identified with $[0, 2\pi]^d$	p. 3
d	spatial dimension of domain	p. 3
\mathbf{u}	(flow) vector field $\mathbf{u} : \mathbb{T}^d \times [0, T] \rightarrow \mathbb{R}^d$	p. 3
$\bar{\mathbf{u}}$	initial data $\bar{\mathbf{u}} : \mathbb{T}^d \rightarrow \mathbb{R}^d$ (for incompressible Euler)	p. 3
$\hat{\mathbf{u}}_k$	(spatial) Fourier coefficient of \mathbf{u}	p. 7
ω	(scalar) curl of \mathbf{u} , $\omega = \text{curl}(\mathbf{u}) \in \mathbb{R}$ (for $d = 2$)	p. 8
Δ	grid scale parameter $\Delta \equiv 1/N$, $N \in \mathbb{N}$	p. 16
\mathbf{u}^Δ	discretized velocity, $\mathbf{u}^\Delta = \sum_{ k _\infty \leq N} \hat{\mathbf{u}}^\Delta e^{ik \cdot x}$	p. 16
ω^Δ	(scalar) curl of \mathbf{u}^Δ , $\omega^\Delta = \text{curl}(\mathbf{u}^\Delta) \in \mathbb{R}$ (for $d = 2$)	p. 23
$\mathcal{P}(X)$, $(\mathcal{P}(L_x^2))$	space of Borel probability measures on Banach space X (L_x^2)	p. 185
$\mathcal{P}_p(X)$	set of $\mu \in \mathcal{P}(X)$ with finite p -th moment	p. 185
\mathcal{M}	set of bounded Radon measures on \mathbb{T}^d	p. 21
\mathcal{M}_+	set of non-negative Radon measures on \mathbb{T}^d	p. 22
ν	viscosity parameter in Navier-Stokes equations	p. 5
μ_t	time-parametrized probability measure (or statistical solution)	p. 50
$\bar{\mu}$	statistical initial data, $\bar{\mu} \in \mathcal{P}(L_x^2)$	
μ_t^Δ	approximate statistical solution	p. 50
$S_2(\mu; r)$	statistical (second-order) structure function	p. 49
$S_2^T(\mu_t; r)$	time-integrated statistical structure function	p. 51
$W_1(\mu, \nu)$	1-Wasserstein distance between $\mu, \nu \in \mathcal{P}_1(L_x^2)$	p. 185
$d_T(\mu_t, \nu_t)$	time-integrated 1-Wasserstein distance	p. 50
$L_t^1(\mathcal{P})$	space of time-parametrized probability measures, s.t. $d_T(\mu_t, \delta_0) < \infty$	p. 50
$S_2(\mathbf{u}; r)$	deterministic structure function	p. 84
$S_2^T(\mathbf{u}; r)$	time-integrated structure function	p. 84
$\bar{\mathbf{u}} \mapsto \mathcal{S}_t(\bar{\mathbf{u}})$	solution operator	
$\bar{\mathbf{u}} \mapsto \mathcal{S}_t^\Delta(\bar{\mathbf{u}})$	approximate solution operator (from discretization)	
$\phi(r)$	modulus of continuity	

Banach spaces

L^2	Space of square-integrable functions	
\dot{L}^2	$\dot{L}^2 \subset L^2$ square-integrable functions with zero mean	p. 180

L_N^2	$L_N^2 \subset L^2$ trigonometric polynomials of degree $\leq N$	p. 180
\dot{L}_N^2	$\dot{L}_N^2 = \dot{L}^2 \cap L_N^2$ trigonometric polynomials with zero mean	p. 180
H^s	Sobolev space of smoothness $s \geq 0$, with norm $\ \cdot\ _{H^s}$	p. 179
H^{-s}	dual of H^s	
\dot{H}^s	Sobolev space with zero mean, with norm $\ \cdot\ _{\dot{H}^s}$	p. 180

Projection operators

P_N	L^2 -orthogonal Fourier projection $P_N : L^2 \rightarrow L_N^2$	p. 180
\dot{P}_N	Fourier projection $\dot{P}_N : L^2 \rightarrow \dot{L}_N^2$ with zero mean	p. 181
\mathcal{I}_N	Pseudo-spectral Fourier projection, i.e. trigonometric interpolation on regular grid $\{x_j\}_{j \in \mathcal{J}_N}$	p. 181
\mathbb{P}	Leray projection onto divergence-free vector fields	p. 161
\mathbb{P}_N	Leray projection followed by projection P_N ; $\mathbb{P}_N = P_N \circ \mathbb{P}$	p. 161

Bayesian inversion

$\mathcal{L}^\Delta(u)$, $\mathcal{L}(u)$	observable	p. 117
y	measurement, $y \in \mathbb{R}^d$	p. 117
η	measurement noise	p. 117
$d\mu^{\Delta,y}(u)$	posterior probability measure	p. 117
$\Phi^{\Delta,y}(u)$	log-likelihood function	p. 117
$\mathcal{G}_j(u)$	Eulerian observable	p. 128
Y_j	measurements $Y_j = (y_1, \dots, y_j)$ in time interval $[0, t_j]$	p. 129
$\nu_t^{\Delta,Y_j}(du)$	Bayesian estimate at time t , given measurements Y_j	p. 129
$\nu_t^{\Delta,y}$	filtering distribution, Bayesian estimate given past measurements	p. 133

Neural networks

σ	activation function	
d_a, d_u, d_v	number of components of input, output and lifting	p. 150
$\mathcal{A}(D; \mathbb{R}^{d_a})$	input function space	p. 150
$\mathcal{U}(D; \mathbb{R}^{d_u})$	output function space	p. 150
$\mathcal{F}, \mathcal{F}^{-1}$	Fourier transform and inverse Fourier transform	p. 179
$\mathcal{F}_N, \mathcal{F}_N^{-1}$	discrete Fourier transform and inverse	p. 182
$\{x_j\}_{j \in \mathcal{J}_N}$	regular periodic grid, $x_j = 2\pi j/(2N+1)$	p. 182
\mathcal{J}_N	grid point indices, $\mathcal{J}_N = \{0, \dots, 2N\}^d$	p. 182
\mathcal{K}_N	Fourier wavenumbers $\mathcal{K}_N = \{k \in \mathbb{Z}^d \mid k _\infty \leq N\}$	
\mathcal{R}	lifting operator	p. 150
\mathcal{L}_ℓ	neural operator layer	p. 151
\mathcal{Q}	projection operator	p. 150
\mathcal{F} -layer	linear, non-local layer; $v(x) \mapsto \mathcal{F}^{-1}(P\mathcal{F}v)(x)$	p. 158
σ -layer	non-linear, local layer; $v(x) \mapsto \sigma(Wv(x) + b(x))$	p. 158

Appendices

Appendix A

Mathematical complements

In this appendix, we summarize frequently used notation in the thesis main text, summarize some essential facts about Fourier analysis and recall two well-known theorems in analysis.

A.1 Fourier analysis

In the main text, we focus on functions defined on the periodic torus \mathbb{T}^d , identified as $\mathbb{T}^d = [0, 2\pi]^d$. Following standard practice, we denote by $L^2(\mathbb{T}^d)$ the space of square-integrable functions. For any such function $v \in L^2(\mathbb{T}^d)$, we can define the **Fourier transform** as,

$$\mathcal{F}(v)(k) := \frac{1}{(2\pi)^d} \int_{\mathbb{T}^d} v(x) e^{-ik \cdot x} dx, \quad \forall k \in \mathbb{Z}^d. \quad (\text{A.1.1})$$

For any $k \in \mathbb{Z}^d$, the k -th Fourier coefficient of v is denoted by $\hat{v}_k = \mathcal{F}(v)(k)$.

Given a set of Fourier coefficients $\{\hat{v}_k\}_{k \in \mathbb{Z}^d}$, the **inverse Fourier transform** is defined as,

$$\mathcal{F}^{-1}(\hat{v})(x) := \sum_{k \in \mathbb{Z}^d} \hat{v}_k e^{ik \cdot x}, \quad \forall x \in \mathbb{T}^d. \quad (\text{A.1.2})$$

We recall Parseval's identity for $u, v \in L^2(\mathbb{T}^d)$:

$$\langle u, v \rangle_{L^2} := \int_{\mathbb{T}^d} u(x) v(x) dx = (2\pi)^d \sum_{k \in \mathbb{Z}^d} \hat{u}_k \hat{v}_k. \quad (\text{A.1.3})$$

Using the Fourier transform (A.1.1) and for $s \geq 0$, we denote by $H^s(\mathbb{T}^d)$ the **Sobolev space** of functions $v \in L^2(\mathbb{T}^d)$, with Fourier coefficients $\{\hat{v}_k\}_{k \in \mathbb{Z}^d}$, having a finite H^s -norm:

$$\|v\|_{H^s} := \left((2\pi)^d \sum_{k \in \mathbb{Z}^d} (1 + |k|)^{2s} |\hat{v}_k|^2 \right)^{1/2} < \infty. \quad (\text{A.1.4})$$

Note that with this definition, we have from Parseval's identity, that $\|v\|_{H^0} = \|v\|_{L^2}$, so that $H^0(\mathbb{T}^d) = L^2(\mathbb{T}^d)$. Furthermore, we note that for any $s \geq 0$, the dual space H^{-s} is the space of distributions $v \in \mathcal{D}'(\mathbb{T}^d)$, with Fourier coefficients \hat{v}_k satisfying

$$\|v\|_{H^{-s}} = \left((2\pi)^d \sum_{k \in \mathbb{Z}^d} \frac{1}{(1 + |k|)^{2s}} |\hat{v}_k|^2 \right)^{1/2} < \infty.$$

Furthermore, for any functions $u, v \in L^2(\mathbb{T}^d)$, we have from Parseval's identity and the Cauchy-Schwarz inequality:

$$\langle u, v \rangle_{L^2} \leq \|u\|_{H^s} \|v\|_{H^{-s}}.$$

We also introduce the corresponding **homogeneous Sobolev spaces** $\dot{H}^s(\mathbb{T}^d)$ (and $\dot{L}^2(\mathbb{T}^d) := \dot{H}^0(\mathbb{T}^d)$), consisting of functions $v(x) \in H^s(\mathbb{T}^d)$ and with zero mean $\int_{\mathbb{T}^d} v(x) dx = \widehat{v}_0 = 0$. The space $\dot{H}^s(\mathbb{T}^d)$ is endowed with the norm

$$\|v\|_{\dot{H}^s} := \left((2\pi)^d \sum_{k \in \mathbb{Z}^d \setminus \{0\}} |k|^{2s} |\widehat{v}_k|^2 \right)^{1/2}. \quad (\text{A.1.5})$$

Given $N \in \mathbb{N}$, throughout this work, we will denote by $L_N^2(\mathbb{T}^d)$, the space of trigonometric polynomials $v_N : \mathbb{T}^d \rightarrow \mathbb{R}$, of the form

$$v_N(x) = \sum_{|k|_\infty \leq N} c_k e^{ix \cdot k}, \quad (\text{A.1.6})$$

where the summation is over all $k = (k_1, \dots, k_d) \in \mathbb{Z}^d$ such that

$$|k|_\infty := \max_{i=1, \dots, d} |k_i| \leq N.$$

The space $L_N^2(\mathbb{T}^d)$ is viewed as a normed vector space with norm $\|\cdot\|_{L^2}$. Similarly, for $s \geq 0$, we denote by $H_N^s(\mathbb{T}^d)$ the normed vector space of trigonometric polynomials v_N of degree $\leq N$, with norm $\|\cdot\|_{H^s}$.

We note that in order to ensure that $v_N(x) \in \mathbb{R}$ is real-valued for all $x \in \mathbb{T}^d$, the coefficients $c_k \in \mathbb{C}$ must satisfy the relations $c_{-k} = \overline{c_k}$ for all $|k|_\infty \leq N$, and where $\overline{c_k}$ denotes the complex conjugate of c_k .

We denote by

$$P_N : L^2(\mathbb{T}^d) \rightarrow L_N^2(\mathbb{T}^d), \quad v \mapsto P_N v, \quad (\text{A.1.7})$$

the **L^2 -orthogonal projection onto $L_N^2(\mathbb{T}^d)$** ; or more explicitly,

$$P_N \left(\sum_{k \in \mathbb{Z}^d} c_k e^{ik \cdot x} \right) = \sum_{|k|_\infty \leq N} c_k e^{ik \cdot x}, \quad \forall (c_k)_{k \in \mathbb{Z}^d} \in \ell^2(\mathbb{Z}^d).$$

In fact, the mapping P_N defines a projection $H^s(\mathbb{T}^d) \rightarrow H_N^s(\mathbb{T}^d)$ for any $s \geq 0$. We have the following spectral approximation estimate: Let $s > 0$ be given. There exists a constant $C = C(s, d) > 0$, such that for any $v \in H^s(\mathbb{T}^d)$, we have

$$\|v - P_N v\|_{H^s} \leq C N^{-(s-\varsigma)} \|v\|_{H^s}, \quad \text{for any } \varsigma \in [0, s]. \quad (\text{A.1.8})$$

We furthermore note that the norm of the projection $P_N : L^1 \rightarrow L^1$ is not uniformly bounded. Instead, we have the following estimate:

Proposition A.1.1. *Let $N \in \mathbb{N}$, $N \geq 2$. The norm of the Fourier projection $P_N : L^1(\mathbb{T}^d) \rightarrow L^1(\mathbb{T}^d)$, interpreted as an operator on L^1 , is bounded by $\|P_N\|_{L^1 \rightarrow L^1} \leq C \log(N)^d$, where $C > 0$ is an absolute constant, independent of N .*

Proof. Let $D_N^1 : \mathbb{T} \rightarrow \mathbb{R}$ be the (one-dimensional) Dirichlet kernel, $D_N^1(\xi) = (2\pi)^{-1} \sum_{\ell=-N}^N e^{i\ell\xi}$. We recall in passing that D_N^1 can be expressed in the closed form

$$D_N^1(\xi) = \frac{\sin((N+1/2)\xi)}{2\pi \sin(\xi)}.$$

Let $D_N(x) := \prod_{k=1}^d D_N^1(x_k)$ be the d -fold tensor product of D_N^1 . We note that the projection P_N can be written as a convolution with D_N , *i.e.* that $P_N u \equiv D_N * u$ for any $u \in L^1(\mathbb{T}^d)$. It follows that

$$\|P_N u\|_{L^1} = \|D_N * u\|_{L^1} \leq \|D_N\|_{L^1} \|u\|_{L^1},$$

and hence, $\|P_N\|_{L^1 \rightarrow L^1} \leq \|D_N\|_{L^1}$. The claim now follows from the well-known fact that $\|D_N^1\|_{L^1} \leq C \log(N)$ for some constant $C > 0$, and from the identity

$$\|D_N\|_{L^1} = \int_{\mathbb{T}^d} \prod_{k=1}^d |D_N^1(x_k)| dx = \prod_{k=1}^d \int_{\mathbb{T}} |D_N^1(x_k)| dx_k = \prod_{k=1}^d \|D_N^1\|_{L^1} \leq C^d \log(N)^d.$$

□

We also define a natural projection

$$\dot{P}_N : L^2(\mathbb{T}^d) \rightarrow \dot{L}_N^2(\mathbb{T}^d), \quad (\text{A.1.9})$$

by removing the mean, *i.e.* $\dot{P}_N v = P_N v - \int_{\mathbb{T}^d} v(x) dx$, or equivalently:

$$\dot{P}_N \left(\sum_{k \in \mathbb{Z}^d} c_k e^{ik \cdot x} \right) = \sum_{0 < |k|_\infty \leq N} c_k e^{ik \cdot x}, \quad \forall (c_k)_{k \in \mathbb{Z}^d} \in \ell^2(\mathbb{Z}^d).$$

Furthermore, we denote by

$$\mathcal{I}_N : C(\mathbb{T}^d) \mapsto L_N^2(\mathbb{T}^d), \quad u \mapsto \mathcal{I}_N u, \quad (\text{A.1.10})$$

the **pseudo-spectral projection** onto $L_N^2(\mathbb{T}^d)$; we recall that the pseudo-spectral projection $\mathcal{I}_N v$ of a continuous function v is defined as the unique trigonometric polynomial $\mathcal{I}_N v \in L_N^2(\mathbb{T}^d)$, such that

$$\mathcal{I}_N v(x_j) = v(x_j), \quad \forall j \in \mathcal{J}_N, \quad (\text{A.1.11})$$

where $\{x_j\}_{j \in \mathcal{J}_N}$ denotes the set of all regular grid points $x_j \in \mathbb{Z}^d$ of the form $x_j = 2\pi j/(2N+1) \in \mathbb{T}^d$, $j \in \mathbb{Z}^d$ (*cp.* equation (A.1.12)).

We also recall the following embedding theorem for the Sobolev spaces $H^s(\mathbb{T}^d)$:

Theorem A.1.2 (Sobolev embedding). *Let $d \in \mathbb{N}$. For any $s > d/2$, we have a compact embedding $H^s(\mathbb{T}^d) \hookrightarrow C(\mathbb{T}^d)$ into the space of continuous functions. In particular, there exists a constant $C = C(s, d) > 0$, such that*

$$\|v\|_{L^\infty} \leq C \|v\|_{H^s}, \quad \forall v \in H^s(\mathbb{T}^d).$$

The Sobolev embedding theorem implies in particular that the pseudo-spectral projection \mathcal{I}_N is well-defined as an operator $\mathcal{I}_N : H^s(\mathbb{T}^d) \rightarrow L_N^2(\mathbb{T}^d)$ for $s > d/2$. In the following theorem, we recall a well-known approximation error estimate for the pseudo-spectral projection \mathcal{I}_N :

Theorem A.1.3 (Pseudo-spectral approximation estimate). *Let $d \in \mathbb{N}$. For any $s > d/2$ and $N \in \mathbb{N}$, the spectral interpolation operator $\mathcal{I}_N : H^s(\mathbb{T}^d) \rightarrow L_N^2(\mathbb{T}^d)$ is well-defined. Furthermore, there exists a constant $C = C(s, d) > 0$, such that the following approximation error estimate holds*

$$\|(1 - \mathcal{I}_N)v\|_{H^s} \leq CN^{-(s-\varsigma)} \|v\|_{H^s}, \quad \forall v \in H^s(\mathbb{T}^d),$$

for any $\varsigma \in [0, s]$.

Finally, for $N \in \mathbb{N}$, we fix a regular grid $\{x_j\}_{j \in \mathcal{J}_N}$ of values

$$x_j = \frac{2\pi j}{2N + 1}, \quad (\text{A.1.12})$$

where the index $j \in \mathcal{J}_N$ belong to the index set

$$\mathcal{J}_N := \{0, \dots, 2N\}^d. \quad (\text{A.1.13})$$

Recall the set of Fourier wave numbers (7.2.10) and we define the **discrete Fourier transform** $\mathcal{F}_N : \mathbb{R}^{\mathcal{J}_N} \rightarrow \mathbb{C}^{\mathcal{K}_N}$ by

$$\mathcal{F}_N(v)(k) := \frac{1}{(2N+1)^d} \sum_{j \in \mathcal{J}_N} v_j e^{-2\pi i(k \cdot x_j)}, \quad (\text{A.1.14})$$

with inverse $\mathcal{F}_N^{-1} : \mathbb{C}^{\mathcal{K}_N} \rightarrow \mathbb{R}^{\mathcal{J}_N}$,

$$\mathcal{F}_N^{-1}(\hat{v})(j) := \sum_{k \in \mathcal{K}_N} \hat{v}_k e^{2\pi i(k \cdot x_j)}. \quad (\text{A.1.15})$$

We finally remark that all of the above notions are extended to functions $\mathbf{u} : \mathbb{T}^d \rightarrow \mathbb{R}^{d'}$ in the obvious way (with multiplication $u(x)v(x)$ replaced by the dot-product $\mathbf{u}(x) \cdot \mathbf{v}(x)$), leading to corresponding spaces $L^2(\mathbb{T}^d; \mathbb{R}^{d'}), H^s(\mathbb{T}^d; \mathbb{R}^{d'}), \dot{H}^s(\mathbb{T}^d; \mathbb{R}^{d'})$. We will use the same notation $P_N, \dot{P}_N, \mathcal{I}_N$ for the corresponding projections defined on vector-fields $\mathbf{u} : \mathbb{T}^d \rightarrow \mathbb{R}^{d'}$. If the domain and co-domain are clear from the context, we will occasionally write H^s , instead of $H^s(\mathbb{T}^d; \mathbb{R}^{d'})$; in order to emphasize the fact that we consider functions with a spatial dependence, we shall also use the short-hand notation $H_x^s = H^s(\mathbb{T}^d; \mathbb{R}^{d'})$. In particular, for a time-parametrized mapping $\mathbf{u} : [0, T] \rightarrow H_x^s$, we will write $\|\mathbf{u}(t)\|_{H_x^s}$ for the H^s -norm of $\mathbf{u}(t) \in H_x^s$ at time $t \in [0, T]$. Corresponding Bochner spaces, such as $L^p([0, T]; H^s(\mathbb{T}^d; \mathbb{R}^{d'}))$ will often be written in the abbreviated form $L_t^p H_x^s$.

A.2 Compactness theorems

We finally recall the following two mathematical facts, which will be used in the main text: The first is the Arzela-Ascoli theorem, characterizing compactness in $C_{\text{loc}}(X, Y)$, for topological spaces X, Y :

Theorem A.2.1 (Arzela-Ascoli). *Let X be a locally compact Hausdorff space. Let Y be a complete metric space. A subset $F \subset C_{\text{loc}}(X, Y)$, of the space of continuous functions $X \rightarrow Y$ in the topology of local uniform convergence, is relatively compact if, and only if, it is equi-continuous and for all $x \in X$, the set $\{f(x) | f \in F\}$ is relatively compact in Y .*

We also recall the following characterization of weakly compact subsets of $L^1([0, T] \times \mathbb{T}^d)$, commonly known as the Dunford-Pettis theorem (for a proof, see [DS58]).

Theorem A.2.2 (Dunford-Pettis). *A subset $K \subset L^1([0, T] \times \mathbb{T}^d)$ is relatively compact in the weak topology (induced by the duality pairing with L^∞) if, and only if,*

- *K is bounded in the L^1 -norm,*
- *for every $\epsilon > 0$, there exists a $\delta > 0$ such that for all Lebesgue-measurable $A \subset [0, T] \times \mathbb{T}^d$,*

$$|A| < \delta \implies \int_A f(x, t) dx dt < \epsilon, \quad \text{for all } f \in K.$$

Appendix B

Wasserstein distance

Here, we summarize a few elementary facts about the Wasserstein distance and the convergence of measures. An excellent reference on this material (and much more) is [Vil08]. Given a separable Banach space X , we denote by $\mathcal{P}(X)$ the space of Borel probability measures on X . The term “measurable” will always refer to Borel measurability. A sequence $\mu_n \in \mathcal{P}(X)$ is said to **converge weakly** to a limit μ , denoted $\mu_n \rightharpoonup \mu$, if

$$\int_X \phi \, d\mu_n \rightarrow \int_X \phi \, d\mu, \quad \forall \phi \in C_b(X), \quad (\text{B.0.1})$$

where $C_b(X)$ denotes the space of bounded, continuous functions on X .

We call a family of probability measures $\{\mu^\Delta\}_{\Delta > 0} \subset \mathcal{P}(X)$ **tight**, provided that for any $\epsilon > 0$ there exists a compact subset $K \subset X$ such that

$$\mu^\Delta(K) \geq 1 - \epsilon, \quad \forall \Delta > 0.$$

It is a classical result due to Prokhorov (see *e.g.* Theorems 8.6.7, 8.6.8 of the monograph [Bog07]) that a family $\mu^\Delta \in \mathcal{P}(X)$, with X a separable Banach space, is tight if and only if μ^Δ is relatively compact under the weak topology.

We denote by $\mathcal{P}_p(X)$ the space of Borel probability measures $\mu \in \mathcal{P}(X)$, possessing finite p -th moments, $\int_X \|u\|_X^p \, d\mu(u) < \infty$, metrized by the p -Wasserstein distance W_p :

$$W_p(\mu, \nu) := \inf_{\pi \in \Gamma(\mu, \nu)} \left(\int_{X \times X} \|u - v\|_X^p \, d\pi(u, v) \right)^{1/p}. \quad (\text{B.0.2})$$

where the infimum is taken over all **transfer plans** $\pi \in \Gamma(\mu, \nu)$ defined as,

$$\Gamma(\mu, \nu) := \left\{ \pi \in \mathcal{P}(X \times X) \mid \int_{X \times X} (F(u) + G(v)) \, d\pi(u, v) = \int_X F(u) \, d\mu(u) + \int_X G(v) \, d\nu(v) \right\},$$

for all $F, G \in C_b(X)$.

Given a measurable map $F : X \rightarrow Y$, we denote by $F_\# \mu \in \mathcal{P}(Y)$ the push-forward of a probability measure $\mu \in \mathcal{P}(X)$ by F , defined by $(F_\# \mu)(A) := \mu(F^{-1}(A))$ for measurable $A \subset Y$; the push-forward measure satisfies the relation

$$\int_Y \phi(v) \, d(F_\# \mu)(v) = \int_X (\phi \circ F)(u) \, d\mu(u),$$

for all measurable functions $\phi : Y \rightarrow \mathbb{R}$ such that $\phi \circ F \in L^1(\mu)$. We recall that the 1-Wasserstein distance $W_1(\mu, \nu)$ between measures $\mu, \nu \in \mathcal{P}_1(X)$ can also be determined via the Kantorovich duality:

$$W_1(\mu, \nu) = \sup_{\Phi} \int \Phi(u) [d\mu(u) - d\nu(u)], \quad (\text{B.0.3})$$

where the supremum is taken over all Lipschitz continuous $\Phi \in \text{Lip}(X)$, with $\|\Phi\|_{\text{Lip}} \leq 1$, and we define the semi-norm $\|\cdot\|_{\text{Lip}}$ by

$$\|\Phi\|_{\text{Lip}} := \sup_{u \neq v} \frac{|\Phi(u) - \Phi(v)|}{\|u - v\|_X}. \quad (\text{B.0.4})$$

We also recall that for a sequence of measures $\mu^\Delta \in \mathcal{P}_1(X)$, $\Delta \rightarrow 0$, and $\mu \in \mathcal{P}_1(X)$, we have

$$\lim_{\Delta \rightarrow 0} W_1(\mu^\Delta, \mu) = 0 \Leftrightarrow \left\{ \begin{array}{l} \mu^\Delta \rightharpoonup \mu \text{ converges weakly and} \\ \int_X \|u\|_X d\mu^\Delta(u) \rightarrow \int_X \|u\|_X d\mu(u). \end{array} \right\} \quad (\text{B.0.5})$$

We will denote the Kullback-Leibler (KL) divergence of a measure $\nu \in \mathcal{P}(X)$ with respect to $\mu \in \mathcal{P}(X)$ by $\mathcal{D}_{\text{KL}}(\nu||\mu)$; We recall that the Kullback-Leibler divergence is defined by

$$\mathcal{D}_{\text{KL}}(\nu||\mu) := \begin{cases} \int_X \log\left(\frac{d\nu}{d\mu}\right) d\nu, & (\nu \ll \mu), \\ +\infty, & (\nu \not\ll \mu). \end{cases} \quad (\text{B.0.6})$$

It is well-known that $\mathcal{P}(X) \rightarrow \mathbb{R}$, $\nu \mapsto \mathcal{D}_{\text{KL}}(\nu||\mu)$ is a strictly convex, coercive and lower semi-continuous function. In particular, for any $\alpha > 0$ the set $\{\nu \in \mathcal{P}(X) \mid \mathcal{D}_{\text{KL}}(\nu||\mu) \leq \alpha\}$ is compact in the weak topology on $\mathcal{P}(X)$.

Bibliography

- [AAB⁺20] Anima Anandkumar, Kamyar Azizzadenesheli, Kaushik Bhattacharya, Nikola Kovachki, Zongyi Li, Burigede Liu, and Andrew Stuart. Neural operator: Graph kernel network for partial differential equations. In *ICLR 2020 Workshop on Integration of Deep Neural Models and Differential Equations*, 2020.
- [AB97] J.J. Alibert and G. Bouchitté. Non-uniform integrability and generalized young measures. *Journal of Convex Analysis*, 4(1):129–147, 1997.
- [Alf11] Giancarlo Alfonsi. On direct numerical simulation of turbulent flows. *Applied Mechanics Reviews*, 64(2), 2011.
- [AM18] R. Abgrall and S. Mishra. Uncertainty quantification for hyperbolic systems of conservation laws. *Handbook of Numerical Analysis*, 18:507–544, 2018.
- [Bar93] A. R. Barron. Universal approximation bounds for superpositions of a sigmoidal function. *IEEE Trans. Inform. Theory.*, 39(3):930–945, 1993.
- [BDLS11] Yann Brenier, Camillo De Lellis, and László Székelyhidi. Weak-strong uniqueness for measure-valued solutions. *Communications in Mathematical Physics*, 305(2):351, May 2011.
- [BdLSV19] Tristan Buckmaster, Camillo de Lellis, László Székelyhidi, Jr., and Vlad Vicol. Onsager’s conjecture for admissible weak solutions. *Comm. Pure Appl. Math.*, 72(2):229–274, 2019.
- [BHKS21] Kaushik Bhattacharya, Bamdad Hosseini, Nikola B. Kovachki, and Andrew M. Stuart. Model Reduction And Neural Networks For Parametric PDEs. *The SMAI journal of computational mathematics*, 7:121–157, 2021.
- [BKM84] J. T. Beale, T. Kato, and A. J. Majda. Remarks on the breakdown of smooth solutions for the 3-D Euler equations. *Communications in Mathematical Physics*, 94(1):61 – 66, 1984.
- [BL10] Oscar P. Bruno and Mark Lyon. High-order unconditionally stable FC-AD solvers for general smooth domains I. Basic elements. *Journal of Computational Physics*, 229(6):2009–2033, 2010.
- [Bog07] V. I. Bogachev. *Measure theory. Vol. I, II*. Springer-Verlag, Berlin, 2007.
- [BT15] Claude Bardos and Eitan Tadmor. Stability and spectral convergence of Fourier method for nonlinear problems: on the shortcomings of the 2/3 de-aliasing method. *Numer. Math.*, 129(4):749–782, 2015.

- [BTB15] Peter Bauer, Alan Thorpe, and Gilbert Brunet. The quiet revolution of numerical weather prediction. *Nature*, 525(7567):47–55, 2015.
- [BvdPPH11] Nicolas Bonneel, Michiel van de Panne, Sylvain Paris, and Wolfgang Heidrich. Displacement interpolation using Lagrangian mass transport. *ACM Trans. Graph.*, 30(6):158:1–158:12, December 2011.
- [Caf88] Russel E Caflisch. Long time existence and singularity formation for vortex sheets. In *Vortex Methods*, pages 1–8. Springer, 1988.
- [CC95] Tianping Chen and Hong Chen. Universal approximation to nonlinear operators by neural networks with arbitrary activation functions and its application to dynamical systems. *IEEE Transactions on Neural Networks*, 6(4):911–917, 1995.
- [CET94] Peter Constantin, Weinan E, and Edriss S. Titi. Onsager’s conjecture on the energy conservation for solutions of Euler’s equation. *Comm. Math. Phys.*, 165(1):207–209, 1994.
- [CFLS16] A. Cheskidov, M. C. Lopes Filho, H. J. Nussenzveig Lopes, and R. Shvydkoy. Energy conservation in two-dimensional incompressible ideal fluids. *Communications in Mathematical Physics*, 348(1):129–143, Nov 2016.
- [CG12] Gui-Qiang Chen and James Glimm. Kolmogorov’s theory of turbulence and inviscid limit of the Navier-Stokes equations in \mathbb{R}^3 . *Communications in Mathematical Physics*, 310(1):267–283, 2012.
- [Cha93] D. H. Chae. Weak solutions of 2-D Euler equations with initial vorticity in $L(\log L)$. *Journal of Differential Equations*, 103:323–337, June 1993.
- [Cha94] Dongho Chae. Weak solutions of 2-D incompressible Euler equations. *Nonlinear Anal.*, 23(5):629–638, September 1994.
- [Cho68] A. Chorin. Numerical solution of the Navier-Stokes equations. *Math. Comput.*, 22:745–762, 1968.
- [CHQZ07] Claudio Canuto, M Yousuff Hussaini, Alfio Quarteroni, and Thomas A Zang. *Spectral methods: fundamentals in single domains*. Springer Science & Business Media, 2007.
- [CM90] Alexandre Joel Chorin and Jerrold E Marsden. *A mathematical introduction to fluid mechanics*, volume 168. Springer, 1990.
- [CT65] James W Cooley and John W Tukey. An algorithm for the machine calculation of complex Fourier series. *Mathematics of computation*, 19(90):297–301, 1965.
- [CV18] Peter Constantin and Vlad Vicol. Remarks on high reynolds numbers hydrodynamics and the inviscid limit. *Journal of Nonlinear Science*, 28(2):711–724, 2018.
- [CWL⁺21] Shengze Cai, Zhicheng Wang, Lu Lu, Tamer A. Zaki, and George Em Karniadakis. DeepM&Mnet: Inferring the electroconvection multiphysics fields based on operator approximation by neural networks. *Journal of Computational Physics*, 436:110296, 2021.
- [Cyb89] G. Cybenko. Approximations by superpositions of sigmoidal functions. *Approximation theory and its applications*, 9(3):17–28, 1989.

- [DE11] Paul Dupuis and Richard S Ellis. *A weak convergence approach to the theory of large deviations*, volume 902. John Wiley & Sons, 2011.
- [DE19] Theodore D Drivas and Gregory L Eyink. An Onsager singularity theorem for Leray solutions of incompressible Navier–Stokes. *Nonlinearity*, 32(11):4465, 2019.
- [Del91] Jean-Marc Delort. Existence de nappes de tourbillon en dimension deux. *J. Am. Math. Soc.*, 4(3):553–586, 1991.
- [DGO84] Y. M. Houssaini D. Gottlieb and S. Orszag. Theory and application of spectral methods. In *Spectral methods for PDEs*, pages 1–54. SIAM, 1984.
- [DiP85] Ronald J DiPerna. Measure-valued solutions to conservation laws. *Archive for Rational Mechanics and Analysis*, 88(3):223–270, 1985.
- [DL89] Ronald J DiPerna and Pierre-Louis Lions. Ordinary differential equations, transport theory and Sobolev spaces. *Inventiones mathematicae*, 98(3):511–547, 1989.
- [DLLM⁺21] P Clark Di Leoni, Lu Lu, Charles Meneveau, George Karniadakis, and Tamer A Zaki. DeepONet prediction of linear instability waves in high-speed boundary layers. *arXiv preprint arXiv:2105.08697*, 2021.
- [DLM21] T. DeRyck, S. Lanthaler, and S. Mishra. On the approximation of functions by tanh neural networks. *arXiv preprint arXiv:2104:08938v1*, 2021.
- [DLS09] Camillo De Lellis and László Székelyhidi, Jr. The Euler equations as a differential inclusion. *Ann. of Math. (2)*, 170(3):1417–1436, 2009.
- [DM87a] Ronald J. Diperna and Andrew J. Majda. Concentrations in regularizations for 2-D incompressible flow. *Communications on Pure and Applied Mathematics*, 40(3):301–345, 1987.
- [DM87b] Ronald J. DiPerna and Andrew J. Majda. Oscillations and concentrations in weak solutions of the incompressible fluid equations. *Comm. Math. Phys.*, 108(4):667–689, 1987.
- [DN19] Theodore D Drivas and Huy Q Nguyen. Remarks on the emergence of weak Euler solutions in the vanishing viscosity limit. *Journal of Nonlinear Science*, 29(2):709–721, 2019.
- [DS58] N. Dunford and J.T. Schwartz. *Linear Operators, Part I*. Wiley-Interscience, New York, 1958.
- [DT95] Charles R. Doering and Edriss S. Titi. Exponential decay rate of the power spectrum for solutions of the Navier-Stokes equations. *Phys. Fluids*, 7(6):1384–1390, 1995.
- [EHJ17] Weinan E, Jiequn Han, and Arnulf Jentzen. Deep learning-based numerical methods for high-dimensional parabolic partial differential equations and backward stochastic differential equations. *Communications in Mathematics and Statistics*, 5(4):349–380, 2017.
- [ES06] Gregory L. Eyink and Katepalli R. Sreenivasan. Onsager and the theory of hydrodynamic turbulence. *Rev. Mod. Phys.*, 78:87–135, Jan 2006.
- [Eul57] Leonhard Euler. Principes généraux du mouvement des fluides. *Mémoires de l'Académie des Sciences de Berlin*, pages 274–315, 1757.

- [Eyi94] Gregory L. Eyink. Energy dissipation without viscosity in ideal hydrodynamics I. Fourier analysis and local energy transfer. *Physica D: Nonlinear Phenomena*, 78(3):222 – 240, 1994.
- [FC17] Rémi Flamary and Nicolas Courty. POT Python Optimal Transport library, 2017.
- [FKMT17] U. S. Fjordholm, R. Käppeli, S. Mishra, and E. Tadmor. Construction of approximate entropy measure valued solutions for hyperbolic systems of conservation laws. *Found. Comput. Math.*, 17(3):763–827, 2017.
- [FLM17] U. S. Fjordholm, S. Lanthaler, and S. Mishra. Statistical solutions of hyperbolic conservation laws I: Foundations. *Arch. Ration. Mech. An.*, 226(2):809–849, 2017.
- [FLM18] U. S. Fjordholm, K. O. Lye, and S. Mishra. Numerical approximation of statistical solutions of scalar conservation laws. *SIAM J. Numer. Anal.*, 56(5):2989–3009, 2018.
- [FLMW20] U. S Fjordholm, K. O. Lye, S. Mishra, and F. Weber. Statistical solutions of hyperbolic systems of conservation law: Numerical approximation. *Math. Models Meth. Appl. Sci (M3AS)*, 30(3):539–609, 2020.
- [FLT00] Milton C Lopes Filho, Helena J Nussenzveig Lopes, and Eitan Tadmor. Approximate solutions of the incompressible Euler equations with no concentrations. *Annales de l'Institut Henri Poincaré (C) Non Linear Analysis*, 17(3):371 – 412, 2000.
- [FMRT08] C. Foias, O. Manley, R. Rosa, and R. Temam. *Navier-Stokes equations and Turbulence*. Cambridge University Press, 2008.
- [FMT16] U. S. Fjordholm, S. Mishra, and E. Tadmor. On the computation of measure-valued solutions. *Acta numerica.*, 25:567–679, 2016.
- [Fri95] Uriel Frisch. *Turbulence: The Legacy of A. N. Kolmogorov*. Cambridge University Press, 1995.
- [FRT10] Ciprian Foias, Ricardo M.S. Rosa, and Roger Temam. A note on statistical solutions of the three-dimensional Navier–Stokes equations: The time-dependent case. *Comptes Rendus Mathematique*, 348(3):235 – 240, 2010.
- [FW18] U.S. Fjordholm and E. Wiedemann. Statistical solutions and Onsager’s conjecture. *Physica D: Nonlinear Phenomena*, 376-377:259 – 265, 2018. Special Issue: Nonlinear Partial Differential Equations in Mathematical Fluid Dynamics.
- [GBC16] Ian Goodfellow, Yoshua Bengio, and Aaron Courville. *Deep learning*. MIT press, 2016.
- [Gey11] Charles J Geyer. Introduction to Markov chain Monte Carlo. *Handbook of markov chain monte carlo*, 20116022:45, 2011.
- [GGL⁺01] J. Glimm, J.W. Grove, X.L. Li, W. Oh, and D.H. Sharp. A critical analysis of Rayleigh–Taylor growth rates. *Journal of Computational Physics*, 169(2):652 – 677, 2001.
- [Gho96] S. Ghoshal. An analysis of numerical errors in large eddy simulations of turbulence. *J. Comput. Phys.*, 125(1):187–206, 1996.
- [GST01] Sigal Gottlieb, Chi-Wang Shu, and Eitan Tadmor. Strong stability-preserving high-order time discretization methods. *SIAM review*, 43(1):89–112, 2001.

- [HKR90] W. D. Henshaw, H. O. Kreiss, and L. G. Reyna. Smallest scale estimates for the Navier-Stokes equations for incompressible fluids. *Arch. Ration. Mech. Anal.*, 112(1):21–44, 1990.
- [HSW89] K. Hornik, M. Stinchcombe, and H. White. Multilayer feedforward networks are universal approximators. *Neural networks*, 2(5):359–366, 1989.
- [HSZ20] Lukas Herrmann, Christoph Schwab, and Jakob Zech. Deep neural network expression of posterior expectations in Bayesian PDE inversion. *Inverse Problems*, 36(12):125011, dec 2020.
- [Ise18] Philip Isett. A proof of Onsager’s conjecture. *Ann. of Math. (2)*, 188(3):871–963, 2018.
- [ISY20] Kartik P Iyer, Katepalli R Sreenivasan, and PK Yeung. Scaling exponents saturate in three-dimensional isotropic turbulence. *Physical Review Fluids*, 5(5):054605, 2020.
- [JBBG89] P. Colella J. B. Bell and H. M. Glaz. A second-order projection method for the incompressible Navier-Stokes equations. *J. Comput. Phys.*, 85(2):257–283, 1989.
- [KK00] G. S. Karamanos and G. E. Karniadakis. A spectral vanishing viscosity method for large-eddy simulations. *J. Comput. Phys.*, 163:22–50, 2000.
- [KLH⁺91] Andrei Nikolaevich Kolmogorov, V. Levin, Julian Charles Roland Hunt, Owen Martin Phillips, and David Williams. Dissipation of energy in the locally isotropic turbulence. *Proceedings of the Royal Society of London. Series A: Mathematical and Physical Sciences*, 434(1890):15–17, 1991.
- [KLM21] Nikola Kovachki, Samuel Lanthaler, and Siddhartha Mishra. On universal approximation and error bounds for Fourier Neural Operators. *arXiv preprint arXiv:2107.07562*, 2021.
- [Kol91] A. N. Kolmogorov. The local structure of turbulence in incompressible viscous fluid for very large Reynolds numbers. *Proceedings: Mathematical and Physical Sciences*, 434(1890):9–13, 1991.
- [KPS19] G. Kutyniok, P. Petersen, and R. Schneider. A theoretical analysis of deep neural networks and parametric partial differential equations. *arXiv preprint arXiv:1904.00377*, 2019.
- [Kra86a] R. Krasny. Desingularization of periodic vortex sheet roll-up. *J. Comput. Phys.*, 65:292–313, 1986.
- [Kra86b] Robert Krasny. A study of singularity formation in a vortex sheet by the point-vortex approximation. *Journal of Fluid Mechanics*, 167:65–93, 1986.
- [Kra87] Robert Krasny. Computation of vortex sheet roll-up in the Trefftz plane. *Journal of Fluid mechanics*, 184:123–155, 1987.
- [KS06] Jari Kaipio and Erkki Somersalo. *Statistical and computational inverse problems*, volume 160. Springer Science & Business Media, 2006.
- [Lat20] Jonas Latz. On the Well-posedness of Bayesian Inverse Problems. *SIAM/ASA Journal on Uncertainty Quantification*, 8(1):451–482, 2020.
- [LB10] Mark Lyon and Oscar P. Bruno. High-order unconditionally stable FC-AD solvers for general smooth domains II. Elliptic, parabolic and hyperbolic PDEs; theoretical considerations. *Journal of Computational Physics*, 229(9):3358–3381, 2010.

- [LBH15] Yann LeCun, Yoshua Bengio, and Geoffrey Hinton. Deep learning. *Nature*, 521(7553):436–444, 2015.
- [Leo18] Filippo Leonardi. *Numerical methods for ensemble based solutions to incompressible flow equations*. PhD thesis, ETH Zürich, 2018.
- [Ler34] Jean Leray. Sur le mouvement d’un liquide visqueux emplissant l’espace. *Acta mathematica*, 63:193–248, 1934.
- [Lév92] Paul Lévy. *Processus stochastiques et mouvement brownien*. Les Grands Classiques Gauthier-Villars. [Gauthier-Villars Great Classics]. Éditions Jacques Gabay, Sceaux, 1992. Followed by a note by M. Loèvre, Reprint of the second (1965) edition.
- [LFLX01] Milton C Lopes Filho, Helena J Nussenzveig Lopes, and Zhouping Xin. Existence of vortex sheets with reflection symmetry in two space dimensions. *Archive for rational mechanics and analysis*, 158(3):235–257, 2001.
- [LFNL00] Milton C Lopes Filho, Helena J Nussenzveig Lopes, and Eitan Tadmor. Approximate solutions of the incompressible Euler equations with no concentrations. In *Annales de l’Institut Henri Poincaré (C) Nonlinear Analysis*, volume 17, pages 371–412. Elsevier Science, 2000.
- [LH19] Guo Luo and Thomas Y Hou. Formation of finite-time singularities in the 3D axisymmetric Euler equations: a numerics guided study. *SIAM Review*, 61(4):793–835, 2019.
- [Lio96] Pierre-Louis Lions. *Mathematical topics in fluid mechanics. Vol. 1*, volume 3 of *Oxford Lecture Series in Mathematics and its Applications*. The Clarendon Press, Oxford University Press, New York, 1996. Incompressible models, Oxford Science Publications.
- [LJK19] Lu Lu, Pengzhan Jin, and George Em Karniadakis. DeepONet: Learning nonlinear operators for identifying differential equations based on the universal approximation theorem of operators. *arXiv preprint arXiv:1910.03193*, 2019.
- [LKA⁺20] Zongyi Li, Nikola Kovachki, Kamyar Azizzadenesheli, Burigede Liu, Andrew Stuart, Kaushik Bhattacharya, and Anima Anandkumar. Multipole graph neural operator for parametric partial differential equations. In H. Larochelle, M. Ranzato, R. Hadsell, M. F. Balcan, and H. Lin, editors, *Advances in Neural Information Processing Systems*, volume 33, pages 6755–6766. Curran Associates, Inc., 2020.
- [LKA⁺21] Zongyi Li, Nikola Borislavov Kovachki, Kamyar Azizzadenesheli, Burigede liu, Kaushik Bhattacharya, Andrew Stuart, and Anima Anandkumar. Fourier neural operator for parametric partial differential equations. In *International Conference on Learning Representations*, 2021.
- [LLL⁺21] Chensen Lin, Zhen Li, Lu Lu, Shengze Cai, Martin Maxey, and George Em Karniadakis. Operator learning for predicting multiscale bubble growth dynamics. *The Journal of Chemical Physics*, 154(10):104118, 2021.
- [LM15] Samuel Lanthaler and Siddhartha Mishra. Computation of measure-valued solutions for the incompressible Euler equations. *Mathematical Models and Methods in Applied Sciences*, 25(11):2043–2088, 2015.

- [LM20] Samuel Lanthaler and Siddhartha Mishra. On the convergence of the spectral viscosity method for the two-dimensional incompressible Euler equations with rough initial data. *Foundations of Computational Mathematics*, 20:1309–1362, 2020.
- [LMCR20] K . O. Lye, S. Mishra, P. Chandrasekhar, and D. Ray. Iterative surrogate model optimization (ISMO): An active learning algorithm for PDE constrained optimization with deep neural networks. *arXiv preprint arXiv:2008.05730*, 2020.
- [LMK21] Samuel Lanthaler, Siddhartha Mishra, and George Em Karniadakis. Error estimates for DeepOnets: A deep learning framework in infinite dimensions. *arXiv preprint arXiv:2102.09618*, 2021.
- [LMPP21a] S Lanthaler, S Mishra, and C Parés-Pulido. On the conservation of energy in two-dimensional incompressible flows. *Nonlinearity*, 34(2):1084–1135, 2021.
- [LMPP21b] S. Lanthaler, S. Mishra, and C. Parés-Pulido. Statistical solutions of the incompressible Euler equations. *Mathematical Models and Methods in Applied Sciences*, 31(02):223–292, 2021.
- [LMR20] Kjetil O Lye, Siddhartha Mishra, and Deep Ray. Deep learning observables in computational fluid dynamics. *Journal of Computational Physics*, page 109339, 2020.
- [LMS16] F. Leonardi, S. Mishra, and C. Schwab. Numerical approximation of statistical solutions of planar, incompressible flows. *Math. Model Meth. Appl. Sci.*, 26:2471–2523, 2016.
- [LMW21] Samuel Lanthaler, Siddhartha Mishra, and Franziska Weber. On the well-posedness of Bayesian inversion for PDEs with ill-posed forward problems. *arXiv preprint arXiv:2107.07593*, 2021.
- [Lor63] Edward N. Lorenz. Deterministic nonperiodic flow. *Journal of Atmospheric Sciences*, 20(2):130 – 141, 1963.
- [LSZ15] Kody Law, Andrew Stuart, and Kostas Zygalakis. Data assimilation. *Cham, Switzerland: Springer*, 214, 2015.
- [LT97] Doron Levy and Eitan Tadmor. Non-oscillatory central schemes for the incompressible 2-D Euler equations. *Mathematical Research Letters*, 4:1–20, 1997.
- [LX95] Jian-Guo Liu and Zhouping Xin. Convergence of vortex methods for weak solutions to the 2-D Euler equations with vortex sheet data. *Communications on Pure and Applied Mathematics*, 48(6):611–628, 1995.
- [LX01] Jian-Guo Liu and Zhouping Xin. Convergence of the point vortex method for 2-D vortex sheet. *Math. Comp.*, 70(234):595–606, 2001.
- [Maj88] Andrew J. Majda. Vortex dynamics: numerical analysis, scientific computing, and mathematical theory. In *ICIAM'87: Proceedings of the First International Conference on Industrial and Applied Mathematics*, pages 153–182, 1988.
- [Maj93] Andrew J. Majda. Remarks on weak solutions for vortex sheets with a distinguished sign. *Indiana Univ. Math. J.*, 42(3):921–939, 1993.
- [MB01] Andrew J. Majda and Andrea L. Bertozzi. *Vorticity and Incompressible Flow*. Cambridge Texts in Applied Mathematics. Cambridge University Press, 2001.

- [MH12] Andrew J Majda and John Harlim. *Filtering complex turbulent systems*. Cambridge University Press, 2012.
- [MLM⁺20] Zhiping Mao, Lu Lu, Olaf Marxen, Tamer A Zaki, and George E Karniadakis. DeepM&Mnet for hypersonics: Predicting the coupled flow and finite-rate chemistry behind a normal shock using neural-network approximation of operators. *arXiv preprint arXiv:2011.03349*, 2020.
- [MM20a] S. Mishra and R. Molinaro. Estimates on the generalization error of physics informed neural networks (PINNs) for approximating PDEs. *arXiv preprint arXiv:2006:16144v1*, 2020.
- [MM20b] S. Mishra and R. Molinaro. Estimates on the generalization error of physics informed neural networks (PINNs) for approximating PDEs ii: A class of inverse problems. *arXiv preprint arXiv:2007:01138v1*, 2020.
- [Mor92] AB Morgulis. On existence of two-dimensional nonstationary flows of an ideal incompressible liquid admitting a curl nonsummable to any power greater than 1. *Siberian Mathematical Journal*, 33(5):934–937, 1992.
- [MSŠ12] S. Mishra, Ch. Schwab, and J. Šukys. Multi-level Monte Carlo finite volume methods for nonlinear systems of conservation laws in multi-dimensions. *J. Comput. Phys.*, 231(8):3365–3388, 2012.
- [MT89] Y Maday and E Tadmor. Analysis of the spectral vanishing viscosity method for periodic conservation laws. *SIAM J. Math. Anal.*, 26(4):854–870, 1989.
- [Nas54] John Nash. C1 isometric imbeddings. *Annals of Mathematics*, 60(3):383–396, 1954.
- [Ons49] L. Onsager. Statistical hydrodynamics. *Il Nuovo Cimento*, 6:279–287, March 1949.
- [PP21] Carlos Parés-Pulido. *Numerical approximation of statistical solutions of the incompressible Euler equations with a finite difference-projection method*. PhD thesis, ETH Zürich, 2021.
- [RC15] Sebastian Reich and Colin Cotter. *Probabilistic forecasting and Bayesian data assimilation*. Cambridge University Press, 2015.
- [RK18] Maziar Raissi and George Em Karniadakis. Hidden physics models: Machine learning of nonlinear partial differential equations. *Journal of Computational Physics*, 357:125–141, 2018.
- [Rog06] Luke G. Rogers. Degree-independent Sobolev extension on locally uniform domains. *Journal of Functional Analysis*, 235(2):619–665, 2006.
- [RPK19] M. Raissi, P. Perdikaris, and G. E. Karniadakis. Physics-informed neural networks: A deep learning framework for solving forward and inverse problems involving nonlinear partial differential equations. *Journal of Computational Physics*, 378:686–707, 2019.
- [SAF92] Z-S She, E. Aurell, and U. Frisch. The inviscid Burgers equation with initial data of Brownian type. *Comm. Math. Phys.*, 148:623–641, 1992.
- [Sch90] Steven Schochet. The rate of convergence of spectral-viscosity methods for periodic scalar conservation laws. *SIAM J. Numer. Anal.*, 27(5):1142–1159, 1990.

- [Sch95] Steven Schochet. The weak vorticity formulation of the 2-D Euler equations and concentration-cancellation. *Communications in Partial Differential Equations*, 20(5-6):1077–1104, 1995.
- [Sch96] Steven Schochet. The point-vortex method for periodic weak solutions of the 2-D Euler equations. *Communications on Pure and Applied Mathematics*, 49(9):911–965, 1996.
- [Shv09] Roman Shvydkoy. On the energy of inviscid singular flows. *Journal of mathematical analysis and applications*, 349(2):583–595, 2009.
- [Sim86] Jacques Simon. Compact sets in the space $L^p(0, T; B)$. *Annali di Matematica Pura ed Applicata*, 146(1):65–96, Dec 1986.
- [Sin92] Ya. G. Sinai. Statistics of shocks in solutions of inviscid Burgers equation. *Communications in Mathematical Physics*, 148(3):601–621, Sep 1992.
- [Spr20] Björn Sprungk. On the local Lipschitz stability of Bayesian inverse problems. *Inverse Problems*, 36(5):055015, may 2020.
- [SS17] J. Guzman, C-W. Shu and A. F. Sequira. $h(\text{div})$ conforming and DG methods for the incompressible Euler's equations. *IMA J. Num. Anal.*, 37(4):1733–1771, 2017.
- [SSBF81] C Sulem, PL Sulem, C Bardos, and U Frisch. Finite time analyticity for the two and three dimensional Kelvin-Helmholtz instability. *Communications in Mathematical Physics*, 80(4):485–516, 1981.
- [Stu10] Andrew M Stuart. Inverse problems: a Bayesian perspective. *Acta numerica*, 19:451–559, 2010.
- [SW12] László Székelyhidi and Emil Wiedemann. Young measures generated by ideal incompressible fluid flows. *Arch. Ration. Mech. Anal.*, 206(1):333–366, 2012.
- [SZ19] Christoph Schwab and Jakob Zech. Deep learning in high dimension: Neural network expression rates for generalized polynomial chaos expansions in UQ. *Analysis and Applications*, 17(01):19–55, 2019.
- [Szé11] László Székelyhidi. Weak solutions to the incompressible Euler equations with vortex sheet initial data. *C. R. Math. Acad. Sci. Paris*, 349(19-20):1063–1066, 2011.
- [Tad89] Eitan Tadmor. Convergence of spectral methods for nonlinear conservation laws. *SIAM J. Numer. Anal.*, 26(1), 1989.
- [Tad04] Eitan Tadmor. Burgers' equation with vanishing hyper-viscosity. *Commun. Math. Sci.*, 2(2):317–324, 2004.
- [Tar05] Albert Tarantola. *Inverse problem theory and methods for model parameter estimation*. SIAM, 2005.
- [VF77] M. I. Vishik and A. V. Fursikov. Homogeneous statistical solutions of the Navier-Stokes system. *Uspehi Mat. Nauk.*, 32:179–180, 1977.
- [Vil08] Cédric Villani. *Optimal transport: old and new*, volume 338. Springer Science & Business Media, 2008.

- [Vis98] Misha Vishik. Hydrodynamics in Besov spaces. *Archive for Rational Mechanics and Analysis*, 145(3):197–214, 1998.
- [Vis99] Misha Vishik. Incompressible flows of an ideal fluid with vorticity in borderline spaces of Besov type. In *Annales Scientifiques de l'École Normale Supérieure*, volume 32, pages 769–812. Elsevier, 1999.
- [VW93] Italo Vecchi and Sijue Wu. On L1-vorticity for 2-D incompressible flow. *manuscripta mathematica*, 78(1):403–412, Dec 1993.
- [Yar17] Dmitry Yarotsky. Error bounds for approximations with deep ReLU networks. *Neural Networks*, 94:103–114, 2017.
- [Yud63] Victor I Yudovich. Non-stationary flow of an ideal incompressible liquid. *USSR Computational Mathematics and Mathematical Physics*, 3(6):1407–1456, 1963.
- [Yud95] Victor Iosifovich Yudovich. Uniqueness theorem for the basic nonstationary problem in the dynamics of an ideal incompressible fluid. *Mathematical Research Letters*, 2(1):27–38, 1995.

Acknowledgments

This thesis is the product of many fruitful interactions over the past years, and I am indebted to my mentors, colleagues and friends for their many contributions during this time.

First and foremost I would like to thank my advisor, *Siddhartha Mishra*, for his guidance and continuous support. He has always found the perfect balance between providing ample room for the exploration of my ideas, giving excellent input and new impetus when needed, and occasionally focusing my research on concrete problems to keep me from wandering too far off the path. I am thankful for all the excellent advice over the last years, mathematical or otherwise, and feel very fortunate to have had Sid as my mentor throughout this endeavour.

I would also like to thank my collaborators, who have contributed to many aspects of the work presented in this thesis: Firstly, I would like to thank *Carlos Parés-Pulido*, who spent many hours (including evenings and weekends) running many of the numerical experiments that put some flesh on the theoretical skeleton of our work on statistical solutions; It has been a great joy working and collaborating during this time. I would like to extend my thanks also to *Tim DeRyck*, who has graciously let me be part of his work on neural network approximations, from which I have learnt a lot on the fundamentals of this field. I would also like to thank my most recent collaborators, *Franziska Weber*, *George Karniadakis* and *Nikola Kovachki*, for their insightful contributions (and corrections) to work on Bayesian inversion and operator learning frameworks.

This thesis has been written at the Seminar for Applied Mathematics (SAM) at ETH Zurich, and despite the peculiar circumstances of a pandemic, has not been written in complete isolation. I would like to thank everyone at SAM for their contributions – be they direct or indirect. I would like to offer my special thanks to *Vasile Grădinaru*, for always keeping my workload for his course manageable, and for generously taking on some of my tasks after the birth of our daughter. I would like to thank *Luc Grosheintz* for his help with the exam scripts and the exam statistics, which has saved me so much time. My thanks also go to *Kthim Imeri*, for his invaluable help with the initial organization of the exercise classes and his general advice. I would like to express my sincere gratitude to *Adrian Ruf* and his family for the fun get-togethers, and for their generosity in leaving us many baby books and toys.

I would like to thank my siblings, my parents and my extended family overseas, for their invaluable help and their thoughtfulness, especially during the last few months. My deepest gratitude goes to *Dahye*, for her patience and support throughout this journey, and to *Leonie* for joining us during the final stretch.

Zürich, 12.10.2021
S.L.

Samuel Lanthaler

Seminar for Applied Mathematics, ETH Zurich, Switzerland

• Google Scholar • ArXiv • Orcid

EDUCATION AND RESEARCH EXPERIENCE

SINCE 11/2018	PhD candidate in Mathematics at ETH Zurich, Switzerland — Advisor: Prof. Siddhartha Mishra
08/2015 – 08/2020	PhD in Physics at EPF Lausanne, Switzerland Thesis: “Kinetic-MHD stability of virtually collisionless plasmas” — Advisor: Prof. Jonathan P. Graves
09/2013 – 03/2015	Master of Science ETH in Mathematics , ETH Zurich Thesis: “Computation of measure-valued solutions of the incompressible Euler equations” — Advisor: Prof. Siddhartha MISHRA
09/2010 – 09/2013	Bachelor of Science ETH in Mathematics , ETH Zurich

- **Research presentations** at the *PhILMs Seminar* (Brown U.; 2021), *SIAM Analysis of PDEs*, (California; 2019), *Numerical Methods for Hyperbolic Problems (NumHyp2019)* (Spain; 2019), workshop on *Interfaces and Instabilities in Fluid Dynamics* (Germany; 2019), *Theory of Fusion Plasmas* (Italy; 2018), *XV International Conference on Hyperbolic Problems (Hyp2014)* (Brazil; 2014).
- **Co-supervision** of master theses (3) and semester projects (1).
- **Teaching assistant** for lectures on Linear Algebra (**head assistant**; 8 TAs, \sim 350 students), Numerical Methods for Hyperbolic PDEs, Mathematical Methods for Physicists, Advanced Physics, Computational Physics, Numerical Mathematics II, Differential Geometry II.
- Extended **programming experience** in C++, Fortran-90/03 (with MPI-parallelization), MATLAB, PYTHON, and basic knowledge of CUDA, OPENACC.

AWARDS AND RECOGNITION

2022 – 2024	GAMM Junior Fellow Elected by the Association of Applied Mathematics and Mechanics (GAMM) for outstanding work in Master's or doctoral thesis (10 junior fellows per year)
01/2015	ETH Medal (ETH Zurich) Awarded for outstanding master's thesis
09/2013 – 01/2015	Excellence Scholarship and Opportunity Programme (ETH Zurich) A special scholarship to cover the full study and living costs for the duration of master's degree, as well as specific supervision.
12/2013	Polya prize (ETH Zurich) Awarded for best bachelor's degree in mathematics and physics.

PUBLICATIONS

Preprints

- [P12] “On universal approximation and error bounds for Fourier neural operators”, N. Kovachki, S. Lanthaler, S. Mishra, (2021), *arXiv:2107.07562*
- [P11] “On the well-posedness of Bayesian inversion for PDEs with ill-posed forward problems”, S. Lanthaler, S. Mishra, F. Weber, (2021), *arXiv:2107.07593*
- [P10] “Error estimates for DeepOnets: A deep learning framework in infinite dimensions”, S. Lanthaler, S. Mishra, G.E. Karniadakis, (2021) *arXiv:2102.09618*
- [P9] “On concentration in vortex sheets”, S. Lanthaler, (2020), *arXiv:2004.01537*

Published articles in peer-reviewed journals

- [P8] “On the approximation of functions by tanh neural networks”, T. De Ryck, S. Lanthaler, S. Mishra, *Neural Networks* **143**, (2021), 732-750
- [P7] “Statistical solutions of the incompressible Euler equations”, S. Lanthaler, S. Mishra, C. Parés-Pulido, *Math. Models Methods Appl. Sci.* (M³AS), **31**(2), (2021), 223-292
- [P6] “On the conservation of energy in two-dimensional incompressible flows”, S. Lanthaler, S. Mishra, C. Parés-Pulido, *Nonlinearity*, **34**(2), (2021), 1084
- [P5] “On the convergence of the spectral viscosity method for the two-dimensional incompressible Euler equations with rough initial data”, S. Lanthaler, S. Mishra, *Found Comput Math*, **20**, (2020), 1309–1362
- [P4] “Guiding-centre theory for kinetic-magnetohydrodynamic modes in strongly flowing plasmas”, S. Lanthaler, J. P. Graves, D. Pfefferl  , W. A. Cooper, *Plasma Phys. Control. Fusion*, **61**, (2019), 074006
- [P3] “Higher order Larmor radius corrections to guiding-centre equations and application to fast ion equilibrium distributions”, S. Lanthaler, D. Pfefferl  , J. P. Graves, W. A. Cooper, *Plasma Phys. Control. Fusion*, **59**, (2017), 044014
- [P2] “Statistical solutions of hyperbolic conservation laws I: Foundations”, U. S. Fjordholm and S. Lanthaler and S. Mishra, *Arch. Ration. Mech. An.*, **226**(2), (2017), 809–849
- [P1] “Computation of measure-valued solutions for the incompressible Euler equations”, S. Lanthaler, S. Mishra, *Math. Models and Methods Appl. Sci.*, **25**, (2015), 2043-2088